Test Set for Initial Value Problem Solvers

Walter M. Lioen
CWI, PO Box 94079, 1090 GB Amsterdam, The Netherlands (Walter.Lioen@cwi.nl)

Jacques J.B. de Swart
CWI, PO Box 94079, 1090 GB Amsterdam, The Netherlands (Jacques.de.Swart@cwi.nl) &
Paragon Decision Technology, PO Box 3277, 2001 DG Haarlem, The Netherlands (jacques@paragon.nl)

Release 2.1 September 1999

ABSTRACT
The CWI test set for IVP solvers presents a collection of Initial Value Problems to test solvers for implicit differential equations. This test set can both decrease the effort for the code developer to test his software in a reliable way, and cross the bridge between the application field and numerical mathematics. This document contains the descriptive part of the test set. It describes the test problems and their origin, and reports on the behavior of a few state-of-the-art solvers on these problems. The latest version of this document and the software part of the test set is available via the world wide web at http://www.cwi.nl/cwi/projects/IVPtestset/. The software part serves as a platform on which one can test the performance of a solver on a particular test problem oneself. Instructions how to use this software are in this paper as well. The idea to develop this test set was discussed at the workshop ODE to NODE, held in Geiranger, Norway, 19–22 June 1995.

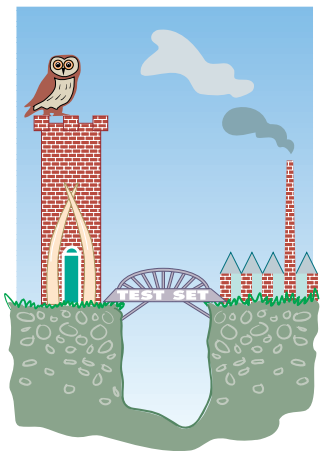

1991 Mathematics Subject Classification: Primary: 65Y20, Secondary: 65-04, 65C20, 65L05.
1991 Computing Reviews Classification System: G.1.7, G.4.
Keywords and Phrases: test problems, software, IVP, IDE, ODE, DAE.
Note: The maintenance of the test set belongs to the project MAS2.2: 'Parallel Software for Implicit Differential Equations'.
Acknowledgements: This work is supported financially by the 'Technologiestichting STW' (Dutch Foundation for Technical Sciences), grants no. CWI.2703, CWI.4533. The use of supercomputer facilities was made possible by the 'Stichting Nationale Computerfaciliteiten' (National Computing Facilities Foundation, NCF), with financial support from the 'Nederlandse Organisatie voor Wetenschappelijk Onderzoek' (Netherlands Organization for Scientific Research, NWO). We thank all contributors to this test set, without whom it would not be possible to collect problems from such a wide variety of application fields.

Contents

Test problems collected so far:

I. Introduction

I.1 The idea behind this test set

Both engineers and computational scientists alike will benefit greatly from having a standard test set for Initial Value Problems (IVPs) which includes documentation of the test problems, experimental results from a number of proven solvers, and Fortran subroutines providing a common interface to the defining problem functions. Engineers will be able to see at a glance which methods will be most effective for their class of problems. Researchers will be able to compare their new methods with the results of existing ones without incurring additional programming workload; they will have a reference with which their colleagues are familiar. This test set tries to fulfill these demands and tries to set a standard for IVP solver testing. We hope that the following features of this set will enable the achievement of this goal:

- uniform presentation of the problems,
- ample description of the origin of the problems,
- robust interfaces between problem and drivers,
- portability among different platforms,
- contributions by people from several application fields,
- presence of real-life problems,
- being used, tested and debugged by a large, international group of researchers,
- comparisons of the performance of well-known solvers,
- interpretation of the numerical solution in terms of the application field,
- ease of access and use.

There exist other test sets, e.g., NSDTST and STDTST by Enright & Pryce [EP87], PADETEST by Bellen [Bel92], the Geneva test set by Hairer & Wanner [HW] and the Test Frame for Ordinary Differential Equations by Nowak and Gebauer [NG97], which all have their own qualities. However, we think that none of those test sets combines all the features listed above.

I.2 Structure of this test set

The test set consists of a descriptive part and a software part. The first part describes test problems and reports on the behavior of a few state-of-the-art solvers when applied to these problems. Section II explains how this information is presented. The software serves as a platform to test the performance of a solver on a particular test problem by a user of the test set. In Section III we specify the format of the Fortran subroutines and explains how to run test problems with the help of drivers that make these codes suitable for runs with a number of solvers. Currently, DASSL, MEBDFDAE, PSIDE, RADAU, RADAU5 and VODE are supported.

I.3 How to obtain this test set

The latest release of this test set can be obtained in two ways. Either via the WWW page with URL

`http://www.cwi.nl/cwi/projects/IVPtestset/` ,

or via anonymous ftp at the site

`ftp.cwi.nl` in the directory `pub/IVPtestset` .

The first release of this test set appeared in [LSV96].

I.4 Acknowledgements

We gratefully acknowledge G. Denk, M. Günther, U. Feldmann, E. Messina and B. Simeon, who contributed one or more test problems; and the cooperation with R. van der Hout of the Akzo Nobel company, which led to two test problems. The many discussions with E. Hairer were very useful too. The standard work by Hairer & Wanner [HW96] turned out to be a fruitful source for well documented test problems.

I.5 People involved

This test set is maintained by the project group 'Parallel Software for Implicit Differential Equations', and is sponsored by the 'Technologiestichting STW' under grant no. CWI.4533. The project is a follow-up of the project 'Parallel Codes for Circuit Analysis and Control Engineering', which was sponsored under grant no. CWI.2703, also by STW.

The members of this project group are

P.J. van der Houwen (*P.J.van.der.Houwen@cwi.nl*),
W. Hoffmann[1] (*walter@wins.uva.nl*),
B.P. Sommeijer (*B.P.Sommeijer@cwi.nl*),
W.M. Lioen (*Walter.Lioen@cwi.nl*),
W.A. van der Veen[2],
J.J.B. de Swart (*Jacques.de.Swart@cwi.nl*),
J.E. Frank (*J.E.Frank@cwi.nl*).

This group belongs to the research theme 'Modelling and Simulation of Industrial Processes' of the cluster 'Modelling, Analysis and Simulation' of the 'Centre for Mathematics and Computer Science' (CWI).

References

[Bel92] A. Bellen. PADETEST: a set of real-life test differential equations for parallel computing. Technical Report 103, Dipartimento di Scienze Matematiche, Università di Trieste, 1992.

[EP87] W.H. Enright and J.D. Pryce. Two Fortran packages for assessing initial value methods. *ACM Transactions on Mathematical Software*, 13-I:1–27, 1987.

[HW] E. Hairer and G. Wanner. *Testset of Stiff ODEs*. Geneva. Available at http://www.unige.ch/math/folks/hairer/testset/testset.html.

[HW96] E. Hairer and G. Wanner. *Solving Ordinary Differential Equations II: Stiff and Differential-algebraic Problems*. Springer-Verlag, second revised edition, 1996.

[LSV96] W.M. Lioen, J.J.B. de Swart, and W.A. van der Veen. Test set for IVP solvers. Technical Report NM-R9615, CWI, Amsterdam, 1996.

[NG97] Ulrich Nowak and Susanna Gebauer. A new test frame for ordinary differential equations. Technical Report SC 97-68, Konrad-Zuse-Zentrum für Informationstechnik, Berlin, 1997.

[1] University of Amsterdam.
[2] Formerly at CWI, co-author of the first version.

II. Format of the problem descriptions

Every problem description contains the four sections, which are described below.

II.1 General information

The problem identification is given; the type of problem (IDE, ODE or DAE), its dimension and index. The contributor and any further relevant information are listed too. What is meant here by IDE, ODE, DAE and index, is explained in §III.

II.2 Mathematical description of the problem

All ingredients that are necessary for implementation are given in mathematical formulas.

II.3 Origin of the problem

A brief description of the origin of the problem, in order to give its physical interpretation. References to the literature are given for further details.

II.4 Numerical solution of the problem

This section contains:

1. **Reference solution at the end of the integration interval.** The values of (some of) the components of a reference solution at the end of the integration interval are listed.

2. **Run characteristics.** Integration statistics, if applicable, of runs with DASSL, MEBDFDAE, PSIDE, RADAU, RADAU5, and VODE serve to give insight in the numerical difficulty of the problem.

   The experiments were done on an SGI workstation, an *Indy* with a 100 MHz R4000SC processor. We used the Fortran 77 compiler with optimization: `f77 -O <source code>`. If a run does not produce correct results then we report what went wrong.

   The characteristics are in the following format:

   - *solver*
     The name of the numerical solver with which the run was performed.
   - *rtol*
     The user supplied relative error tolerance.
   - *atol*
     The user supplied absolute error tolerance.
   - *h0*
     The user supplied initial step size (if relevant).
   - *scd*
     The scd values denote the minimum number of significant correct digits in the numerical solution at the end of the integration interval, i.e.

     $$\text{scd} := -\log_{10}(\| \text{ relative error at the end of the integration interval } \|_\infty). \qquad \text{(II.1)}$$

     If some components of the solution vector are not taken into account for the computation of the scd value, or if the absolute error is computed instead of the relative error, then this is specified locally.
   - *steps*
     Total number of steps taken by the solver (including rejected steps due to error test failures and/or convergence test failures).
   - *accept*
     The number of accepted steps.

- *# f* and *# Jac*
  The number of evaluations of the derivative function and its Jacobians, respectively.
- *# LU*
  The number of LU-decompositions (not for DASSL). The codes, except for RADAU and RADAU5, count the LU-decompositions of systems of dimension d, where d is the dimension of the test problem.

  RADAU and RADAU5 use an s-stage Radau IIA method. For RADAU5, $s = 3$ and for RADAU, $s = 3$, 5 or 7. Every iteration of the inexact Newton process, used for solving systems of non-linear equations, requires the solution of a linear system of dimension sd. By means of transformations, this linear system is reduced to $(s + 1)/2$ linear systems of dimension d. Of these systems, one system is real, and $(s - 1)/2$ systems are complex. The decompositions of all $(s + 1)/2$ linear systems are counted by RADAU and RADAU5 as 1 LU-decomposition.
- *CPU*
  The CPU time in seconds to perform the run on the aforementioned computer. Since timings may depend on other processes (like e.g. daemons), the minimum of the CPU times of 10 runs is listed.

PSIDE – Parallel Software for Implicit Differential Equations – is a Fortran 77 code for solving IDE problems. It is developed for parallel, shared memory computers. The integration characteristics in the tables refer to a one-processor computer. Since PSIDE can do four function evaluations and four linear system solves concurrently on a computer with four processors, one may divide the number of function evaluations, decompositions and solves in the tables by four to obtain the analogous *effective* characteristics for four-processor machines.

3. **Behavior of the numerical solution.** Plots of (some of) the solution components over (part of) the integration interval are presented.

4. **Work-precision diagram.** For every relevant solver, a range of input tolerances and, if necessary, a range of initial stepsizes, were used to produce a plot of the resulting scd values, defined in Formula (II.1), against the number of CPU seconds needed for the run on the aforementioned computer, with the setting as described before. Here we took again the minimum of the CPU times of 10 runs. The format of these diagrams is as in Hairer & Wanner [HW96, pp. 166–167, 324–325]. The range of input tolerances and initial stepsizes is problem dependent and specified locally. The input parameters for the runs in the tables with run characteristics are such that these runs appear in the work-precision diagrams as well.

   To give an impression of the performance of PSIDE on a parallel computer we plotted two PSIDE curves in the work-precision diagrams, PSIDE-1 and PSIDE-4. The first curve refers to PSIDE on one processor. The latter curve was obtained by dividing the CPU timings of the runs on one processor by the speed-up factor for one single run as obtained using ATExpert on a Cray C90. The speed-up factor is also listed separately. For more details on ATExpert, we refer to [Cra94].

We want to emphasize that the reader should be careful with using these diagrams for a mutual comparison of the solvers. The diagrams just show the result of runs with the prescribed input on the specified computer. A more sophisticated setting of the input parameters, another computer or compiler, as well as another range of tolerances might change the diagrams considerably.

References

[Cra94] Cray Research, Inc. *UNICOS Performance Utilities Reference Manual*, SR-2040 8.0 edition, 1994.

[HW96] E. Hairer and G. Wanner. *Solving Ordinary Differential Equations II: Stiff and Differential-algebraic Problems.* Springer-Verlag, second revised edition, 1996.

III. The software part of the test set

III.1 Classification of test problems

We have categorized the test problems in three classes: IDEs, ODEs and DAEs.

In this test set, we call a problem an **IDE** (system of Implicit Differential Equations) if it is of the form

$$\begin{aligned} &f(t, y, y') = 0, \qquad t_0 \le t \le t_{\text{end}}, \\ &y, f \in \mathbf{R}^d, \\ &y(t_0) \text{ and } y'(t_0) \text{ are given.} \end{aligned}$$

A problem is named an **ODE** (system of Ordinary Differential Equations), if it has the form

$$\begin{aligned} &y' = f(t, y), \qquad t_0 \le t \le t_{\text{end}}, \\ &y, f \in \mathbf{R}^d, \\ &y(t_0) \text{ is given,} \end{aligned}$$

whereas the label **DAE** is given to problems which can be cast in the form

$$\begin{aligned} &My' = f(t, y), \qquad t_0 \le t \le t_{\text{end}}, \\ &y, f \in \mathbf{R}^d, \qquad M \in \mathbf{R}^{d \times d}, \\ &y(t_0) \text{ and } y'(t_0) \text{ are given,} \end{aligned}$$

where M is a constant, possibly singular matrix. Note that ODEs and DAEs are subclasses of IDEs.

III.2 How to perform tests

You can perform one of the following types of tests:

- solve test set problems with solvers that are supported in the test set,
- solve test set problems with your own solver, or
- solve your own problem with solvers that are supported in the test set.

For all types of tests, four types of codes are involved: a solver, a driver, a problem code and auxiliary routines. Currently, there are 6 solvers available:

1. DASSL[Pet91] for ODEs and IDEs/DAEs of index less than or equal to 1,
2. MEBDFDAE[Cas98] for ODEs and DAEs of index less than or equal to 3,
3. PSIDE[SLV98] for ODEs and IDEs/DAEs of index upto at least 3,
4. RADAU[HW98] for ODEs and DAEs of index less than or equal to 3,
5. RADAU5[HW96] for ODEs and DAEs of index less than or equal to 3, and
6. VODE[BHB97] for ODEs.

These solvers can be obtained via [LS98] in the files `ddassl.f`, `mebdfdae.f`, `pside.f`, `radau.f`, `radau5.f` and `vode.f`. These files contain versions of the solvers with which the numerical experiments were conducted. The official links to the solvers, which possibly direct to more recent versions, can be found at [LS98] too.

The drivers `dassld.f`, `mebdfdaed.f`, `psided.f`, `radaud.f`, `radau5d.f` and `voded.f`, which are available at [LS98], are such that runs can be performed that solve the problem numerically with the aforementioned solvers. Although DASSL is a code written for problems of index ≤ 1, it can handle some of the higher index problems by adjusting the error control. If possible, this is done in the driver `dassld.f`. Unless stated otherwise, all input parameters are set to their default values in the drivers.

For every test problem, the file `problem.f` contains a set of six Fortran 77 subroutines defining the problem. Although the format of the subroutines is the same for all three classes, the meaning of the arguments may depend on the problem class. Section III.3 describes the format of the problem codes.

The auxiliary linear algebra routines for the solvers are in `dassla.f`, `psidea.f`, `radaua.f` (for both RADAU and RADAU5) and `vodea.f`. For MEBDFDAE, the linear algebra routines are included in `medbdfdae.f`. The auxiliary file `report.f` contains a user interface. All these files are available at [LS98] as well.

III.2.1 How to solve test problems with available solvers Compiling

```
f77  -o dotest  dassld.f     problem.f  ddassl.f    dassla.f  report.f,
f77  -o dotest  mebdfdaed.f  problem.f  mebdfdae.f            report.f,
f77  -o dotest  psided.f     problem.f  pside.f     psidea.f  report.f,
f77  -o dotest  radaud.f     problem.f  radau.f     radaua.f  report.f   or
f77  -o dotest  radau5d.f    problem.f  radau5.f    radaua.f  report.f,
f77  -o dotest  voded.f      problem.f  vode.f      vodea.f   report.f,
```

will yield an executable `dotest` that solves the problem, of which the Fortran routines in the format described in Section III.3 are in the file `problem.f`. As an example, we perform a test run, in which we solve problem HIRES. Figure III.1 shows what one has to do.

III.2.2 How to solve test problems with your own solver The following guidelines serve to test your own solver with the test set.

- Write your own solver in a format similar to existing solvers in the file `own.f`.
- (Optional) You may like to put the linear algebra subroutines in a seperate file `owna.f`. In this way you can, for example, use the linear algebra of an existing solver.
- Write driver subroutines in the file `ownd.f`. If the format of your solver is similar to that of a solver that is already available in the test set, then this will only require minor modifications of the driver routines of that solver.
- Adjust the file `report.f` as indicated in the comment lines of this file. This will only be a minor modification.
- Compiling

  ```
  f77  -o dotest  ownd.f  problem.f  own.f  owna.f  report.f,
  ```

  will yield an executable `dotest` that solves the problem, of which the Fortran routines are in the file `problem.f`

III.2.3 How to solve your own problem with available solvers The following guidelines serve to solve your own problem with the solvers that are supported in the test set.

- Write your own problem in a format similar to that of the test set problems in the file `newprob.f`. This format is described precisely in Section III.3.
- Adjust the file `report.f` as indicated in the comment lines of this file. This will only be a minor modification.
- To solve your problem with, for example, DASSL, compiling

  ```
  f77  -o dotest  dassld.f  newprob.f  ddassl.f  dassla.f  report.f,
  ```

  will give you the desired executable `dotest`.

```
$ f77 -O -o dotest radaud.f hires.f radau5.f radaua.f report.f
$ dotest
Solving Problem HIRES using RADAU5

User input:

give relative error tolerance: 1d-4
give absolute error tolerance: 1d-4
give initial stepsize: 1d-7

Numerical solution:

                                        scd
       solution component              ----------------   ignore
                                        abs        rel
---------------------------------      -----      -----   ------
y(  1) =   0.7421645857497393E-03       5.30       2.17
y(  2) =   0.1452408987422247E-03       6.00       2.16
y(  3) =   0.5982382362740506E-04       6.03       1.80
y(  4) =   0.1185056912601290E-02       5.03       2.10
y(  5) =   0.2537002003509868E-02       3.82       1.20
y(  6) =   0.6714837054158053E-02       3.32       1.12
y(  7) =   0.2953745838879603E-02       3.98       1.44
y(  8) =   0.2746254161120250E-02       3.98       1.44

used components for scd                    8          8
scd of Y (maximum norm)                 3.32       1.12
using relative error yields scd                   1.12

Integration characteristics:

   number of integration steps         43
   number of accepted steps            35
   number of f evaluations            314
   number of Jacobian evaluations      22
   number of LU decompositions         43

CPU-time used:                          0.03 sec
```

FIGURE III.1: *Example of performing a test run, in which we solve problem HIRES with RADAU5. The experiment was done on an SGI workstation, an* Indy *with a 100 MHz R4000SC processor. We used the Fortran 77 compiler* `f77` *with the optimization flag* `-O`.

III.3 Format of the problem codes
The six subroutines that define the problem are called `PROB`, `INIT`, `FEVAL`, `JEVAL`, `MEVAL`, and `SOLUT`. The following subsections describe the format of these subroutines in full detail. In the sequel, the variables listed under `INTENT(IN)`, `INTENT(INOUT)`, and `INTENT(OUT)` are input, update and output variables, respectively.

III.3.1 Subroutine `PROB` This routine gives some general information about the test problem.

```
      SUBROUTINE PROB(FULLNM,PROBLM,TYPE,
     +                NEQN,NDISC,T,
     +                NUMJAC,MLJAC,MUJAC,
     +                NUMMAS,MLMAS,MUMAS,
     +                IND)
      CHARACTER*(*) FULLNM, PROBLM, TYPE
      INTEGER NEQN,NDISC,MLJAC,MUJAC,MLMAS,MUMAS,IND(*)
      DOUBLE PRECISION T(0:*)
      LOGICAL NUMJAC, NUMMAS
C     INTENT(OUT) FULLNM,PROBLM,TYPE,NEQN,NDISC,T,NUMJAC,MLJAC,
C    +            MUJAC,NUMMAS,MLMAS,MUMAS,IND
```

Meaning of the arguments:

`FULLNM`
: This character string contains the long name of the problem, e.g. `Chemical Akzo Nobel problem`.

`PROBLM`
: This character string contains the short name of the problem, e.g. `chemakzo`, and corresponds to the name of the Fortran source file.

`TYPE`
: This character string takes the value `IDE`, `ODE` or `DAE`, depending on the type of problem.

`NEQN`
: The dimension d of the problem, which is the number of equations to be solved.

`NDISC`
: The number of discontinuities in time of the function f or its derivative. The solver is restarted at every such discontinuity by the driver.

`T`
: An array containing time points.
  - If `NDISC .EQ. 0`, then `T(0)` contains t_0 and `T(1)` contains t_{end}.
  - If `NDISC .GT. 0`, then `T(0)` contains t_0, `T(NDISC+1)` contains t_{end} and `T(1)` ... `T(NDISC)` are the time points where the function f or its derivative has a discontinuity in time.

`NUMJAC`
: To solve the problem numerically, it is necessary to use the partial derivative $J := \partial f/\partial y$. If J is available analytically, then `NUMJAC = .FALSE.` and J is provided via subroutine `JEVAL`. If J is not available, then `NUMJAC = .TRUE.` and `JEVAL` is a dummy subroutine. In this case, the solvers approximate J by numerical differencing.

`MLJAC` and `MUJAC`
: These integers contain information about the structure of $J := \partial f/\partial y$. If J is a full matrix, then `MLJAC = NEQN`, otherwise `MLJAC` and `MUJAC` equal the number of nonzero lower co-diagonals and the number of nonzero upper co-diagonals of J, respectively.

`NUMMAS`
Only relevant for IDEs.

- For IDEs, it is necessary to use the partial derivative $M := \partial f/\partial y'$. If M is available analytically, then `NUMMAS = .FALSE.` and M is provided via subroutine `MEVAL`. If M is not available, then `NUMMAS = .TRUE.` and `MEVAL` is a dummy subroutine. In this case, the solvers have to approximate M by numerical differencing.
- For DAEs and ODEs, `NUMMAS` is not referenced.

`MLMAS` and `MUMAS`
These integers contain information about the structure of the constant matrix M (for DAEs) or the matrix $M := \partial f/\partial y'$ (for IDEs).

- For IDEs and DAEs: If M is a full matrix, then `MLMAS = NEQN`, otherwise `MLMAS` and `MUMAS` equal the number of nonzero lower co-diagonals and the number of nonzero upper co-diagonals of M, respectively.
- For ODEs, `MLMAS` and `MUMAS` are not referenced.

`IND`
Connected to IDEs and DAEs is the concept of index.

- For ODEs, `IND` is not referenced.
- For IDEs and DAEs, `IND` is an array of length `NEQN` and `IND(I)` specifies the index of variable `I`.

III.3.2 Subroutine `INIT` This routine contains the initial values $y(t_0)$ and $y'(t_0)$.

```
      SUBROUTINE INIT(NEQN,T,Y,YPRIME,CONSIS)
      INTEGER NEQN
      DOUBLE PRECISION T,Y(NEQN),YPRIME(NEQN)
      LOGICAL CONSIS
C     INTENT(IN)  NEQN,T
C     INTENT(OUT) Y,YPRIME,CONSIS
```

Meaning of the arguments:

`NEQN`
The dimension of the problem.

`Y(NEQN)`
Contains the initial value $y(t_0)$.

`YPRIME(NEQN)`
Only relevant for IDEs and DAEs.

- For IDEs and DAEs, `YPRIME` contains the initial value $y'(t_0)$.
- For ODEs, `YPRIME` is not set. If needed by the solver, it is computed in the driver as $y'(t_0) = f(t_0, y_0)$.

`CONSIS`
Only relevant for IDEs and DAEs.

- For IDEs and DAEs, CONSIS is a switch for the consistency of the initial values. If CONSIS .EQ. .TRUE., then $y(t_0)$ and $y'(t_0)$ are assumed to be consistent. If CONSIS .EQ. .FALSE., then $y(t_0)$ and $y'(t_0)$ are possibly inconsistent. Solvers with a facility to compute consistent initial values internally, will try to do so in this case. Currently, all problems in the test set have consistent initial values.
- For ODEs, CONSIS is not referenced.

III.3.3 Subroutine FEVAL This subroutine evaluates the function f.

```
      SUBROUTINE FEVAL(NEQN,T,Y,YPRIME,F,IERR,RPAR,IPAR)
      INTEGER NEQN,IERR,IPAR(*)
      DOUBLE PRECISION T,Y(NEQN),YPRIME(NEQN),F(NEQN),RPAR(*)
C     INTENT(IN)    NEQN,T,Y,YPRIME
C     INTENT(INOUT) RPAR,IPAR
C     INTENT(OUT)   F,IERR
```

Meaning of the arguments:

NEQN
: The dimension of the problem.

T
: The time point where the function is evaluated.

Y(NEQN)
: The value of y in which the function is evaluated.

YPRIME(NEQN)
: Only relevant for IDEs.
  - For IDEs, this is the value of y' in which the function f is evaluated.
  - For ODEs and DAEs, YPRIME is not referenced.

F(NEQN)
: The resulting function value f(T, Y) (for ODEs and DAEs), or f(T, Y, YPRIME) (for IDEs).

IERR
: IERR is an integer flag which is always equal to zero on input. Subroutine FEVAL sets IERR = -1 if FEVAL can not be evaluated for the current values of T, Y and YPRIME. Some solvers have the facility to attempt to prevent the occurrence of IERR = -1, or return to the driver in that case.

  IERR has an analogous meaning in subroutines JEVAL and MEVAL.

RPAR and IPAR
: RPAR and IPAR are double precision and integer arrays, respectively, which can be used for communication between the driver and the subroutines FEVAL, JEVAL and MEVAL. If RPAR and IPAR are not needed, then these parameters are ignored by treating them as dummy arguments.

  RPAR and IPAR have the same meaning in subroutines JEVAL and MEVAL.

III.3.4 Subroutine JEVAL This subroutine evaluates the derivative (or Jacobian) of the function f with respect to y.

```
      SUBROUTINE JEVAL(LDIM,NEQN,T,Y,YPRIME,DFDY,IERR,RPAR,IPAR)
      INTEGER LDIM,NEQN,IERR,IPAR(*)
      DOUBLE PRECISION T,Y(NEQN),YPRIME(NEQN),DFDY(LDIM,NEQN),RPAR(*)
C     INTENT(IN)    LDIM,NEQN,T,Y,YPRIME
C     INTENT(INOUT) RPAR,IPAR
C     INTENT(OUT)   DFDY,IERR
```

Meaning of the arguments:

`LDIM`
: The leading dimension of the array `DFDY`.

`NEQN`
: The dimension of the problem.

`T`
: The time point where the derivative is evaluated.

`Y(NEQN)`
: The value of y in which the derivative is evaluated.

`YPRIME(NEQN)`
: Only relevant for IDEs.

  – For IDEs, this is the value of y' in which the derivative $\partial f(t, y, y')/\partial y$ is evaluated.

  – For ODEs and DAEs, `YPRIME` is not referenced.

`DFDY(LDIM,NEQN)`
: The array with the resulting Jacobian matrix.

  – If $\partial f/\partial y$ is a full matrix (`MLJAC` = `NEQN`), then `DFDY(I,J)` contains $\partial f_{\mathtt{I}}/\partial y_{\mathtt{J}}$.

  – If $\partial f/\partial y$ is a band matrix ($0 \leq$ `MLJAC` $<$ `NEQN`), then `DFDY(I-J+MUJAC+1,J)` contains $\partial f_{\mathtt{I}}/\partial y_{\mathtt{J}}$ (LAPACK / LINPACK / BLAS storage).

`IERR`, `RPAR` and `IPAR`
: See the description of subroutine `FEVAL`.

III.3.5 Subroutine `MEVAL` For ODEs, `MEVAL` is not called and a dummy subroutine is supplied. For DAEs, it supplies the constant matrix M. For IDEs, it evaluates the matrix $M := \partial f/\partial y'$.

```
      SUBROUTINE MEVAL(LDIM,NEQN,T,Y,YPRIME,DFDDY,IERR,RPAR,IPAR)
      INTEGER LDIM,NEQN,IERR,IPAR(*)
      DOUBLE PRECISION T,Y(NEQN),YPRIME(NEQN),DFDDY(LDIM,NEQN),RPAR(*)
C     INTENT(IN)    LDIM,NEQN,T,Y,YPRIME
C     INTENT(INOUT) RPAR,IPAR
C     INTENT(OUT)   DFDDY,IERR
```

Meaning of the arguments:

`LDIM`
: The leading dimension of the matrix M.

`NEQN`
: The dimension of the problem.

`T`
The time point where M is evaluated. (For DAEs, `T` is not referenced.)

`Y(NEQN)`
The value of y in which M is evaluated. (For DAEs, `Y` is not referenced.)

`YPRIME(NEQN)`
The value of y' in which M is evaluated. (For DAEs, `YPRIME` is not referenced.)

`DFDDY(LDIM,NEQN)`
This array contains the constant matrix M (for DAEs) or $M := \partial f/\partial y'$ (for IDEs).

- If M is a full matrix (`MLMAS` = `NEQN`), then `DFDDY(I,J)` contains $M_{\mathtt{I},\mathtt{J}}$ for DAEs and $\partial f_{\mathtt{I}}/\partial y'_{\mathtt{J}}$ for IDEs.
- If M is a band matrix ($0 \le$ `MLMAS` $<$ `NEQN`), then `DFDDY(I-J+MUMAS+1,J)` contains $M_{\mathtt{I},\mathtt{J}}$ for DAEs and $\partial f_{\mathtt{I}}/\partial y'_{\mathtt{J}}$ for IDEs. (LAPACK / LINPACK / BLAS storage).

`IERR`, `RPAR` and `IPAR`
See the description of subroutine `FEVAL`.

III.3.6 Subroutine `SOLUT` This routine contains the reference solution.

```
      SUBROUTINE SOLUT(NEQN,T,Y)
      INTEGER NEQN
      DOUBLE PRECISION T,Y(NEQN)
C     INTENT(IN)  NEQN,T
C     INTENT(OUT) Y
```

Meaning of the arguments:

`NEQN`
The dimension of the problem.

`T`
The value of t, in which the reference solution is given (normally t_{end}).

`Y(NEQN)`
This array contains the reference solution in $t =$ `T`.

References

[BHB97] Peter N. Brown, Alan C. Hindmarsh, and George D. Byrne. *VODE: A variable coefficient ODE solver*, May 15, 1997. Bug fix release November 12, 1998. Available at http://www.netlib.org/ode/vode.f.

[Cas98] J. Cash. *MEBDFDAE*, November 6, 1998. Available at http://www.ma.ic.ac.uk/~jcash/IVP_software/finaldae/readme.html.

[HW96] E. Hairer and G. Wanner. *RADAU5*, July 9, 1996. Available at ftp://ftp.unige.ch/pub/doc/math/stiff/radau5.f.

[HW98] E. Hairer and G. Wanner. *RADAU*, September 18, 1998. Available at ftp://ftp.unige.ch/pub/doc/math/stiff/radau.f.

[LS98] W.M. Lioen and J.J.B. de Swart. *Test Set for Initial Value Problem Solvers*, December 1998. Available at http://www.cwi.nl/cwi/projects/IVPtestset/.

[Pet91] L.R. Petzold. *DASSL: A Differential/Algebraic System Solver*, June 24, 1991. Available at http://www.netlib.org/ode/ddassl.f.

[SLV98] J.J.B. de Swart, W.M. Lioen, and W.A. van der Veen. *PSIDE*, November 25, 1998. Available at http://www.cwi.nl/cwi/projects/PSIDE/.

1. Chemical Akzo Nobel problem

1.1 General information

This IVP is a stiff system of 6 non-linear DAEs of index 1 and has been taken from [Sto98]. The parallel-IVP-algorithm group of CWI contributed this problem to the test set in collaboration with W.J.H. Stortelder. We acknowledge the remarks of Dotsikas Ioannis, which improved the formulation of this problem considerably.

1.2 Mathematical description of the problem

The problem is of the form

$$M\frac{\mathrm{d}y}{\mathrm{d}t} = f(y), \qquad y(0) = y_0, \quad y'(0) = y'_0,$$

with

$$y \in \mathbb{R}^6, \quad 0 \le t \le 180.$$

The matrix M is of rank 5 and given by

$$M = \begin{pmatrix} 1 & 0 & 0 & 0 & 0 & 0 \\ 0 & 1 & 0 & 0 & 0 & 0 \\ 0 & 0 & 1 & 0 & 0 & 0 \\ 0 & 0 & 0 & 1 & 0 & 0 \\ 0 & 0 & 0 & 0 & 1 & 0 \\ 0 & 0 & 0 & 0 & 0 & 0 \end{pmatrix}$$

and the function f by

$$f(y) = \begin{pmatrix} -2r_1 & +r_2 & -r_3 & -r_4 & & \\ -\frac{1}{2}r_1 & & & -r_4 & -\frac{1}{2}r_5 & +F_{in} \\ r_1 & -r_2 & +r_3 & & & \\ & -r_2 & +r_3 & -2r_4 & & \\ & r_2 & -r_3 & & +r_5 & \\ K_s \cdot y_1 \cdot y_4 - y_6 & & & & & \end{pmatrix},$$

where the r_i and F_{in} are auxiliary variables, given by

$$\begin{aligned} r_1 &= k_1 \cdot y_1^4 \cdot y_2^{\frac{1}{2}}, \\ r_2 &= k_2 \cdot y_3 \cdot y_4, \\ r_3 &= \frac{k_2}{K} \cdot y_1 \cdot y_5, \\ r_4 &= k_3 \cdot y_1 \cdot y_4^2, \\ r_5 &= k_4 \cdot y_6^2 \cdot y_2^{\frac{1}{2}}, \\ F_{in} &= klA \cdot (\frac{p(\mathrm{CO}_2)}{H} - y_2). \end{aligned}$$

The values of the parameters k_1, k_2, k_3, k_4, K, klA, $p(\mathrm{CO}_2)$ and H are

$$\begin{array}{rclrclrcl} k_1 &=& 18.7, & k_4 &=& 0.42, & K_s &=& 115.83, \\ k_2 &=& 0.58, & K &=& 34.4, & p(\mathrm{CO}_2) &=& 0.9, \\ k_3 &=& 0.09, & klA &=& 3.3, & H &=& 737. \end{array}$$

The consistent initial vectors are

$$y_0 = \begin{pmatrix} 0.444, 0.00123, 0, 0.007, 0, K_s \cdot y_{0,1} \cdot y_{0,4} \end{pmatrix}^{\mathrm{T}} \qquad y'_0 = f(y_0).$$

It is clear from the definition of r_1 and r_5 that the function f can not be evaluated for negative values of y_2. In the Fortran subroutine that defines f, we set `IERR=-1` if $y_2 < 0$ to prevent this situation. See page *III-vi* of the the description of the software part of the test set for more details on `IERR`.

1.3 Origin of the problem

The problem originates from Akzo Nobel Central Research in Arnhem, The Netherlands. It describes a chemical process, in which 2 species, FLB and ZHU, are mixed, while carbon dioxide is continuously added. The resulting species of importance is ZLA. In the interest of commercial competition, the names of the chemical species are fictitious. The reaction equations, as given by Akzo Nobel [CBS93], are given in Figure 1.1. The last reaction equation describes an equilibrium

$$
\begin{aligned}
2\,\mathrm{FLB} + \frac{1}{2}\mathrm{CO_2} &\xrightarrow{k_1} \mathrm{FLBT} + \mathrm{H_2O} \\
\mathrm{ZLA} + \mathrm{FLB} &\underset{k_2}{\overset{k_2/K}{\rightleftharpoons}} \mathrm{FLBT} + \mathrm{ZHU} \\
\mathrm{FLB} + 2\,\mathrm{ZHU} + \mathrm{CO_2} &\xrightarrow{k_3} \mathrm{LB} + \mathrm{nitrate} \\
\mathrm{FLB.ZHU} + \frac{1}{2}\mathrm{CO_2} &\xrightarrow{k_4} \mathrm{ZLA} + \mathrm{H_2O} \\
\mathrm{FLB} + \mathrm{ZHU} &\rightleftharpoons \mathrm{FLB.ZHU}
\end{aligned}
$$

FIGURE 1.1: *Reaction scheme for Chemical Akzo Nobel problem.*

$$K_s = \frac{[\mathrm{FLB.ZHU}]}{[\mathrm{FLB}] \cdot [\mathrm{ZHU}]}.$$

The value of K_s plays a role in parameter estimation. The other equations describe reactions with velocities given by

$$
\begin{aligned}
r_1 &= k_1 \cdot [\mathrm{FLB}]^4 \cdot [\mathrm{CO_2}]^{\frac{1}{2}}, && (1.1)\\
r_2 &= k_2 \cdot [\mathrm{FLBT}] \cdot [\mathrm{ZHU}], \\
r_3 &= \frac{k_2}{K} \cdot [\mathrm{FLB}] \cdot [\mathrm{ZLA}], \\
r_4 &= k_3 \cdot [\mathrm{FLB}] \cdot [\mathrm{ZHU}]^2, && (1.2)\\
r_5 &= k_4 \cdot [\mathrm{FLB.ZHU}]^2 \cdot [\mathrm{CO_2}]^{\frac{1}{2}}, && (1.3)
\end{aligned}
$$

respectively. Here the square brackets '[ ]' denote concentrations. One would expect from the reaction scheme in Figure 1.1, that reaction velocities r_1, r_4 and r_5 would read

$$
\begin{aligned}
r_1 &= k_1 \cdot [\mathrm{FLB}]^2 \cdot [\mathrm{CO_2}]^{\frac{1}{2}}, \\
r_4 &= k_3 \cdot [\mathrm{FLB}] \cdot [\mathrm{ZHU}]^2 \cdot [\mathrm{CO_2}], \\
r_5 &= k_4 \cdot [\mathrm{FLB.ZHU}] \cdot [\mathrm{CO_2}]^{\frac{1}{2}}.
\end{aligned}
$$

However, it turns out that the chemical process under consideration is modeled more appropiately using (1.1)–(1.3).

The inflow of carbon dioxide per volume unit is denoted by F_{in}, and satisfies

$$F_{in} = klA \cdot (\frac{p(\mathrm{CO_2})}{H} - [\mathrm{CO_2}]),$$

where *klA* is the mass transfer coefficient, H is the Henry constant and $p(CO_2)$ is the partial carbon dioxide pressure. $p(CO_2)$ is assumed to be independent of $[CO_2]$. The parameters k_1, k_2, k_3, k_4, K, *klA*, K_s, H and $p(CO_2)$ are given constants*.

The process is started by mixing 0.444 mol/liter FLB with 0.007 mol/liter ZHU. The concentration of carbon dioxide at the beginning is 0.00123 mol/liter. Initially, no other species are present. The simulation is performed on the time interval $[0, 180$ minutes$]$.

Identifying the concentrations [FLB], $[CO_2]$, [FLBT], [ZHU], [ZLA], [FLB.ZHU] with $y_1, \ldots, y_6$, respectively, one easily arrives at the mathematical formulation of the preceding section.

1.4 Numerical solution of the problem

Tables 1.1–1.2 and Figures 1.2–1.4 present the reference solution at the end of the integration interval, the run characteristics, the behavior of the solution over the integration interval and the work-precision diagrams, respectively. The reference solution was computed by PSIDE on a Cray C90, using double precision, `rtol = atol` 10^{-19}. To get more insight in the exact behavior of the second component, we included a plot of y_2 on $[0, 3]$ in Figure 1.2. For the work-precision diagrams, we used: rtol = $10^{-(4+m/4)}$, $m = 0, 1, \ldots, 24$; atol = rtol; h0 = rtol for RADAU, RADAU5 and MEBDFDAE. The

TABLE 1.1: *Reference solution at the end of the integration interval.*

y_1	0.1150794920661702	y_4	$0.3656156421249283 \cdot 10^{-3}$
y_2	$0.1203831471567715 \cdot 10^{-2}$	y_5	$0.1708010885264404 \cdot 10^{-1}$
y_3	0.1611562887407974	y_6	$0.4873531310307455 \cdot 10^{-2}$

TABLE 1.2: *Run characteristics.*

solver	rtol	atol	h0	scd	steps	accept	# f	# Jac	# LU	CPU
DASSL	10^{-4}	10^{-4}		2.77	57	57	81	12		0.02
	10^{-7}	10^{-7}		5.49	174	172	223	26		0.06
	10^{-10}	10^{-10}		8.55	521	515	668	38		0.16
MEBDFDAE	10^{-4}	10^{-4}	10^{-4}	2.87	63	63	96	14	14	0.04
	10^{-7}	10^{-7}	10^{-7}	6.24	142	141	228	20	20	0.08
	10^{-10}	10^{-10}	10^{-10}	9.59	287	287	429	33	33	0.15
PSIDE-1	10^{-4}	10^{-4}		4.07	25	25	353	12	96	0.05
	10^{-7}	10^{-7}		7.13	35	34	643	13	124	0.07
	10^{-10}	10^{-10}		9.91	87	85	1671	15	204	0.15
RADAU	10^{-7}	10^{-7}	10^{-7}	6.25	43	39	372	33	43	0.04
	10^{-10}	10^{-10}	10^{-10}	8.39	43	41	696	30	43	0.06
RADAU5	10^{-7}	10^{-7}	10^{-7}	6.25	43	39	372	33	43	0.04
	10^{-10}	10^{-10}	10^{-10}	7.99	94	94	850	81	91	0.08

failed runs are in Table 1.3; listed are the name of the solver that failed, for which values of m this happened, and the reason for failing. The speed-up factor for PSIDE is 1.19.

REFERENCES

[CBS93] CBS-reaction-meeting Köln. Handouts, May 1993. Br/ARLO-CRC.

*Apart from H, which is generally known, all parameters have been estimated by W. Stortelder [Sto95].

TABLE 1.3: *Failed runs.*

solver	m	reason
RADAU	$0, 1, \ldots, 9$	solver cannot handle `IERR=-1`.
RADAU5	$0, 1, \ldots, 9$	solver cannot handle `IERR=-1`.

[Sto95] W.J.H. Stortelder, 1995. Private communication.

[Sto98] W.J.H. de Stortelder. *Parameter Estimation in Nonlinear Dynamical Systems.* PhD thesis, University of Amsterdam, March 12, 1998.

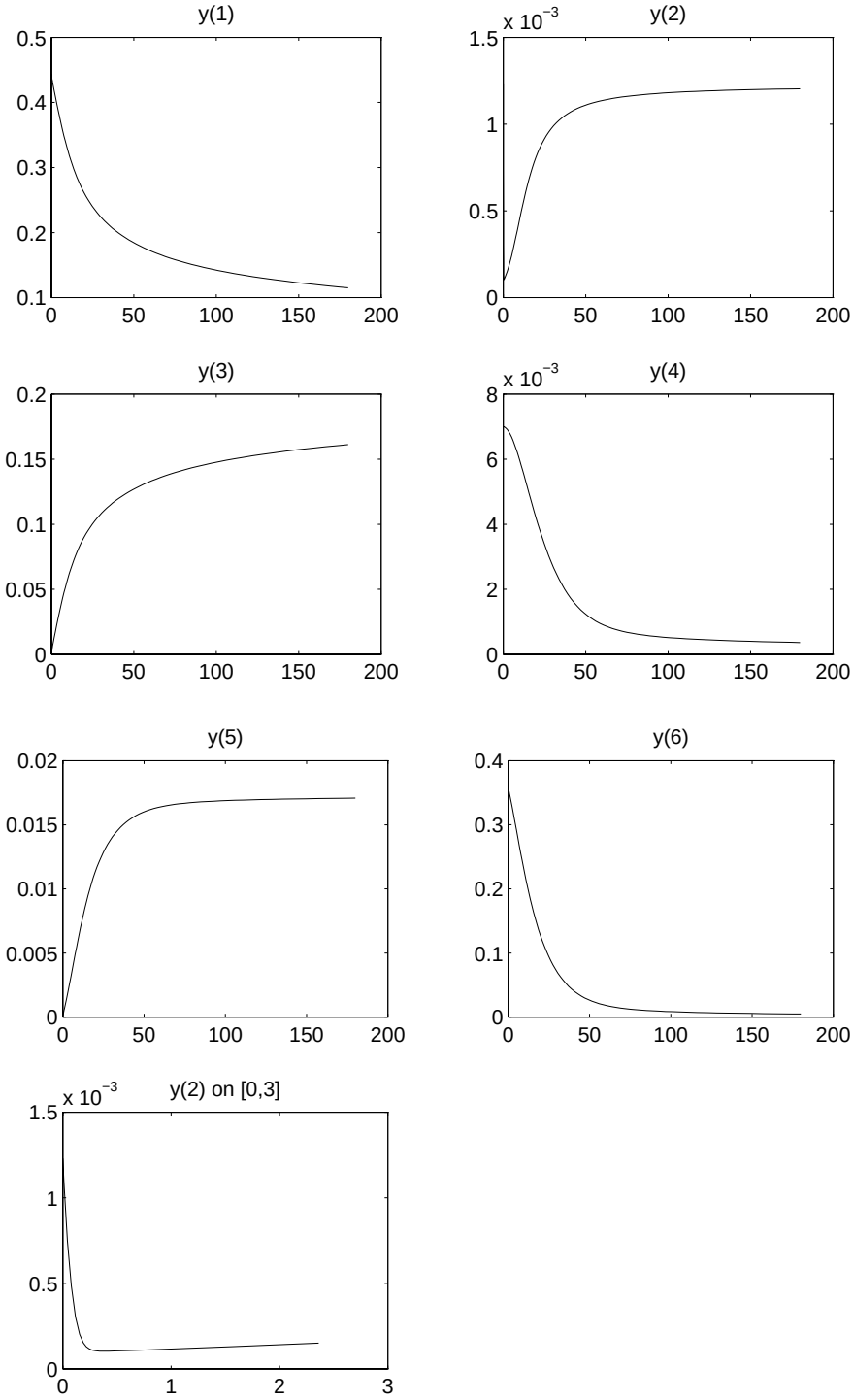

FIGURE 1.2: *Behavior of the solution over the integration interval.*

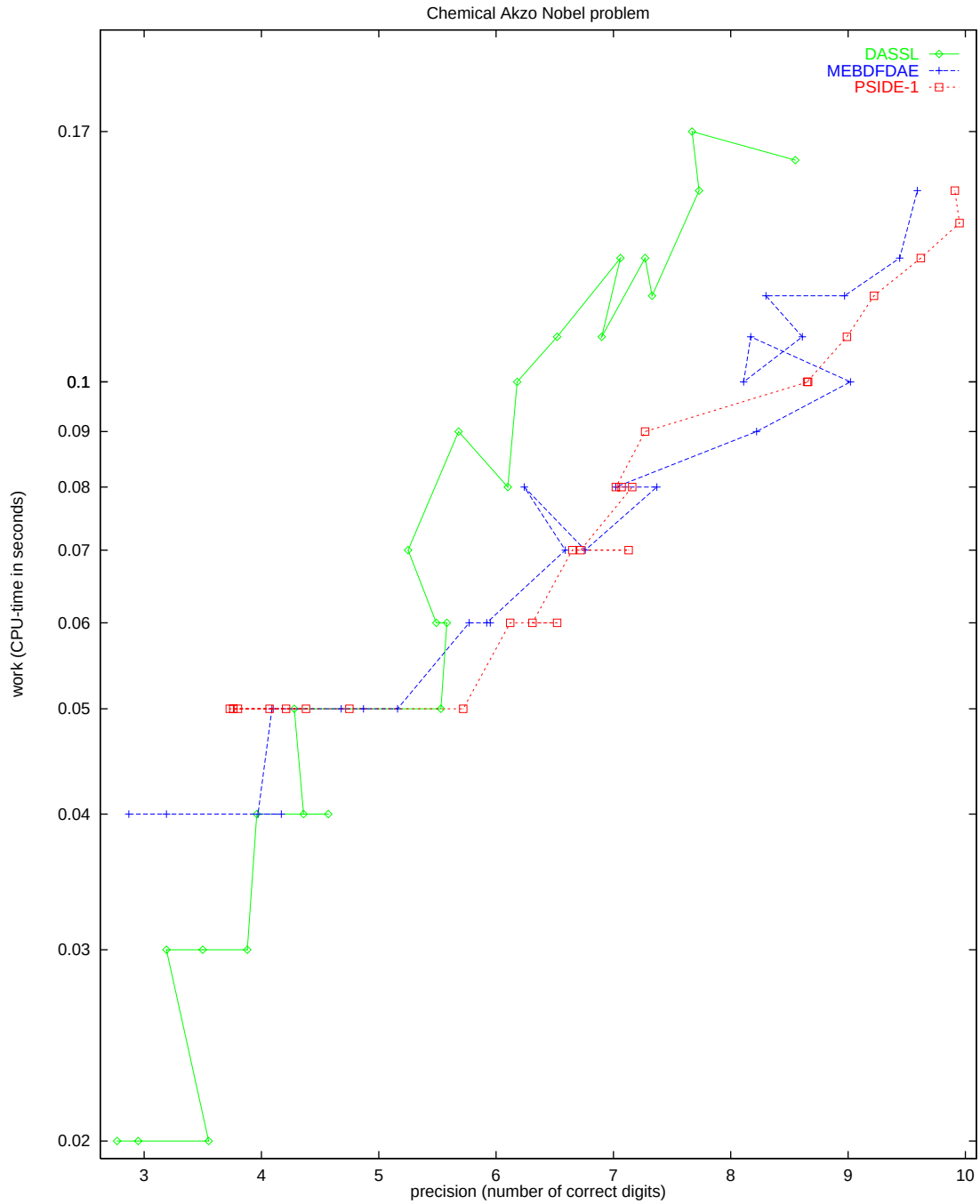

FIGURE 1.3: *Work-precision diagram.*

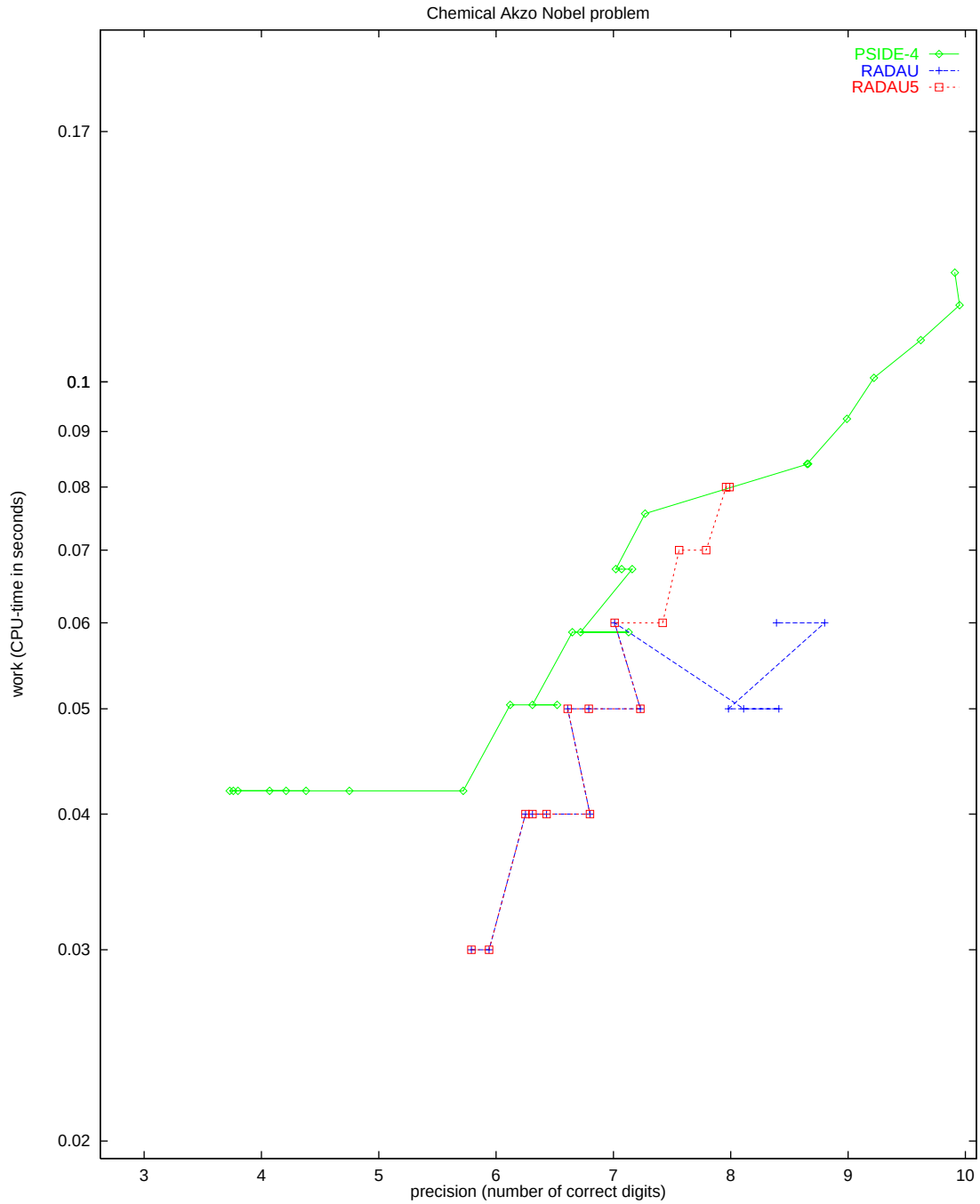

FIGURE 1.4: *Work-precision diagram.*

2. Problem HIRES

2.1 General information

This IVP is a stiff system of 8 non-linear Ordinary Differential Equations. It was proposed by Schäfer in 1975 [Sch75]. The name HIRES was given by Hairer & Wanner [HW96]. It refers to 'High Irradiance RESponse', which is described by this ODE. The parallel-IVP-algorithm group of CWI contributed this problem to the test set.

2.2 Mathematical description of the problem

The problem is of the form

$$\frac{\mathrm{d}y}{\mathrm{d}t} = f(y), \quad y(0) = y_0,$$

with

$$y \in \mathbb{R}^8, \quad 0 \le t \le 321.8122.$$

The function f is defined by

$$f(y) = \begin{pmatrix} -1.71y_1 & +0.43y_2 & +8.32y_3 & +0.0007 & & \\ 1.71y_1 & -8.75y_2 & & & & \\ -10.03y_3 & +0.43y_4 & +0.035y_5 & & & \\ 8.32y_2 & +1.71y_3 & -1.12y_4 & & & \\ -1.745y_5 & +0.43y_6 & +0.43y_7 & & & \\ -280y_6y_8 & +0.69y_4 & +1.71y_5 & -0.43y_6 & +0.69y_7 & \\ 280y_6y_8 & -1.81y_7 & & & & \\ -280y_6y_8 & +1.81y_7 & & & & \end{pmatrix}.$$

The initial vector y_0 is given by $(1, 0, 0, 0, 0, 0, 0, 0.0057)^{\mathrm{T}}$.

2.3 Origin of the problem

The HIRES problem originates from plant physiology and describes how light is involved in morphogenesis. To be precise, it explains the 'High Irradiance Responses' (HIRES) of photomorphogenesis on the basis of phytochrome, by means of a chemical reaction involving eight reactants. It has been promoted as a test problem by Gottwald in [Got77]. The reaction scheme is given in Figure 2.1.

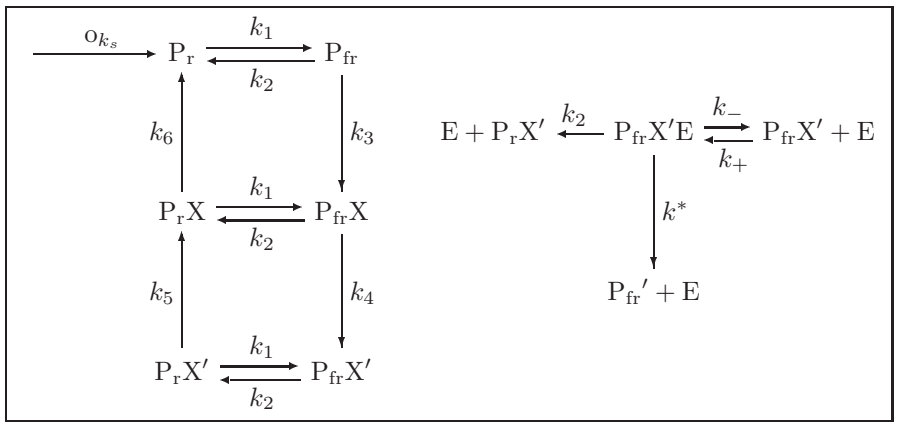

Figure 2.1: *Reaction scheme for problem HIRES.*

P_r and P_{fr} refer to the red and far-red absorbing form of phytochrome, respectively. They can be bound by two receptors X and X′, partially influenced by the enzyme E. The values of the parameters were taken from [HW96]

k_1	=	1.71	k_3	=	8.32	k_5	=	0.035	k_+	=	280	k^*	=	0.69
k_2	=	0.43	k_4	=	0.69	k_6	=	8.32	k_-	=	0.69	o_{k_s}	=	0.0007

For more details, we refer to [Sch75].

Identifying the concentrations of P_r, P_{fr}, P_rX, $P_{fr}X$, P_rX', $P_{fr}X'$, $P_{fr}X'E$ and E with y_i, $i \in \{1, \ldots, 8\}$, respectively, the differential equations mentioned in §2.2 easily follow. See [SL98] for a more detailed description of this modeling process.

The end point of the integration interval, 321.8122, was chosen arbitrarily[Wan98].

2.4 Numerical solution of the problem

Tables 2.1–2.2 and Figures 2.2–2.4 present the reference solution at the end of the integration interval, the run characteristics, the behavior of the solution over (part of) the integration interval and the work-precision diagrams, respectively. The reference solution was computed by RADAU5 on a Cray C90, using double precision, `work(1) = uround` $= 1.01 \cdot 10^{-19}$, `rtol = atol = h0` $= 1.1 \cdot 10^{-18}$. For the work-precision diagrams, we used: rtol $= 10^{-(4+m/4)}$, $m = 0, 1, \ldots, 24$; atol = rtol; h0 $= 10^{-2} \cdot$ rtol for RADAU, RADAU5 and MEBDFDAE. The speed-up factor for PSIDE is 1.26.

TABLE 2.1: *Reference solution at the end of the integration interval.*

y_1	$0.7371312573325668 \cdot 10^{-3}$	y_5	$0.2386356198831331 \cdot 10^{-2}$
y_2	$0.1442485726316185 \cdot 10^{-3}$	y_6	$0.6238968252742796 \cdot 10^{-2}$
y_3	$0.5888729740967575 \cdot 10^{-4}$	y_7	$0.2849998395185769 \cdot 10^{-2}$
y_4	$0.1175651343283149 \cdot 10^{-2}$	y_8	$0.2850001604814231 \cdot 10^{-2}$

TABLE 2.2: *Run characteristics.*

solver	rtol	atol	h0	scd	steps	accept	# f	# Jac	# LU	CPU
DASSL	10^{-4}	10^{-4}		1.03	108	99	173	31		0.04
	10^{-7}	10^{-7}		3.87	320	309	473	40		0.11
	10^{-10}	10^{-10}		6.70	1150	1134	1588	55		0.39
MEBDFDAE	10^{-4}	10^{-4}	10^{-6}	1.11	97	94	168	21	21	0.05
	10^{-7}	10^{-7}	10^{-9}	4.99	265	265	463	31	31	0.13
	10^{-10}	10^{-10}	10^{-12}	7.79	488	484	812	53	53	0.23
PSIDE-1	10^{-4}	10^{-4}		3.03	43	37	665	20	168	0.08
	10^{-7}	10^{-7}		4.88	68	60	1208	25	252	0.13
	10^{-10}	10^{-10}		8.85	152	151	2528	35	344	0.24
RADAU	10^{-4}	10^{-4}	10^{-6}	0.72	42	33	333	21	42	0.03
	10^{-7}	10^{-7}	10^{-9}	4.91	51	40	985	22	51	0.09
	10^{-10}	10^{-10}	10^{-12}	8.03	69	58	1511	29	68	0.13
RADAU5	10^{-4}	10^{-4}	10^{-6}	0.72	42	33	333	21	41	0.03
	10^{-7}	10^{-7}	10^{-9}	4.31	79	72	684	31	61	0.06
	10^{-10}	10^{-10}	10^{-12}	6.88	203	202	1684	61	100	0.14
VODE	10^{-4}	10^{-4}		1.39	133	131	191	10	25	0.03
	10^{-7}	10^{-7}		3.98	415	390	608	9	70	0.10
	10^{-10}	10^{-10}		6.20	933	880	1224	15	134	0.21

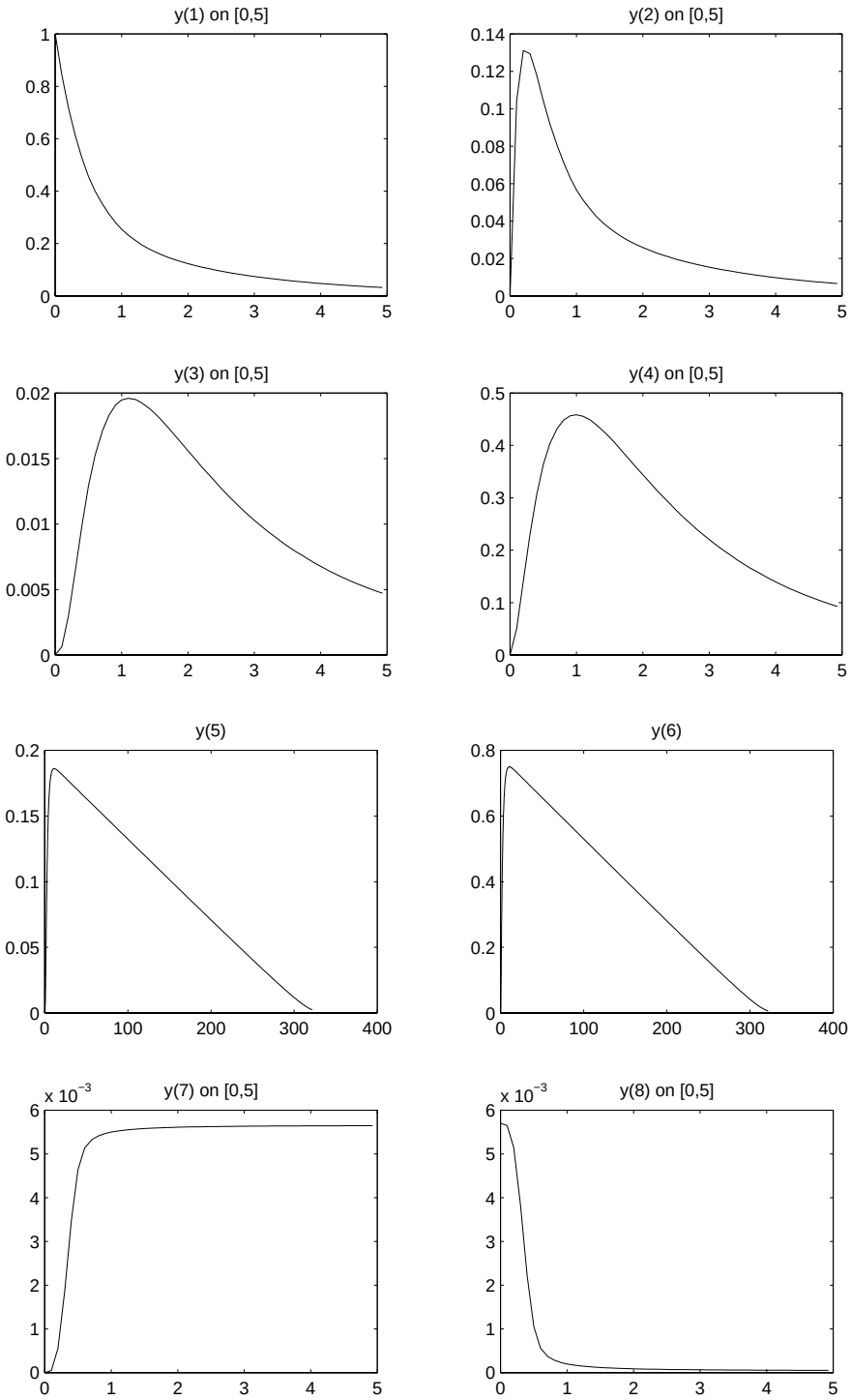

FIGURE 2.2: *Behavior of the solution over the integration interval.*

REFERENCES

[Got77] B.A. Gottwald. MISS - ein einfaches Simulations-System für biologische und chemische Prozesse. *EDV in Medizin und Biologie*, 3:85–90, 1977.

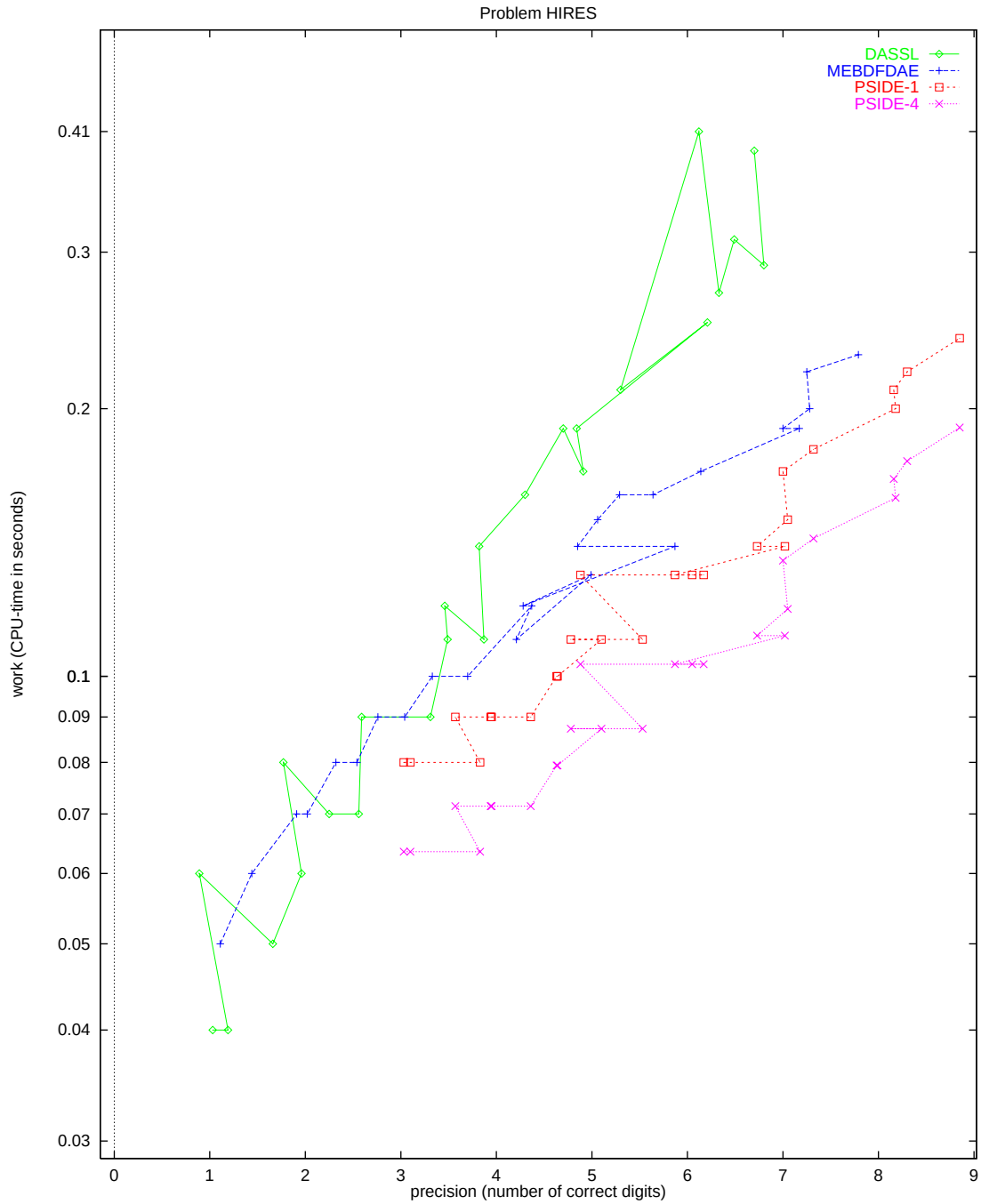

FIGURE 2.3: *Work-precision diagram.*

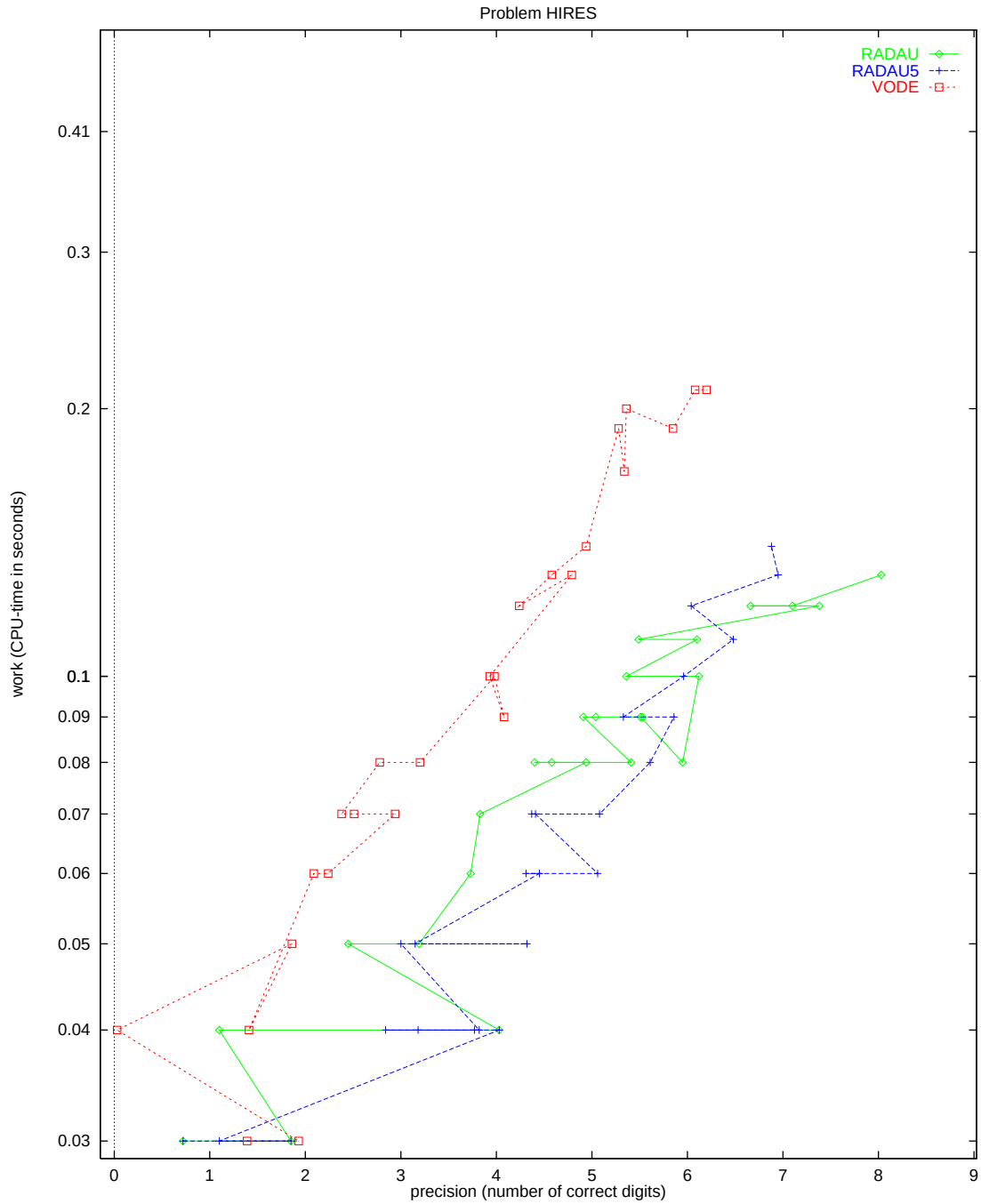

FIGURE 2.4: *Work-precision diagram.*

[HW96] E. Hairer and G. Wanner. *Solving Ordinary Differential Equations II: Stiff and Differential-algebraic Problems*. Springer-Verlag, second revised edition, 1996.

[Sch75] E. Schäfer. A new approach to explain the 'high irradiance responses' of photomorphogenesis on the basis of phytochrome. *J. of Math. Biology*, 2:41–56, 1975.

[SL98] J.J.B. de Swart and W.M. Lioen. Collecting real-life problems to test solvers for implicit differential equations. *CWI Quarterly*, 11(1):83–100, 1998.

[Wan98] G. Wanner, 1998. Private communication.

3. Pollution problem

3.1 General information

This IVP is a stiff system of 20 non-linear Ordinary Differential Equations. It is the chemical reaction part of the air pollution model developed at The Dutch National Institute of Public Health and Environmental Protection (RIVM) and it is described by Verwer in [Ver94]. The parallel-IVP-algorithm group of CWI contributed this problem to the test set.

3.2 Mathematical description of the problem

The problem is of the form

$$\frac{\mathrm{d}y}{\mathrm{d}t} = f(y), \quad y(0) = y_0, \tag{3.1}$$

with

$$y \in \mathbb{R}^{20}, \quad 0 \le t \le 60.$$

The function f is defined by

$$f = \begin{pmatrix} -\sum_{j\in\{1,10,14,23,24\}} r_j + \sum_{j\in\{2,3,9,11,12,22,25\}} r_j \\ -r_2 - r_3 - r_9 - r_{12} + r_1 + r_{21} \\ -r_{15} + r_1 + r_{17} + r_{19} + r_{22} \\ -r_2 - r_{16} - r_{17} - r_{23} + r_{15} \\ -r_3 + 2r_4 + r_6 + r_7 + r_{13} + r_{20} \\ -r_6 - r_8 - r_{14} - r_{20} + r_3 + 2r_{18} \\ -r_4 - r_5 - r_6 + r_{13} \\ r_4 + r_5 + r_6 + r_7 \\ -r_7 - r_8 \\ -r_{12} + r_7 + r_9 \\ -r_9 - r_{10} + r_8 + r_{11} \\ r_9 \\ -r_{11} + r_{10} \\ -r_{13} + r_{12} \\ r_{14} \\ -r_{18} - r_{19} + r_{16} \\ -r_{20} \\ r_{20} \\ -r_{21} - r_{22} - r_{24} + r_{23} + r_{25} \\ -r_{25} + r_{24} \end{pmatrix},$$

where the r_i are auxiliary variables, given in Table 3.1. The values of the parameters k_j are in Table 3.2. Finally, the initial vector y_0 is given by

$$y_0 = (0, 0.2, 0, 0.04, 0, 0, 0.1, 0.3, 0.01, 0, 0, 0, 0, 0, 0, 0, 0.007, 0, 0, 0)^{\mathrm{T}}.$$

3.3 Origin of the problem

The problem is a chemical model consisting of 25 reactions and 20 reacting compounds. Figure 3.1 shows the reaction scheme. Writing down the reaction velocities r_j for every reaction equation and making the identification in Table 3.3, which also lists the concentrations at $t = 0$, one arrives at the system of differential equations (3.1). The time interval [0,60] represents the behavior of the reactants sufficiently.

TABLE 3.1: *Auxiliary variables.*

r_1	=	$k_1 \cdot y_1$	r_{10}	=	$k_{10} \cdot y_{11} \cdot y_1$	r_{19}	=	$k_{19} \cdot y_{16}$
r_2	=	$k_2 \cdot y_2 \cdot y_4$	r_{11}	=	$k_{11} \cdot y_{13}$	r_{20}	=	$k_{20} \cdot y_{17} \cdot y_6$
r_3	=	$k_3 \cdot y_5 \cdot y_2$	r_{12}	=	$k_{12} \cdot y_{10} \cdot y_2$	r_{21}	=	$k_{21} \cdot y_{19}$
r_4	=	$k_4 \cdot y_7$	r_{13}	=	$k_{13} \cdot y_{14}$	r_{22}	=	$k_{22} \cdot y_{19}$
r_5	=	$k_5 \cdot y_7$	r_{14}	=	$k_{14} \cdot y_1 \cdot y_6$	r_{23}	=	$k_{23} \cdot y_1 \cdot y_4$
r_6	=	$k_6 \cdot y_7 \cdot y_6$	r_{15}	=	$k_{15} \cdot y_3$	r_{24}	=	$k_{24} \cdot y_{19} \cdot y_1$
r_7	=	$k_7 \cdot y_9$	r_{16}	=	$k_{16} \cdot y_4$	r_{25}	=	$k_{25} \cdot y_{20}$
r_8	=	$k_8 \cdot y_9 \cdot y_6$	r_{17}	=	$k_{17} \cdot y_4$			
r_9	=	$k_9 \cdot y_{11} \cdot y_2$	r_{18}	=	$k_{18} \cdot y_{16}$			

TABLE 3.2: *Parameter values.*

k_1	$= 0.350$	k_{10}	$= 0.900 \cdot 10^4$	k_{19}	$= 0.444 \cdot 10^{12}$
k_2	$= 0.266 \cdot 10^2$	k_{11}	$= 0.220 \cdot 10^{-1}$	k_{20}	$= 0.124 \cdot 10^4$
k_3[†]	$= 0.123 \cdot 10^5$	k_{12}	$= 0.120 \cdot 10^5$	k_{21}	$= 0.210 \cdot 10$
k_4	$= 0.860 \cdot 10^{-3}$	k_{13}	$= 0.188 \cdot 10$	k_{22}	$= 0.578 \cdot 10$
k_5	$= 0.820 \cdot 10^{-3}$	k_{14}	$= 0.163 \cdot 10^5$	k_{23}	$= 0.474 \cdot 10^{-1}$
k_6	$= 0.150 \cdot 10^5$	k_{15}	$= 0.480 \cdot 10^7$	k_{24}	$= 0.178 \cdot 10^4$
k_7	$= 0.130 \cdot 10^{-3}$	k_{16}	$= 0.350 \cdot 10^{-3}$	k_{25}	$= 0.312 \cdot 10$
k_8	$= 0.240 \cdot 10^5$	k_{17}	$= 0.175 \cdot 10^{-1}$		
k_9	$= 0.165 \cdot 10^5$	k_{18}	$= 0.100 \cdot 10^9$		

[†] Notice that this constant has a typing error in [Ver94].

1.	NO2	→	NO+O3P	14.	NO2+OH	→	HNO3
2.	NO+O3	→	NO2	15.	O3P	→	O3
3.	HO2+NO	→	NO2+OH	16.	O3	→	O1D
4.	HCHO	→	2 HO2+CO	17.	O3	→	O3P
5.	HCHO	→	CO	18.	O1D	→	2 OH
6.	HCHO+OH	→	HO2+CO	19.	O1D	→	O3P
7.	ALD	→	MEO2+HO2+CO	20.	SO2+OH	→	SO4+HO2
8.	ALD+OH	→	C2O3	21.	NO3	→	NO
9.	C2O3+NO	→	NO2+MEO2+CO2	22.	NO3	→	NO2+O3P
10.	C2O3+NO2	→	PAN	23.	NO2+O3	→	NO3
11.	PAN	→	C2O3+NO2	24.	NO3+NO2	→	N2O5
12.	MEO2+NO	→	CH3O+NO2	25.	N2O5	→	NO3+NO2
13.	CH3O	→	HCHO+HO2				

FIGURE 3.1: *Reaction scheme.*

TABLE 3.3: *Identification of variables with species. The square brackets '[ ]' denote concentrations.*

variable	species	initial value	variable	species	initial value
y_1	[NO2]	0	y_{11}	[C2O3]	0
y_2	[NO]	0.2	y_{12}	[CO2]	0
y_3	[O3P]	0	y_{13}	[PAN]	0
y_4	[O3]	0.04	y_{14}	[CH3O]	0
y_5	[HO2]	0	y_{15}	[HNO3]	0
y_6	[OH]	0	y_{16}	[O1D]	0
y_7	[HCHO]	0.1	y_{17}	[SO2]	0.007
y_8	[CO]	0.3	y_{18}	[SO4]	0
y_9	[ALD]	0.01	y_{19}	[NO3]	0
y_{10}	[MEO2]	0	y_{20}	[N2O5]	0

TABLE 3.4: *Reference solution at the end of the integration interval.*

y_1	$0.5646255480022769 \cdot 10^{-1}$	y_{11}	$0.1135863833257075 \cdot 10^{-7}$
y_2	0.1342484130422339	y_{12}	$0.2230505975721359 \cdot 10^{-2}$
y_3	$0.4139734331099427 \cdot 10^{-8}$	y_{13}	$0.2087162882798630 \cdot 10^{-3}$
y_4	$0.5523140207484359 \cdot 10^{-2}$	y_{14}	$0.1396921016840158 \cdot 10^{-4}$
y_5	$0.2018977262302196 \cdot 10^{-6}$	y_{15}	$0.8964884856898295 \cdot 10^{-2}$
y_6	$0.1464541863493966 \cdot 10^{-6}$	y_{16}	$0.4352846369330103 \cdot 10^{-17}$
y_7	$0.7784249118997964 \cdot 10^{-1}$	y_{17}	$0.6899219696263405 \cdot 10^{-2}$
y_8	0.3245075353396018	y_{18}	$0.1007803037365946 \cdot 10^{-3}$
y_9	$0.7494013383880406 \cdot 10^{-2}$	y_{19}	$0.1772146513969984 \cdot 10^{-5}$
y_{10}	$0.1622293157301561 \cdot 10^{-7}$	y_{20}	$0.5682943292316392 \cdot 10^{-4}$

3.4 Numerical solution of the problem

Tables 3.4–3.5 and Figures 3.2–3.4 present the reference solution at the end of the integration interval, the run characteristics, the behavior of the solution over the interval [0,12] and the work-precision diagrams, respectively. The reference solution was computed by RADAU5 on a Cray C90, using double precision, `work(1) = uround` $= 1.01 \cdot 10^{-19}$, `rtol = atol = h0` $= 1.1 \cdot 10^{-18}$. For the work-precision diagrams, we used: rtol $= 10^{-(4+m/4)}$, $m = 0, 1, \ldots, 24$; atol = rtol; h0 = rtol for RADAU, RADAU5 and MEBDFDAE. The speed-up factor for PSIDE is 1.41.

REFERENCES

[Ver94] J.G. Verwer. Gauss-Seidel iteration for stiff ODEs from chemical kinetics. *SIAM J. Sci. Comput.*, 15(5):1243–1259, 1994.

TABLE 3.5: *Run characteristics.*

solver	rtol	atol	h0	scd	steps	accept	# f	# Jac	# LU	CPU
DASSL	10^{-4}	10^{-4}		2.00	36	35	56	13		0.03
	10^{-7}	10^{-7}		4.13	135	135	190	23		0.11
	10^{-10}	10^{-10}		6.14	384	381	497	37		0.28
MEBDFDAE	10^{-4}	10^{-4}	10^{-4}	3.15	37	37	57	10	10	0.05
	10^{-7}	10^{-7}	10^{-7}	4.74	123	123	184	19	19	0.13
	10^{-10}	10^{-10}	10^{-10}	6.98	247	247	352	34	34	0.25
PSIDE-1	10^{-4}	10^{-4}		2.82	24	24	296	11	96	0.13
	10^{-7}	10^{-7}		4.84	31	29	465	9	124	0.18
	10^{-10}	10^{-10}		8.04	63	62	970	12	188	0.34
RADAU	10^{-4}	10^{-4}	10^{-4}	1.23	22	18	156	15	21	0.07
	10^{-7}	10^{-7}	10^{-7}	3.78	32	29	227	21	32	0.10
	10^{-10}	10^{-10}	10^{-10}	7.75	35	35	449	21	35	0.18
RADAU5	10^{-4}	10^{-4}	10^{-4}	1.23	22	18	156	15	21	0.07
	10^{-7}	10^{-7}	10^{-7}	3.78	32	29	227	21	32	0.10
	10^{-10}	10^{-10}	10^{-10}	7.39	65	65	458	31	46	0.17
VODE	10^{-4}	10^{-4}		1.12	55	55	102	4	15	0.04
	10^{-7}	10^{-7}		3.32	149	149	208	4	27	0.08
	10^{-10}	10^{-10}		4.78	393	375	528	7	61	0.20

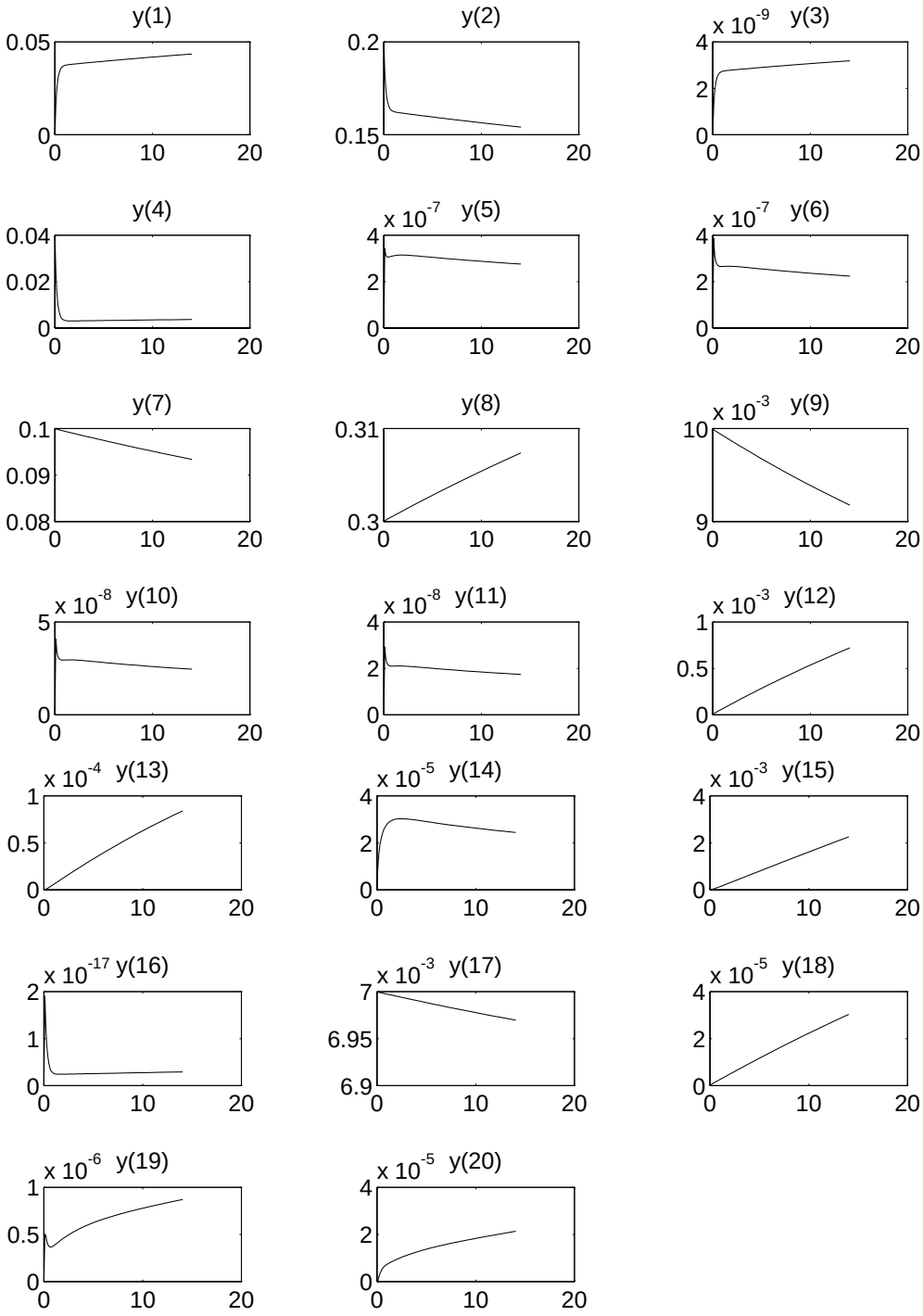

FIGURE 3.2: *Behavior of the solution over the interval [0,12].*

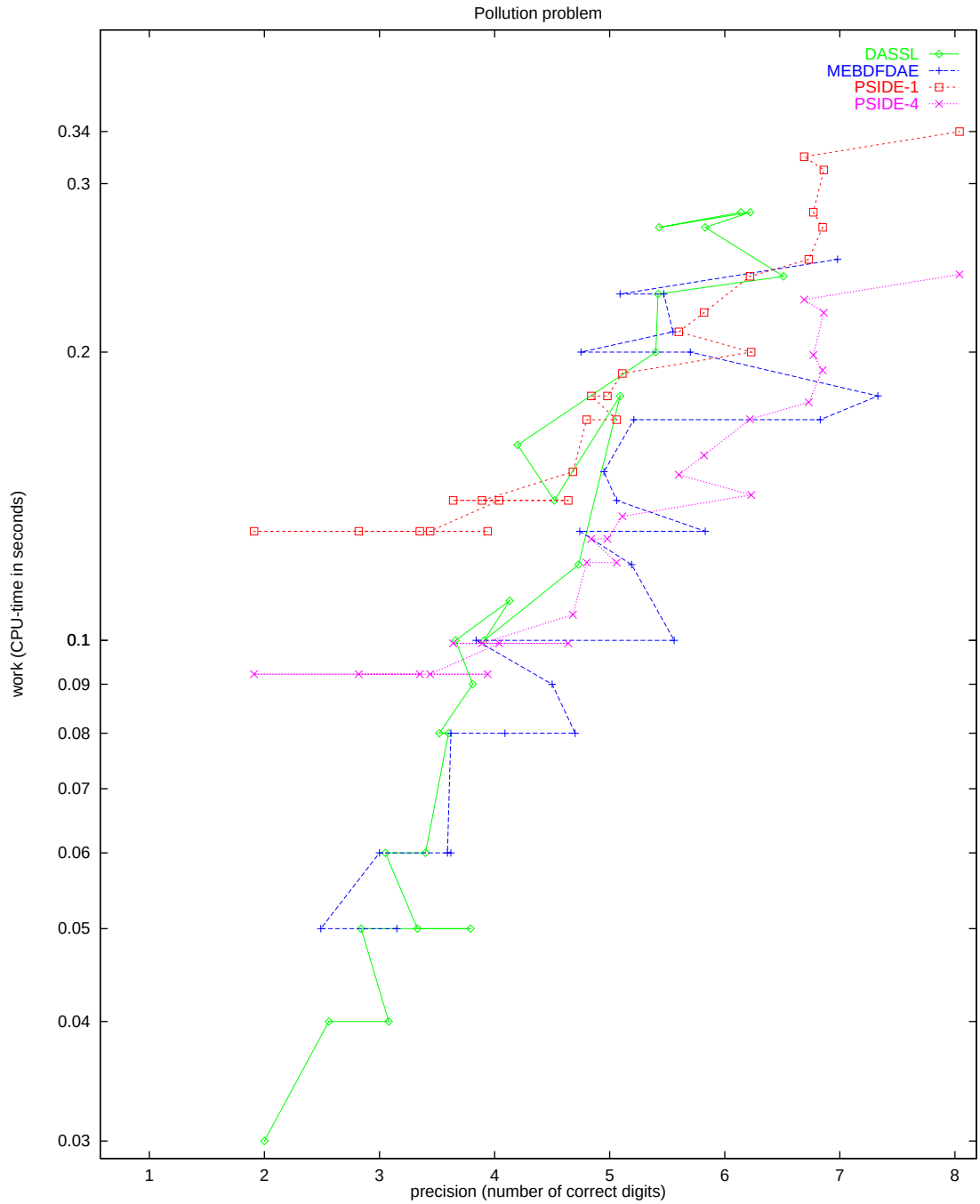

FIGURE 3.3: *Work-precision diagram.*

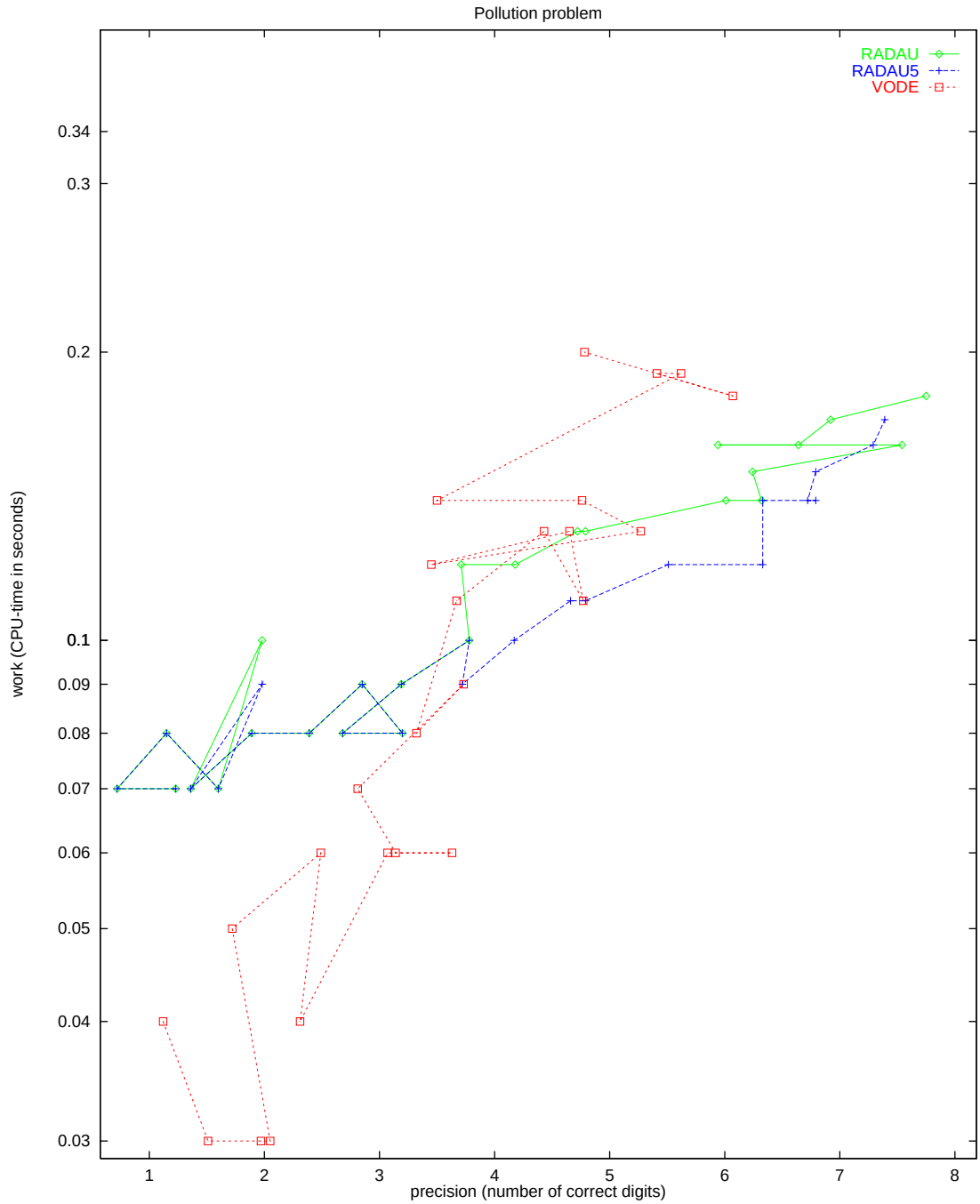

FIGURE 3.4: *Work-precision diagram.*

4. Ring modulator

4.1 General information

The type of the problem depends on the parameter C_s. If $C_s \neq 0$, then it is a stiff system of 15 non-linear ordinary differential equations. For $C_s = 0$ we have a DAE of index 2, consisting of 11 differential equations and 4 algebraic equations. The numerical results presented here refer to $C_s = 2 \cdot 10^{-12}$. The problem has been taken from [KRS92], where the approach of Horneber [Hor76] is followed. The parallel-IVP-algorithm group of CWI contributed this problem to the test set.

4.2 Mathematical description of the problem

For the ODE case, the problem is of the form

$$\frac{\mathrm{d}y}{\mathrm{d}t} = f(t,y), \quad y(0) = y_0,$$

with

$$y \in \mathbb{R}^{15}, \quad 0 \leq t \leq 10^{-3}.$$

The function f is defined by

$$f(t,y) = \begin{pmatrix} C^{-1}(y_8 - 0.5y_{10} + 0.5y_{11} + y_{14} - R^{-1}y_1) \\ C^{-1}(y_9 - 0.5y_{12} + 0.5y_{13} + y_{15} - R^{-1}y_2) \\ C_s^{-1}(y_{10} - q(U_{D1}) + q(U_{D4})) \\ C_s^{-1}(-y_{11} + q(U_{D2}) - q(U_{D3})) \\ C_s^{-1}(y_{12} + q(U_{D1}) - q(U_{D3})) \\ C_s^{-1}(-y_{13} - q(U_{D2}) + q(U_{D4})) \\ C_p^{-1}(-R_p^{-1}y_7 + q(U_{D1}) + q(U_{D2}) - q(U_{D3}) - q(U_{D4})) \\ -L_h^{-1}y_1 \\ -L_h^{-1}y_2 \\ L_{s2}^{-1}(0.5y_1 - y_3 - R_{g2}y_{10}) \\ L_{s3}^{-1}(-0.5y_1 + y_4 - R_{g3}y_{11}) \\ L_{s2}^{-1}(0.5y_2 - y_5 - R_{g2}y_{12}) \\ L_{s3}^{-1}(-0.5y_2 + y_6 - R_{g3}y_{13}) \\ L_{s1}^{-1}(-y_1 + U_{in1}(t) - (R_i + R_{g1})y_{14}) \\ L_{s1}^{-1}(-y_2 - (R_c + R_{g1})y_{15}) \end{pmatrix}. \tag{4.1}$$

The auxiliary functions $U_{D1}, U_{D2}, U_{D3}, U_{D4}, q, U_{in1}$ and U_{in2} are given by

$$\begin{aligned} U_{D1} &= y_3 - y_5 - y_7 - U_{in2}(t), \\ U_{D2} &= -y_4 + y_6 - y_7 - U_{in2}(t), \\ U_{D3} &= y_4 + y_5 + y_7 + U_{in2}(t), \\ U_{D4} &= -y_3 - y_6 + y_7 + U_{in2}(t), \\ q(U) &= \gamma(e^{\delta U} - 1), \\ U_{in1}(t) &= 0.5\sin(2000\pi t), \\ U_{in2}(t) &= 2\sin(20000\pi t). \end{aligned} \tag{4.2}$$

The values of the parameters are:

C	=	$1.6 \cdot 10^{-8}$	R	=	25000
C_s	=	$2 \cdot 10^{-12}$	R_p	=	50
C_p	=	10^{-8}	R_{g1}	=	36.3
L_h	=	4.45	R_{g2}	=	17.3
L_{s1}	=	0.002	R_{g3}	=	17.3
L_{s2}	=	$5 \cdot 10^{-4}$	R_i	=	50
L_{s3}	=	$5 \cdot 10^{-4}$	R_c	=	600
γ	=	$40.67286402 \cdot 10^{-9}$	δ	=	17.7493332

The initial vector y_0 is given by

$$y_0 = (0, 0, 0, 0, 0, 0, 0, 0, 0, 0, 0, 0, 0, 0, 0)^{\mathrm{T}}.$$

The definition of the function $q(U)$ in (4.2) may cause overflow if δU becomes too large. In the Fortran subroutine that defines f, we set `IERR=-1` if $\delta U > 172$ to prevent this situation. See page *III-vi* of the description of the software part of the test set for more details on `IERR`.

4.3 Origin of the problem

The problem originates from electrical circuit analysis. It describes the behavior of the ring modulator, of which the circuit diagram is given in Figure 4.1. Given a low-frequency signal U_{in1} and a high-frequency signal U_{in2}, the ring modulator produces a mixed signal in U_2.

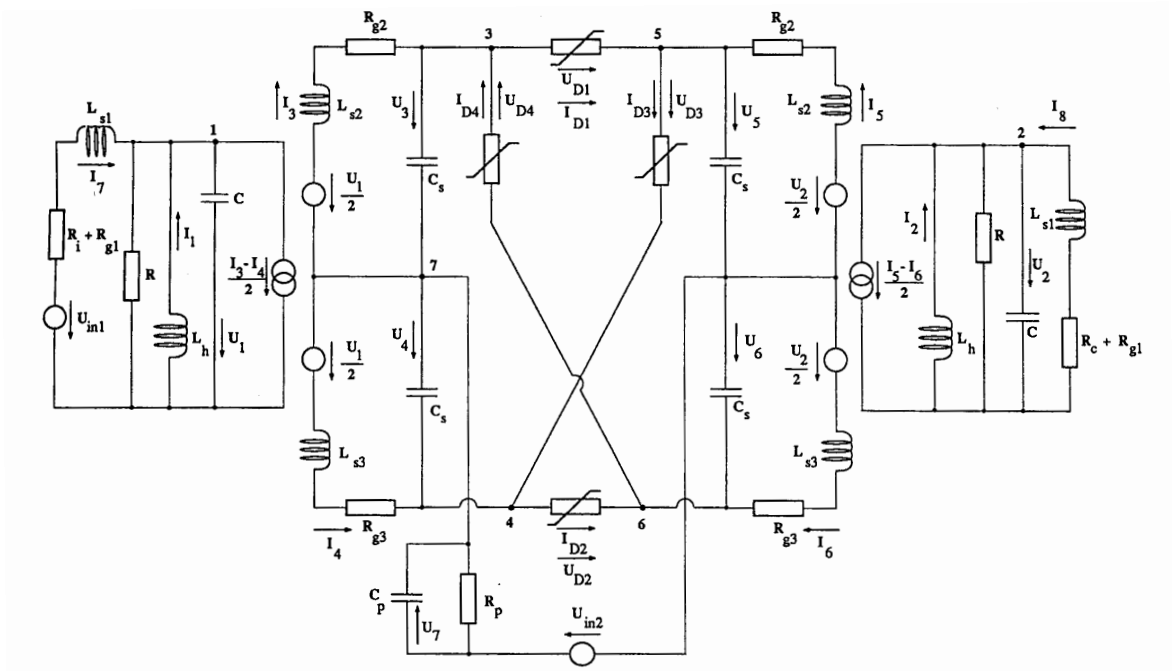

FIGURE 4.1: *Circuit diagram for Ring Modulator (taken from [KRS92]).*

Every capacitor in the diagram leads to a differential equation:

$$C\dot{U} = I.$$

Applying Kirchhoff's Current Law yields the following differential equations:

$$\begin{aligned}
C\dot{U}_1 &= I_1 - 0.5I_3 + 0.5I_4 + I_7 - R^{-1}U_1,\\
C\dot{U}_2 &= I_2 - 0.5I_5 + 0.5I_6 + I_8 - R^{-1}U_2,\\
C_s\dot{U}_3 &= I_3 - q(U_{D1}) + q(U_{D4}),\\
C_s\dot{U}_4 &= -I_4 + q(U_{D2}) - q(U_{D3}),\\
C_s\dot{U}_5 &= I_5 + q(U_{D1}) - q(U_{D3}),\\
C_s\dot{U}_6 &= -I_6 - q(U_{D2}) + q(U_{D4}),\\
C_p\dot{U}_7 &= -R_p^{-1}U_7 + q(U_{D1}) + q(U_{D2}) - q(U_{D3}) - q(U_{D4}),
\end{aligned}$$

where U_{D1}, U_{D1}, U_{D1} and U_{D1} stand for:

$$\begin{aligned}
U_{D1} &= U_3 - U_5 - U_7 - U_{in2},\\
U_{D2} &= -U_4 + U_6 - U_7 - U_{in2},\\
U_{D3} &= U_4 + U_5 + U_7 + U_{in2},\\
U_{D4} &= -U_3 - U_6 + U_7 + U_{in2}.
\end{aligned}$$

The diode function q is given by

$$q(U) = \gamma(e^{\delta U} - 1),$$

where γ and δ are fixed constants.

Every inductor leads to a differential equation as well:

$$L\dot{I} = U.$$

Applying Kirchoff's Voltage Law to closed loops that contains an inductor, results in another 8 differential equations:

$$\begin{aligned}
L_h\dot{I}_1 &= -U_1,\\
L_h\dot{I}_2 &= -U_2,\\
L_{s2}\dot{I}_3 &= 0.5U_1 - U_3 - R_{g2}I_3,\\
L_{s3}\dot{I}_4 &= -0.5U_1 + U_4 - R_{g3}I_4,\\
L_{s2}\dot{I}_5 &= 0.5U_2 - U_5 - R_{g2}I_5,\\
L_{s3}\dot{I}_6 &= -0.5U_2 + U_6 - R_{g3}I_6,\\
L_{s1}\dot{I}_7 &= -U_1 + U_{in1} - (R_i + R_{g1})I_7,\\
L_{s1}\dot{I}_8 &= -U_2 - (R_c + R_{g1})I_8.
\end{aligned}$$

Initially, all voltages and currents are zero.

Identifying the voltages with $y_1, \ldots, y_7$ and the currents with $y_8, \ldots, y_{15}$, we obtain the 15 differential equations (4.1). From the plot of $y_2 = U_2$ in Figure 4.2 we see how the low and high frequency input signals are mixed by the ring modulator.

4.4 Numerical solution of the problem

Tables 4.2–4.3 and Figures 4.2–4.5 present the reference solution at the end of the integration interval, the run characteristics, the behavior of the solution over the integration interval and the work-precision diagrams, respectively. The reference solution was computed using PSIDE with `atol = rtol =` 10^{-13}. For the work-precision diagrams, we used: rtol $= 10^{-(4+m/8)}$, $m = 0, 1, \ldots, 24$; atol = rtol; h0 $= 10^{-2} \cdot$ rtol for RADAU, RADAU5 and MEBDFDAE. The failed runs are in Table 4.1; listed are the name of the solver that failed, for which values of m this happened, and the reason for failing. The speed-up factor for PSIDE is 2.29.

TABLE 4.1: *Failed runs.*

solver	m	reason
RADAU	$0, 1, \ldots, 24$	solver cannot handle `IERR=-1`.
RADAU5	$0, 1, \ldots, 18$	solver cannot handle `IERR=-1`.
VODE	$4, 5$	error test failed repeatedly.

TABLE 4.2: *Reference solution at the end of the integration interval.*

y_1	$-0.2339057358486745 \cdot 10^{-1}$	y_9	$-0.2840029933642329 \cdot 10^{-7}$
y_2	$-0.7367485485540825 \cdot 10^{-2}$	y_{10}	$0.7267198267264553 \cdot 10^{-3}$
y_3	0.2582956709291169	y_{11}	$0.7929487196960840 \cdot 10^{-3}$
y_4	-0.4064465721283450	y_{12}	$-0.7255283495698965 \cdot 10^{-3}$
y_5	-0.4039455665149794	y_{13}	$-0.7941401968526521 \cdot 10^{-3}$
y_6	0.2607966765422943	y_{14}	$0.7088495416976114 \cdot 10^{-4}$
y_7	0.1106761861269975	y_{15}	$0.2390059075236570 \cdot 10^{-4}$
y_8	$0.2939904342435596 \cdot 10^{-6}$		

TABLE 4.3: *Run characteristics.*

solver	rtol	atol	h0	scd	steps	accept	# f	# Jac	# LU	CPU
DASSL	10^{-4}	10^{-4}		0.46	87550	85182	115053	3390		53.22
	10^{-7}	10^{-7}		2.54	252945	249289	321989	7943		151.20
MEBDFDAE	10^{-4}	10^{-4}	10^{-6}	1.94	66718	66403	100491	6801	6801	53.90
	10^{-7}	10^{-7}	10^{-9}	4.60	155662	155062	217642	13706	13706	124.51
PSIDE-1	10^{-4}	10^{-4}		0.60	9791	8241	267721	6834	38184	57.88
	10^{-7}	10^{-7}		4.53	55067	45545	883758	3978	110648	191.04
RADAU5	10^{-7}	10^{-7}	10^{-9}	3.80	102488	93103	544974	12300	55122	137.80
VODE	10^{-4}	10^{-4}		0.36	110268	102207	144377	1923	16022	47.31
	10^{-7}	10^{-7}		2.15	217438	207614	261420	3610	22655	87.87

References

[Hor76] E.H. Horneber. *Analyse nichtlinearer RLCÜ-Netzwerke mit Hilfe der gemischten Potentialfunktion mit einer systematischen Darstellung der Analyse nichtlinearer dynamischer Netzwerke*. PhD thesis, Universität Kaiserslautern, 1976.

[KRS92] W. Kampowski, P. Rentrop, and W. Schmidt. Classification and numerical simulation of electric circuits. *Surveys on Mathematics for Industry*, 2(1):23–65, 1992.

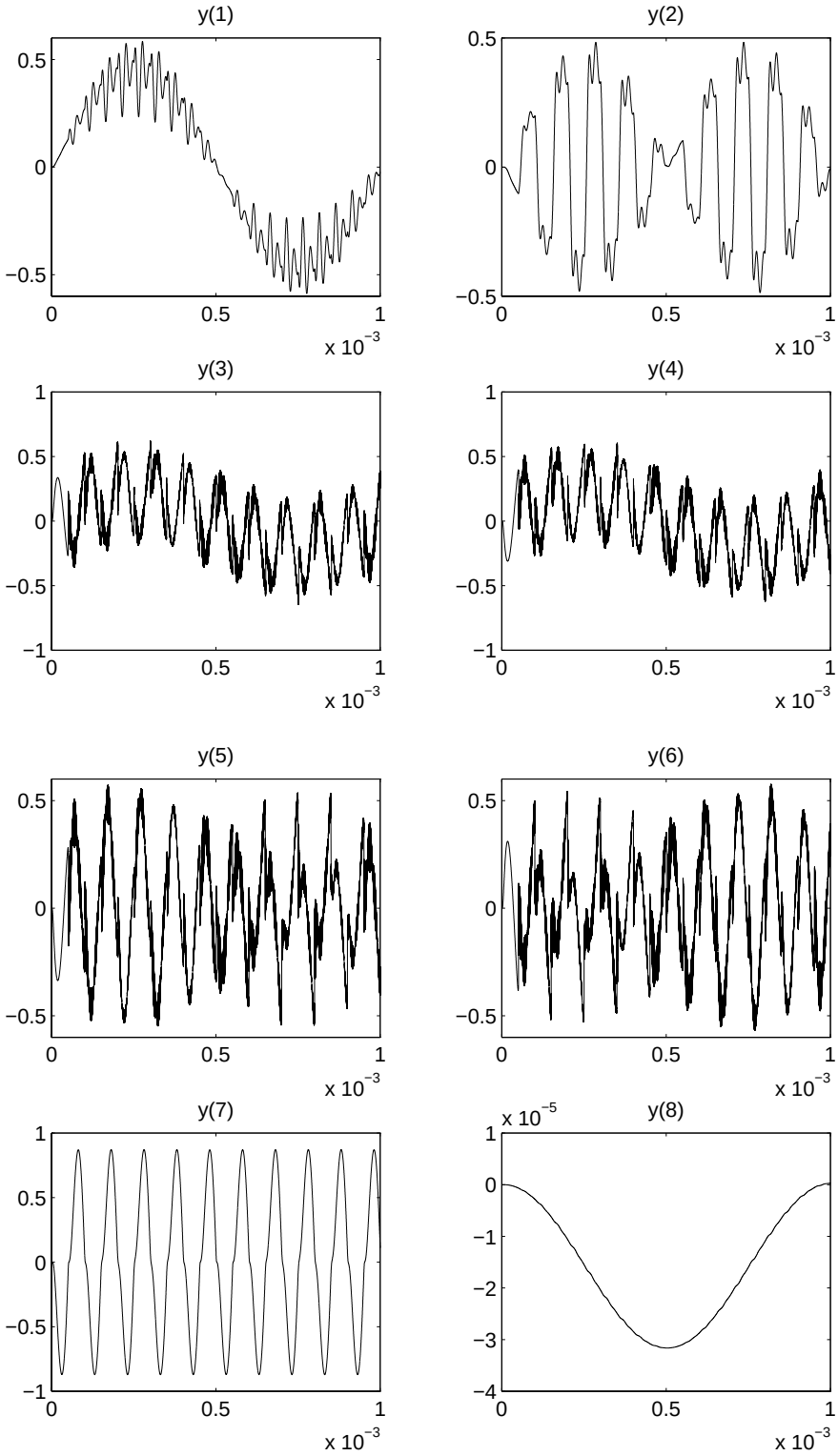

FIGURE 4.2: *Behavior of the first eight solution components solution over the integration interval.*

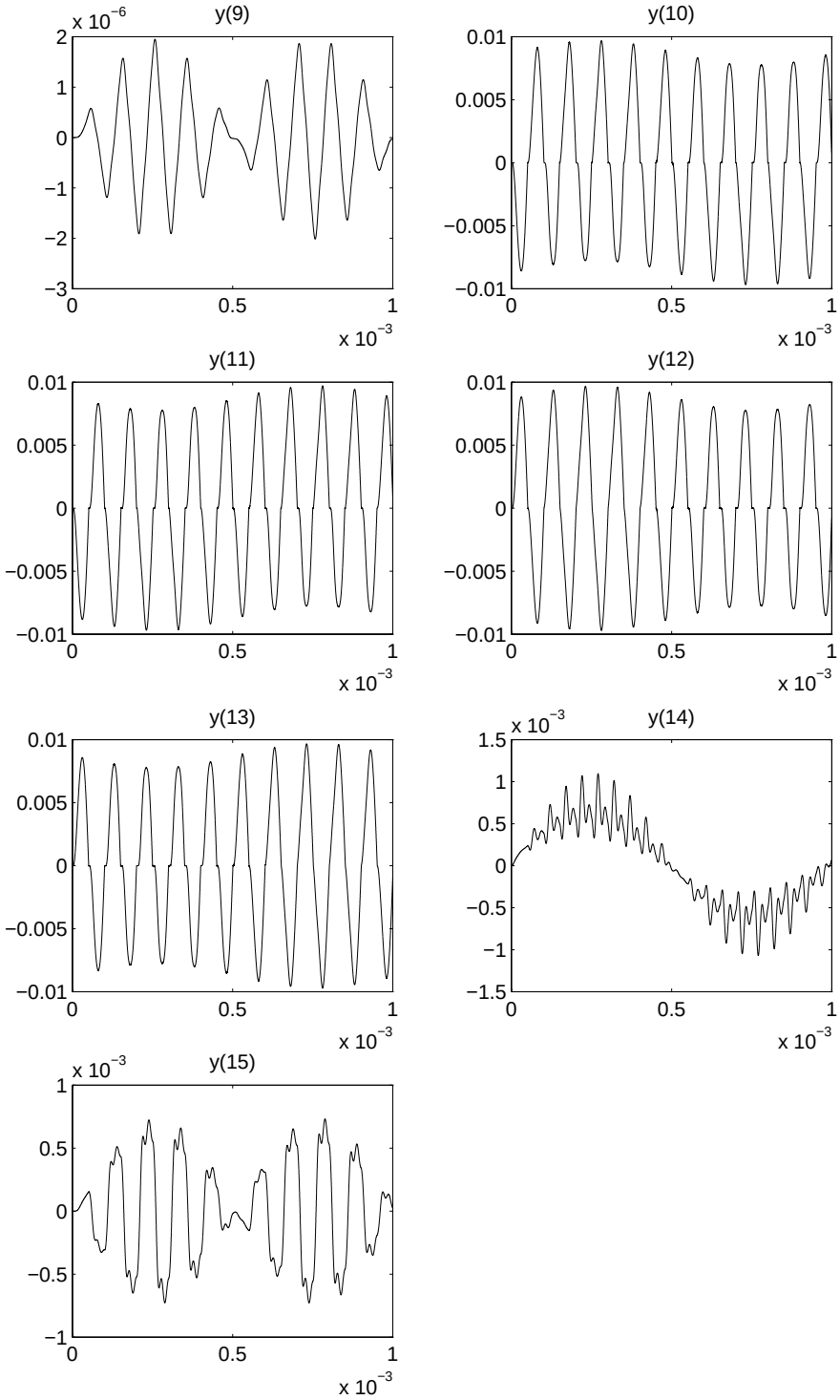

FIGURE 4.3: *Behavior of the last seven solution components solution over the integration interval.*

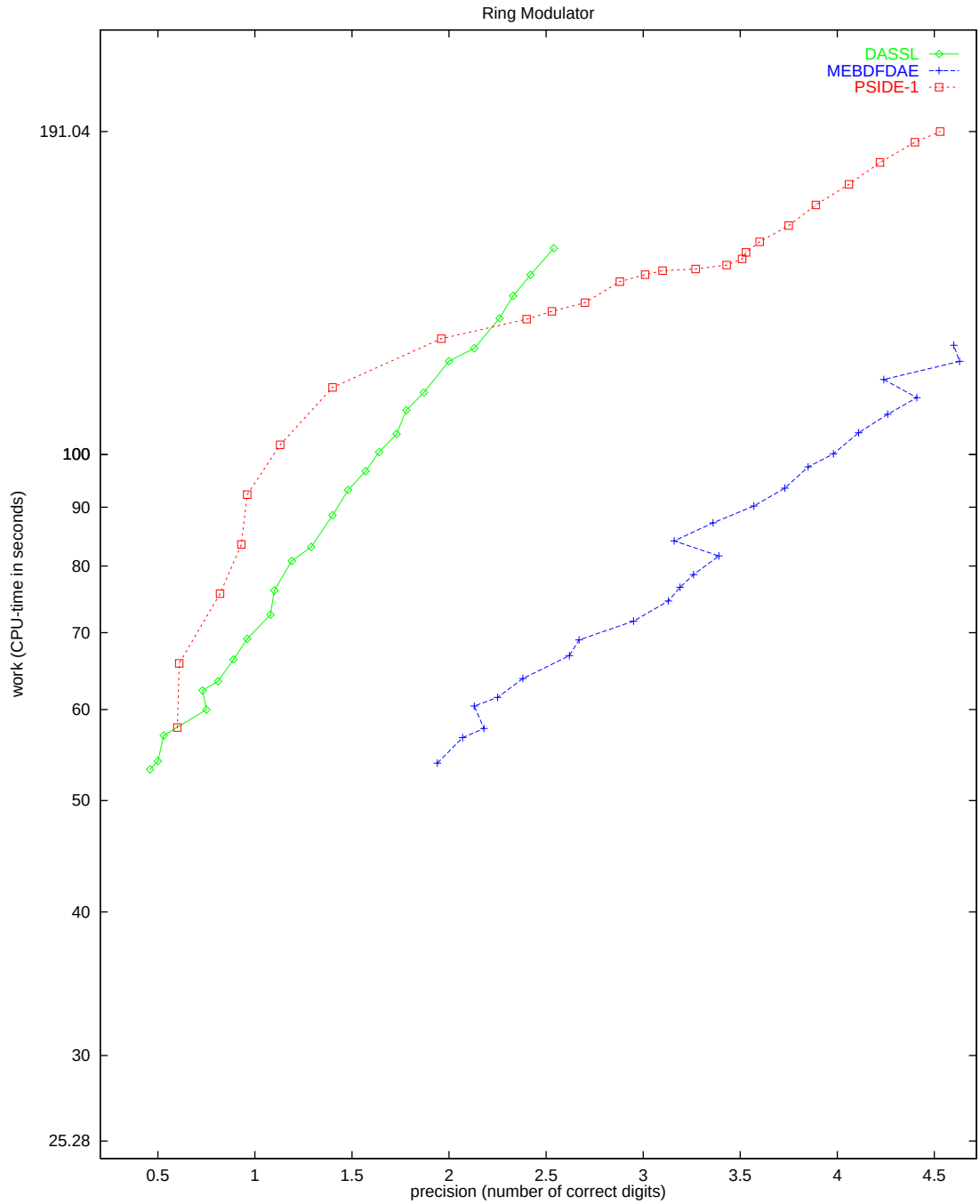

FIGURE 4.4: *Work-precision diagram.*

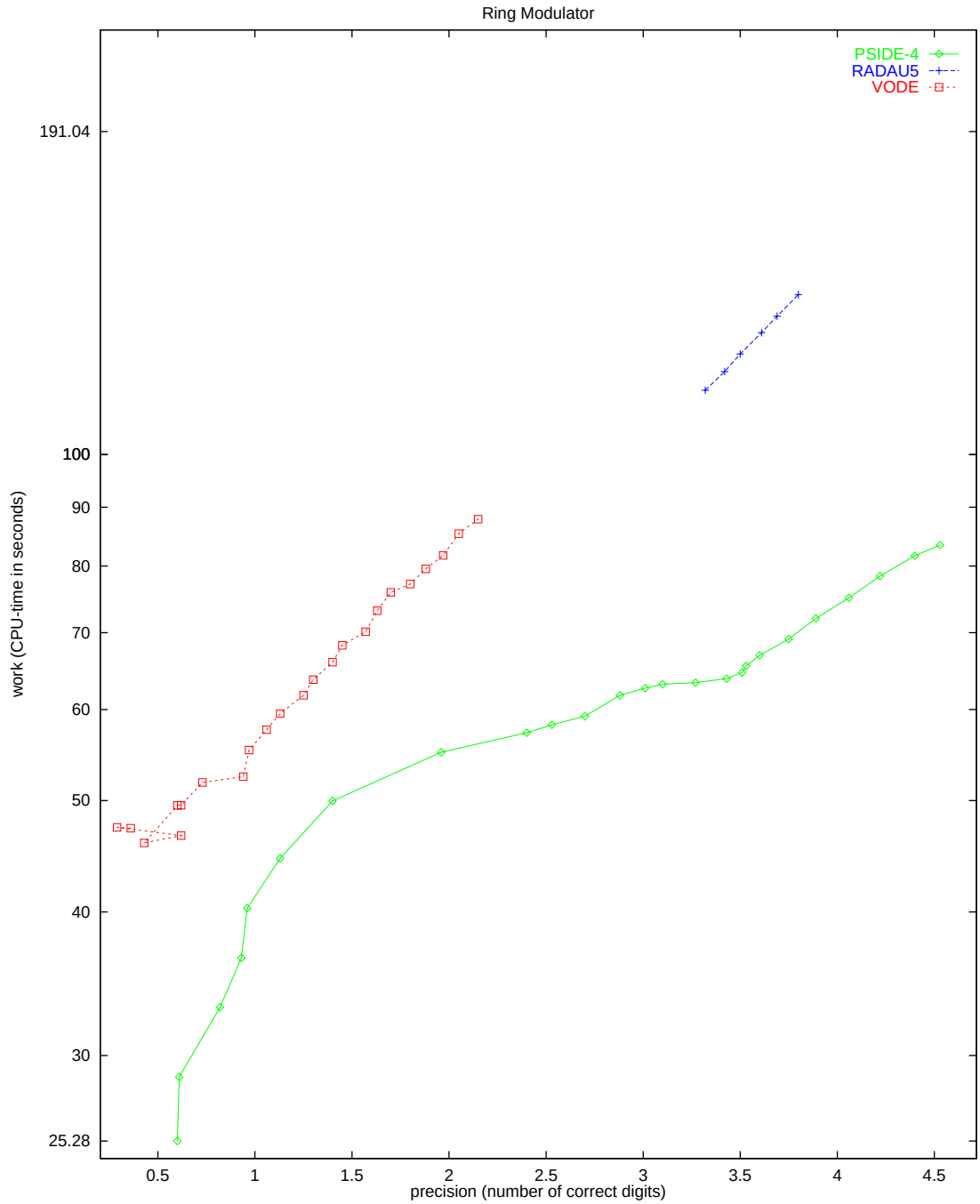

FIGURE 4.5: *Work-precision diagram.*

5. Andrews' squeezing mechanism

5.1 General information

The problem is a non-stiff second order DAE of index 3, consisting of 21 differential and 6 algebraic equations. It has been promoted as a test problem by Giles [Gil78] and Manning [Man81]. The formulation here corresponds to the one presented in Hairer & Wanner [HW96]. The parallel-IVP-algorithm group of CWI contributed this problem to the test set.

5.2 Mathematical description of the problem

The problem is of the form

$$K\frac{\mathrm{d}y}{\mathrm{d}t} \;=\; \phi(y), \qquad y(0)=y_0, \quad y'(0)=y'_0, \tag{5.1}$$

where

$$y=\begin{pmatrix} q \\ \dot q \\ \ddot q \\ \lambda \end{pmatrix}, \quad K=\begin{bmatrix} I & O & O & O \\ O & I & O & O \\ O & O & O & O \\ O & O & O & O \end{bmatrix}, \quad \phi(y)=\begin{pmatrix} \dot q \\ \ddot q \\ M(q)\ddot q - f(q,\dot q) + G^{\mathrm{T}}(q)\lambda \\ g(q) \end{pmatrix}.$$

Here,

$$\begin{aligned} 0 &\le t \le 0.03, \\ q &\in \mathbb{R}^7, \\ \lambda &\in \mathbb{R}^6, \\ M &: \mathbb{R}^7 \to \mathbb{R}^{7\times 7}, \\ f &: \mathbb{R}^{14} \to \mathbb{R}^7, \\ g &: \mathbb{R}^7 \to \mathbb{R}^6, \\ G &= \frac{\partial g}{\partial q}. \end{aligned}$$

The function $M(q)=(M_{ij}(q))$ is given by:

$$\begin{aligned} M_{11}(q) &= m_1\cdot ra^2 + m_2(rr^2 - 2da\cdot rr\cdot\cos q_2 + da^2) + I_1 + I_2, \\ M_{21}(q) &= M_{12}(q) \;=\; m_2(da^2 - da\cdot rr\cdot\cos q_2) + I_2, \\ M_{22}(q) &= m_2\cdot da^2 + I_2, \\ M_{33}(q) &= m_3(sa^2 + sb^2) + I_3, \\ M_{44}(q) &= m_4(e-ea)^2 + I_4, \\ M_{54}(q) &= M_{45}(q) \;=\; m_4((e-ea)^2 + zt(e-ea)\sin q_4) + I_4, \\ M_{55}(q) &= m_4(zt^2 + 2zt(e-ea)\sin q_4 + (e-ea)^2) + m_5(ta^2+tb^2) + I_4 + I_5, \\ M_{66}(q) &= m_6(zf-fa)^2 + I_6, \\ M_{76}(q) &= M_{67}(q) \;=\; m_6((zf-fa)^2 - u(zf-fa)\sin q_6) + I_6, \\ M_{77}(q) &= m_6((zf-fa)^2 - 2u(zf-fa)\sin q_6 + u^2) + m_7(ua^2+ub^2) + I_6 + I_7, \\ M_{ij}(q) &= 0 \quad \text{for all other cases.} \end{aligned}$$

The function $f = (f_i(q, \dot{q}))$ reads:

$$\begin{aligned}
f_1(q,\dot{q}) &= mom - m_2 \cdot da \cdot rr \cdot \dot{q}_2(\dot{q}_2 + 2\dot{q}_1)\sin q_2,\\
f_2(q,\dot{q}) &= m_2 \cdot da \cdot rr \cdot \dot{q}_1^2 \cdot \sin q_2,\\
f_3(q,\dot{q}) &= F_x(sc \cdot \cos q_3 - sd \cdot \sin q_3) + F_y(sd \cdot \cos q_3 + sc \cdot \sin q_3),\\
f_4(q,\dot{q}) &= m_4 \cdot zt(e - ea)\dot{q}_5^2 \cdot \cos q_4,\\
f_5(q,\dot{q}) &= -m_4 \cdot zt(e - ea)\dot{q}_4(\dot{q}_4 + 2\dot{q}_5)\cos q_4,\\
f_6(q,\dot{q}) &= -m_6 \cdot u(zf - fa)\dot{q}_7^2 \cdot \cos q_6,\\
f_7(q,\dot{q}) &= m_6 \cdot u(zf - fa)\dot{q}_6(\dot{q}_6 + 2\dot{q}_7)\cos q_6.
\end{aligned}$$

F_x and F_y are defined by:

$$\begin{aligned}
F_x &= F(xd - xc),\\
F_y &= F(yd - yc),\\
F &= -c_0(L - l_0)/L,\\
L &= \sqrt{(xd - xc)^2 + (yd - yc)^2},\\
xd &= sd \cdot \cos q_3 + sc \cdot \sin q_3 + xb,\\
yd &= sd \cdot \sin q_3 - sc \cdot \cos q_3 + yb.
\end{aligned}$$

The function $g = (g_i(q))$ is given by:

$$\begin{aligned}
g_1(q) &= rr \cdot \cos q_1 - d \cdot \cos(q_1 + q_2) - ss \cdot \sin q_3 - xb,\\
g_2(q) &= rr \cdot \sin q_1 - d \cdot \sin(q_1 + q_2) + ss \cdot \cos q_3 - yb,\\
g_3(q) &= rr \cdot \cos q_1 - d \cdot \cos(q_1 + q_2) - e \cdot \sin(q_4 + q_5) - zt \cdot \cos q_5 - xa,\\
g_4(q) &= rr \cdot \sin q_1 - d \cdot \sin(q_1 + q_2) + e \cdot \cos(q_4 + q_5) - zt \cdot \sin q_5 - ya,\\
g_5(q) &= rr \cdot \cos q_1 - d \cdot \cos(q_1 + q_2) - zf \cdot \cos(q_6 + q_7) - u \cdot \sin q_7 - xa,\\
g_6(q) &= rr \cdot \sin q_1 - d \cdot \sin(q_1 + q_2) - zf \cdot \sin(q_6 + q_7) + u \cdot \cos q_7 - ya.
\end{aligned}$$

The constants arising in these formulas are given by:

m_1	=	0.04325	I_1	=	$2.194 \cdot 10^{-6}$	ss	=	0.035
m_2	=	0.00365	I_2	=	$4.410 \cdot 10^{-7}$	sa	=	0.01874
m_3	=	0.02373	I_3	=	$5.255 \cdot 10^{-6}$	sb	=	0.01043
m_4	=	0.00706	I_4	=	$5.667 \cdot 10^{-7}$	sc	=	0.018
m_5	=	0.07050	I_5	=	$1.169 \cdot 10^{-5}$	sd	=	0.02
m_6	=	0.00706	I_6	=	$5.667 \cdot 10^{-7}$	ta	=	0.02308
m_7	=	0.05498	I_7	=	$1.912 \cdot 10^{-5}$	tb	=	0.00916
xa	=	−0.06934	d	=	0.028	u	=	0.04
ya	=	−0.00227	da	=	0.0115	ua	=	0.01228
xb	=	−0.03635	e	=	0.02	ub	=	0.00449
yb	=	0.03273	ea	=	0.01421	zf	=	0.02
xc	=	0.014	rr	=	0.007	zt	=	0.04
yc	=	0.072	ra	=	0.00092	fa	=	0.01421
c_0	=	4530	l_0	=	0.07785	mom	=	0.033

Consistent initial values are

$$y_0 = (q_0, \dot{q}_0, \ddot{q}_0, \lambda_0)^{\mathrm{T}} \text{ and } y_0' = (\dot{q}_0, \ddot{q}_0, \dddot{q}_0, \dot{\lambda}_0)^{\mathrm{T}},$$

where

$$q_0 = \begin{pmatrix} -0.06171389001427644963589484580 01 \\ 0 \\ 0.45527981916307038025591238244 9 \\ 0.22266839016588588467447318560 9 \\ 0.48736497954384255022559895353 0 \\ -0.22266839016588588467447318560 9 \\ 1.23054744454982119249735015568 \end{pmatrix},$$

$$\dot{q}_0 = \ddot{q}_0 = (0,0,0,0,0,0,0)^{\mathrm{T}},$$

$$\ddot{q}_0 = \begin{pmatrix} 14222.44391995411387059116258 87 \\ -10666.83293996558540294337194 15 \\ 0 \\ 0 \\ 0 \\ 0 \\ 0 \end{pmatrix},$$

$$\lambda_0 = \begin{pmatrix} 98.56687039624108960576549821 70 \\ -6.12268834425566265503114393122 \\ 0 \\ 0 \\ 0 \\ 0 \end{pmatrix},$$

$$\dot{\lambda}_0 = (0,0,0,0,0,0)^{\mathrm{T}}.$$

The index of the q, $\dot{q}$, $\ddot{q}$ and λ components in y is 1, 2, 3 and 3, respectively.

5.3 Origin of the problem

Formulation (5.1) can be rewritten as

$$\begin{aligned} M(q)\ddot{q} &= f(q,\dot{q}) - G^{\mathrm{T}}(q)\lambda, \\ 0 &= g(q), \end{aligned}$$

which is the general form of a constrained mechanical system. More precisely, the problem describes the motion of 7 rigid bodies connected by joints without friction. It was promoted by [Gil78] and [Man81] as a test problem for numerical codes. [HW96, pp. 530–536] describes the system and the modeling process in full detail.

5.4 Numerical solution of the problem

The Jacobian $\partial\phi/\partial y$, needed by the numerical solver, was approximated by

$$\begin{bmatrix} O & I & O & O \\ O & O & I & O \\ O & O & M & G^{\mathrm{T}} \\ G & O & O & O \end{bmatrix},$$

which means that we neglect the derivatives of $f(q,\dot{q})$ as well as those of $M(q)$ and $G(q)$. Note that the evaluation of such a Jacobian does not cost anything, because M and G are already computed in the evaluation of ϕ. However, we did not exploit this in the numerical computations.

Tables 5.1–5.2 and Figures 5.1–5.3 present the reference solution at the end of the integration interval, the run characteristics, the behavior of the solution over the integration interval and the work-precision diagrams, respectively. In computing the scd values, only the first seven components

TABLE 5.1: *Reference solution (first 7 components) at the end of the integration interval.*

y_1	$0.15810771 \cdot 10^2$	y_4	-0.53473012	y_6	0.53473012
y_2	$-0.15756371 \cdot 10^2$	y_5	0.52440997	y_7	$0.10480807 \cdot 10$
y_3	$0.40822240 \cdot 10^{-1}$				

TABLE 5.2: *Run characteristics.*

solver	rtol	atol	h0	scd	steps	accept	# f	# Jac	# LU	CPU
MEBDFDAE	10^{-4}	10^{-4}	10^{-4}	-0.30	149	133	345	28	28	0.32
	10^{-7}	10^{-7}	10^{-7}	3.01	398	386	849	46	46	0.86
PSIDE-1	10^{-4}	10^{-4}		2.95	92	75	1675	52	368	1.47
	10^{-7}	10^{-7}		4.98	113	93	2637	63	428	2.24
RADAU	10^{-4}	10^{-4}	10^{-4}	1.36	96	56	810	54	96	0.55
	10^{-7}	10^{-7}	10^{-7}	4.46	117	97	1321	92	117	0.84
RADAU5	10^{-4}	10^{-4}	10^{-4}	1.36	96	56	810	54	96	0.54
	10^{-7}	10^{-7}	10^{-7}	4.46	117	97	1321	92	117	0.83

were considered, since they refer to the physically important quantities. The reference solution was computed on the Cray C90, using PSIDE with Cray double precision and atol = rtol = 10^{-14}. For the work-precision diagrams, we used: rtol = $10^{-(4+m/8)}$, $m = 0, 1, \ldots, 24$; atol = rtol; h0 = rtol for RADAU, RADAU5 and MEBDFDAE. The speed-up factor for PSIDE is 2.16.

REFERENCES

[Gil78] D.R.A. Giles. An algebraic approach to A-stable linear multistep-multiderivative integration formulas. *BIT*, 14:382–406, 1978.

[HW96] E. Hairer and G. Wanner. *Solving Ordinary Differential Equations II: Stiff and Differential-algebraic Problems*. Springer-Verlag, second revised edition, 1996.

[Man81] D.W. Manning. *A computer technique for simulating dynamic multibody systems based on dynamic formalism*. PhD thesis, Univ. Waterloo, Ontario, 1981.

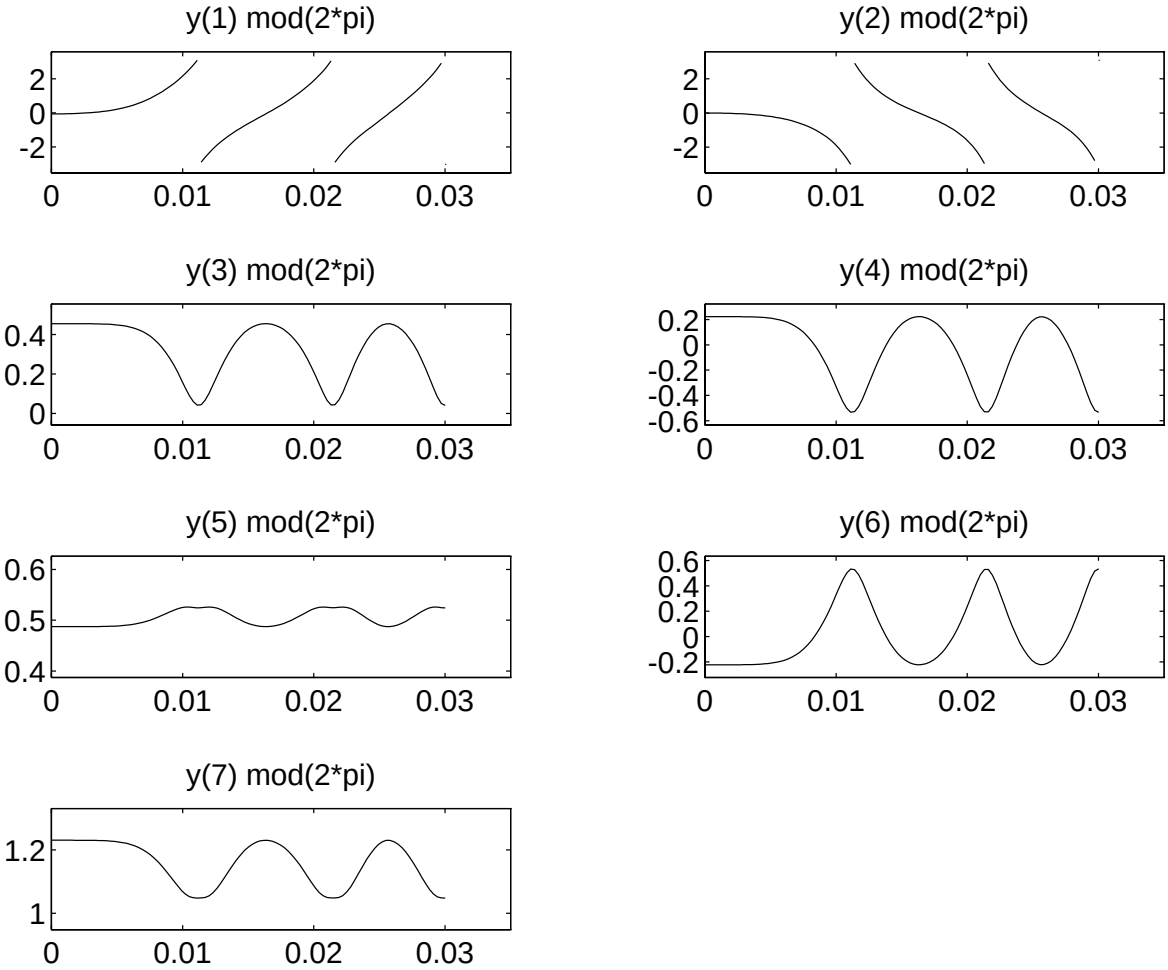

FIGURE 5.1: *Behavior of the solution modulo* 2π *over the integration interval.*

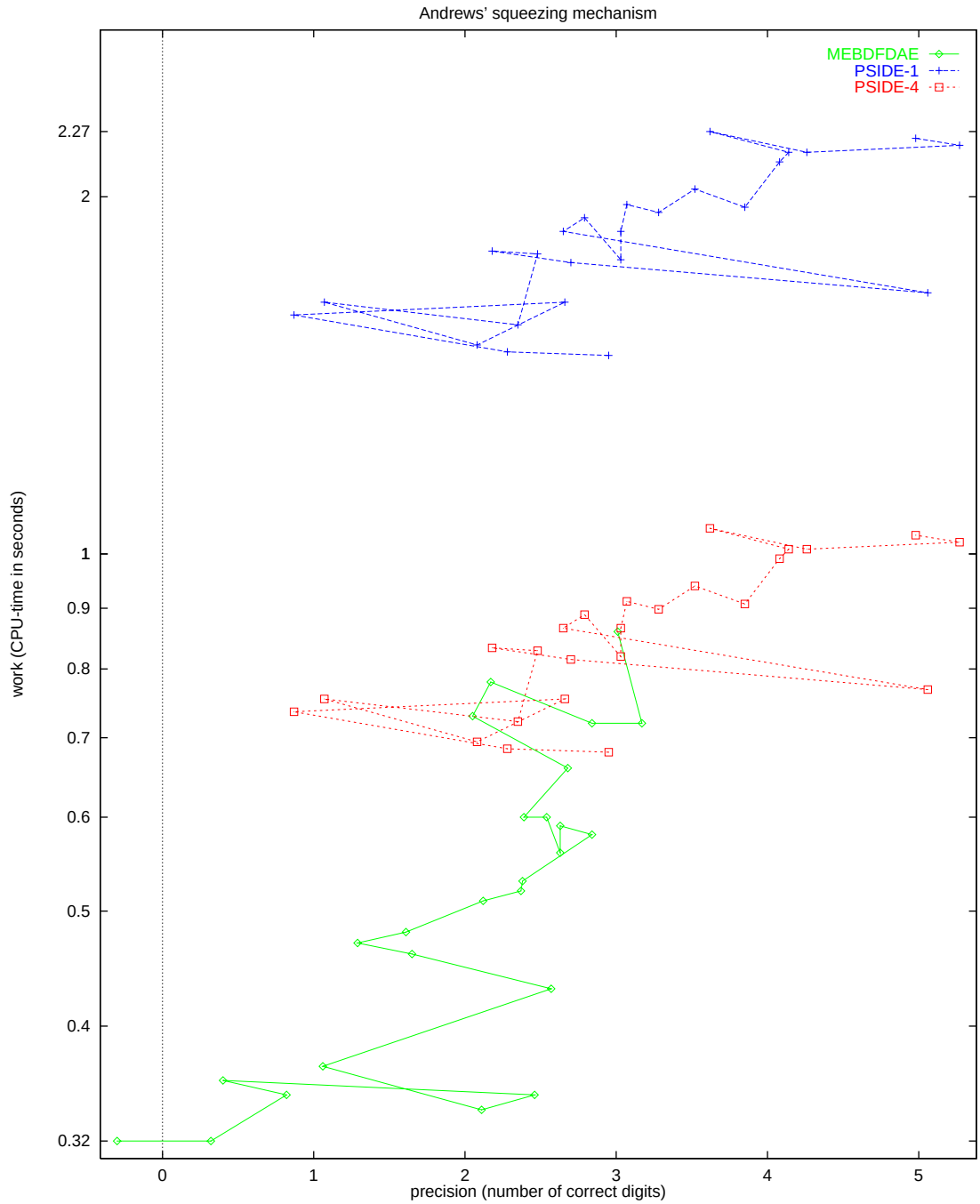

FIGURE 5.2: *Work-precision diagram.*

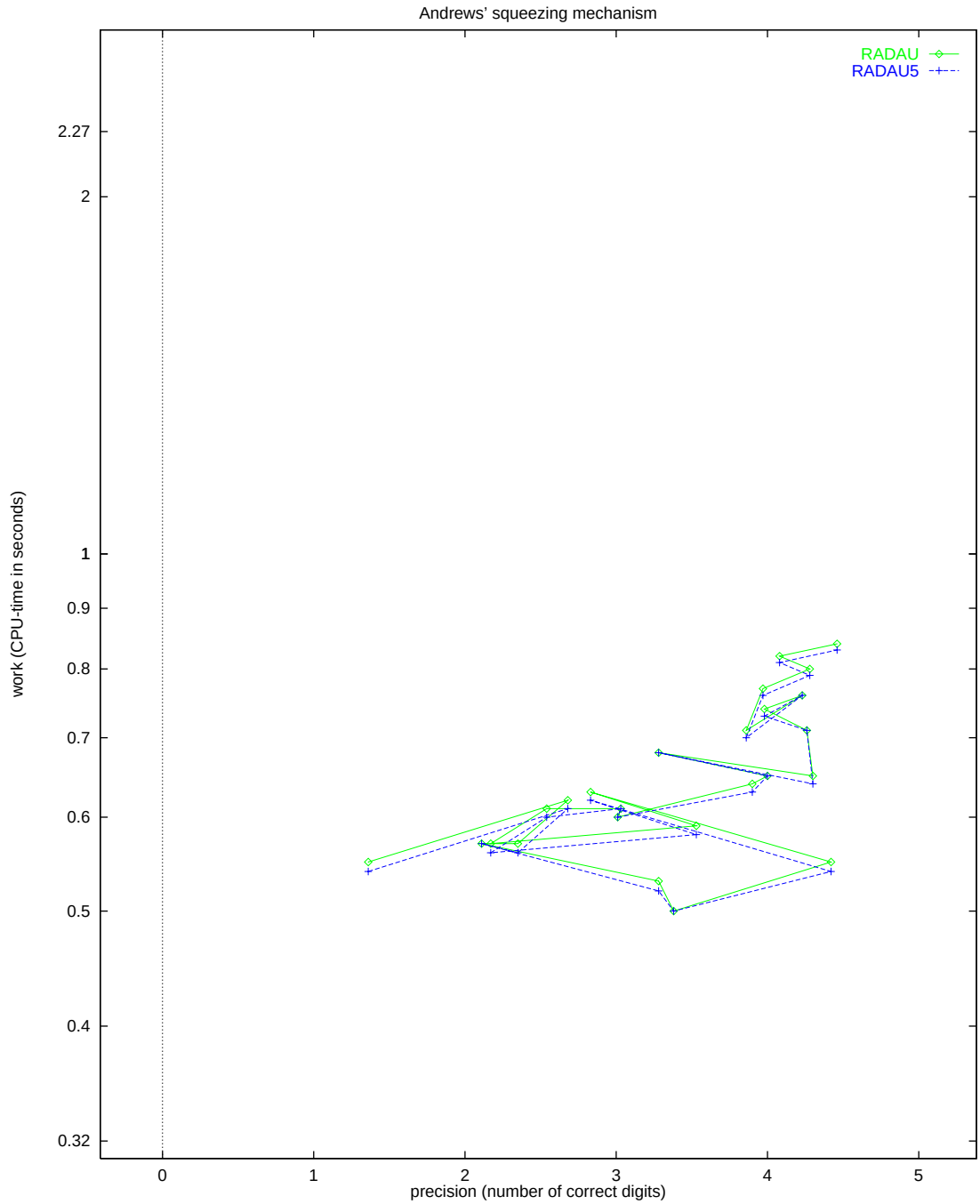

FIGURE 5.3: *Work-precision diagram.*

6. Transistor amplifier

6.1 General information

The problem is a stiff DAE of index 1 consisting of 8 equations P. Rentrop has received it from K. Glashoff & H.J. Oberle and has documented it in [RRS89]. The formulation presented here has been taken from [HLR89]. The parallel-IVP-algorithm group of CWI contributed this problem to the test set.

6.2 Mathematical description of the problem

The problem is of the form

$$M\frac{\mathrm{d}y}{\mathrm{d}t} = f(y), \qquad y(0) = y_0, \quad y'(0) = y'_0,$$

with

$$y \in \mathbb{R}^8, \quad 0 \le t \le 0.2.$$

The matrix M is of rank 5 and given by

$$M = \begin{pmatrix} -C_1 & C_1 & 0 & 0 & 0 & 0 & 0 & 0 \\ C_1 & -C_1 & 0 & 0 & 0 & 0 & 0 & 0 \\ 0 & 0 & -C_2 & 0 & 0 & 0 & 0 & 0 \\ 0 & 0 & 0 & -C_3 & C_3 & 0 & 0 & 0 \\ 0 & 0 & 0 & C_3 & -C_3 & 0 & 0 & 0 \\ 0 & 0 & 0 & 0 & 0 & -C_4 & 0 & 0 \\ 0 & 0 & 0 & 0 & 0 & 0 & -C_5 & C_5 \\ 0 & 0 & 0 & 0 & 0 & 0 & C_5 & -C_5 \end{pmatrix},$$

and the function f by

$$f(y) = \begin{pmatrix} -\frac{U_e(t)}{R_0} + \frac{y_1}{R_0} \\ -\frac{U_b}{R_2} + y_2(\frac{1}{R_1} + \frac{1}{R_2}) - (\alpha - 1)g(y_2 - y_3) \\ -g(y_2 - y_3) + \frac{y_3}{R_3} \\ -\frac{U_b}{R_4} + \frac{y_4}{R_4} + \alpha g(y_2 - y_3) \\ -\frac{U_b}{R_6} + y_5(\frac{1}{R_5} + \frac{1}{R_6}) - (\alpha - 1)g(y_5 - y_6) \\ -g(y_5 - y_6) + \frac{y_6}{R_7} \\ -\frac{U_b}{R_8} + \frac{y_7}{R_8} + \alpha g(y_5 - y_6) \\ \frac{y_8}{R_9} \end{pmatrix},$$

where g and U_e are auxiliary functions given by

$$g(x) = \beta(e^{\frac{x}{U_F}} - 1) \quad \text{and} \quad U_e(t) = 0.1\sin(200\pi t).$$

The values of the technical parameters are:

U_b	=	6,	R_0	=	1000,		
U_F	=	0.026,	R_k	=	9000	for	$k = 1, \ldots, 9,$
α	=	0.99,	C_k	=	$k \cdot 10^{-6}$	for	$k = 1, \ldots, 5.$
β	=	10^{-6},					

Consistent initial values at $t = 0$ are

$$y_0 = \begin{pmatrix} 0 \\ U_b/(\frac{R_2}{R_1}+1) \\ U_b/(\frac{R_2}{R_1}+1) \\ U_b \\ U_b/(\frac{R_6}{R_5}+1) \\ U_b/(\frac{R_6}{R_5}+1) \\ U_b \\ 0 \end{pmatrix}, \qquad y_0' = \begin{pmatrix} 51.338775 \\ 51.338775 \\ -U_b/((\frac{R_2}{R_1}+1)(C_2 \cdot R_3)) \\ -24.9757667 \\ -24.9757667 \\ -U_b/((\frac{R_6}{R_5}+1)(C_4 \cdot R_7)) \\ -10.00564453 \\ -10.00564453 \end{pmatrix}.$$

The first, fourth and seventh component of y_0' were determined numerically. All components of y are of index 1.

6.3 Origin of the problem

The problem originates from electrical circuit analysis. It is a model for the transistor amplifier. The diagram of the circuit is given in Figure 6.1. Here U_e is the input signal and U_8 is the amplified output

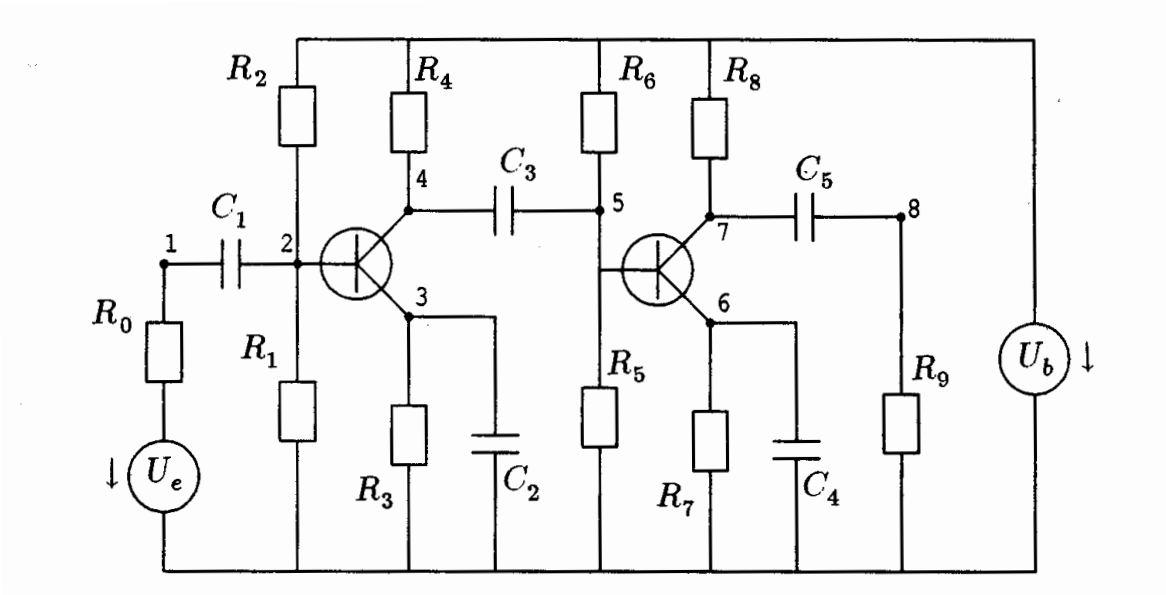

FIGURE 6.1: *Circuit diagram of Transistor Amplifier (taken from [HLR89]).*

voltage. The circuit contains two transistors of the form depicted in Figure 6.2. As a simple model for the behavior of the transistors we assume that the currents through the gate, drain and source, which are denoted by I_G, I_D and I_S, respectively, are

$$\begin{aligned} I_G &= (1-\alpha)g(U_G - U_S), \\ I_D &= \alpha g(U_G - U_S), \\ I_S &= g(U_G - U_S), \end{aligned}$$

where U_G and U_S denote the voltage at the gate and source, respectively, and $\alpha = 0.99$. For the function g we take

$$g(U_i - U_j) = \beta(\mathrm{e}^{\frac{U_i - U_j}{U_F}} - 1),$$

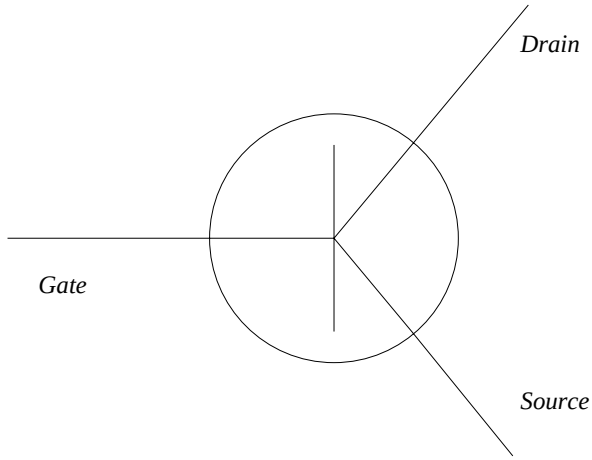

FIGURE 6.2: *Schematic representation of a transistor.*

where $\beta = 10^{-6}$ and $U_F = 0.026$.

To formulate the governing equations, Kirchoff's Current Law is used in each numbered node. This law states that the total sum of all currents entering a node must be zero. All currents passing through the circuit components can be expressed in terms of the unknown voltages $U_1, \ldots, U_8$. Consider for instance node 1. The current I_{C_1} passing through capacitor C_1 is given by

$$I_{C_1} = \frac{\mathrm{d}}{\mathrm{d}t}(C_1(U_2 - U_1)),$$

and the current I_{R_0} passing through the resistor R_0 by

$$I_{R_0} = \frac{U_e - U_1}{R_0}.$$

Here, the currents are directed towards node 1 if the current is positive. A similar derivation for the other nodes gives the system:

$$\begin{aligned}
\text{node 1:} \quad & \tfrac{\mathrm{d}}{\mathrm{d}t}(C_1(U_2 - U_1)) + \tfrac{U_e(t)}{R_0} - \tfrac{U_1}{R_0} && = 0,\\
\text{node 2:} \quad & \tfrac{\mathrm{d}}{\mathrm{d}t}(C_1(U_1 - U_2)) + \tfrac{U_b}{R_2} - U_2(\tfrac{1}{R_1} + \tfrac{1}{R_2}) + (\alpha - 1)g(U_2 - U_3) && = 0,\\
\text{node 3:} \quad & -\tfrac{\mathrm{d}}{\mathrm{d}t}(C_2 U_3) + g(U_2 - U_3) - \tfrac{U_3}{R_3} && = 0,\\
\text{node 4:} \quad & -\tfrac{\mathrm{d}}{\mathrm{d}t}(C_3(U_4 - U_5)) + \tfrac{U_b}{R_4} - \tfrac{U_4}{R_4} - \alpha g(U_2 - U_3) && = 0,\\
\text{node 5:} \quad & \tfrac{\mathrm{d}}{\mathrm{d}t}(C_3(U_4 - U_5)) + \tfrac{U_b}{R_6} - U_5(\tfrac{1}{R_5} + \tfrac{1}{R_6}) + (\alpha - 1)g(U_5 - U_6) && = 0,\\
\text{node 6:} \quad & -\tfrac{\mathrm{d}}{\mathrm{d}t}(C_4 U_6) + g(U_5 - U_6) - \tfrac{U_6}{R_7} && = 0,\\
\text{node 7:} \quad & -\tfrac{\mathrm{d}}{\mathrm{d}t}(C_5(U_7 - U_8)) + \tfrac{U_b}{R_8} - \tfrac{U_7}{R_8} - \alpha g(U_5 - U_6) && = 0.\\
\text{node 8:} \quad & -\tfrac{\mathrm{d}}{\mathrm{d}t}(C_5(U_7 - U_8)) + \tfrac{U_8}{R_9} && = 0,
\end{aligned}$$

The input signal $U_e(t)$ is

$$U_e(t) = 0.1\sin(200\pi t).$$

TABLE 6.1: *Reference solution at the end of the integration interval.*

y_1	$-0.5562145012262709 \cdot 10^{-2}$	y_5	$0.2704617865010554 \cdot 10$
y_2	$0.3006522471903042 \cdot 10$	y_6	$0.2761837778393145 \cdot 10$
y_3	$0.2849958788608128 \cdot 10$	y_7	$0.4770927631616772 \cdot 10$
y_4	$0.2926422536206241 \cdot 10$	y_8	$0.1236995868091548 \cdot 10$

TABLE 6.2: *Run characteristics.*

solver	rtol	atol	h0	scd	steps	accept	# f	# Jac	# LU	CPU
DASSL	10^{-4}	10^{-4}		2.57	9666	6003	18201	7213		4.36
	10^{-7}	10^{-7}		4.56	59485	33008	115182	52726		27.54
MEBDFDAE	10^{-4}	10^{-4}	10^{-6}	4.46	1788	1691	3772	307	307	1.23
	10^{-7}	10^{-7}	10^{-9}	7.62	4624	4441	8209	608	608	3.10
PSIDE-1	10^{-4}	10^{-4}		4.76	516	362	9742	253	2008	1.12
	10^{-7}	10^{-7}		7.07	829	652	21753	411	2748	2.35
RADAU	10^{-5}	10^{-5}	10^{-7}	5.67	956	740	9109	734	956	0.99
	10^{-7}	10^{-7}	10^{-9}	6.83	1787	1555	17746	1547	1787	1.92
RADAU5	10^{-5}	10^{-5}	10^{-7}	5.67	956	740	9109	734	956	0.95
	10^{-7}	10^{-7}	10^{-9}	6.83	1787	1555	17746	1547	1786	1.86

To arrive at the mathematical formulation of the preceding subsection, one just has to identify U_i with y_i.

From the plot of output signal $U_8 = y(8)$ in Figure 6.1 we see that the amplitude of the input signal U_e is indeed amplified.

6.4 Numerical solution of the problem

Tables 6.1–6.2 and Figures 6.3–6.5 present the reference solution at the end of the integration interval, the run characteristics, the behavior of the solution over the integration interval and the work-precision diagrams, respectively. The reference solution was computed on the Cray C90, using PSIDE with Cray double precision and atol = rtol = 10^{-14}. For the work-precision diagrams, we used: rtol = $10^{-(4+m/8)}$, $m = 0, 1, \ldots, 24$; atol = rtol; h0 = $10^{-2} \cdot$ rtol for RADAU, RADAU5 and MEBDFDAE. The speed-up factor for PSIDE is 1.72.

REFERENCES

[HLR89] E. Hairer, C. Lubich, and M. Roche. *The Numerical Solution of Differential-Algebraic Systems by Runge–Kutta Methods*. Lecture Notes in Mathematics 1409. Springer-Verlag, 1989.

[RRS89] P. Rentrop, M. Roche, and G. Steinebach. The application of Rosenbrock-Wanner type methods with stepsize control in differential-algebraic equations. *Numer. Math.*, 55:545–563, 1989.

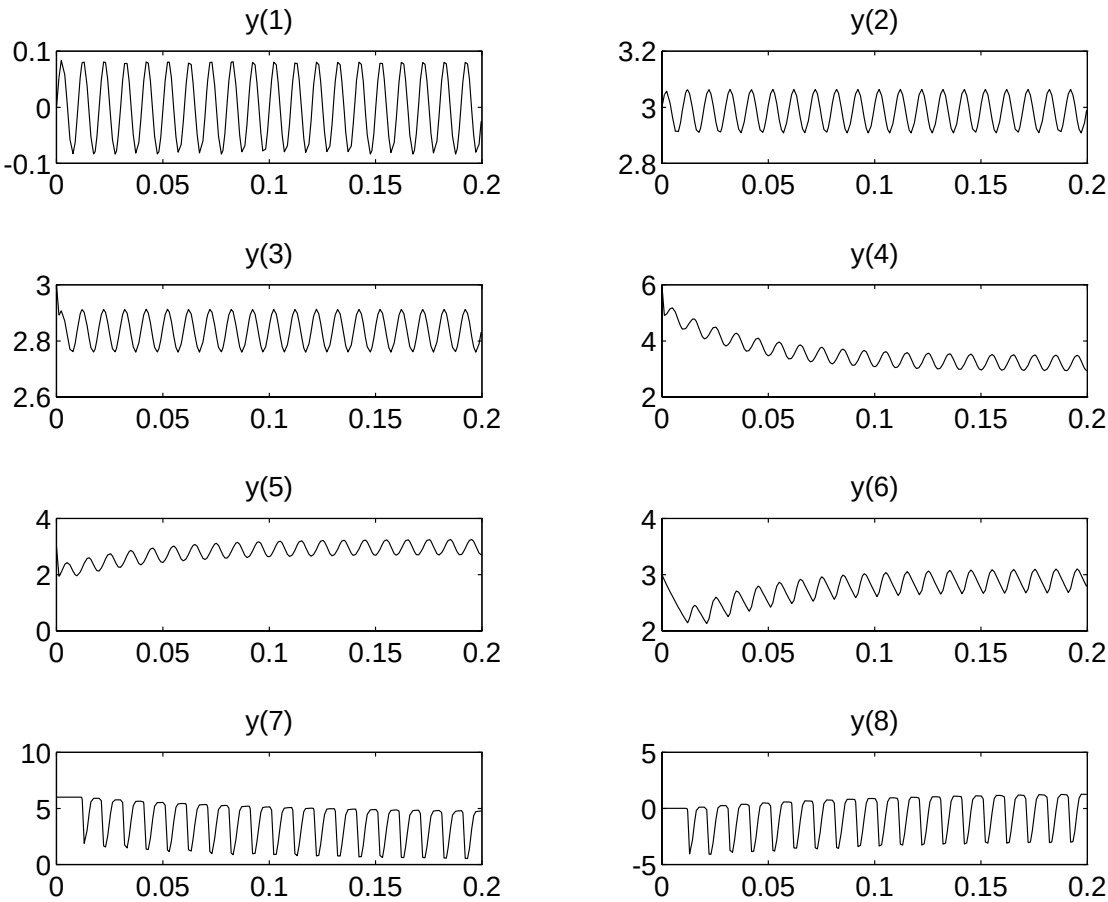

FIGURE 6.3: *Behavior of the solution over the integration interval.*

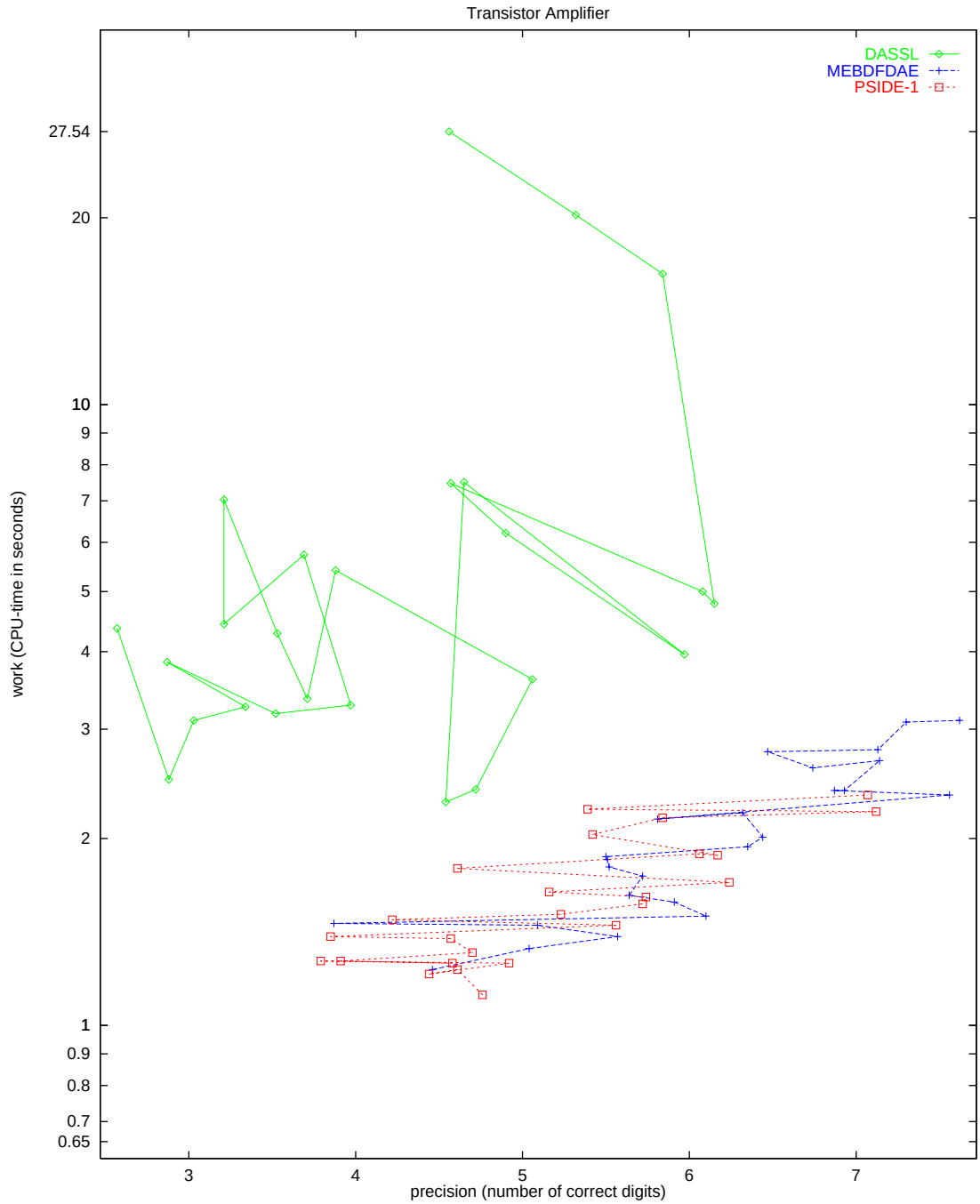

FIGURE 6.4: *Work-precision diagram.*

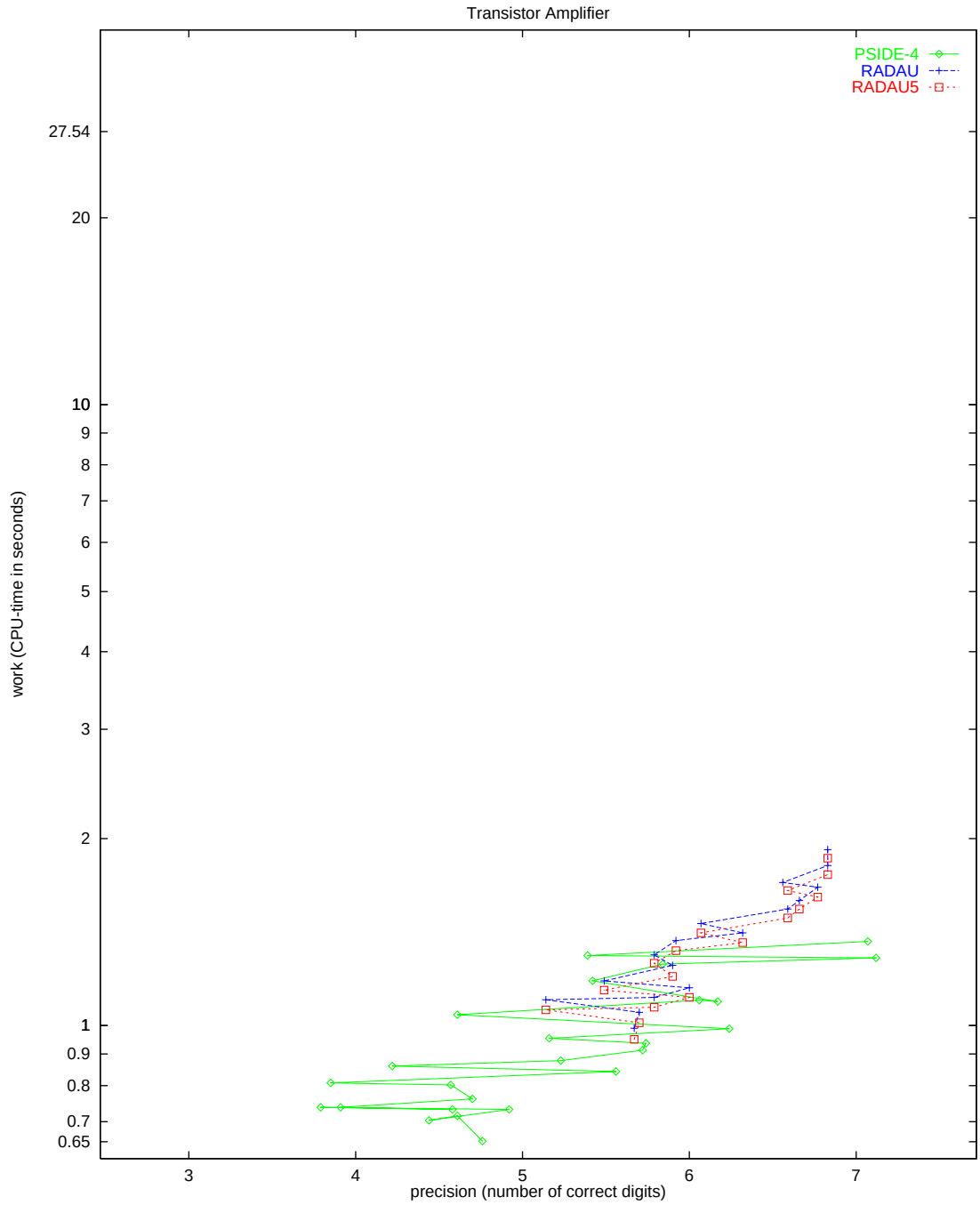

FIGURE 6.5: *Work-precision diagram.*

7. Medical Akzo Nobel problem

7.1 General information

The problem consists of 2 partial differential equations. Semi-discretization of this system yields a stiff ODE. The parallel-IVP-algorithm group of CWI contributed this problem to the test set in collaboration with R. van der Hout from Akzo Nobel Central Research.

7.2 Mathematical description of the problem

The problem is of the form

$$\frac{\mathrm{d}y}{\mathrm{d}t} = f(t,y), \quad y(0) = g, \tag{7.1}$$

with

$$y \in \mathbb{R}^{2N}, \quad 0 \le t \le 20.$$

Here, the integer N is a user-supplied parameter. The function f is given by

$$\begin{aligned} f_{2j-1} &= \alpha_j \frac{y_{2j+1} - y_{2j-3}}{2\Delta\zeta} + \beta_j \frac{y_{2j-3} - 2y_{2j-1} + y_{2j+1}}{(\Delta\zeta)^2} - k\, y_{2j-1} y_{2j}, \\ f_{2j} &= -k\, y_{2j} y_{2j-1}, \end{aligned}$$

where

$$\begin{aligned} \alpha_j &= \frac{2(j\Delta\zeta - 1)^3}{c^2}, \\ \beta_j &= \frac{(j\Delta\zeta - 1)^4}{c^2}. \end{aligned}$$

Here, j ranges from 1 to N, $\Delta\zeta = \frac{1}{N}$, $y_{-1}(t) = \phi(t)$, $y_{2N+1} = y_{2N-1}$ and $g \in \mathbb{R}^{2N}$ is given by

$$g = (0, v_0, 0, v_0, \ldots, 0, v_0)^{\mathrm{T}}.$$

The function ϕ is given by

$$\phi(t) = \begin{cases} 2 & \text{for} \quad t \in (0,5], \\ 0 & \text{for} \quad t \in (5,20]. \end{cases}$$

which means that f undergoes a discontinuity in time at $t = 5$. Suitable values for the parameters k, v_0 and c are 100, 1 and 4, respectively.

7.3 Origin of the problem

The Akzo Nobel research laboratories formulated this problem in their study of the penetration of radio-labeled antibodies into a tissue that has been infected by a tumor [Hou94]. This study was carried out for diagnostic as well as therapeutic purposes.

Let us consider a reaction diffusion system in one spatial dimension:

$$\frac{\partial u}{\partial t} = \frac{\partial^2 u}{\partial x^2} - kuv, \tag{7.2}$$

$$\frac{\partial v}{\partial t} = -kuv, \tag{7.3}$$

which originates from the chemical reaction

$$A + B \xrightarrow{k} C.$$

Here A, the radio-labeled antibody, reacts with substrate B, the tissue with the tumor, and k denotes the rate constant. The concentrations of A and B are denoted by u and v, respectively. In the derivation of the equations (7.2) and (7.3) it was assumed that the reaction is governed by mass action kinetics and in addition that the chemical A is mobile while B is immobile.

Consider a clean semi-infinite slab, in which the substrate B is uniformly distributed. When the slab is exposed at its surface to the chemical A, this chemical starts to penetrate into the slab.

To model this penetration, the equations (7.2) and (7.3) are considered in the strip

$$S_T = \{(x,t) : 0 < x < \infty,\ 0 < t < T\} \quad \text{for some } T,$$

along with the following initial and boundary conditions:

$$u(x,0) = 0, \quad v(x,0) = v_0 \quad \text{for } x > 0,$$

where v_0 is a constant, and

$$u(0,t) = \phi(t) \quad \text{for } 0 < t < T.$$

In order to solve the problem numerically, we transform the variable x in such a way that the semi-infinite slab is transformed into a finite one. A suitable transformation is provided by the following special family of Möbius transformations:

$$\zeta = \frac{x}{x+c}, \quad \text{with } c > 0.$$

Each transformation in this class transforms S_T into the slab:

$$\{(\zeta,t) : 0 < \zeta < 1,\ 0 < t < T\}.$$

In terms of ζ the problem now reads:

$$\frac{\partial u}{\partial t} = \frac{(\zeta-1)^4}{c^2}\frac{\partial^2 u}{\partial \zeta^2} + \frac{2(\zeta-1)^3}{c^2}\frac{\partial u}{\partial \zeta} - kuv, \tag{7.4}$$

$$\frac{\partial v}{\partial t} = -kuv, \tag{7.5}$$

with initial conditions

$$u(\zeta,0) = 0, \quad v(\zeta,0) = v_0 \quad \text{for } \zeta > 0, \tag{7.6}$$

and boundary conditions

$$u(0,t) = \phi(t), \quad \frac{\partial u}{\partial \zeta}(1,t) = 0 \quad \text{for } 0 < t < T. \tag{7.7}$$

The last boundary condition is derived from $\frac{\partial u}{\partial x}(\infty,t) = 0$.

The system consisting of (7.4), (7.5), (7.6) and (7.7) will be written as a system of ordinary differential equations by using the method of lines, i.e. by discretizing the spatial derivatives. We use the uniform grid $\{\zeta_j\}_{j=1,\ldots,N}$ defined by:

$$\zeta_j = j \cdot \Delta\zeta, \quad j = 1,\ldots,N, \quad \Delta\zeta = \frac{1}{N}.$$

Let u_j and v_j denote the approximations of $u(\zeta_j,t)$ and $v(\zeta_j,t)$, respectively. Obviously, u_j and v_j are functions of t. In terms of the function u_j, our choices for the discretization of the spatial first and second order derivatives read

$$\frac{\partial u_j}{\partial \zeta} = \frac{u_{j+1} - u_{j-1}}{2\Delta\zeta} \quad \text{and} \quad \frac{\partial^2 u_j}{\partial \zeta^2} = \frac{u_{j-1} - 2u_j + u_{j+1}}{(\Delta\zeta)^2},$$

respectively, where $j = 1, \ldots, N$. Suitable values for u_0 and u_{N+1} are obtained from the boundary conditions. They are given by $u_0 = \phi(t)$ and $u_{N+1} = u_N$.

Defining $y(t)$ by $y = (u_1, v_1, u_2, v_2, \ldots, u_N, v_N)^{\mathrm{T}}$, and choosing $T = 20$, this semi-discretized problem is precisely the ODE (7.1).

To give an idea of the solution to the PDE (7.4)–(7.7), Figure 7.1 plots u and v as function of x and t. We nicely see that injection of chemical A (locally) destroys B.

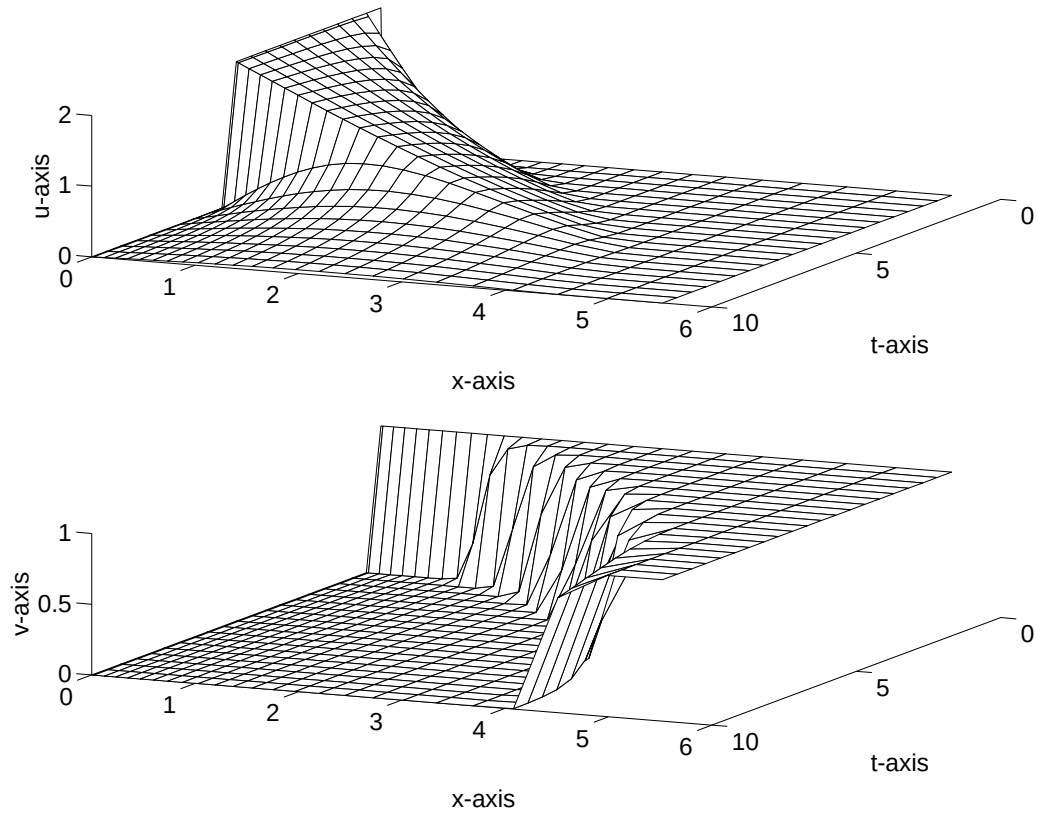

FIGURE 7.1: *u and v as function of time and space.*

7.4 Numerical solution of the problem

The numerical experiments were done for the case $N = 200$. In Table 7.1 we give the value of some components of the reference solution at the end of the integration interval. These components correspond to the values of u and v in $x = 1$, 2.4, 4.0 and 6.0. For the complete reference solution we refer to the Fortran subroutine `solut`. Figure 7.2 plots the behavior of the solution components y_i for $i \in \{79, 80, 133, 134, 171, 172, 199, 200\}$, which correspond to approximations of the PDE solutions u and v on the grid lines $x = 1$, 2, 3 and 4. Table 7.2 and Figures 7.3–7.4 show the run characteristics, and the work-precision diagrams, respectively. The reference solution was computed on the Cray C90, using PSIDE with Cray double precision and atol = rtol = 10^{-10}. For the work-precision diagrams, we used: rtol = $10^{-(4+m/8)}$, $m = 0, 1, \ldots, 24$; atol = rtol; h0 = $10^{-5} \cdot$ rtol for RADAU, RADAU5 and MEBDFDAE. Since some solution components are zero, all scd values presented here denote absolute precision. The speed-up factor for PSIDE is 2.91.

REFERENCES

[Hou94] R. van der Hout, 1994. Private communication.

TABLE 7.1: *Reference solution at the end of the integration interval.*

y_{79}	$0.2339942217046434 \cdot 10^{-3}$	y_{199}	$0.11737412926802 \cdot 10^{-3}$
y_{80}	$-0.1127916494884468 \cdot 10^{-141}$	y_{200}	$0.61908071460151 \cdot 10^{-5}$
y_{149}	$0.3595616017506735 \cdot 10^{-3}$	y_{239}	$0.68600948191191 \cdot 10^{-11}$
y_{150}	$0.1649638439865233 \cdot 10^{-86}$	y_{240}	0.99999973258552

TABLE 7.2: *Run characteristics.*

solver	rtol	atol	h0	scd	steps	accept	# f	# Jac	# LU	CPU
DASSL	10^{-4}	10^{-4}		3.37	367	362	545	47		4.34
	10^{-7}	10^{-7}		6.36	1387	1380	1840	58		15.37
MEBDFDAE	10^{-4}	10^{-4}	10^{-9}	4.08	365	352	564	68	68	6.20
	10^{-7}	10^{-7}	10^{-12}	6.45	862	839	1266	111	111	16.00
PSIDE-1	10^{-4}	10^{-4}		5.00	118	83	1263	34	456	6.77
	10^{-7}	10^{-7}		7.12	159	145	2838	109	624	13.65
RADAU	10^{-4}	10^{-4}	10^{-9}	3.82	93	93	747	60	93	3.29
	10^{-7}	10^{-7}	10^{-12}	6.92	100	100	1807	58	100	8.10
RADAU5	10^{-4}	10^{-4}	10^{-9}	3.82	93	93	747	60	93	3.25
	10^{-7}	10^{-7}	10^{-12}	6.52	256	256	1885	174	223	8.19
VODE	10^{-4}	10^{-4}		2.84	364	359	506	10	62	2.41
	10^{-7}	10^{-7}		5.61	1036	1023	1217	19	101	6.14

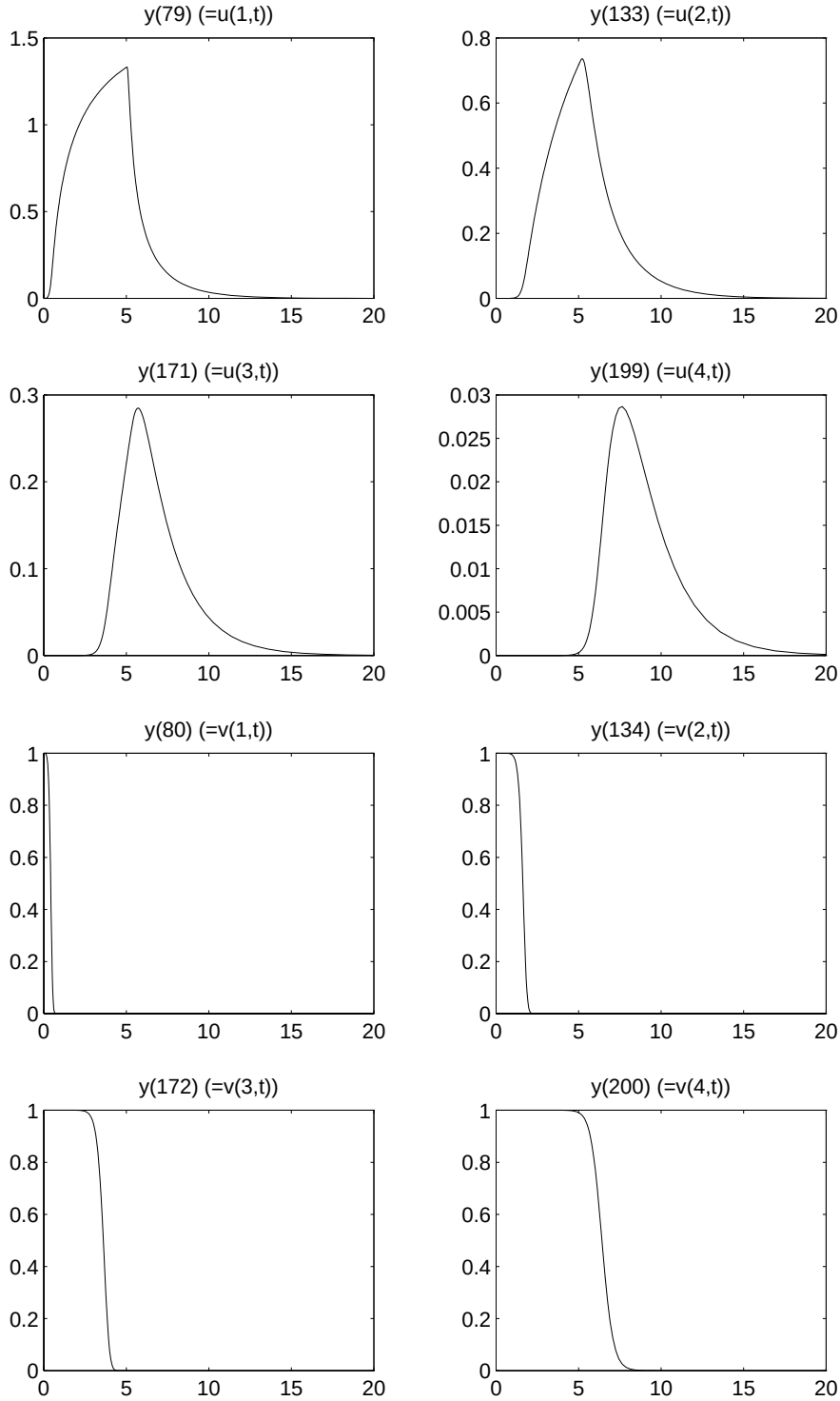

FIGURE 7.2: *Behavior of some solution components over the integration interval.*

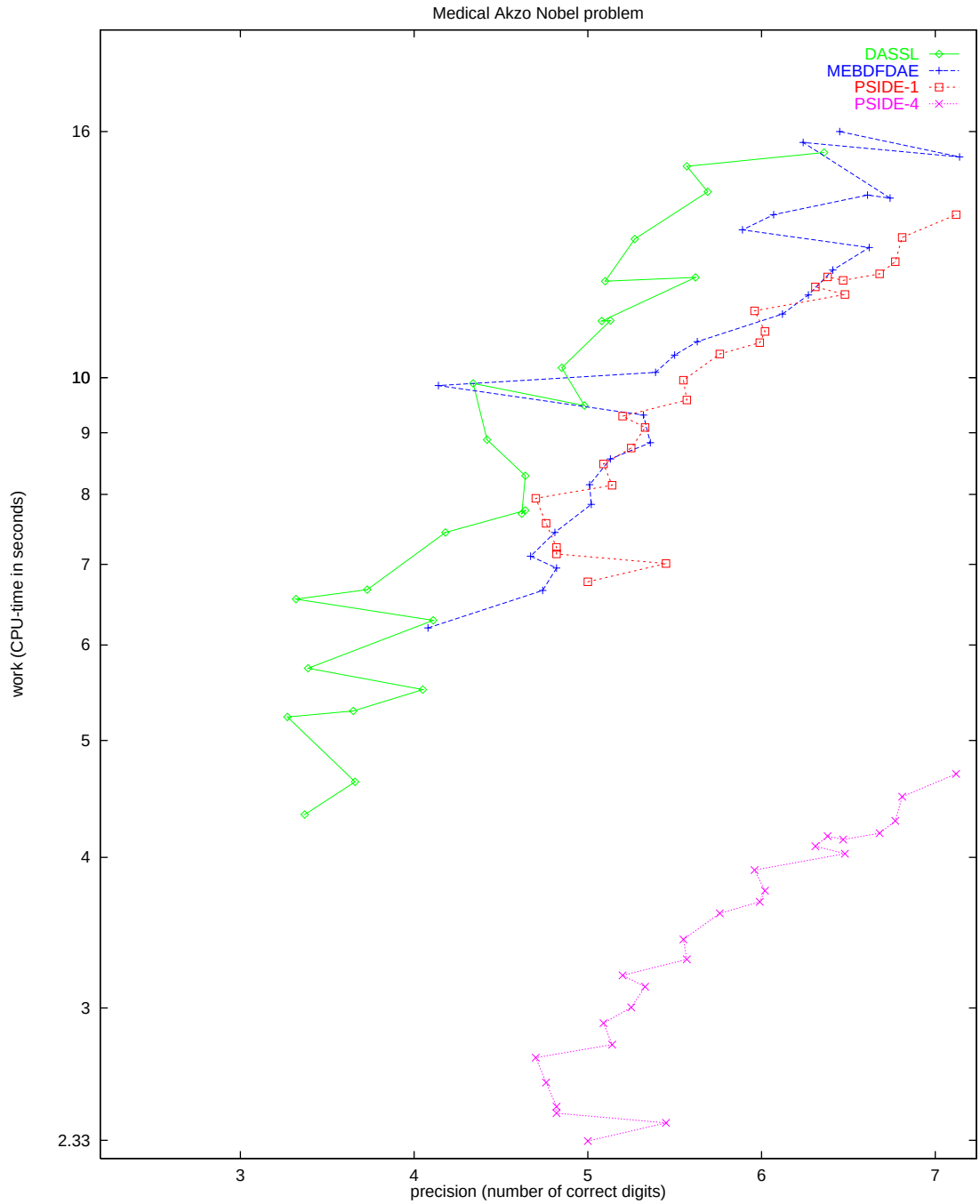

FIGURE 7.3: *Work-precision diagram.*

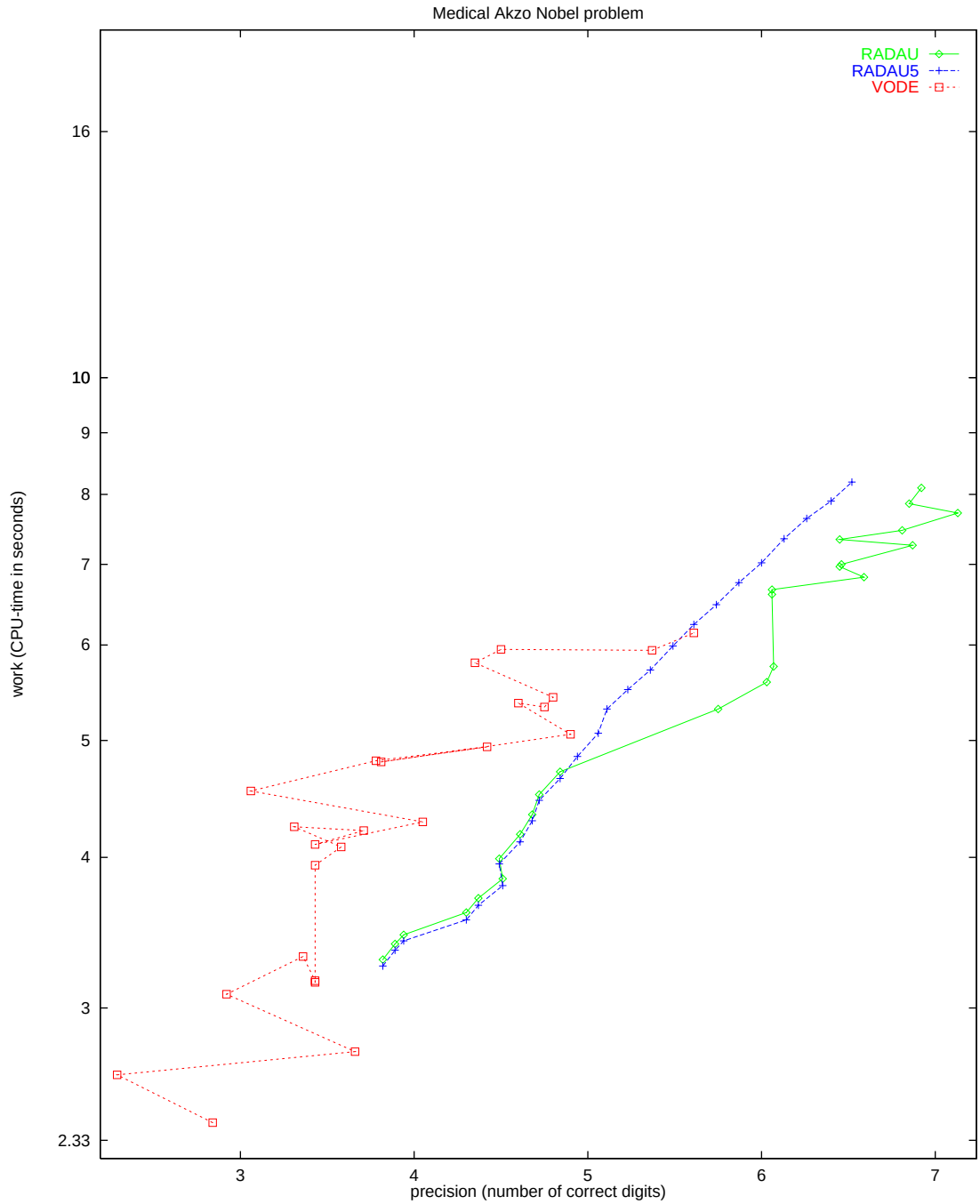

FIGURE 7.4: *Work-precision diagram.*

8. EMEP problem

8.1 General information

The problem is a stiff system of 66 ordinary differential equations. The 'Mathematics and the Environment' project group at CWI contributed this problem to the test set.

8.2 Mathematical description of the problem

The problem is of the form

$$\frac{\mathrm{d}y}{\mathrm{d}t} = f(t,y), \quad y(0) = g,$$

with

$$y \in \mathbb{R}^{66}, \quad 14400 \le t \le 417600.$$

The initial vector $g = (g_i)$ is given by

$$g_i = \begin{cases} 1.0 \cdot 10^{9} & \text{for} \quad i = 1, \\ 5.0 \cdot 10^{9} & \text{for} \quad i \in \{2,3\}, \\ 3.8 \cdot 10^{12} & \text{for} \quad i = 4, \\ 3.5 \cdot 10^{13} & \text{for} \quad i = 5, \\ 1.0 \cdot 10^{7} & \text{for} \quad i \in \{6,7,\ldots,13\}, \\ 5.0 \cdot 10^{11} & \text{for} \quad i = 14, \\ 1.0 \cdot 10^{2} & \text{for} \quad i \in \{15,16,\ldots,37\}, \\ 1.0 \cdot 10^{-3} & \text{for} \quad i = 38, \\ 1.0 \cdot 10^{2} & \text{for} \quad i \in \{39,40,\ldots,66\}. \end{cases}$$

The function f has discontinuities in time at $t = 3600(4{+}24i)$ and $t = 3600(-4{+}24i)$ for $i = 1,2,3,4,5$. Since f is too voluminous to be described here, we refer to the Fortran subroutine `feval` and to [VS94] to get more insight in the function.

8.3 Origin of the problem

The problem is the chemistry part of the EMEP MSC-W ozone chemistry model, which is in development at the Norwegian Meteorological Institute in Oslo, Norway. About 140 reactions with a total of 66 species are involved. Below we give the correspondence between the solution vector y and the chemical species.

$y = ($ NO, NO2, SO2, CO, CH4, C2H6,
NC4H10, C2H4, C3H6, OXYL, HCHO, CH3CHO,
MEK, O3, HO2, HNO3, H2O2, H2,
CH3O2, C2H5OH, SA, CH3O2H, C2H5O2, CH3COO,
PAN, SECC4H, MEKO2, R2OOH, ETRO2, MGLYOX,
PRRO2, GLYOX, OXYO2, MAL, MALO2, OP,
OH, OD, NO3, N2O5, ISOPRE, NITRAT,
ISRO2, MVK, MVKO2, CH3OH, RCO3H, OXYO2H,
BURO2H, ETRO2H, PRRO2H, MEKO2H, MALO2H, MACR,
ISNI, ISRO2H, MARO2, MAPAN, CH2CCH3, ISONO3,
ISNIR, MVKO2H, CH2CHR, ISNO3H, ISNIRH, MARO2H $)^{\mathrm{T}}$.

The integration interval covers 112 hours. Rate coefficients are often variable. Some of them undergo a discontinuity at sunrise and sunset, which correspond to $t = 3600(\pm 4 + 24i)$, respectively, for $i = 1,2,3,4,5$. The unit of the species is number of molecules per cm^3, the time t is in seconds. The test problem corresponds to the rural case in [VS94]. From the plot of O3 versus time in Figure 8.1 we see that in this model the ozone concentration steadily grows over the integration interval. A more elaborate description of the model can be found in [VS94], [Sim93] and [SASJ93].

TABLE 8.1: *Reference solution at the end of the integration interval.*

NO	$=0.25645805093601 \cdot 10^{8}$	CH4	$=0.34592853260350 \cdot 10^{14}$
NO2	$=0.51461347708556 \cdot 10^{11}$	O3	$=0.31503085853931 \cdot 10^{13}$
SO2	$=0.23156799577319 \cdot 10^{12}$	N2O5	$=0.76845966195032 \cdot 10^{9}$

TABLE 8.2: *Run characteristics.*

solver	rtol	atol	h0	scd	steps	accept	# f	# Jac	# LU	CPU
DASSL	10^{-2}	1		1.79	714	677	1309	167		5.40
	10^{-4}	1		3.46	1983	1928	3375	252		12.06
	10^{-6}	1		5.00	4135	4013	6491	398		22.81
MEBDFDAE	10^{-2}	1	10^{-7}	1.93	707	653	1576	138	138	6.92
	10^{-4}	1	10^{-7}	2.89	1480	1406	2939	239	239	13.70
	10^{-6}	1	10^{-7}	5.28	2922	2760	5361	450	450	26.78
PSIDE-1	10^{-2}	1		2.39	490	438	6954	175	1908	37.24
	10^{-4}	1		2.29	509	447	9241	213	1980	42.72
	10^{-6}	1		3.95	769	650	15861	335	2716	64.95
RADAU	10^{-2}	1	10^{-7}	2.57	398	325	3510	224	398	25.74
	10^{-4}	1	10^{-7}	2.68	542	492	4815	377	542	35.44
	10^{-6}	1	10^{-7}	3.60	463	390	10241	281	463	59.18
RADAU5	10^{-2}	1	10^{-7}	2.57	398	325	3510	224	395	25.51
	10^{-4}	1	10^{-7}	2.68	542	492	4815	377	537	35.09
	10^{-6}	1	10^{-7}	4.43	965	905	8026	760	930	60.47
VODE	10^{-2}	1		0.61	879	854	1416	61	254	6.15
	10^{-4}	1		2.33	2180	2081	3339	64	386	11.86
	10^{-6}	1		4.56	4270	4048	6011	80	637	21.04

8.4 Numerical solution of the problem

Table 8.1 and Figure 8.1 present the the value of reference solution at the end of the integration interval $t = 417600$ and the behavior of the solution over the integration interval of the components of y corresponding to NO, NO2, SO2, CH4, O3 and N2O5 (i.e. y_1, y_2, y_3, y_5, y_{14} and y_{40}). For the complete reference solution at the end of the integration interval we refer to the Fortran subroutine `solut`. The values at the horizontal axis in Figure 8.1 denote the time t in hours modulo 24 hours. Table 8.2 and Figures 8.2–8.3 contain the run characteristics and the work-precision diagrams, respectively. Since components y_{36} and y_{38} are relatively very small and physically unimportant, we did not include these components in the computation of the scd value. The reference solution was computed using RADAU5 with rtol $= 10^{-12}$, atol $= 1$, h0 $= 10^{-10}$, and a maximal stepsize of 10. For the work-precision diagrams, we used: rtol $= 10^{-(2+m/4)}$, $m = 0, 1, \ldots, 32$; atol $= 1$ and h0 $= 10^{-7}$ for RADAU, RADAU5 and MEBDFDAE. The speed-up factor for PSIDE is 3.26.

REFERENCES

[SASJ93] D. Simpson, Y. Andersson-Skold, and M.E. Jenkin. Updating the chemical scheme for the EMEP MSC-W model: Current status. Report EMEP MSC-W Note 2/93, The Norwegian Meteorological Institute, Oslo, 1993.

[Sim93] D. Simpson. Photochemical model calculations over Europe for two extended summer periods: 1985 and 1989. model results and comparisons with observations. *Atmospheric Envi-*

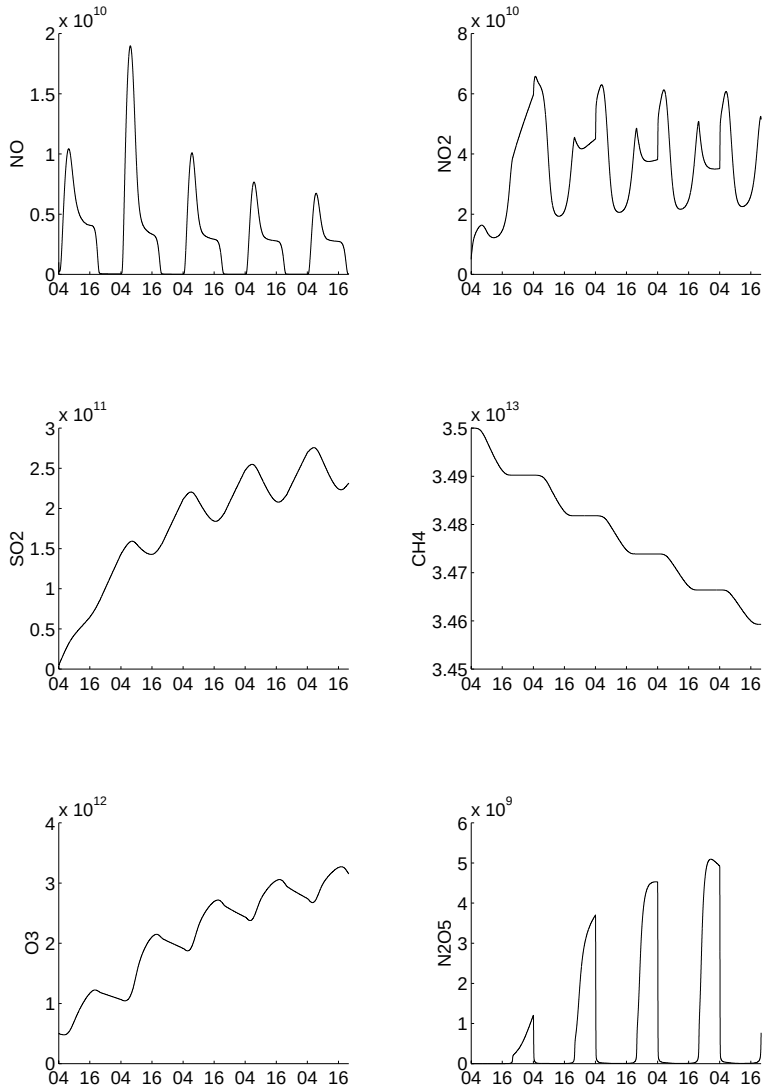

FIGURE 8.1: *Behavior of the solution over the integration interval.*

ronment, 27A:921–943, 1993.

[VS94] J.G. Verwer and D. Simpson. Explicit methods for stiff ODEs from atmospheric chemistry. Report NM-R9409, CWI, Amsterdam, 1994.

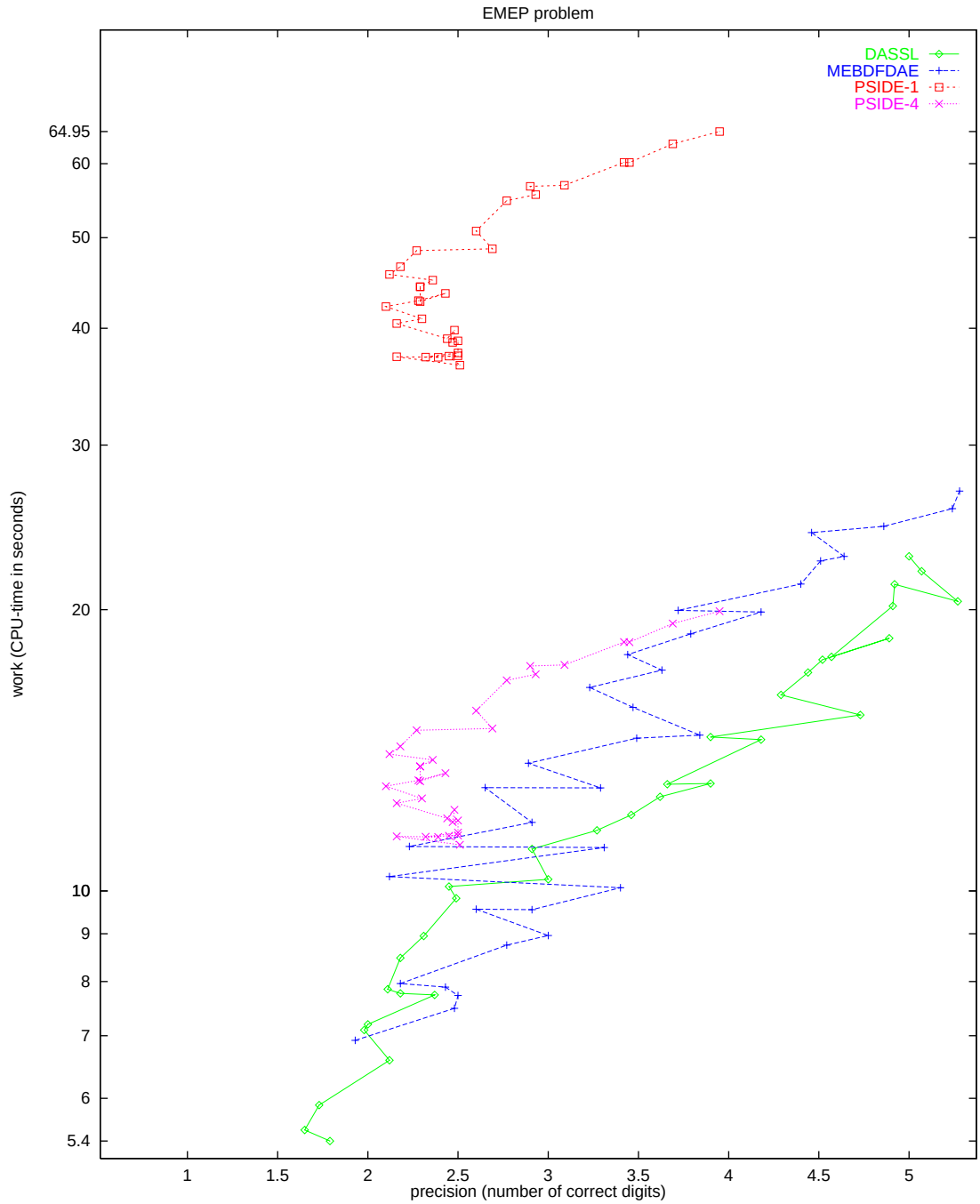

FIGURE 8.2: *Work-precision diagram.*

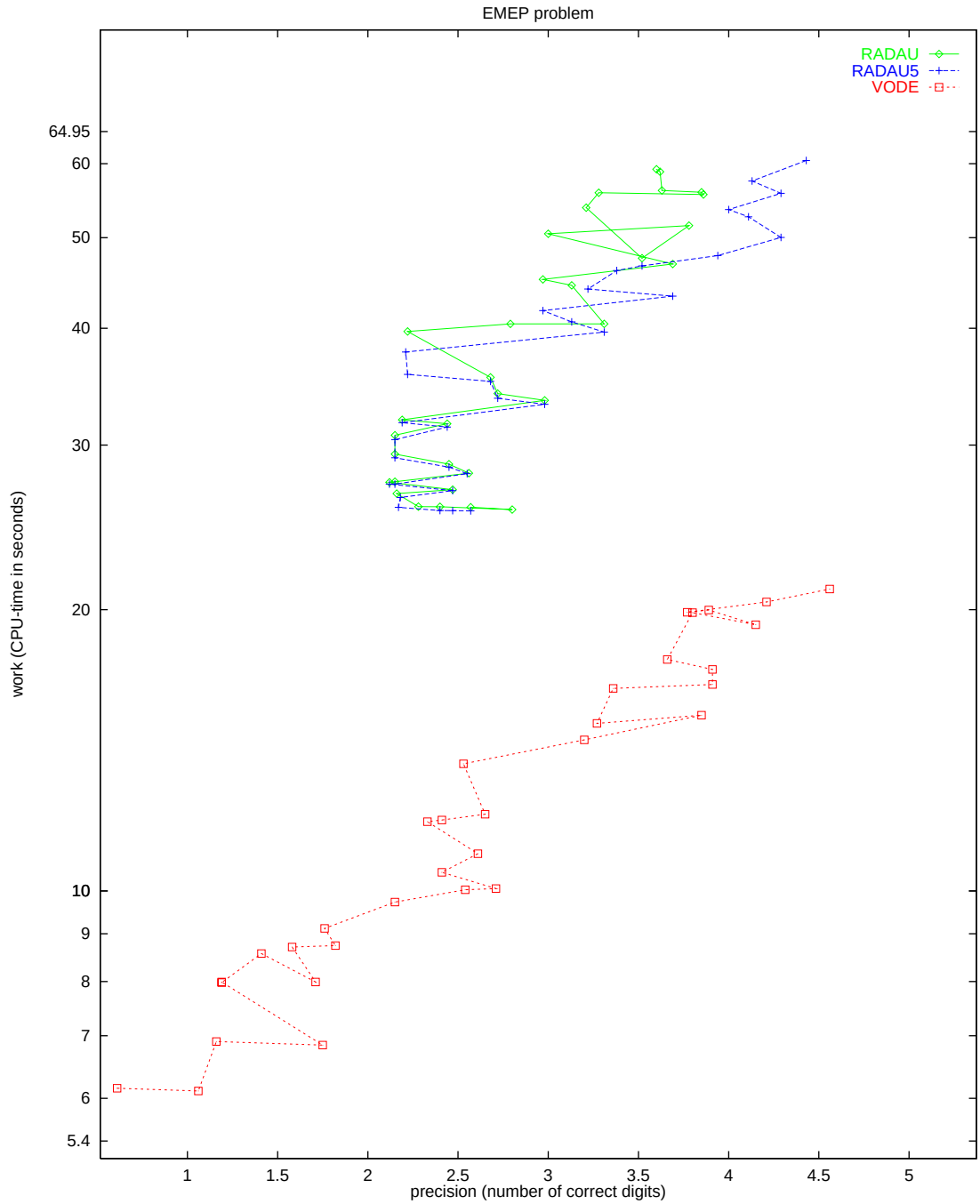

FIGURE 8.3: *Work-precision diagram.*

9. NAND GATE

9.1 General information

The problem is a system of 14 stiff IDEs of index 1. It has been contributed by Michael Günther and Peter Rentrop [GR96].

9.2 Mathematical description of the problem

The problem is of the form:

$$C(y(t))\,\frac{\mathrm{d}y}{\mathrm{d}t} \;=\; f(t,y(t)), \qquad y(0)=y_0, \quad y'(0)=y_0' \tag{9.1}$$

with

$$y\in \mathbb{R}^{14}, \qquad 0\le t\le 80.$$

The equations are given by:

$$C_{GS}\cdot(\dot y_5-\dot y_1) = i^D_{DS}(y_2-y_1,y_5-y_1,y_3-y_5,y_5-y_2,y_4-V_{DD}) + \frac{y_1-y_5}{R_{GS}} \tag{9.2}$$

$$C_{GD}\cdot(\dot y_5-\dot y_2) = -i^D_{DS}(y_2-y_1,y_5-y_1,y_3-y_5,y_5-y_2,y_4-V_{DD}) + \frac{y_2-V_{DD}}{R_{GD}}, \tag{9.3}$$

$$C_{BS}(y_3-y_5)\cdot(\dot y_5-\dot y_3) = \frac{y_3-V_{BB}}{R_{BS}} - i^D_{BS}(y_3-y_5), \tag{9.4}$$

$$C_{BD}(y_4-V_{DD})\cdot(-\dot y_4) = \frac{y_4-V_{BB}}{R_{BD}} - i^D_{BD}(y_4-V_{DD}), \tag{9.5}$$

$$\begin{aligned} &C_{GS}\cdot\dot y_1 + C_{GD}\cdot\dot y_2 + C_{BS}(y_3-y_5)\cdot\dot y_3 - (C_{GS}+C_{GD}+C_{BS}(y_3-y_5)+C_5)\cdot\dot y_5 \\ &\quad -C_{BD}(y_9-y_5)\cdot(\dot y_5-\dot y_9) \;=\; \tfrac{y_5-y_1}{R_{GS}} + i^D_{BS}(y_3-y_5) + \tfrac{y_5-y_7}{R_{GD}} + i^E_{BD}(y_9-y_5), \end{aligned} \tag{9.6}$$

$$C_{GS}\cdot\dot y_6 = -i^E_{DS}(y_7-y_6,V_1(t)-y_6,y_8-y_{10},V_1(t)-y_7,y_9-y_5) + C_{GS}\cdot\dot V_1(t) - \frac{y_6-y_{10}}{R_{GS}}, \tag{9.7}$$

$$C_{GD}\cdot\dot y_7 = i^E_{DS}(y_7-y_6,V_1(t)-y_6,y_8-y_{10},V_1(t)-y_7,y_9-y_5) + C_{GD}\cdot\dot V_1(t) - \frac{y_7-y_5}{R_{GD}}, \tag{9.8}$$

$$C_{BS}(y_8-y_{10})\cdot(\dot y_8-\dot y_{10}) = -\frac{y_8-V_{BB}}{R_{BS}} + i^E_{BS}(y_8-y_{10}), \tag{9.9}$$

$$C_{BD}(y_9-y_5)\cdot(\dot y_9-\dot y_5) = -\frac{y_9-V_{BB}}{R_{BD}} + i^E_{BD}(y_9-y_5), \tag{9.10}$$

$$\begin{aligned} &C_{BS}(y_8-y_{10})\cdot(\dot y_8-\dot y_{10}) - C_{BD}(y_{14}-y_{10})\cdot(\dot y_{10}-\dot y_{14}) + C_{10}\cdot\dot y_{10} \\ &\quad = \tfrac{y_{10}-y_6}{R_{GS}} + i^E_{BS}(y_8-y_{10}) + \tfrac{y_{10}-y_{12}}{R_{GD}} + i^E_{BD}(y_{14}-y_{10}), \end{aligned} \tag{9.11}$$

$$C_{GS}\cdot\dot{y}_{11} = -i^E_{DS}(y_{12}-y_{11}, V_2(t)-y_{11}, y_{13}, V_2(t)-y_{12}, y_{14}-y_{10}) + C_{GS}\cdot\dot{V}_2(t) - \frac{y_{11}}{R_{GS}}, \quad (9.12)$$

$$C_{GD}\cdot\dot{y}_{12} = i^E_{DS}(y_{12}-y_{11}, V_2(t)-y_{11}, y_{13}, V_2(t)-y_{12}, y_{14}-y_{10}) + C_{GD}\cdot\dot{V}_2(t) - \frac{y_{12}-y_{10}}{R_{GD}}, \quad (9.13)$$

$$C_{BS}(y_{13})\cdot\dot{y}_{13} = -\frac{y_{13}-V_{BB}}{R_{BS}} + i^E_{BS}(y_{13}), \quad (9.14)$$

$$C_{BD}(y_{14}-y_{10})\cdot(\dot{y}_{14}-\dot{y}_{10}) = -\frac{y_{14}-V_{BB}}{R_{BS}} + i^E_{BD}(y_{14}-y_{10}). \quad (9.15)$$

The functions C_{BD} and C_{BS} read

$$C_{BD}(U) = C_{BS}(U) = \begin{cases} C_0\cdot\left(1-\frac{U}{\phi_B}\right)^{-\frac{1}{2}} & \text{for} \quad U\le 0, \\ C_0\cdot\left(1+\frac{U}{2\cdot\phi_B}\right) & \text{for} \quad U>0 \end{cases}$$

with $C_0 = 0.24\cdot 10^{-4}$ and $\phi_B = 0.87$.

The functions i^D_{BS} and i^E_{BS} have the same form denoted by i_{BS}. The only difference between them is that the constants used in i_{BS} depend on the superscript D and E. The same holds for the functions $i^{D/E}_{BD}$ and $i^{D/E}_{DS}$. The functions i_{BS}, i_{BD} and i_{DS} are defined by

$$i_{BS}(U_{BS}) = \begin{cases} -i_S\cdot\left(\exp(\frac{U_{BS}}{U_T})-1\right) & \text{for} \quad U_{BS}\le 0, \\ 0 & \text{for} \quad U_{BS}>0, \end{cases}$$

$$i_{BD}(U_{BD}) = \begin{cases} -i_S\cdot\left(\exp(\frac{U_{BD}}{U_T})-1\right) & \text{for} \quad U_{BD}\le 0, \\ 0 & \text{for} \quad U_{BD}>0, \end{cases}$$

$$i_{DS}(U_{DS},U_{GS},U_{BS},U_{GD},U_{BD}) = \begin{cases} GDS_+(U_{DS},U_{GS},U_{BS}) & \text{for} \quad U_{DS}>0, \\ 0 & \text{for} \quad U_{DS}=0, \\ GDS_-(U_{DS},U_{GD},U_{BD}) & \text{for} \quad U_{DS}<0, \end{cases}$$

where

$$GDS_+(U_{DS},U_{GS},U_{BS}) =$$

$$\begin{cases} 0 & \text{for} \quad U_{GS}-U_{TE}\le 0, \\ -\beta\cdot(1+\delta\cdot U_{DS})\cdot(U_{GS}-U_{TE})^2 & \text{for} \quad 0<U_{GS}-U_{TE}\le U_{DS}, \\ -\beta\cdot U_{DS}\cdot(1+\delta\cdot U_{DS})\cdot(2\cdot(U_{GS}-U_{TE})-U_{DS}) & \text{for} \quad 0<U_{DS}<U_{GS}-U_{TE}, \end{cases}$$

with

$$U_{TE} = U_{T0} + \gamma\cdot\left(\sqrt{\Phi-U_{BS}}-\sqrt{\Phi}\right), \quad (9.16)$$

and

$$GDS_-(U_{DS},U_{GD},U_{BD}) =$$

$$\begin{cases} 0 & \text{for} \quad U_{GD}-U_{TE}\le 0, \\ \beta\cdot(1-\delta\cdot U_{DS})\cdot(U_{GD}-U_{TE})^2 & \text{for} \quad 0<U_{GD}-U_{TE}\le -U_{DS}, \\ -\beta\cdot U_{DS}\cdot(1-\delta\cdot U_{DS})\cdot(2\cdot(U_{GD}-U_{TE})+U_{DS}) & \text{for} \quad 0<-U_{DS}<U_{GD}-U_{TE}, \end{cases}$$

TABLE 9.1: *Dependence of constants on D and E for i_{BS}, i_{BD} and i_{DS}.*

	E	D
i_S	10^{-14}	10^{-14}
U_T	25.85	25.85
U_{T0}	0.2	-2.43

	E	D
β	$1.748 \cdot 10^{-3}$	$5.35 \cdot 10^{-4}$
γ	0.035	0.2
δ	0.02	0.02
Φ	1.01	1.28

with

$$U_{TE} = U_{T0} + \gamma \cdot \left(\sqrt{\Phi - U_{BD}} - \sqrt{\Phi} \right). \tag{9.17}$$

The constants used in the definition of i_{BS}, i_{BD} and i_{DS} carry a superscript D or E. Using for example the constants with superscript E in the functions i_{BS} yields the function i_{BS}^E. These constants are shown in Table 9.1. The other constants are given by

$$\begin{aligned} V_{BB} &= -2.5, \\ V_{DD} &= 5, \\ C_5 &= C_{10} = 0.5 \cdot 10^{-4}, \\ R_{GS} &= R_{GD} = 4, \\ R_{BS} &= R_{BD} = 10, \\ C_{GS} &= C_{GD} = 0.6 \cdot 10^{-4}. \end{aligned}$$

The functions $V_1(t)$ and $V_2(t)$ are

$$V_1(t) = \begin{cases} 20 - tm & \text{if} \quad 15 < tm \le 20, \\ 5 & \text{if} \quad 10 < tm \le 15, \\ tm - 5 & \text{if} \quad 5 < tm \le 10, \\ 0 & \text{if} \quad tm \le 5, \end{cases}$$

with $tm = t \bmod 20$ and

$$V_2(t) = \begin{cases} 40 - tm & \text{if} \quad 35 < tm \le 40, \\ 5 & \text{if} \quad 20 < tm \le 35, \\ tm - 15 & \text{if} \quad 15 < tm \le 20, \\ 0 & \text{if} \quad tm \le 15, \end{cases}$$

with $tm = t \bmod 40$. From these definitions for $V_1(t)$ and $V_2(t)$ we see that the function f in (9.1) has discontinuities in its derivative at $tm = 5, 10, 15, 20$. Therefore, we restart the solvers at $t = 5, 10, \ldots, 75$.

Consistent initial values are given by $y_0' = 0$ and

$$\begin{aligned} &y_1 = y_2 = y_5 = y_7 = 5.0, \\ &y_3 = y_4 = y_8 = y_9 = y_{13} = y_{14} = V_{BB} = -2.5, \\ &y_6 = y_{10} = y_{12} = 3.62385, \\ &y_{11} = 0. \end{aligned}$$

All components of y are of index 1.

It is clear from Formulas (9.16) and (9.17) that the function f can not be evaluated if one of the values $\Phi - U_{BS}$, $\Phi - U_{BD}$ or Φ becomes negative. To prevent this situation, we set `IERR=-1` in the Fortran subroutine that defines f if this happens. See page *III-vi* of the the description of the software part of the test set for more details on `IERR`.

9.3 Origin of the problem

The NAND gate in Figure 9.1 consists of two n-channel enhancement MOSFETs (ME), one n-channel depletion MOSFET (MD) and two load capacitances C_5 and C_{10}. MOSFETs are special transistors, which have four terminals: the drain, the bulk, the source and the gate, see also Figure 9.3. The drain voltage of MD is constant at $V_{DD} = 5$[V]. The bulk voltages are constantly $V_{BB} = -2.5$[V]. The gate voltages of both enhancement transistors are controlled by two voltage sources V_1 and V_2. Depending

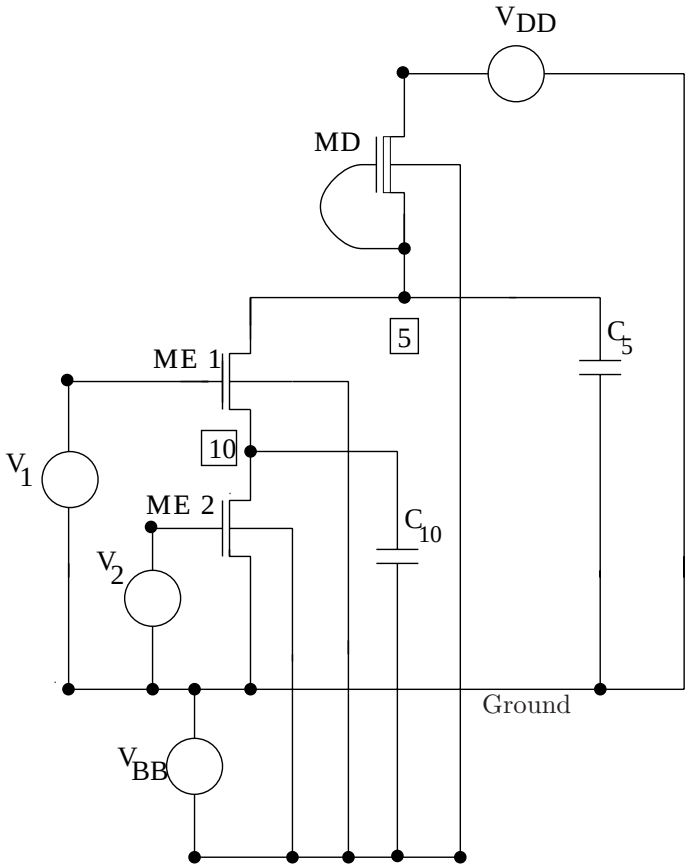

FIGURE 9.1: *Circuit diagram of the NAND gate (taken from [GR96])*

		V2	
		LOW	HIGH
V1	LOW	HIGH	HIGH
	HIGH	HIGH	LOW

FIGURE 9.2: *Response of the NAND gate*

on the input voltages, the NAND gate generates a response at node 5 as shown in Figure 9.2. If we represent the logical values 1 and 0 by high respectively low voltage levels, we see that the NAND gate

executes the *Not AND* operation. This behavior can be explained from Figure 9.1 as follows. Roughly speaking, a transistor acts as a switch between drain and source; it closes if the voltage between gate and source drops below a certain threshold value. The circuit is constructed such that the voltage at node 10 drops to zero unless V_1 is high and V_2 is low, in which case it is approximately 5[V]. This means that as soon either V_1 or V_2 is low, then the corresponding enhancement transistors lock; the voltage at node 5 is high at $V_{DD} = 5$[V] due to MD. If both V_1 and V_2 exceed a given threshold voltage, then a drain current through both enhancement transistors occurs. The MOSFETs open and the voltage at node 5 breaks down. The response is low. In the circuit analysis the three MOSFETs

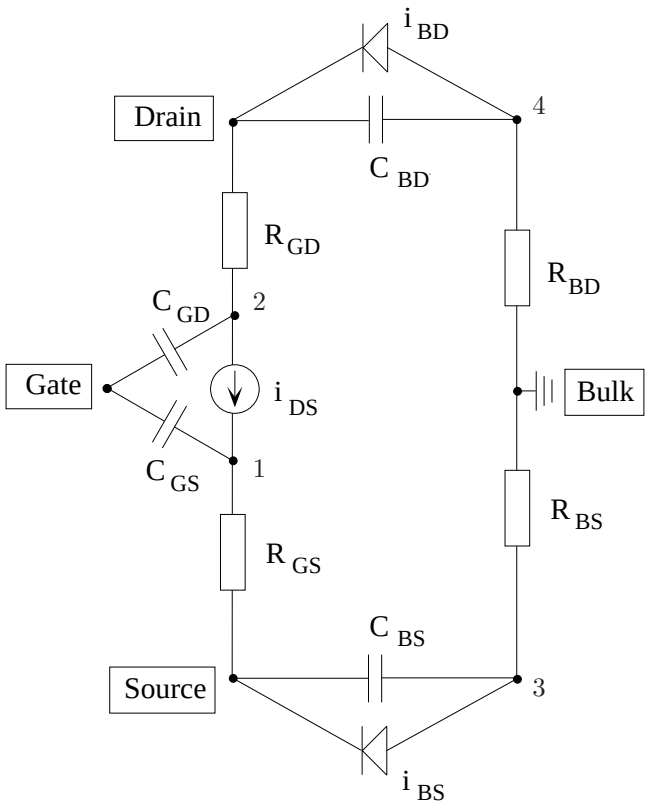

FIGURE 9.3: *Companion model of a MOSFET (taken from [GR96])*

are replaced by the circuit shown in Figure 9.3. Here, the well-known companion model of Shichmann and Hodges [SH68] is used. The characteristics of the circuit elements can differ depending on the MD or ME case. This circuit has four internal nodes indicated by 1, 2, 3 and 4. The static behavior of the transistor is described by the drain current i_{DS}. To include secondary effects, load capacitances like R_{GS}, R_{GD}, R_{BS}, and R_{BD} are introduced. The so-called *pn*-junction between source and bulk is modeled by the diode i_{BS} and the non-linear capacitance C_{BS}. Analogously, i_{BD} and C_{BD} model the *pn*-junction between bulk and drain. Linear gate capacitances C_{GS} and C_{GD} are used to describe the intrinsic charge flow effects roughly.

To formulate the circuit equations, we note that the circuit consists of 14 nodes. These 14 nodes are the nodes 5 and 10 and the 12 internal nodes of the three transistors. For every node a variable is introduced that represents the voltage in that node. Table 9.2 shows the variable–node correspondence.

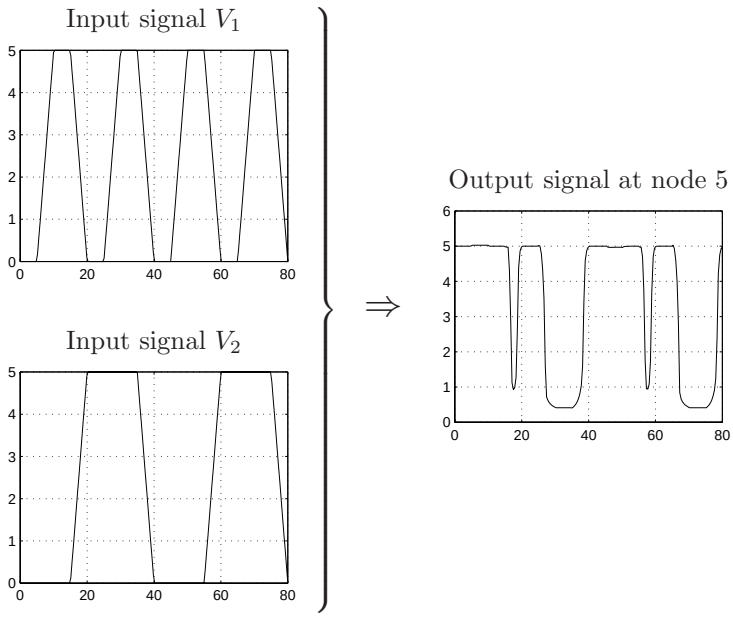

FIGURE 9.4: *Plots of V_1, V_2 and the output of the NAND gate.*

In terms of these voltages the circuit equations are formulated by using the Kirchoff Current Law (KCL) along with the transistor model shown in Figure 9.3. In Figure 9.4, we check the behavior of

TABLE 9.2: *Correspondence between variables and nodes*

variables	nodes
1–4	internal nodes MD-transistor
5	node 5
6–9	internal nodes ME1-transistor
10	node 10
11–14	internal nodes ME2-transistor

the NAND gate by plotting V_1 and V_2 together with the numerical value for the voltage at node 5, which is obtained as y_{10} in §9.4. The picture confirms that the NAND gate produces a high signal in the intervals $[0, 5]$, $[10, 15]$, $[20, 25]$, $[40, 45]$, $[50, 55]$ and $[60, 65]$, whereas the output signal on $[30, 35]$ and $[70, 75]$ is low.

We remark that in this description the unit of time is the nanosecond, while in the report [GR96] the unit of time is the second.

9.4 Numerical solution of the problem

Tables 9.3–9.4 and Figures 9.5–9.6 present the reference solution at the end of the integration interval, the run characteristics, the behavior of the solution over the integration interval and the work-precision diagram, respectively. In computing the scd values, only y_5, the response of the gate at node 5, was considered. The reference solution was computed on the Cray C90, using PSIDE with Cray double precision and atol = rtol = 10^{-16}. For the work-precision diagram, we used: rtol = $10^{-(4+m/8)}$, $m = 0, 1, \ldots, 24$; atol = rtol. The speed-up factor for PSIDE is 1.95.

TABLE 9.3: *Reference solution at the end of the integration interval.*

y_1	$0.4971088699385777 \cdot 10$	y_8	$-0.2500077409198803 \cdot 10$
y_2	$0.4999752103929311 \cdot 10$	y_9	$-0.2499998781491227 \cdot 10$
y_3	$-0.2499998781491227 \cdot 10$	y_{10}	-0.2090289583878100
y_4	$-0.2499999999999975 \cdot 10$	y_{11}	$-0.2399999999966269 \cdot 10^{-3}$
y_5	$0.4970837023296724 \cdot 10$	y_{12}	-0.2091214032073855
y_6	-0.2091214032073855	y_{13}	$-0.2499999999999991 \cdot 10$
y_7	$0.4970593243278363 \cdot 10$	y_{14}	$-0.2500077409198803 \cdot 10$

TABLE 9.4: *Run characteristics.*

solver	rtol	atol	h0	scd	steps	accept	# f	# Jac	# LU	CPU
DASSL	10^{-4}	10^{-4}		6.22	1019	942	1590	232		1.87
	10^{-7}	10^{-7}		7.37	3765	3572	5315	554		5.71
PSIDE-1	10^{-4}	10^{-4}		3.33	464	411	6574	109	1796	3.88
	10^{-7}	10^{-7}		8.48	773	643	13134	222	2760	7.60

REFERENCES

[GR96] M. Günther and P. Rentrop. The NAND-gate – a benchmark for the numerical simulation of digital circuits. In W. Mathis and P. Noll, editors, *2.ITG-Diskussionssitzung "Neue Anwendungen Theoretischer Konzepte in der Elektrotechnik" - mit Gedenksitzung zum 50. Todestag von Wilhelm Cauer*, pages 27–33, Berlin, 1996. VDE-Verlag.

[SH68] H. Shichman and D.A. Hodges. Insulated-gate field-effect transistor switching circuits. *IEEE J. Solid State Circuits*, SC-3:285–289, 1968.

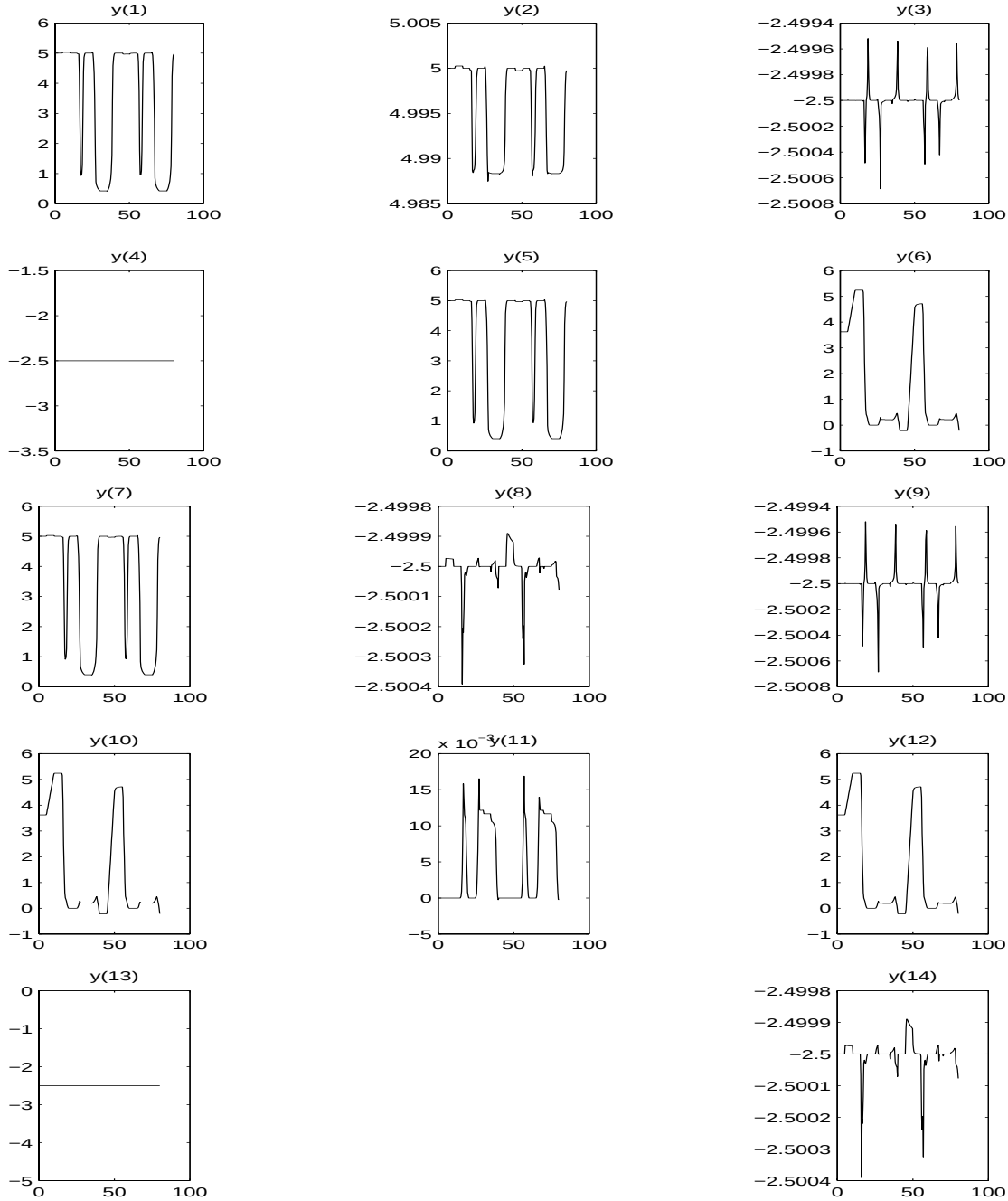

FIGURE 9.5: *Behavior of the solution over the integration interval.*

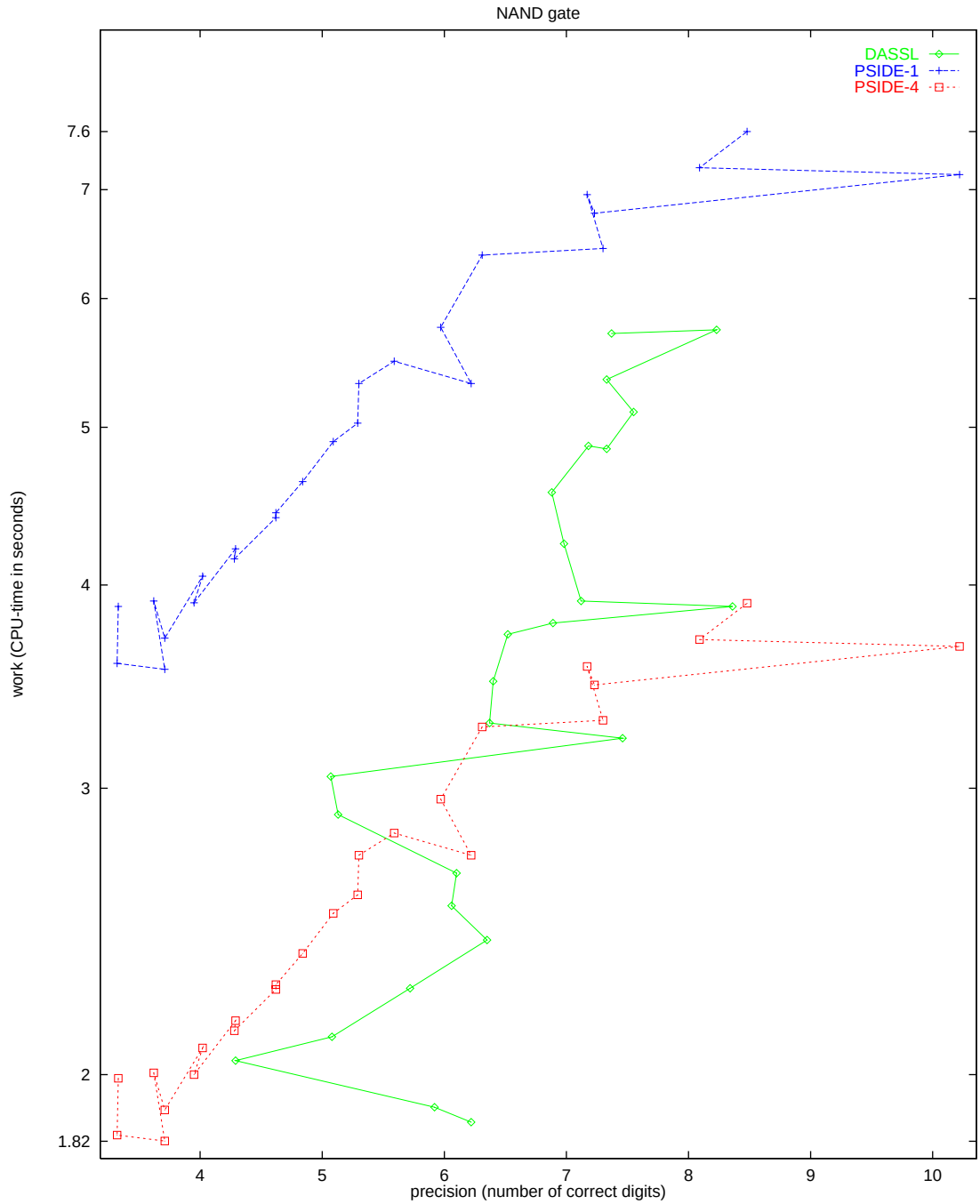

FIGURE 9.6: *Work-precision diagram.*

10. Charge pump

10.1 General information

The problem is a stiff DAE of index 2, consisting of 3 differential and 6 algebraic equations. It has been contributed by Michael Günther, Georg Denk and Uwe Feldmann [GDF95].

10.2 Mathematical description

The problem is of the form

$$M\frac{\mathrm{d}y}{\mathrm{d}t} \;=\; f(t,y(t)), \qquad y(0)=y_0, \quad y'(0)=y_0',$$

with

$$y\in\mathbb{R}^9, \qquad 0\le t\le 1.2\cdot 10^{-6}.$$

The 9×9 matrix M is the zero matrix except for the the minor $M_{1..3,1..5}$, that is given by

$$M_{1..3,1..5}=\begin{pmatrix}1&0&0&0&0\\0&1&1&0&0\\0&0&0&1&1\end{pmatrix}.$$

The function f is defined by

$$f(t,y)=\begin{pmatrix}-y_9\\0\\0\\-y_6+V_{in}(t)\\y_1-Q_G(v)\\y_2-C_S\cdot y_7\\y_3-Q_S(v)\\y_4-C_D\cdot y_8\\y_5-Q_D(v)\end{pmatrix},$$

with $v:=(v_1,v_2,v_3)=(y_6,y_6-y_7,y_6-y_8)$, $C_D=0.4\cdot 10^{-12}$ and $C_S=1.6\cdot 10^{-12}$. The functions Q_G, Q_S and Q_D are given by:

1. If $v_1\le V_{FB}:=U_{T0}-\gamma\sqrt{\Phi}-\Phi$, then

   $$\begin{aligned}Q_G(v) &= C_{ox}(v_1-V_{FB}),\\ Q_S(v) &= Q_D(v)=0,\end{aligned}$$

   with $C_{ox}=4\cdot 10^{-12}$, $U_{T0}=0.2$, $\gamma=0.035$ and $\Phi=1.01$.

2. If $v_1>V_{FB}$ and $v_2\le U_{TE}:=U_{T0}+\gamma(\sqrt{\Phi-U_{BS}}-\sqrt{\Phi})$, then

   $$\begin{aligned}Q_G(v) &= C_{ox}\gamma\left(\sqrt{(\gamma/2)^2+v_1-V_{FB}}-\gamma/2\right),\\ Q_S(v) &= Q_D(v)=0.\end{aligned}$$

3. If $v_1>V_{FB}$ and $v_2>U_{TE}$, then

   $$\begin{aligned}Q_G(v) &= C_{ox}\left(\frac{2}{3}(U_{GDT}+U_{GST}-\frac{U_{GDT}U_{GST}}{U_{GDT}+U_{GST}})+\gamma\sqrt{\Phi-U_{BS}}\right),\\ Q_S(v) &= Q_D(v)=-\frac{1}{2}\left(Q_G-C_{ox}\gamma\sqrt{\Phi-U_{BS}}\right).\end{aligned}$$

Here, U_{BS}, U_{GST} and U_{GDT} are given by

$$\begin{aligned} U_{BS} &= v_2 - v_1, \\ U_{GST} &= v_2 - U_{TE}, \\ U_{GDT} &= \begin{cases} v_3 - U_{TE} & \text{for} \quad v_3 > U_{TE}, \\ 0 & \text{for} \quad v_3 \le U_{TE}. \end{cases} \end{aligned}$$

The function $V_{in}(t)$ is defined using $\tau = (10^9 \cdot t) \bmod 120$ by

$$V_{in}(t) = \begin{cases} 0 & \text{if} \quad \tau < 50, \\ 20(\tau - 50) & \text{if} \quad 50 \le \tau < 60, \\ 20 & \text{if} \quad 60 \le \tau < 110, \\ 20(120 - \tau) & \text{if} \quad \tau \ge 110. \end{cases}$$

This means that the function f has discontinuities in its derivative at $\tau = 50, 60, 90, 110, 120$.

Consistent initial values are

$$y_0 = (Q_G(0,0,0), 0, Q_S(0,0,0), 0, Q_D(0,0,0), 0, 0, 0, 0)^T \quad \text{and} \quad y_0' = (0,0,0,0,0,0,0,0,0)^T.$$

The index of the first eight variables is 1, whereas the index of y_9 is 2.

10.3 Origin of the problem

The Charge-pump circuit shown in Figure 10.1 consists of two capacitors and an n-channel MOS-transistor. The nodes gate, source, gate, and drain of the MOS-transistor are connected with the nodes 1, 2, 3, and Ground, respectively. In formulating the circuit equations, the transistor is replaced by four non-linear current sources in each of the connecting branches. They model the transistor.

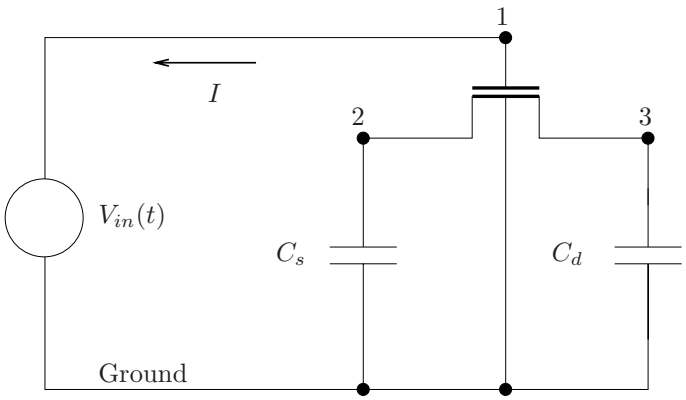

FIGURE 10.1: *Circuit diagram of Charge-pump circuit (taken from [GDF95])*

After inserting the transistor model in the circuit, we get the final circuit, which can be obtained from the circuit in Figure 10.1 by applying the following changes:

- Remove the transistor and replace it by a solid line between the nodes 2 and 3. The point where the lines 2–3 and 1–Ground cross each other becomes a node, which will be denoted by T.
- Add current sources between nodes 1 and T, between 2 and T and between 3 and T. There should also be a current source between the ground and node T, but as the node Ground does not enter the circuit equations, it will not be discussed. The currents produced by these sources are written as the derivatives of charges: current from 1 to T: Q_G', from T to 2: Q_S' and from T to 3: Q_D'. Here, the functions Q_G, Q_S and Q_D depend on the voltage drops U_1, $U_1 - U_2$ and $U_1 - U_3$, where U_i denotes the potential in node i.

The unknowns in the circuit are given by:

- The charges produced by the current sources: Y_{T1}, Y_{T2}, Y_{T3}. They are aliases for respectively Q_G, Q_S and Q_D. Consequently, Y'_{Ti} is the current between node T and node i.
- The charges Y_S and Y_D in the capacitors C_S and C_D.
- Potentials in nodes 1 to 3: U_1, U_2, U_3.
- The current through the voltage source $V_{in}(t)$: I.

In terms of these physical variables, the vector y introduced earlier reads

$$y = (Y_{T1}, Y_S, Y_{T2}, Y_D, Y_{T3}, U_1, U_2, U_3, I)^T.$$

Now, the following equations hold:

$$\begin{aligned} Y'_{T1} &= -I, \\ Y'_S + Y'_{T2} &= 0, \\ Y'_D + Y'_{T3} &= 0, \\ U_1 &= V_{in}(t). \end{aligned}$$

The charges depend on the potentials and are given by

$$\begin{aligned} Y_{T1} &= Q_G(U_1, U_1 - U_2, U_1 - U_3), \\ Y_S &= C_S \cdot U_2, \\ Y_{T2} &= Q_S(U_1, U_1 - U_2, U_1 - U_3), \\ Y_D &= C_D \cdot U_3, \\ Y_{T3} &= Q_D(U_1, U_1 - U_2, U_1 - U_3). \end{aligned}$$

The functions Q_G, Q_S and Q_D are given in the previous section.
Remark: the potential U_1 is known. Here, it is treated as an unknown in order to keep the formulation general and leaving open the possibility to extend the circuit. In addition, removing U_1 by hand contradicts a Computer Aided Design (CAD) approach in circuit simulation.

10.4 Numerical solution of the problem
The various components differ enormously in magnitude. Therefore, the absolute and relative input tolerances atol and rtol were chosen to be component-dependent. Furthermore, we neglect the index 2 variable y_9 in the error control of DASSL. This leads to the following input tolerances:

$$\begin{aligned} \text{atol}(i) &= \text{Tol} \cdot 10^{-6} \quad \text{for} \quad i = 1, \ldots, 5, \\ \text{atol}(i) &= \text{Tol} \quad \text{for} \quad i = 6, \ldots, 8, \\ \text{rtol}(i) &= \text{Tol} \quad \text{for} \quad i = 1, \ldots, 8, \\ \text{atol}(9) = \text{rtol}(9) &= 1000 \quad \text{for} \quad \text{DASSL}, \\ \text{atol}(9) = \text{rtol}(9) &= \text{Tol} \quad \text{for} \quad \text{other solvers}. \end{aligned}$$

The reference solution was produced by PSIDE using $\text{Tol} = 2 \cdot 10^{-8}$.

Table 10.1 and Figures 10.3–10.3 present the run characteristics and the work-precision diagram, respectively. For the computation of the number of significant correct digits (scd), only the first component is taken into account. The second up to eighth component are ignored because these components are zero in the true solution; the ninth component is neglected because it was excluded from DASSL's error control. The first component of the reference solution equals $0.1262800429876759 \cdot 10^{-12}$ at the end of the integration interval. We remark that the magnitude of this component

TABLE 10.1: *Run characteristics.*

solver	Tol	scd	steps	accept	# f	# Jac	# LU	CPU
DASSL	10^{-1}	0.14	447	438	604	369		0.42
	10^{-3}	15.40	923	803	1539	773		0.90
	10^{-5}	3.43	1647	1427	2790	1218		1.52
	10^{-7}	3.78	2435	1993	4029	1732		2.23
PSIDE-1	10^{-1}	0.37	938	839	9843	140	3752	2.51
	10^{-5}	4.47	1366	1068	13424	160	5424	3.43
	10^{-7}	15.40	2404	1547	24011	294	9540	6.12

TABLE 10.2: *Failed runs.*

solver	m	reason
MEBDFDAE	$0, 1, \ldots, 14$	stepsize too small
PSIDE-1	$4, 13, 14$	stepsize too small
RADAU	$0, 1, \ldots, 14$	stepsize too small
RADAU5	$0, 1, \ldots, 14$	stepsize too small

is at most 10^{-10}. For the work-precision diagram, we used: Tol $= 10^{-(1+m/2)}$, $m = 0, 1, \ldots, 14$; h0 $= 10^{-6} \cdot$ Tol for RADAU, RADAU5 and MEBDFDAE. From Table 10.1 and Figure 10.3 we see that the numerical solution computed by DASSL results for some rather large values of Tol in an scd value of 15.4, which equals the accuracy of the reference solution.

Figure 10.2 shows the behavior of the solution over the integration interval. Only the last four components have been plotted, since they are the physically important quantities. The other five components refer to charge flows inside the transistor, which are quantities the user is not interested in. These components have a similar behavior as the components 6, 7 and 8, but their magnitude is at most 10^{-10}.

The failed runs are in Table 10.2; listed are the name of the solver that failed, for which values of m this happened, and the reason for failing. The speed-up factor for PSIDE is 2.12.

REFERENCES

[GDF95] M. Günther, G. Denk, and U. Feldmann. How models for MOS transistors reflect charge distribution effects. Technical Report 1745, Technische Hochschule Darmstadt, Fachbereich Mathematik, Darmstadt, 1995.

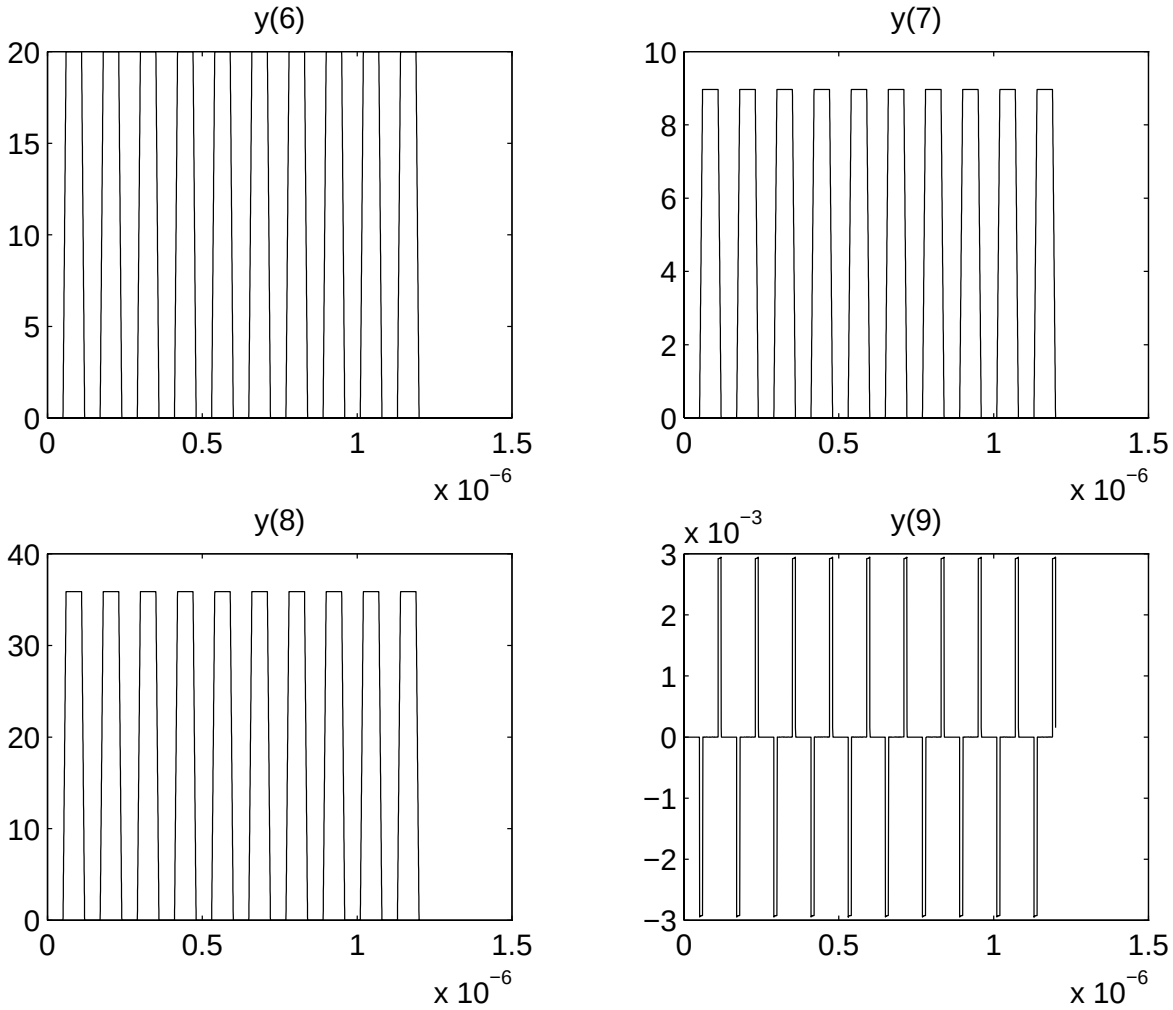

FIGURE 10.2: *Behavior of the solution over the integration interval.*

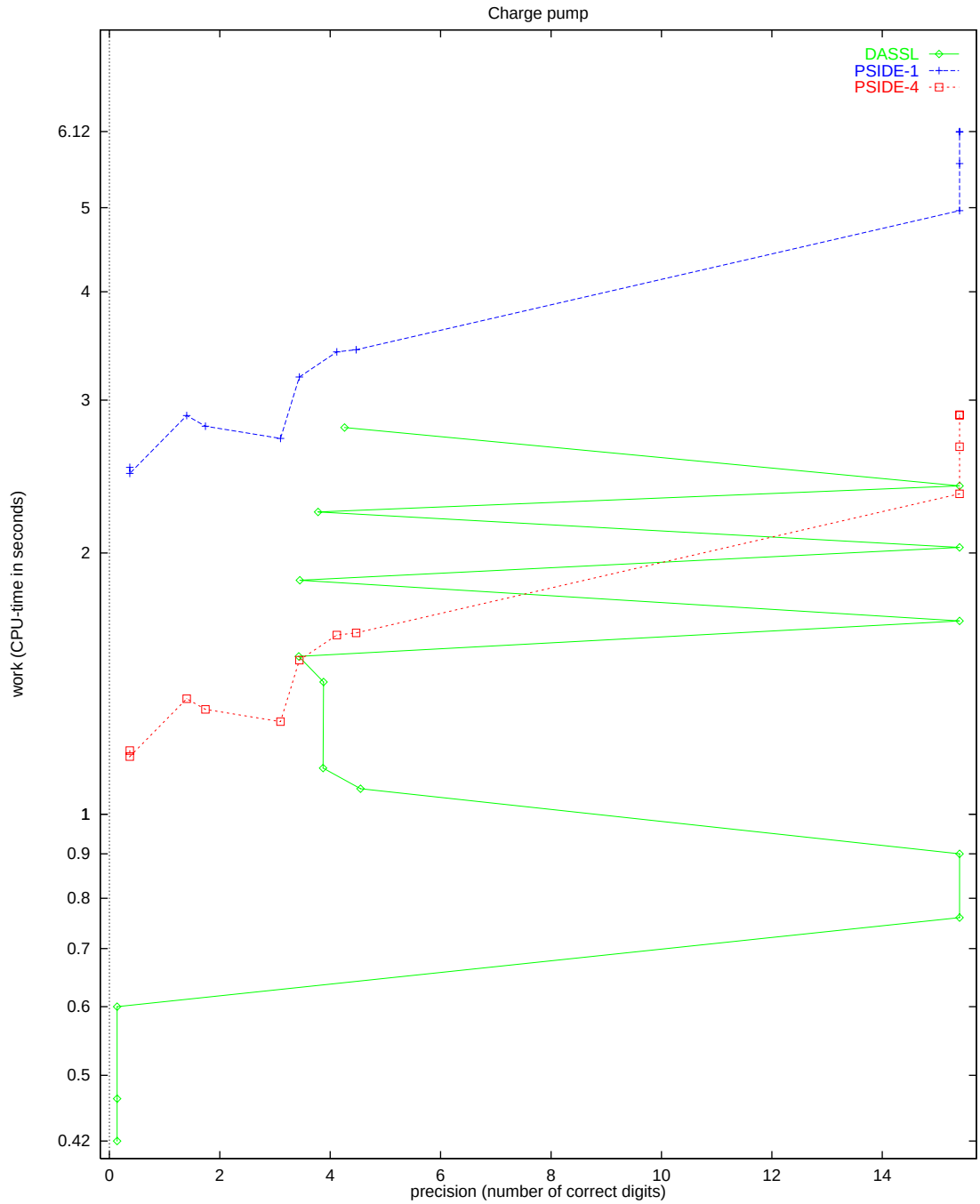

FIGURE 10.3: *Work-precision diagram.*

11. Wheelset

11.1 General Information

The wheelset is an IDE of dimension 17 which shows some typical properties of simulation problems in contact mechanics, i.e., friction, contact conditions, stiffness, etc.. This problem is originally described by an index 3 IDE with additional index 1 equations, but can be reduced to index 2. Test results are based on the index-2 formulation. This problem was contributed by Bernd Simeon, Claus Führer, Peter Rentrop, Nov. 1995. Comments to `bernd.simeon@mathematik.th-darmstadt.de` or `claus@dna.lth.se`. See also [SFR91].

11.2 Mathematical description of the problem

The index 3 formulation of the wheelset problem reads

$$\dot{p} = v, \tag{11.1}$$

$$M(p)\begin{pmatrix} \dot{v} \\ \dot{\beta} \end{pmatrix} = \begin{pmatrix} f(u) - (\partial g_1(p,q)/\partial p)^{\mathrm{T}}\, C\lambda \\ d(u) \end{pmatrix}, \tag{11.2}$$

$$0 = g_1(p,q), \tag{11.3}$$

$$0 = g_2(p,q), \tag{11.4}$$

where $u := (p, v, \beta, q, \lambda)^{\mathrm{T}} \in \mathbb{R}^{17}$, $p, v \in \mathbb{R}^5$, $\beta \in \mathbb{R}$, $q \in \mathbb{R}^4$, $\lambda \in \mathbb{R}^2$ and C is a scalar constant. Furthermore, $M : \mathbb{R}^5 \to \mathbb{R}^6 \times \mathbb{R}^6$, $f : \mathbb{R}^{17} \to \mathbb{R}^5$, $d : \mathbb{R}^{17} \to \mathbb{R}$, $g_1 : \mathbb{R}^9 \to \mathbb{R}^2$ and $g_2 : \mathbb{R}^9 \to \mathbb{R}^4$. The integration interval is from 0 to 10 [s].

For the index 2 formulation of the problem (11.3) is replaced by

$$0 = (\partial g_1(p,q)/\partial p)\, v. \tag{11.5}$$

The non-zero components of the consistent initial values $u(0) := u_0$ and $u'(0) := u_0'$ are given by

$u_{0,1}$	$0.1494100000000000 \cdot 10^{-2}$	$u_{0,12}$	$7.4122380357667139 \cdot 10^{-6}$
$u_{0,2}$	$0.4008900000000000 \cdot 10^{-6}$	$u_{0,13}$	0.1521364296121248
$u_{0,3}$	$0.1124100000000000 \cdot 10^{-5}$	$u_{0,14}$	$7.5634406395172940 \cdot 10^{-6}$
$u_{0,4}$	$-0.2857300000000000 \cdot 10^{-3}$	$u_{0,15}$	0.1490635714733819
$u_{0,5}$	$0.2645900000000000 \cdot 10^{-3}$	$u_{0,16}$	$-0.8359300000000000 \cdot 10^{-2}$
		$u_{0,17}$	$-0.7414400000000000 \cdot 10^{-2}$
$u_{0,6}'$	-1.9752588940112850	$u_{0,9}'$	-5.5333628217315490
$u_{0,7}'$	$-1.0898297102811276 \cdot 10^{-3}$	$u_{0,10}'$	-0.3487021489546511
$u_{0,8}'$	$7.8855083626142589 \cdot 10^{-2}$	$u_{0,11}'$	-2.1329687243809270

The other components of u_0 and u_0' are zero. For the index 3 formulation, the index of variables p, v, β, q and λ equals 1, 2, 2, 1 and 3. For the index 2 problem, these numbers read 1, 1, 1, 1 and 2.

The equations are given in detail in the next subsections, in which some references to the origin of the problem, treated in §11.3, are already given. Table 11.1 lists all problem parameters.

11.2.1 Differential equations

The position coordinates p are defined as

$$p := \begin{pmatrix} x \\ y \\ z \\ \theta \\ \varphi \end{pmatrix} \quad \begin{array}{l} \text{lateral displacement} \\ \text{vertical displacement} \\ \text{longitudinal displacement} \\ \text{yaw angle} \\ \text{roll angle} \end{array}$$

and the contact variables as $q^{\mathrm{T}} := \begin{pmatrix} \psi_L & \xi_L & \psi_R & \xi_R \end{pmatrix}$ with

$$\begin{aligned} \xi_{L|R} &:= \text{coordinate of the contact point left/right,} \\ \psi_{L|R} &:= \text{shift angle left/right.} \end{aligned}$$

The first three equations in (11.2) yield the momentum equations:

$$
\begin{aligned}
m_R\,\ddot{x} &= m_R\left(2\,v_0\,\kappa\,\cos\alpha\,\dot{z} + v_0^2\,\kappa\,\cos\alpha\,(1+\kappa\,(x\cos\alpha - y\sin\alpha))\right)\\
&\quad + T_{L_1} + T_{R_1} + Q_1 - m_R\,\tilde{g}\,\sin\alpha - b_{1,1}\,\lambda_1 - b_{1,2}\,\lambda_2 - 2\,c_x\,x\,,\\
m_R\,\ddot{y} &= -m_R\left(2\,v_0\,\kappa\,\sin\alpha\,\dot{z} + v_0^2\,\kappa\,\sin\alpha\,(1+\kappa\,(x\cos\alpha - y\sin\alpha))\right)\\
&\quad + T_{L_2} + T_{R_2} + Q_2 - m_R\,\tilde{g}\,\cos\alpha - b_{2,1}\,\lambda_1 - b_{2,2}\,\lambda_2\,,\\
m_R\,\ddot{z} &= m_R\left(-2\,v_0\,\kappa\,(\dot{x}\cos\alpha - \dot{y}\sin\alpha) + v_0^2\,\kappa^2\,z\right)\\
&\quad + T_{L_3} + T_{R_3} + Q_3 + F_A - b_{3,1}\,\lambda_1 - b_{3,2}\,\lambda_2\,,
\end{aligned}
$$

where $b_{i,j}$ denotes the (i,j) element of the constraint Jacobian $\partial g_1(p,q)/\partial p$. The next three equations yield the spin equations:

$$
\begin{aligned}
I_2\,\ddot{\theta}\,\cos\varphi &= -\dot{\theta}\,\dot{\varphi}\sin\varphi + v_0\,\kappa\Big(\dot{\varphi}(\sin\alpha\cos\theta\cos\varphi + \cos\alpha\sin\varphi) - \dot{\theta}\sin\alpha\sin\theta\sin\varphi\Big)\\
&\quad - I_1\,(\omega_0+\beta)\,(\dot{\varphi} - v_0\kappa\sin\theta\sin\alpha)\\
&\quad - (I_1 - I_2)\left(\dot{\theta}\,\sin\varphi - v_0\,\kappa\,(\cos\theta\cos\varphi\sin\alpha + \sin\varphi\cos\alpha)\right)\\
&\qquad\qquad \left(\dot{\varphi} - v_0\,\kappa\,\sin\alpha\sin\theta\right)\\
&\quad + \Big[-(\xi_L\sin\theta + R(\xi_L)\sin\psi_L\cos\theta\cos\varphi)\,T_{L_1}\\
&\qquad -R(\xi_L)\sin\psi_L\sin\varphi\,T_{L_2}\\
&\qquad +(-\xi_L\cos\theta + R(\xi_L)\sin\psi_L\sin\theta\cos\varphi)\,T_{L_3}\Big]\\
&\quad + \Big[\quad \text{corresponding terms of the right side} \quad\Big]\\
&\quad - \cos\theta\,\sin\varphi\,M_1 + \cos\varphi\,M_2 + \sin\theta\,\sin\varphi\,M_3 - b_{4,1}\,\lambda_1 - b_{4,2}\,\lambda_2\,,\\
I_2\,\ddot{\varphi} &= I_2\,\dot{\theta}\,v_0\,\kappa\,\sin\alpha\,\cos\theta\\
&\quad + I_1\,(\omega_0+\beta)\left(\dot{\theta}\cos\varphi + v_0\,\kappa\,(\cos\theta\sin\varphi\sin\alpha - \cos\varphi\cos\alpha)\right)\\
&\quad + (I_1 - I_2)\Big(\dot{\theta}\,\sin\varphi - v_0\,\kappa(\cos\theta\cos\varphi\sin\alpha + \sin\varphi\cos\alpha)\Big)\\
&\qquad\qquad \Big(\dot{\theta}\,\cos\varphi + v_0\,\kappa(\cos\theta\sin\varphi\sin\alpha - \cos\varphi\cos\alpha)\Big)\\
&\quad + \Big[-(\xi_L\cos\theta\sin\varphi - R(\xi_L)\cos\psi_L\cos\theta\cos\varphi)\,T_{L_1}\\
&\qquad +(\xi_L\cos\varphi + R(\xi_L)\cos\psi_L\sin\varphi)\,T_{L_2}\\
&\qquad +(\xi_L\sin\theta\sin\varphi - R(\xi_L)\cos\psi_L\sin\theta\cos\varphi)\,T_{L_3}\Big]\\
&\quad + \Big[\quad \text{corresponding terms of the right side} \quad\Big]\\
&\quad + \sin\theta\,M_1 + \cos\theta\,M_3 - b_{5,1}\,\lambda_1 - b_{5,2}\,\lambda_2\,,\\
I_1\,(\dot{\beta} + \ddot{\theta}\,\sin\varphi) &= \dot{\theta}\,\dot{\varphi}\cos\varphi - v_0\,\kappa\,(\dot{\varphi}(\cos\alpha\cos\varphi - \sin\alpha\cos\theta\sin\varphi) - \dot{\theta}\sin\alpha\sin\theta\cos\varphi)\\
&\quad + \Big[-R(\xi_L)\,(\cos\psi_L\sin\theta + \sin\psi_L\cos\theta\sin\varphi)\,T_{L_1}\\
&\qquad +R(\xi_L)\,\sin\psi_L\,\cos\varphi\,T_{L_2}\\
&\qquad -R(\xi_L)\,(\cos\psi_L\cos\theta - \sin\psi_L\sin\theta\sin\varphi)\,T_{L_3}\Big]\\
&\quad + \Big[\quad \text{corresponding terms of the right side} \quad\Big]\\
&\quad + \cos\theta\,\cos\varphi\,M_1 + \sin\varphi\,M_2 - \sin\theta\,\cos\varphi\,M_3 + L_A\,.
\end{aligned}
$$

The forces Q and moments M of the wagon body satisfy the following equations:

$$\begin{aligned}
Q_1 &= \tfrac{m_A\,\tilde g}{\cos\alpha}\left(\tfrac{v_0^2\,\kappa}{\tilde g} - \tan\alpha\right) && \text{(lateral force)},\\
Q_2 &= -m_A\,\tilde g\,\cos\alpha\,\left(\tfrac{v_0^2\,\kappa}{\tilde g}\,\tan\alpha + 1\right) && \text{(vertical force)},\\
Q_3 &= -2\,c_z\,z && \text{(longitudinal force)},\\
M_1 &= 0 &&\\
M_2 &= Q_3\,x_l && \text{(yaw moment)},\\
M_3 &= -h_A\,Q_1 && \text{(roll moment)},\\
0 &= \cos\theta\,M_1 - \sin\theta\,M_3 && \text{(no pitch moment)}.
\end{aligned}$$

The creep forces $T_{L_{1,2,3}}$ and $T_{R_{1,2,3}}$ of the left and right contact point are obtained via the transformation

$$\begin{pmatrix} T_{L|R_1}\\ T_{L|R_2}\\ T_{L|R_3}\end{pmatrix} = \begin{pmatrix} \sin\theta & \cos\theta\cos\Delta_{L|R} & \mp\cos\theta\sin\Delta_{L|R}\\ 0 & \pm\sin\Delta_{L|R} & \cos\Delta_{L|R}\\ \cos\theta & -\sin\theta\cos\Delta_{L|R} & \pm\sin\theta\sin\Delta_{L|R}\end{pmatrix}\begin{pmatrix} T_{1_{L|R}}\\ T_{2_{L|R}}\\ 0\end{pmatrix},$$

where $T_{1_{L|R}}$ and $T_{2_{L|R}}$ denote the creep forces with respect to the local reference frame of the contact point and $\pm$ stands for the left and right side, respectively. The creep forces are approximated by

$$\begin{aligned}
T_{1_{L|R}} &:= -\mu N_{L|R}\tanh\left(\frac{GC_{11}c^2}{\mu N_{L|R}}\nu_1\right),\\
T_{2_{L|R}} &:= -\mu N_{L|R}\tanh\left(\frac{GC_{22}c^2}{\mu N_{L|R}}\nu_2 + \frac{GC_{23}c^3}{\mu N_{L|R}}\varphi_3\right),
\end{aligned}$$

and corrected by

$$\text{if}\quad T_1^2 + T_2^2 > (\mu N)^2\,,\quad \text{then}$$
$$\tilde T_1 := \frac{T_1}{\sqrt{T_1^2+T_2^2}}\,\mu N \quad\text{and}\quad \tilde T_2 := \frac{T_2}{\sqrt{T_1^2+T_2^2}}\,\mu N.$$

The constant parameters

$$\mu, G, C_{11}, C_{22}, C_{23}$$

(friction coefficient, glide module, Kalker coefficients) are listed in Table 11.1. For the computation of c, the size of contact ellipse, which uses the parameters σ, $\widehat G$ and ϵ, we refer to [Jas87]. For alternative creep force models see also [Jas87].

The normal forces N are given by

$$\begin{pmatrix} N_L\\ N_R\end{pmatrix} = \gamma\begin{pmatrix} \cos\Delta_R & -\sin\Delta_R\\ -\cos\Delta_L & -\sin\Delta_L\end{pmatrix}\begin{pmatrix} b_{1,1} & b_{1,2}\\ b_{2,1} & b_{2,2}\end{pmatrix}\begin{pmatrix}\lambda_1\\ \lambda_2\end{pmatrix},$$

where

$$\gamma := \frac{1}{\sin\Delta_L\cos\Delta_R + \sin\Delta_R\cos\Delta_L}\,.$$

Here, $\Delta_{L|R}$ denotes the contact angles and is defined as

$$\begin{aligned}
\tan\Delta_L &= \frac{(R'(\xi_L)\cos\varphi - \sin\varphi\cos\psi_L)\cos\theta + \sin\psi_L\sin\theta}{-R'(\xi_L)\sin\varphi - \cos\psi_L\cos\varphi}\,;\\
\tan\Delta_R &= \frac{(R'(\xi_R)\cos\varphi - \sin\varphi\cos\psi_R)\cos\theta + \sin\psi_R\sin\theta}{+R'(\xi_R)\sin\varphi + \cos\psi_R\cos\varphi}\,.
\end{aligned}$$

For the creepages we have the relations

$$\begin{aligned}
\nu_1 &= \frac{1}{v_{roll}}\left(\sin\theta v_{r1} + \cos\theta v_{r3}\right)\\
\nu_2 &= \frac{1}{v_{roll}}\left(\cos\theta\cos\Delta_{L|R} v_{r1} \pm \sin\Delta_{L|R} v_{r2} - \sin\theta\cos\Delta_{L|R} v_{r3}\right)\\
\varphi_3 &= \frac{1}{v_{roll}}\Big(\mp\sin\Delta_{L|R}(\omega+\beta-v_0\,\kappa\,\sin\alpha) + \cos\Delta_{L|R}(\dot\theta - v_0\,\kappa\cos\alpha)\Big)
\end{aligned}$$

where $v_{r1,2,3}$ (relative velocity at the contact point) and v_{roll} (rolling velocity) are given by (correspondingly for the right side)

$$\begin{aligned}
v_{r1} &= \dot x - \dot\theta(R(\xi_L)(\sin\theta\sin\varphi\cos\psi_L + \cos\theta\sin\psi_L) + \xi_L\sin\theta\cos\varphi)\\
&\quad -\dot\varphi\cos\theta(\xi_L\sin\varphi - R(\xi_L)\cos\varphi\cos\psi_L)\\
&\quad +(\omega_0+\beta)R(\xi_L)(-\sin\theta\cos\psi_L - \sin\varphi\cos\theta\sin\psi_L)\\
&\quad +v_0\kappa\cos\alpha(R(\xi_L)(\sin\theta\sin\varphi\cos\psi_L + \cos\theta\sin\psi_L) + \xi_L\sin\theta\cos\varphi - z),\\
v_{r2} &= \dot y + \dot\varphi(\xi_L\cos\varphi + R(\xi_L)\sin\varphi\cos\psi_L) + (\omega_0+\beta)R(\xi_L)\cos\varphi\sin\psi_L\\
&\quad +v_0\kappa\sin\alpha(z - \xi_L\sin\theta\cos\varphi - R(\xi_L)(\sin\theta\sin\varphi\cos\psi_L + \cos\theta\sin\psi_L)),\\
v_{r3} &= \dot z + v_0 + v_0\kappa(x\cos\alpha - y\sin\alpha)\\
&\quad -\dot\theta(\xi_L\cos\theta\cos\varphi + R(\xi_L)(\cos\theta\sin\varphi\cos\psi_L - \sin\theta\sin\psi_L))\\
&\quad +\dot\varphi\sin\theta(\xi_L\sin\varphi - R(\xi_L)\cos\varphi\cos\psi_L)\\
&\quad +(\omega+\beta)R(\xi_L)(\sin\theta\sin\varphi\sin\psi_L - \cos\theta\cos\psi_L)\\
&\quad -v_0\kappa\sin\alpha(\xi_L\sin\varphi - R(\xi_L)\cos\varphi\cos\psi_L)\\
&\quad +v_0\cos\alpha(\xi_L\cos\theta\cos\varphi + R(\xi_L)(\cos\theta\sin\varphi\cos\psi_L - \sin\theta\sin\psi_L)),
\end{aligned}$$

and

$$v_{roll} = \frac{1}{2}\left\|\begin{pmatrix} -2\dot x + 2v_0\kappa z\cos\alpha\\ -2\dot y - 2v_0\kappa z\sin\alpha\\ -2\dot z - 2v_0 - 2v_0\kappa(x\cos\alpha - y\sin\alpha)\end{pmatrix} + \begin{pmatrix} v_{r1}\\ v_{r2}\\ v_{r3}\end{pmatrix}\right\|_2 .$$

11.2.2 Constraints The constraints (11.3) read

$$\begin{pmatrix} G(\hat\xi_L) - y - \xi_L\sin\varphi + R(\xi_L)\cos\varphi\cos\psi_L\\ G(\hat\xi_R) - y - \xi_R\sin\varphi + R(\xi_R)\cos\varphi\cos\psi_R\end{pmatrix} = 0$$

with profile functions R (wheel) and G (rail), see Figure 11.1,

$$R(\xi) = \rho_0 + \tan\delta_0\,(a_0 - |\xi|) \qquad \text{for } a_0 - \Delta a < |\xi| < b_2\,;$$

$$G(\hat\xi) = \sqrt{\rho_1^2 - \left(|\hat\xi| - a_0 - \rho_1\sin\delta_0\right)^2} - \rho_0 - \cos\delta_0\,\rho_1 \qquad \text{for } c_1 < |\hat\xi| < c_2\,.$$

Here, ξ stands for the left or right coordinate $\xi_{L/R}$, respectively, and $\hat\xi$ is defined by

$$\hat\xi_{L|R} := x + \xi_{L|R}\cos\theta\cos\varphi + R(\xi_{L|R})\left(\cos\theta\sin\varphi\cos\psi_{L|R} - \sin\theta\sin\psi_{L|R}\right).$$

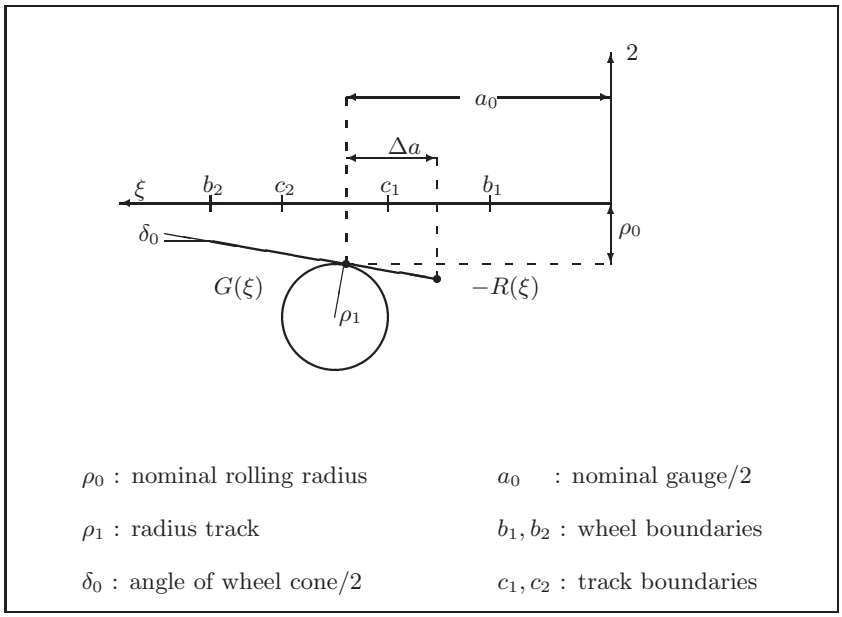

FIGURE 11.1: *Profile functions (left side).*

The constraints (11.4) read

$$\begin{aligned} G'(\hat{\xi}_L)\,(R'(\xi_L)\sin\varphi + \cos\varphi\cos\psi_L) + R'(\xi_L)\cos\theta\cos\varphi \\ -\cos\theta\sin\varphi\cos\psi_L + \sin\theta\sin\psi_L &= 0, \\ R'(\xi_L)\sin\theta\cos\varphi - \sin\theta\sin\varphi\cos\psi_L - \cos\theta\sin\psi_L &= 0, \\ G'(\hat{\xi}_R)\,(R'(\xi_R)\sin\varphi + \cos\varphi\cos\psi_R) + R'(\xi_R)\cos\theta\cos\varphi \\ -\cos\theta\sin\varphi\cos\psi_R + \sin\theta\sin\psi_R &= 0, \\ R'(\xi_R)\sin\theta\cos\varphi - \sin\theta\sin\varphi\cos\psi_R - \cos\theta\sin\psi_R &= 0, \end{aligned}$$

where $G'(\hat{\xi}_{L|R}) := \frac{\mathrm{d}}{\mathrm{d}\hat{\xi}_{L|R}} G(\hat{\xi}_{L|R})\,, R'(\xi_{L|R}) := \frac{\mathrm{d}}{\mathrm{d}\xi_{L|R}} R(\xi_{L|R})$.

11.3 Origin of the problem

The motion of a simple wheelset on a rail track exhibits a lot of the difficulties which occur in the simulation of contact problems in mechanics. The state space form approach for this class of problems requires simplifications and table look ups in order to eliminate the nonlinear constraints. The above example provides thus an alternative by using the IDE approach.

Figure 11.2 shows the mechanical model. The coordinates p denote the displacements and rotations of the wheelset with respect to the reference frame which is centered in the middle of the track. The wheelset is subjected to

- the gravity and centrifugal forces;
- creep forces in the contact points of wheel and rail;
- forces of the wagon body, which is represented by a frame connected to the wheelset via springs and dampers and proceeding with constant speed v_0;
- constraint forces which enforce the contact of wheel and rail on both sides.

TABLE 11.1: *Parameter values according to [Jas90], where a hardware bogie model, scaled 1:4, is investigated.*

Parameter	Meaning	Unit	Value
m_R	mass wheelset	kg	16.08
$\tilde{g}$	gravity constant	m/s^2	9.81
v_0	nominal velocity	m/s	30.0
F_A	propulsion force	N	0
L_A	propulsion moment	kg m^2	0
κ	describes track geometry		0
α	describes track geometry	rad	0
ω_0	nominal angular velocity	1/s	v_0/ρ_0
I_1	lateral moment of inertia	kg m^2	0.0605
I_2	vertical moment of inertia	kg m^2	0.366
m_A	mass of wagon body	kg	0.0
h_A	height of wagon body	m	0.2
c_x	spring constant	N/m	6400.0
c_z	spring constant	N/m	6400.0
x_l	width of wheelset/2	m	0.19
δ_0	cone angle/2	rad	0.0262
ρ_0	nominal radius	m	0.1
a_0	gauge/2	m	0.1506
ρ_1	radius track	m	0.06
μ	friction coefficient		0.12
G	glide module	N/m^2	$7.92 \cdot 10^{10}$
C_{11}	Kalker coefficient		4.72772197
C_{22}	Kalker coefficient		4.27526987
C_{23}	Kalker coefficient		1.97203505
$\widehat{G}$	parameter for computation of contact ellipse		0.7115218
ϵ	parameter for computation of contact ellipse		1.3537956
σ	parameter for computation of contact ellipse		0.28
C	scaling factor for Lagrange multipliers		10^4

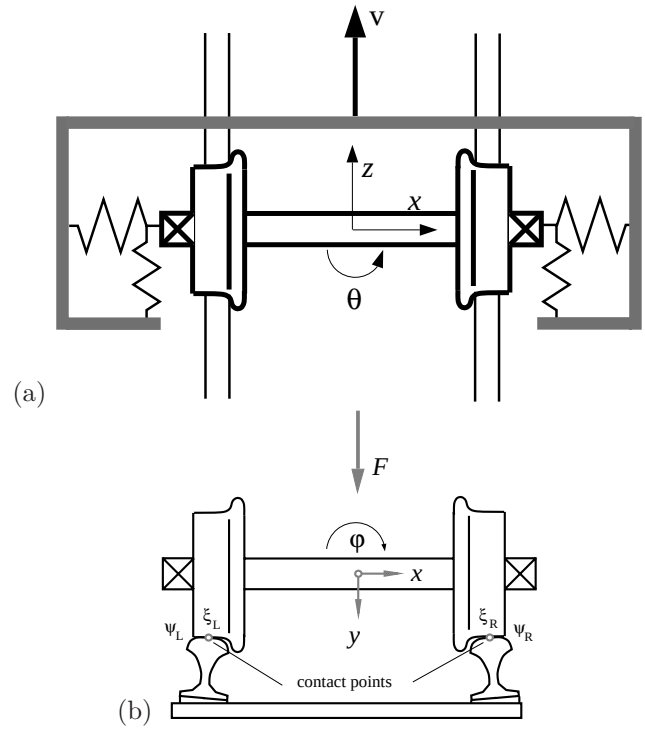

FIGURE 11.2: *The wheelset and the track. (a) View from above, (b) lateral cross section.*

We are particularly interested in a complete and correct formulation of the nonlinear constraint equations. An elimination of the constraints without severe simplifications or the introduction of tables for the dependent variables is impossible. In this example thus a reduction to state space form involves various obstacles, whereas the IDE formulation is straightforward.

Equations (11.1)–(11.2) stand for the kinematic and dynamic equations with positive definite mass matrix $M(p)$. By means of the profile functions R and G which describe the cross sections of wheel and rail depending on the contact points we first express the constraint equations as $0 = g_1$, see Figure 11.3. These constraints are of index 3 and enforce that the contact points of wheel and rail coincide on both sides. Additionally, we have to guarantee that wheel and rail do not intersect, which is accomplished by the conditions $0 = g_2$. Note that $\partial g_2/\partial q$ is regular, which means that we can apply formally the implicit function theorem to eliminate the additional contact variables q and that these constraints are of index 1. The equations of motion of the wheelset are then derived by applying the formalism of Newton and Euler. Here we used the property that this class of contact problems $(\partial g_1/\partial) q\, \dot{q} \equiv 0$. This also implies that if we, in order to get the index 2 formulation, differentiate the constraint (11.3) with respect to t, then we get

$$0 = \frac{\mathrm{d}g_1}{\mathrm{d}t}(p,q) = \frac{\partial g_1}{\partial p}\dot{p} + \frac{\partial g_1}{\partial q}\dot{q} = \frac{\partial g_1}{\partial p}\dot{p} - \frac{\partial g_1}{\partial q}\left(\frac{\partial g_2}{\partial q}\right)^{-1}\frac{\partial g_2}{\partial p}\dot{p},$$

which simplifies to (11.5).

Remarks

- $N(p,q,\lambda) \in \mathbb{R}^2$ denotes the normal forces which act in the contact points. They are necessary to evaluate the creep forces.
- The variable $\beta \in \mathbb{R}$ denotes the deviation of the angular velocity and is given by an additional differential equation.

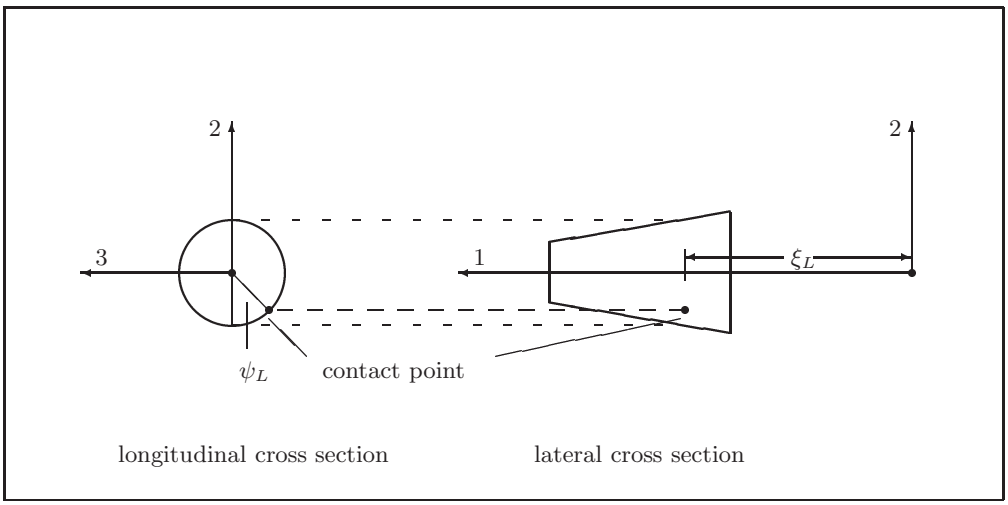

FIGURE 11.3: *Shift angle and coordinate of contact point on the left side.*

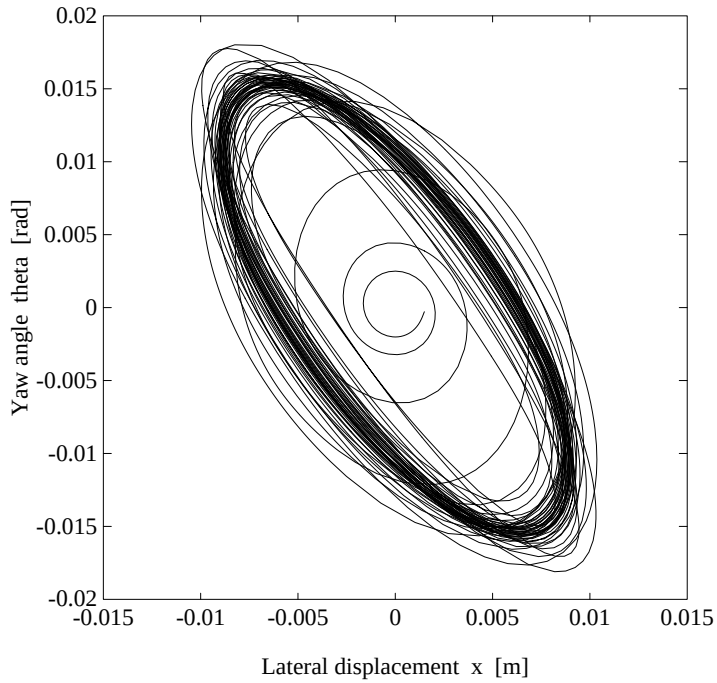

FIGURE 11.4: *Limit cycle or 'hunting motion' of wheelset.*

- The parameters κ and α describe the track geometry. The setting $\kappa = \alpha = 0$ refers to a straight track.
- The constant C in (11.2) means that we internally scaled the Lagrange multipliers.

The initial values correspond to a setting in which the dynamic behavior of the wheelset model is investigated when the wheelset starts with an initial deflection in lateral direction (x-direction) of 0.14941 [cm]. In [Jas90], a limit cycle was observed for this problem and the model data given above. This type of limit cycle, the so-called hunting motion, is a well known phenomenon in railway vehicle dynamics. In Figure 11.4 we see this limit cycle as computed by DASSL applied to the index-2 formulation of the problem. The results are in good agreement with those given in [Jas90], which were obtained by a state space form approach and with measurements on a hardware model.

11.4 Numerical solution of the problem

Tables 11.2–11.3 present the reference solution at the end of the integration interval, and the run characteristics, respectively. Figure 11.5 shows the the behavior of the components of p and the angular velocity β over the integration interval. Figure 11.6 contains the work-precision diagram. For this diagram, we used: rtol $= 10^{-(4+m/8)}$, $m = 0, 1, \ldots, 16$; atol = rtol. The speed-up factor for PSIDE is 2.29.

Remarks

- The Jacobian was computed internally by the solvers.
- For the runs with DASSL, we excluded the Lagrange multipliers from the error control by setting `atol(16)=atol(17)=rtol(16)=atol(17)=`10^{10}.

TABLE 11.2: *Reference solution at the end of the integration interval.*

u_1	$0.86355386965811 \cdot 10^{-2}$	u_{10}	$-0.13633468454173 \cdot 10^{-1}$
u_2	$0.13038281022727 \cdot 10^{-4}$	u_{11}	-0.24421377661131
u_3	$-0.93635784016818 \cdot 10^{-4}$	u_{12}	$-0.33666751972196 \cdot 10^{-3}$
u_4	$-0.13642299804033 \cdot 10^{-1}$	u_{13}	-0.15949425684022
u_5	$0.15292895005422 \cdot 10^{-2}$	u_{14}	$0.37839614386969 \cdot 10^{-3}$
u_6	$-0.76985374142666 \cdot 10^{-1}$	u_{15}	0.14173214964613
u_7	$-0.25151106429207 \cdot 10^{-3}$	u_{16}	$-0.10124044903201 \cdot 10^{-1}$
u_8	$0.20541188079539 \cdot 10^{-2}$	u_{17}	$-0.56285630573753 \cdot 10^{-2}$
u_9	-0.23904837703692		

TABLE 11.3: *Run characteristics.*

solver	rtol	atol	h0	scd	steps	accept	# f	# Jac	# LU	CPU
DASSL	10^{-4}	10^{-4}		0.13	5951	5094	10561	1547		17.82
	10^{-5}	10^{-5}		1.40	9835	8588	16120	1858		24.76
	10^{-6}	10^{-6}		2.25	15893	14204	25046	2561		36.91
PSIDE-1	10^{-4}	10^{-4}		1.13	1279	934	21805	555	4888	24.10
	10^{-5}	10^{-5}		1.27	2309	1500	38905	626	8632	38.53
	10^{-6}	10^{-6}		3.35	3107	2076	55294	562	10856	50.14

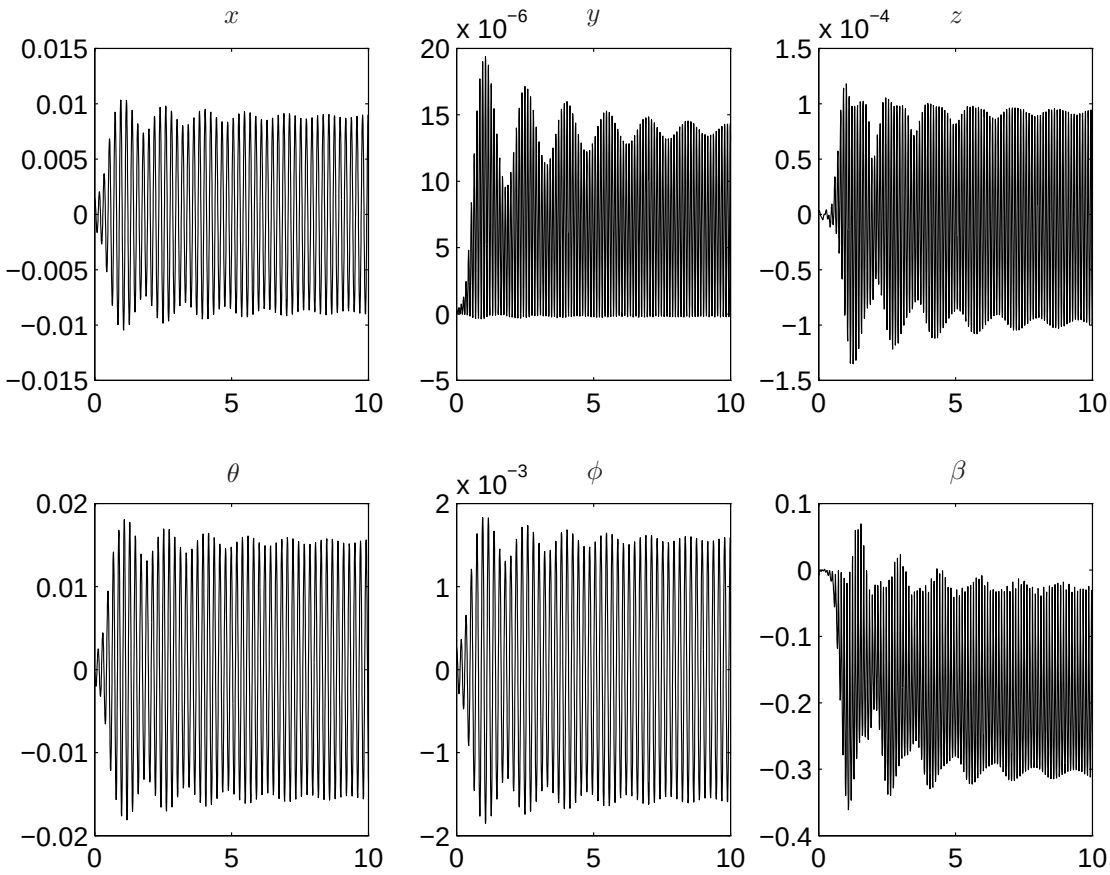

FIGURE 11.5: *Behavior of some solution components over the integration interval.*

- The reference solution was computed using DASSL with atol = rtol = 10^{-9} for p, v and q, and atol = rtol = 10^{10} for λ.

REFERENCES

[Jas87] A. Jaschinski. Anwendung der Kalkerschen Rollreibungstheorie zur dynamischen Simulation von Schienenfahrzeugen. Technical Report DFVLR 87-07, DFVLR Deutsche Forschungs- und Versuchsanstalt für Luft- und Raumfahrt, D-8031 Oberpfaffenhofen, 1987.

[Jas90] A. Jaschinski. *On the Application of Similarity Laws to a Scaled Railway Bogie Model*. PhD thesis, Technische Universiteit Delft, 1990.

[SFR91] B. Simeon, C. Führer, and P. Rentrop. Differential-algebraic equations in vehicle system dynamics. *Surv. Math. Ind.*, 1:1–37, 1991.

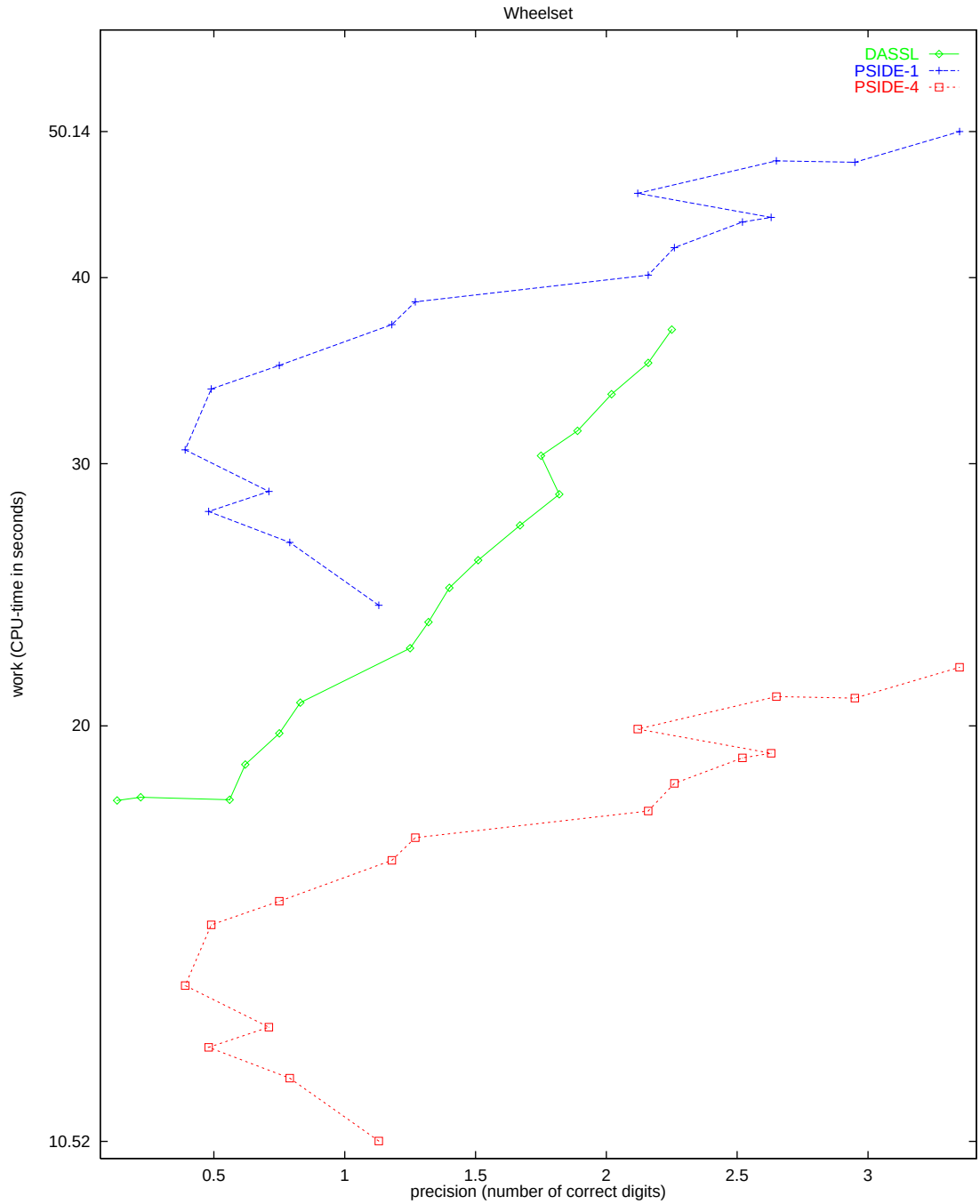

FIGURE 11.6: *Work-precision diagram.*

12. Two bit adding unit

12.1 General Information

The problem is a stiff DAE of index 1, consisting of 175 differential equations and 175 algebraic equations. It has been contributed by M. Günther [Gün95, Gün98].

12.2 Mathematical description of the problem

The problem is of the form

$$\begin{aligned} \frac{\mathrm{d}y}{\mathrm{d}t} &= f(t,x), \\ 0 &= y - g(x), \end{aligned} \tag{12.1}$$

where

$$y, x \in \mathbb{R}^{175}, \quad f : \mathbb{R}^{351} \to \mathbb{R}^{350},\ g : \mathbb{R}^{350} \to \mathbb{R}^{350}, \quad 0 \le t \le 320, \quad y(0) = y_0,\ x(0) = x_0.$$

Since the functions $f(t,x)$ and $g(x)$ and the (consistent) initial values y_0 and x_0 are too voluminous to be printed here, we refer to the subroutines `feval` and `init` for their definitions. The function f has discontinuities in its derivative at $t = 0, 5, 10, \ldots, 320$. The index of the components of x and y equals 1.

The function f contains several square roots. It is clear that the function can not be evaluated if one of the arguments of one of these square roots becomes negative. To prevent this situation, we set `IERR=-1` in the Fortran subroutine that defines f if this happens. See page *III-vi* of the the description of the software part of the test set for more details on `IERR`.

12.3 Origin of the problem

The two bit adding unit computes the sum of two base-2 numbers (each two digits long) and a carry bit. These numbers are fed into the circuit in the form of input signals. As a result the circuit gives their sum coded as three output signals.

The two bit adding unit circuit is a digital circuit. These circuits are used to compute boolean expressions. This is accomplished by associating voltages with boolean variables. By convention the boolean is true if the voltage exceeds $2V$, and false if it is lower than $0.8V$. In between the boolean is undefined. Using CMOS technique, however, sharper bounds are possible for the representation of booleans.

Digital circuits that compute elementary logical operations are called gates. An example of a gate is the NAND gate of test problem 9. This circuit is used to compute the logical expression $\neg(V_1 \wedge V_2)$, where V_1 and V_2 are the booleans that are fed into the circuit as input signals.

The two bit adding unit is depicted in Figure 12.1. In this figure the symbols '&', '≥ 1' and a little white circle respectively stand for the AND, OR and NOT gate. A number of input signals and output signals enter and leave the circuit. Each signal is described by a time-dependent voltage and the boolean it represents. For these two quantities we shall use one symbol: the symbol of this boolean variable. Which one of the two quantities is meant by the symbol, is always clear from the context. With this convention, the input signals are referred to by the boolean variable they represent.

The circuit is designed to perform the addition

$$A_1\ A_0 + B_1\ B_0 + C_{in} = C\ S_1\ S_0.$$

The input signals representing the two numbers and the carry bit C_{in} are fed into the circuit at the nodes indicated by $\overline{\text{A0}}$, $\overline{\text{A1}}$, $\overline{\text{B0}}$, $\overline{\text{B1}}$ and Cin. Here, a bar denotes the logical inversion. The output signals are delivered by the nodes indicated by S0, S1 and $\overline{\text{C}}$.

In Figure 12.1, a number of boxes are drawn using dashed lines. Each of them represents one of the following gates: the NOR (first box to the left in the top-row), the ORANI gate (the box besides S_1), the NAND (the box besides the ORANI gate) and the ANDOI(the box at the bottom). The

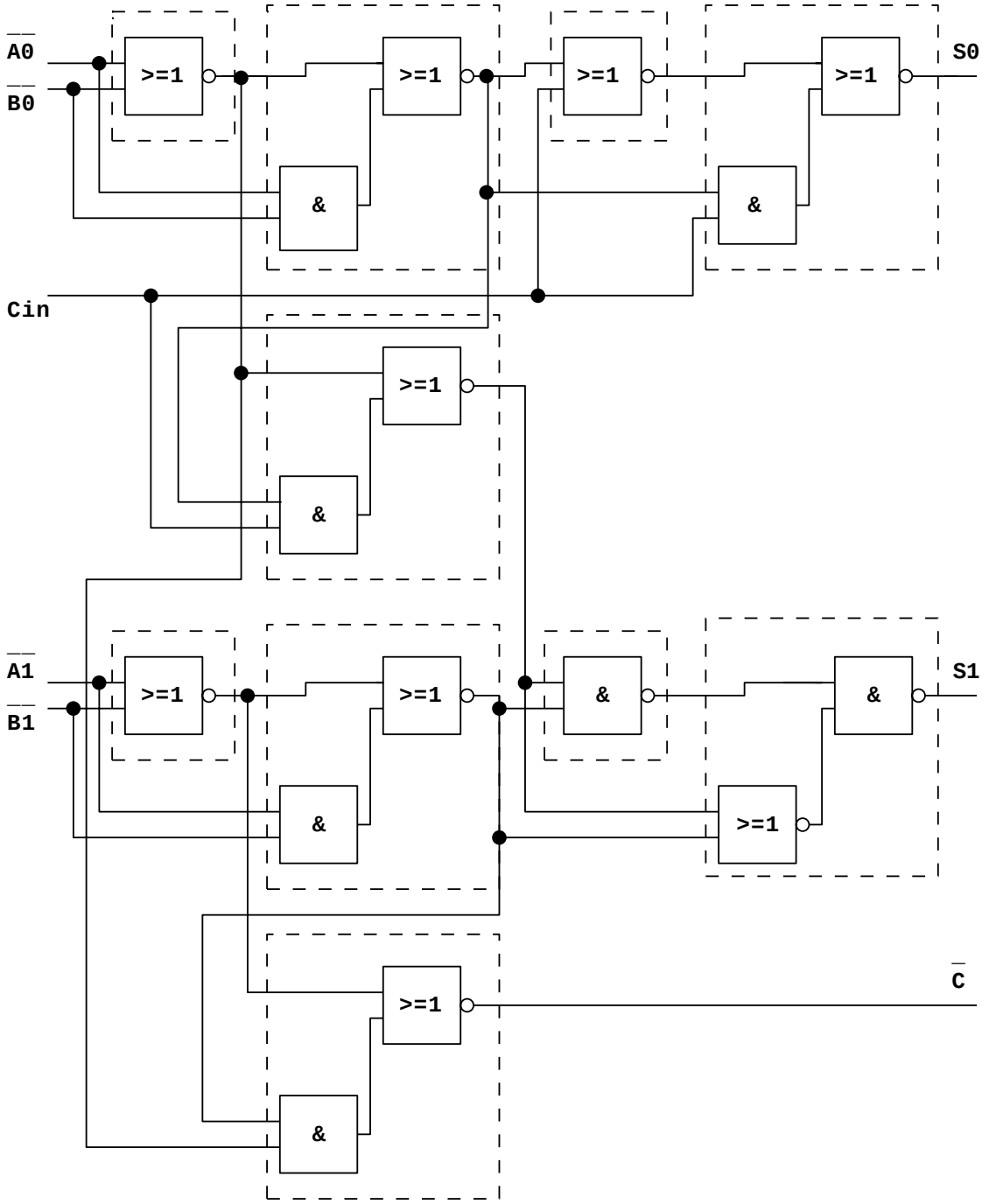

FIGURE 12.1: *Circuit diagram of the two bit adder (taken from [Gün95]).*

TABLE 12.1: *Characteristics of the gates that occur in the two bit adding unit.*

Name	logical expression	# nodes	# times
NOR	$\neg(V_1 \vee V_2)$	$3 \cdot 4 + 1 = 13$	3
NAND	$\neg(V_1 \wedge V_2)$	$3 \cdot 4 + 2 = 14$	1
ANDOI	$\neg(V_1 \vee (V_2 \wedge V_3))$	$4 \cdot 4 + 2 = 18$	5
ORANI	$\neg(V_1 \wedge (V_2 \vee V_3))$	$4 \cdot 4 + 2 = 18$	1

circuit diagram of the NAND-gate is given in test problem 9. For the circuit diagrams of the NOR, ANDOI and ORANI gate see Figures 12.2, 12.3 and 12.4. What logical expressions they compute, is listed in Table 12.1. The fourth column in this table lists the number of times the gate occurs in the big circuit. The third column tabulates the number of nodes in the gate. These nodes consist of two types. The first type of nodes consists of the internal nodes of the transistors due to the MOS transistor model of Shichmann and Hodges [SH68]. Each transistor has four internal nodes that are also the links between transistor and the rest of the circuit. The second type of nodes comprises the usual nodes that are used to link circuit components together. These nodes are indicated by a number placed inside a square. To prevent any misunderstanding, we remark that the big dots in Figures 12.2–12.4 do not represent nodes.

The connection of a gate with the rest of the circuit consists of the input nodes and the output node of the gate. The input signals enter the gate at the nodes with symbol V_1, V_2 and V_3. The output signal leaves the gate from one of the numbered nodes. To ensure stability of the circuit, such an output node is always connected to a capacitance (we refer to the Fortran driver: `CLOAD` denoting the value of a load capacitance for the logical gates, and `COUT` for the output nodes S_0, S_1 and $\overline{C}$). Finally, three enhancement transistors are coupled with the ANDOI gate at the bottom for a correct treatment of C_{in}. This yields 12 internal nodes and two additional nodes, because the three transistors

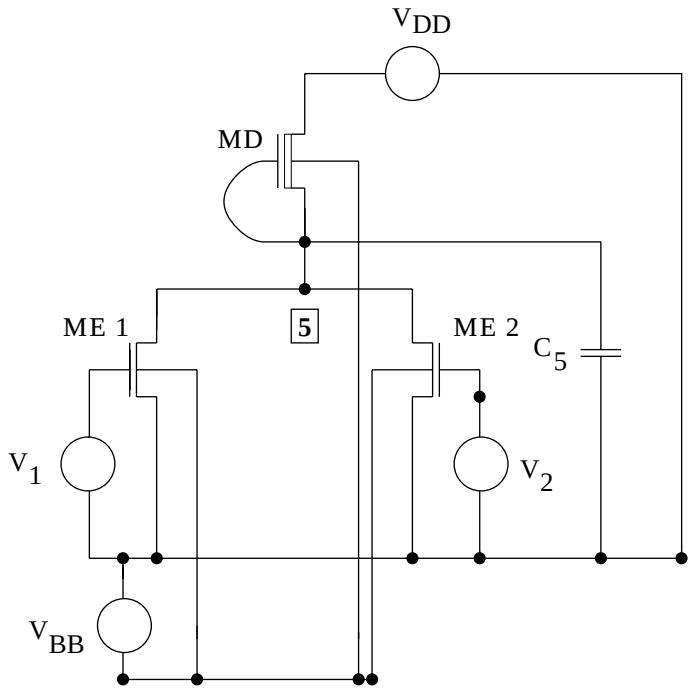

FIGURE 12.2: *Circuit diagram of the NOR gate (taken from [Gün95]).*

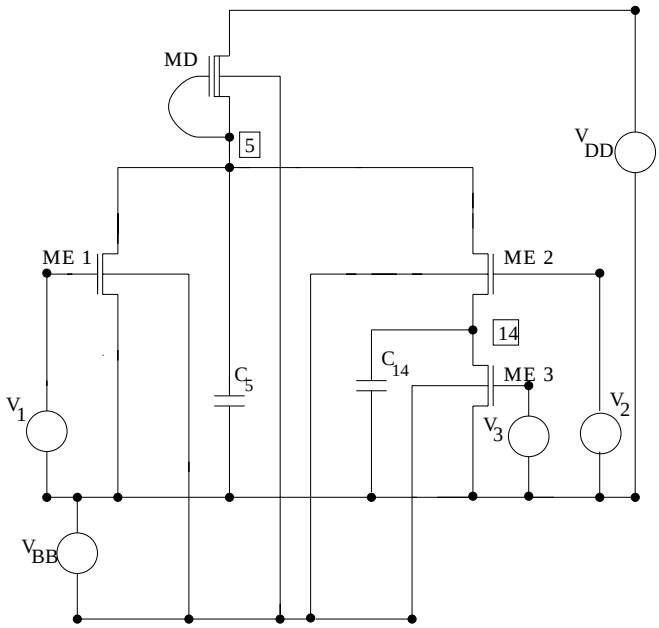

FIGURE 12.3: *Circuit diagram of the ANDOI gate (taken from [Gün95]).*

are coupled in series. Counting all nodes we have $3 \cdot 13 + 1 \cdot 14 + 5 \cdot 18 + 1 \cdot 18 + 14 = 175$ nodes.

Applying Kirchoff's law to all nodes yields a system of 175 equations. This system is an integral form DAE of the special form

$$A \cdot \dot{q}(V) = f(t, V).$$

The function q is a generally nonlinear function of node potentials V, which describes the charges stored in all charge storing elements [GDF96]. Assembling the charge flow at each node by an incidence matrix A, the dynamic part $A \cdot \dot{q}(V)$ equals the contribution of static currents denoted by $f(t, V)$. If all load capacitances at the output nodes are nonzero, then the integral form DAE has differential index 0. If only one of the load capacitances equals zero, the generalized capacitance matrix $A \cdot \partial q(V)/\partial V$ is singular, yielding a system of differential index 1. This shows the regularization effects by applying additional capacitances. Here, we use `CLOAD=0` and `COUT=2.0`.

To make this problem suitable for the solvers used in this test set, the variable $Q = A \cdot q(V)$ of assembled charges is introduced leading to

$$\begin{aligned} \dot{Q} &= f(t, V), \\ 0 &= Q - Aq(V). \end{aligned}$$

This transformation of the integral form DAE into a linearly implicit system raises the differential index by one. However, in the case of singular load capacitances, no higher index effects are detected in the sense of an appropriate perturbation index [Gün98].

Some of the 175 variables have a special meaning. These are the voltage variables of the nodes that deliver the output signals. The output signals S_0, S_1 and $\overline{C}$ are given by the variables x_{49}, x_{130} and x_{148}, respectively. Only these variables are of interest to the engineer.

In the next section we shall see the two bit adder in operation. Every 10 units of time the addition

$$A_1\ A_0 + B_1\ B_0 + C_{in} = C\ S_1\ S_0,$$

is carried out. The numbers that are added are represented by the input signals depicted in Figure 12.5. The outcome of the addition is represented by output signals given in Figure 12.6. Often the output

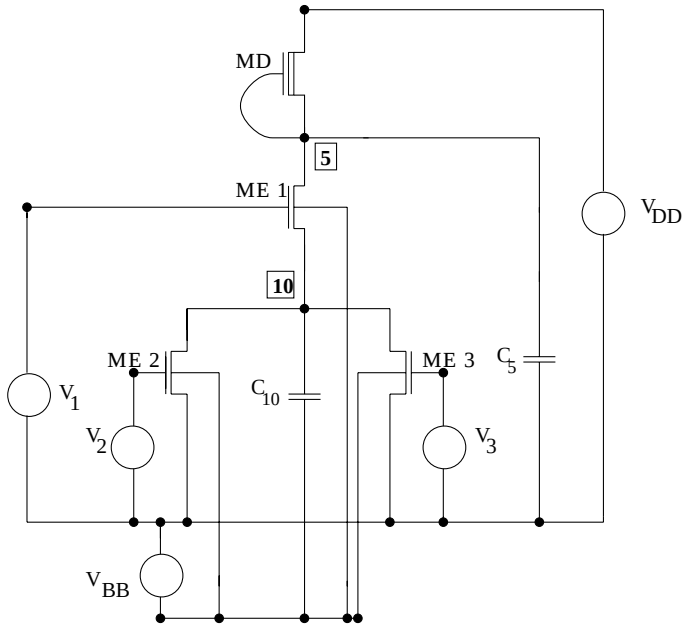

FIGURE 12.4: *Circuit diagram of the ORANI gate (taken from [Gün95]).*

signals need time to adjust to changes in the input signal. Therefore, only during certain periods the sum is correctly represented by the output signals. The two bit adding unit has been designed in such a way that after each 10 units of time the output signal represents the sum correctly.

To see the two bit adding unit performing an addition let us see what happens at $t = 200$. Then the input signals read:

$$\overline{A}_0 = 0,\ \overline{A}_1 = 1,\ \overline{B}_0 = 0, \overline{B}_1 = 0,\ C_{in} = 1,$$

and the output signals are

$$S_0 = 1,\ S_1 = 0,\ \overline{C} = 0.$$

Recall, that a bar denotes the logical inverse. Clearly, the addition 01+11+1=101 has been carried out.

12.4 Numerical solution of the problem

M. Günther provided the source code that defines the problem.

Table 11.2 lists the voltages of the output signals in the reference solution. For the complete reference solution at $t = 320$ we refer to subroutine `solut`. Since these components refer to the output signals

TABLE 12.2: *Value at the end of the integration interval of the components of the reference solution that correspond to the output signals.*

x_{49}	0.2040419147264534
x_{130}	$0.4997238455712048 \cdot 10$
x_{148}	0.2038985905095614

S_0, S_1 and $\overline{C}$, they are the physically relevant quantities.

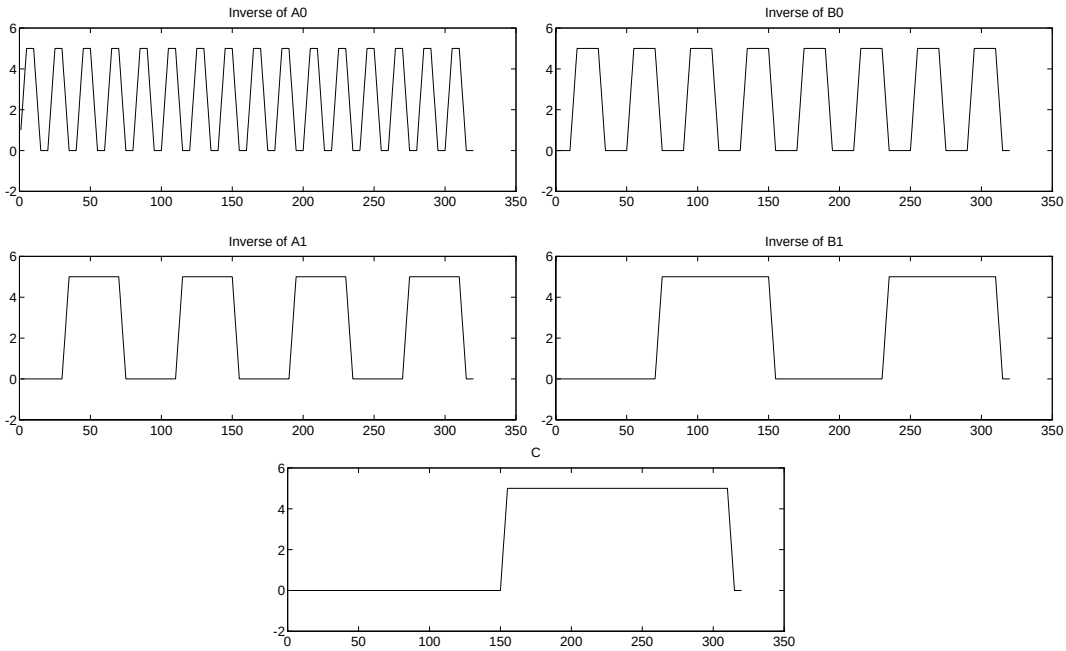

FIGURE 12.5: *The input signals* $\overline{A}_0$, $\overline{A}_1$, $\overline{B}_0$, $\overline{B}_1$ *and* C.

TABLE 12.3: *Failed runs.*

solver	m	reason
PSIDE-1	$8, 9, \ldots, 16$	stepsize too small
RADAU	$0, 1, \ldots, 16$	solver cannot handle `IERR=-1`.
RADAU5	$0, 1, \ldots, 16$	solver cannot handle `IERR=-1`.

Although the function f in (12.1) has discontinuities in its derivative at $t = 0, 5, 10, \ldots, 320$, the results presented here refer to the case in which the solvers are not restarted at these time points. For this case, the argument of the square roots in the function f becomes often negative and the solvers that cannot handle `IERR=-1` break down. If we would restart, then all solvers except DASSL produce too small stepsizes for many input tolerances. Currently, we do not understand this phenomenon.

Table 12.4 and Figures 12.6–12.7 present the run characteristics, the behavior of the output signals over the integration interval and the work-precision diagram, respectively. In computing the scd values, only x_{49}, x_{130} and x_{148} were considered, since they refer to the physically important quantities.

The reference solution was computed using RADAU5 without restarts in the discontinuities in time of the derivative of the problem defining function f, with rtol = atol = 10^{-5} and h0 = $4 \cdot 10^{-5}$.

For the work-precision diagram, we used: rtol = $10^{-(2+m/8)}$, $m = 0, 1, \ldots, 16$; atol = rtol; h0 = $10 \cdot$ rtol for RADAU, RADAU5 and MEBDFDAE. The failed runs are in Table 12.3; listed are the name of the solver that failed, for which values of m this happened, and the reason for failing. The speed-up factor for PSIDE could not be determined because all PSIDE runs failed on the Cray C90.

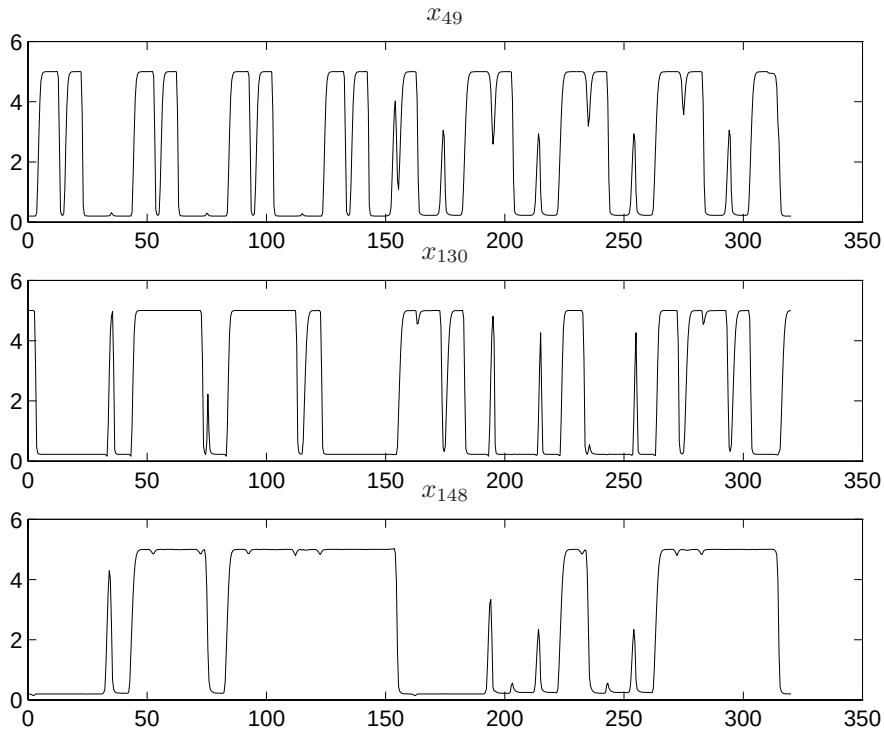

FIGURE 12.6: *Behavior of the output signals S_0, S_1 and $\overline{C}$ over the integration interval.*

Remark M. Günther also wrote a special purpose solver called CHORAL, which stands for CHarge-ORiented ALgorithm [Gün95, Gün98] for integrating equations of the form

$$\begin{aligned} \frac{dy}{dt} &= f(t,x), \\ 0 &= y - q(x). \end{aligned}$$

Most equations occurring in circuit analysis are of this form. In these equations the variables y and x represent respectively (assembled) charges and voltages. CHORAL is based on Rosenbrock-Wanner methods, while the special structure of the problem is exploited. The code eliminates the y variables, reducing the linear algebra work to solving systems of order 175 instead of 350. Correspondingly, a step size prediction and error control based directly on node potentials and currents is offered. For more information see

`http://www.mathematik.th-darmstadt.de/~guenther/Welcome.html`.

TABLE 12.4: *Run characteristics.*

solver	rtol	atol	h0	scd	steps	accept	# f	# Jac	# LU	CPU
DASSL	10^{-2}	10^{-2}		2.08	1550	1385	3085	502		724.18
	10^{-4}	10^{-4}		4.84	5951	5516	9531	833		1393.74
MEBDFDAE	10^{-2}	10^{-2}	10^{-1}	2.85	2027	1758	214802	601	601	998.52
	10^{-4}	10^{-4}	10^{-3}	3.72	5312	4962	345254	957	957	1883.89
PSIDE-1	10^{-2}	10^{-2}		3.73	1277	832	18312	615	5000	2154.62

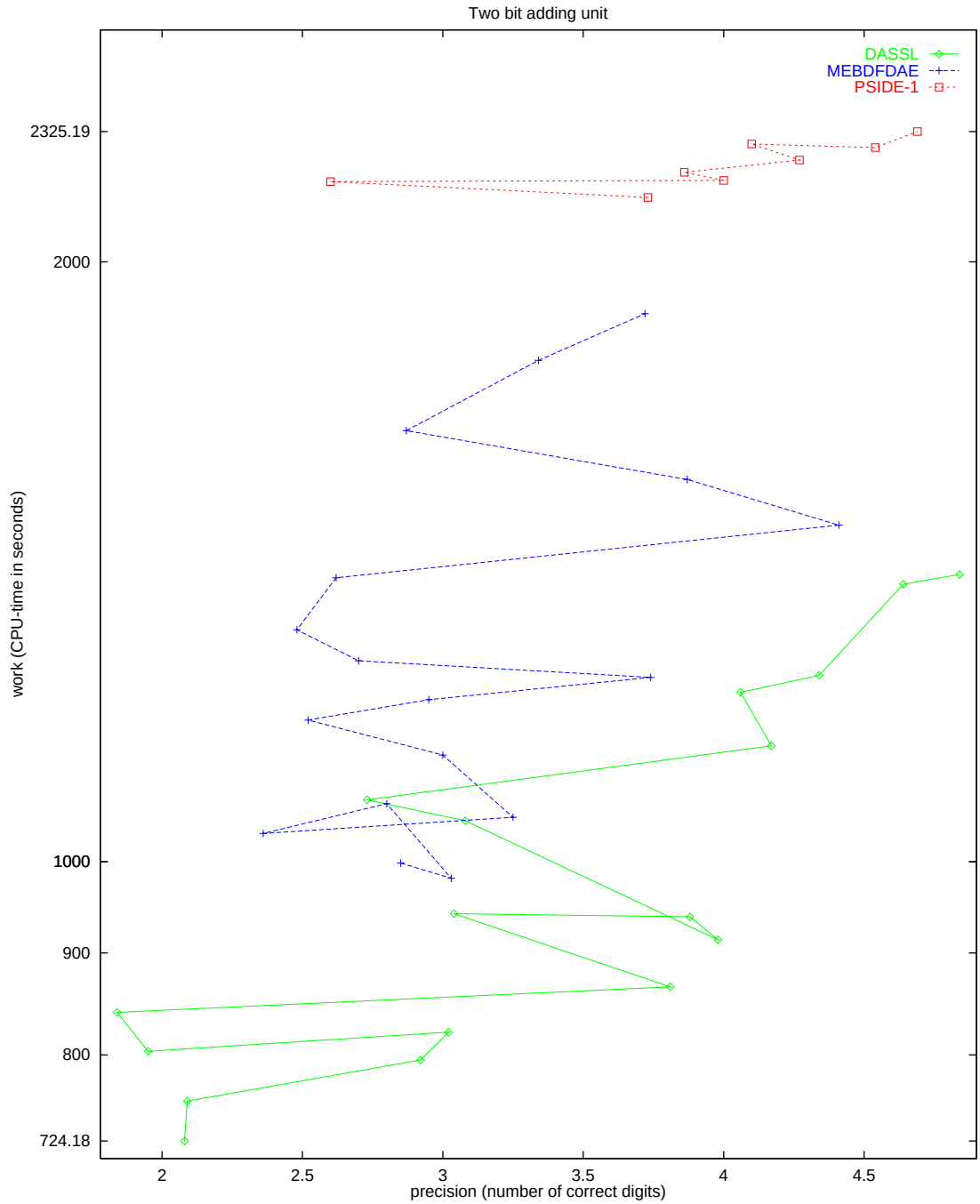

FIGURE 12.7: *Work-precision diagram.*

References

[GDF96] M. Günther, G. Denk, and U. Feldmann. Modeling and simulating charge sensitive circuits. *Math. Modelling of Systems*, 2:69–81, 1996.

[Gün95] M. Günther. *Ladungsorientierte Rosenbrock–Wanner–Methoden zur numerischen Simulation digitaler Schaltungen.* Number 168 in Fortschritt-Berichte VDI Reihe 20. VDI-Verlag, Düsseldorf, 1995.

[Gün98] M. Günther. Simulating digital circuits numerically – a charge-oriented ROW approach. *Numer. Math.*, 79(2):203–212, 1998.

[SH68] H. Shichman and D.A. Hodges. Insulated-gate field-effect transistor switching circuits. *IEEE J. Solid State Circuits*, SC-3:285–289, 1968.

13. The car axis problem

13.1 General information

The problem is a stiff DAE of index 3, consisting of 8 differential and 2 algebraic equations. It has been taken from [Sch94]. Since not all initial conditions were given, we have chosen a consistent set of initial conditions.

13.2 Mathematical description of the problem

The problem is of the form

$$\begin{aligned} p' &= q, && (13.1)\\ Kq' &= f(t,p,\lambda), \qquad p,q \in \mathbb{R}^4, \quad \lambda \in \mathbb{R}^2, \quad 0 \le t \le 3, && (13.2)\\ 0 &= \phi(t,p), && (13.3) \end{aligned}$$

with initial conditions $p(0) = p_0$, $q(0) = q_0$, $p'(0) = q_0$, $q'(0) = q_0'$, $\lambda(0) = \lambda_0$ and $\lambda'(0) = \lambda_0'$.

The matrix K reads $\varepsilon^2 \frac{M}{2} I_4$, where I_4 is the 4×4 identity matrix. The function $f : \mathbb{R}^9 \to \mathbb{R}^4$ is given by

$$f(t,p,\lambda) = \begin{pmatrix} (l_0 - l_l)\dfrac{x_l}{l_l} & +\lambda_1 x_b + 2\lambda_2(x_l - x_r) & \\ (l_0 - l_l)\dfrac{y_l}{l_l} & +\lambda_1 y_b + 2\lambda_2(y_l - y_r) & -\varepsilon^2\dfrac{M}{2} \\ (l_0 - l_r)\dfrac{x_r - x_b}{l_r} & -2\lambda_2(x_l - x_r) & \\ (l_0 - l_r)\dfrac{y_r - y_b}{l_r} & -2\lambda_2(y_l - y_r) & -\varepsilon^2\dfrac{M}{2} \end{pmatrix}.$$

Here, $(x_l, y_l, x_r, y_r)^{\mathrm{T}} := p$, and l_l and l_r are given by

$$\sqrt{x_l^2 + y_l^2} \quad \text{and} \quad \sqrt{(x_r - x_b)^2 + (y_r - y_b)^2}.$$

Furthermore, the functions $x_b(t)$ and $y_b(t)$ are defined by

$$\begin{aligned} x_b(t) &= \sqrt{l^2 - y_b^2(t)}, && (13.4)\\ y_b(t) &= r\sin(\omega t). && (13.5) \end{aligned}$$

The function $\phi : \mathbb{R}^5 \to \mathbb{R}^2$ reads

$$\phi(t,p) = \begin{pmatrix} x_l x_b + y_l y_b \\ (x_l - x_r)^2 + (y_l - y_r)^2 - l^2 \end{pmatrix}.$$

The constants are listed below.

l	=	1	ϵ	=	10^{-2}	h	=	1/5	ω	=	10
l_0	=	1/2	M	=	10	τ	=	$\pi/5$			

Consistent initial values are

$$p_0 = \begin{pmatrix} 0 \\ 1/2 \\ 1 \\ 1/2 \end{pmatrix}, \quad q_0 = \begin{pmatrix} -1/2 \\ 0 \\ -1/2 \\ 0 \end{pmatrix}, \quad q_0' = \frac{2}{M\varepsilon^2} f(0, p_0, \lambda_0), \quad \lambda_0 = \lambda_0' = (0,0)^{\mathrm{T}}.$$

The index of the variables p, q and λ is 1, 2 and 3, respectively.

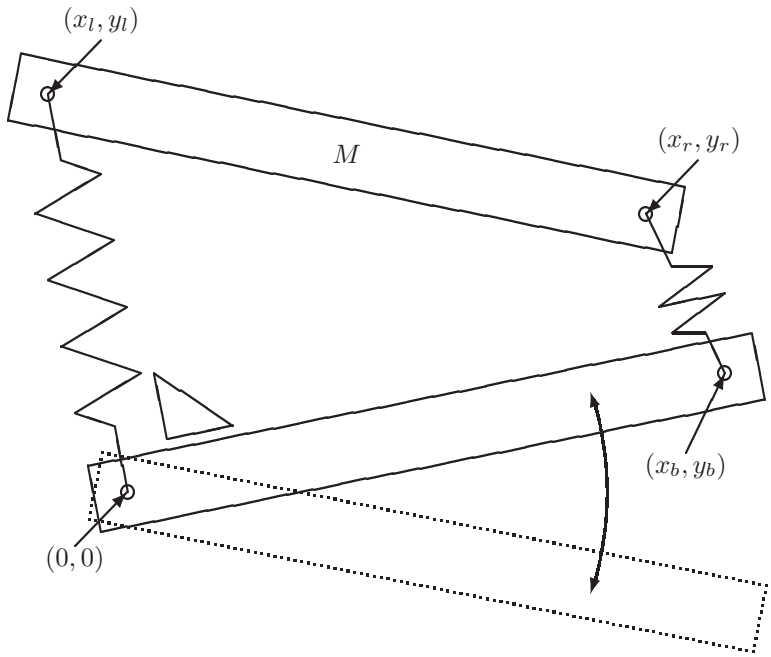

FIGURE 13.1: *Model of the car axis.*

13.3 Origin of the problem

The car axis problem is an example of a rather simple multibody system, in which the behavior of a car axis on a bumpy road is modeled by a set of differential-algebraic equations.

A simplification of the car is depicted in Figure 13.1. We model the situation that the left wheel at the origin $(0, 0)$ rolls on a flat surface and the right wheel at coordinates (x_b, y_b) rolls over a hill of height h every τ seconds. This means that y_b varies over time according to (13.5). The length of the axis, denoted by l, remains constant over time, which means that x_b has to fulfill (13.4). Two springs carry over the movement of the axis between the wheels to the chassis of the car, which is represented by the bar (x_l, y_l)–(x_r, y_r) of mass M. The two springs are assumed to be massless and have Hooke's constant $1/\epsilon^2$ and length l_0 at rest.

There are two position constraints. Firstly, the distance between (x_l, y_l) and (x_r, y_r) must remain constantly l and secondly, for simplicity of the model, we assume that the left spring remains orthogonal to the axis. If we identify p with the vector $(x_l, y_l, x_r, y_r)^{\mathrm{T}}$, then we see that Equation (13.3) reflects these constraints.

Using Lagrangian mechanics, the equations of motions for the car axis are given by

$$\frac{M}{2}\frac{\mathrm{d}^2 p}{\mathrm{d}t^2} = F_{\mathrm{H}} + G^{\mathrm{T}}\lambda + F_{\mathrm{g}}. \tag{13.6}$$

Here, G is the 2×4 Jacobian matrix of the function ϕ with respect to p and λ is the 2-dimensional vector containing the so-called Lagrange multipliers. The factor $M/2$ is explained by the fact that the mass M is divided equally over (x_l, y_l) and (x_r, y_r). The force F_{H} represents the spring forces:

$$F_{\mathrm{H}} = -(\cos(\alpha_l)F_l, \sin(\alpha_l)F_l, \cos(\alpha_r)F_r, \sin(\alpha_r)F_r)^{\mathrm{T}},$$

where F_l and F_r are the forces induced by the left and right spring, respectively, according to Hooke's law:

$$\begin{aligned} F_l &= (l_l - l_0)/\epsilon^2, \\ F_r &= (l_r - l_0)/\epsilon^2. \end{aligned}$$

Here, l_l and l_r are the actual lengths of the left and right spring, respectively:

$$\begin{aligned} l_l &= \sqrt{x_l^2 + y_l^2}, \\ l_r &= \sqrt{(x_r - x_b)^2 + (y_r - y_b)^2}. \end{aligned}$$

Furthermore, α_l and α_r are the angles of the left and right spring with respect to the horizontal axis of the coordinate system:

$$\begin{aligned} \alpha_l &= \arctan(y_l/x_l), \\ \alpha_r &= \arctan((y_r - y_b)/(x_r - x_b)). \end{aligned}$$

Finally, F_g represents the gravitational force

$$F_g = -(0, 1, 0, 1)^{\mathrm{T}} \frac{M}{2} g.$$

The original formulation [Sch94] sets $g = 1$.

We rewrite (13.6) as a system of first order differential equations by introducing the velocity vector q, so that we obtain the first order differential equations (13.1) and

$$\frac{M}{2} \frac{\mathrm{d}q}{\mathrm{d}t} = F_{\mathrm{H}} + G^{\mathrm{T}} \lambda + F_{\mathrm{g}}. \tag{13.7}$$

Setting $f = F_{\mathrm{H}} + G^{\mathrm{T}} \lambda + F_g$, it is easily checked that multiplying (13.7) by ε^2 yields (13.2).

To arrive at a consistent set of initial values p_0, q_0 and λ_0, we have to solve the system of equations consisting of the constraint

$$\phi(t_0, p_0) = 0, \tag{13.8}$$

and the 1 up to $k-1$ times differentiated constraint (13.8), where k is the highest variable index. To facilitate notation, we introduce $\tilde{p} := (t, p^{\mathrm{T}})^{\mathrm{T}}$ and its derivative $\tilde{q} := \frac{\mathrm{d}\tilde{p}}{\mathrm{d}t} = (1, q^{\mathrm{T}})^{\mathrm{T}}$. The Jacobian of ϕ with respect to $\tilde{p}$ will be denoted by $\tilde{G}$. Here, $k = 3$, yielding the additional conditions

$$\tilde{G}(\tilde{p}_0)\tilde{q}_0 = 0 \tag{13.9}$$

and

$$\phi_{\tilde{p}\tilde{p}}(\tilde{p}_0)(\tilde{q}_0, \tilde{q}_0) + \tilde{G}(\tilde{p}_0)\tilde{q}_0' = 0,$$

where $\phi_{\tilde{p}\tilde{p}}$ denotes the second derivative of ϕ with respect to $\tilde{p}$. Using (13.6) and the fact that the first component of $\tilde{q}_0'$ vanishes, the latter condition equals

$$\phi_{\tilde{p}\tilde{p}}(\tilde{p}_0)(\tilde{q}_0, \tilde{q}_0) + \frac{2}{M} G(p_0) \left(F_{\mathrm{H}}(p_0) + G^{\mathrm{T}}(p_0)\lambda_0 + F_{\mathrm{g}}(p_0) \right) = 0. \tag{13.10}$$

The equations (13.8)–(13.10) are solved for

$$\begin{aligned} x_r &= l, \\ x_l &= 0, \\ y_r &= y_l = l_0, \\ x_r' &= x_l' = -\frac{l_0}{l} \frac{\pi}{\tau} h, \\ y_r' &= \frac{l^2 \tau}{M \pi h} (2\lambda_1 - \lambda_2), \\ y_l' &= \frac{l^2 \tau}{M \pi h} (2\lambda_1 - \lambda_2) \pm l \sqrt{\frac{-8\lambda_1 + 2\lambda_2}{M}}. \end{aligned}$$

Choosing $\lambda_1 = \lambda_2 = 0$, we arrive at the initial conditions listed in §13.2,

TABLE 13.1: *Reference solution at the end of the integration interval.*

y_1	$0.4934557842755629 \cdot 10^{-1}$	y_6	$0.7446866596327776 \cdot 10^{-2}$
y_2	0.4969894602303324	y_7	$0.1755681574942899 \cdot 10^{-1}$
y_3	$0.1041742524885400 \cdot 10$	y_8	0.7703410437794031
y_4	0.3739110272652214	y_9	$-0.4736886750784630 \cdot 10^{-2}$
y_5	$-0.7705836840321485 \cdot 10^{-1}$	y_{10}	$-0.1104680411345730 \cdot 10^{-2}$

13.4 Numerical solution of the problem

Tables 13.1–13.2 and Figures 13.2–13.4 present the reference solution at the end of the integration interval, the run characteristics, the behavior of some solution components over the integration interval and the work-precision diagrams, respectively. The reference solution was computed on the Cray C90, using PSIDE with Cray double precision and atol = rtol = 10^{-16}. For the work-precision diagrams, we used: rtol = $10^{-(4+m/4)}$, $m = 0, 1, \ldots, 24$; atol = rtol; h0 = rtol for RADAU, RADAU5 and MEBDFDAE. The speed-up factor for PSIDE is 1.78.

TABLE 13.2: *Run characteristics.*

solver	rtol	atol	h0	scd	steps	accept	# f	# Jac	# LU	CPU
MEBDFDAE	10^{-4}	10^{-4}	10^{-4}	-0.50	275	273	754	26	26	0.22
	10^{-7}	10^{-7}	10^{-7}	1.59	787	783	1968	72	72	0.60
	10^{-10}	10^{-10}	10^{-10}	4.42	1717	1713	4152	166	166	1.29
PSIDE-1	10^{-4}	10^{-4}		-0.28	55	54	1403	42	220	0.30
	10^{-7}	10^{-7}		2.27	179	172	4103	83	464	0.83
	10^{-10}	10^{-10}		4.86	625	612	13751	115	964	2.63
RADAU	10^{-4}	10^{-4}	10^{-4}	0.19	98	97	850	95	98	0.16
	10^{-7}	10^{-7}	10^{-7}	2.51	289	288	2559	282	288	0.48
	10^{-10}	10^{-10}	10^{-10}	4.22	179	178	4281	170	179	0.61
RADAU5	10^{-4}	10^{-4}	10^{-4}	0.19	98	97	850	95	98	0.15
	10^{-7}	10^{-7}	10^{-7}	2.51	289	288	2559	282	288	0.46
	10^{-10}	10^{-10}	10^{-10}	3.15	884	883	8101	861	883	1.42

REFERENCES

[Sch94] S. Schneider. *Intégration de systèmes d'équations différentielles raides et différentielles-algébriques par des méthodes de collocations et méthodes générales linéaires.* PhD thesis, Université de Genève, 1994.

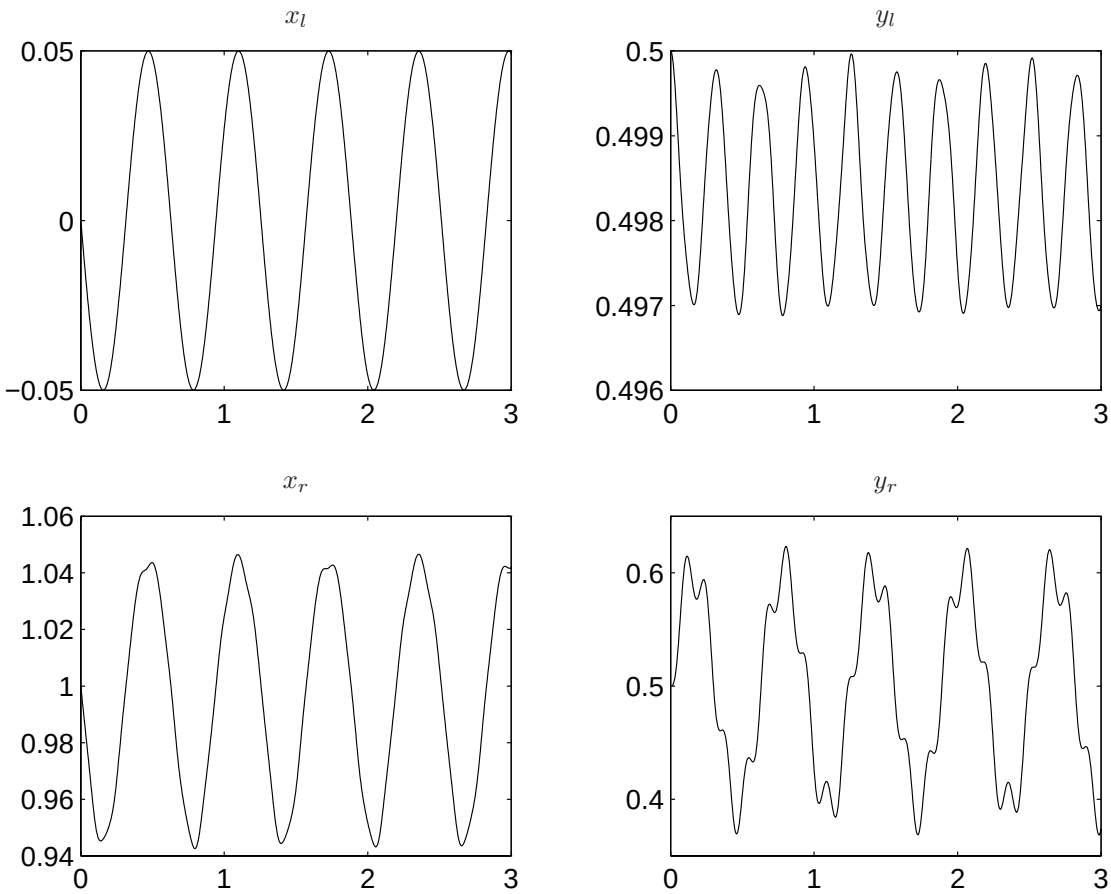

FIGURE 13.2: *Behavior of* (x_l, y_l) *and* (x_r, y_r) *over the integration interval.*

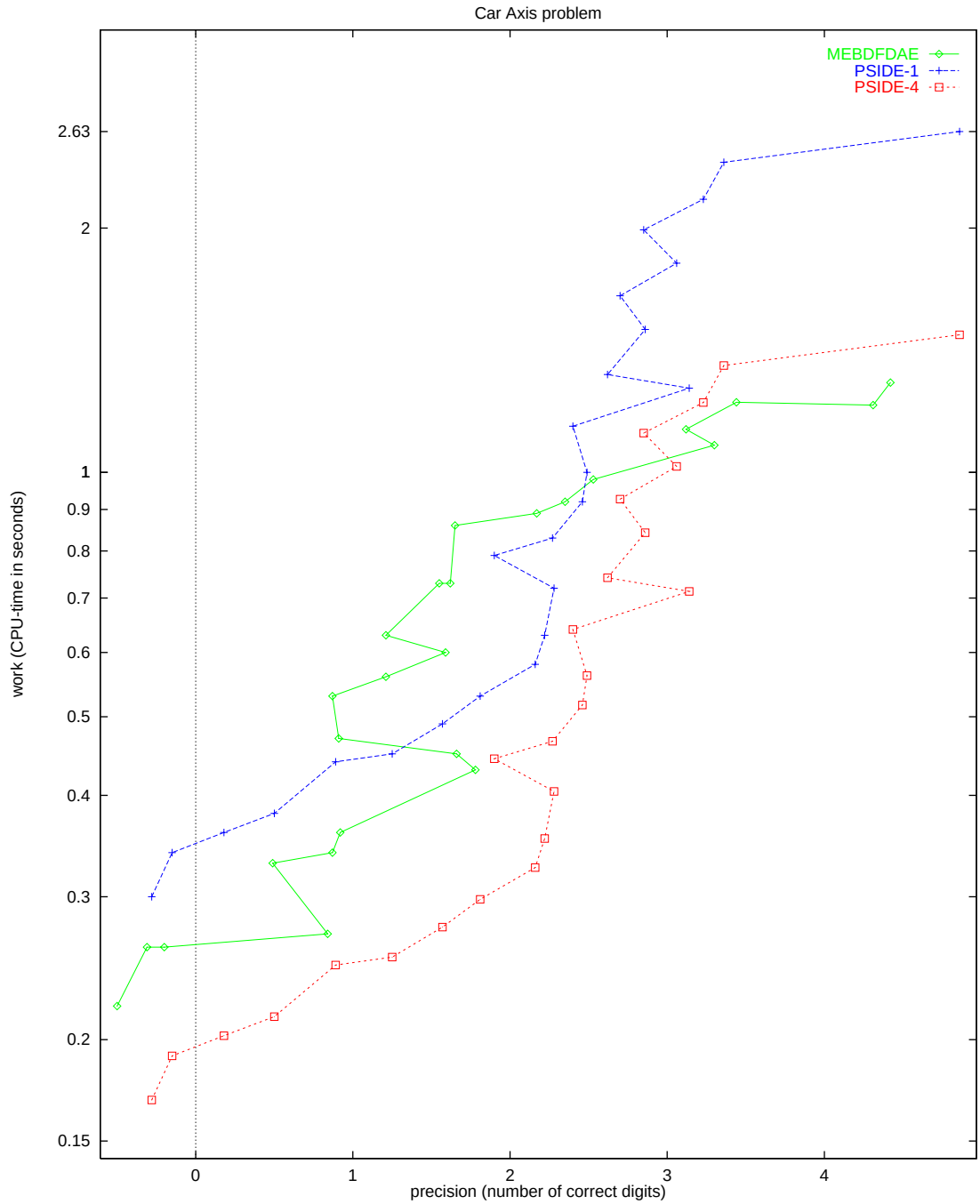

FIGURE 13.3: *Work-precision diagram.*

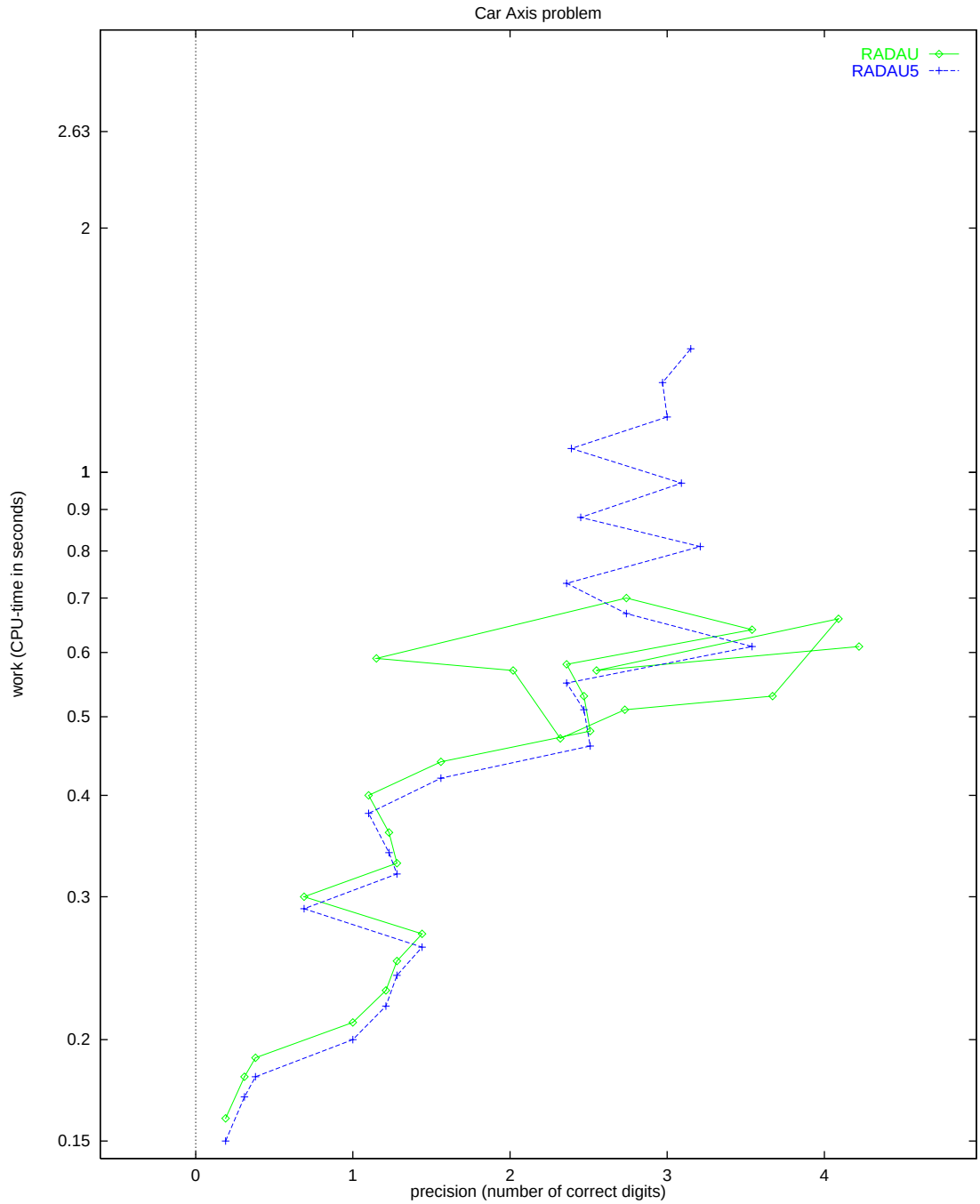

FIGURE 13.4: *Work-precision diagram.*

14. Fekete problem

14.1 General information

The problem is an index 2 DAE from mechanics. The dimension is $8N$, where N is a user supplied integer. The numerical tests shown here correspond to $N = 20$. The problem is of interest for the computation of the elliptic Fekete points [Par95]. The parallel-IVP-algorithm group of CWI contributed this problem to the test set, in collaboration with W. J. H. Stortelder.

14.2 Mathematical description of the problem

The problem is of the form

$$M\frac{\mathrm{d}y}{\mathrm{d}t} = f(y), \quad y(0) = y_0, \quad y'(0) = y'_0, \tag{14.1}$$

with

$$y, f \in \mathbb{R}^{8N}, \quad 0 \le t \le t_{\mathrm{end}}.$$

Here, $t_{\mathrm{end}} = 1000$, $N = 20$ and M is the (constant) mass matrix given by

$$M = \begin{pmatrix} I_{6N} & 0 \\ 0 & 0 \end{pmatrix},$$

where I_{6N} is the identity matrix of dimension $6N$. For the definition of the function f, we refer to §14.3.

The components $y_{0,i}$ of of the initial vector y_0 are defined by

$$\begin{pmatrix} y_{0,3(j-1)+1} \\ y_{0,3(j-1)+2} \\ y_{0,3(j-1)+3} \end{pmatrix} = \begin{pmatrix} \cos(\omega_j)\cos(\beta_j) \\ \sin(\omega_j)\cos(\beta_j) \\ \sin(\beta_j) \end{pmatrix} \quad \text{for} \quad j = 1, \ldots, N,$$

where

$$\begin{array}{lllllll}
\beta_j &=& \frac{3}{8}\pi & \text{and} & \omega_j &=& \frac{2j}{3}\pi + \frac{1}{13}\pi \quad \text{for} \quad j = 1, \ldots, 3, \\
\beta_j &=& \frac{1}{8}\pi & \text{and} & \omega_j &=& \frac{2(j-3)}{7}\pi + \frac{1}{29}\pi \quad \text{for} \quad j = 4, \ldots, 10, \\
\beta_j &=& -\frac{2}{15}\pi & \text{and} & \omega_j &=& \frac{2(j-10)}{6}\pi + \frac{1}{7}\pi \quad \text{for} \quad j = 11, \ldots, 16, \\
\beta_j &=& -\frac{3}{10}\pi & \text{and} & \omega_j &=& \frac{2(j-17)}{4}\pi + \frac{1}{17}\pi \quad \text{for} \quad j = 17, \ldots, 20,
\end{array}$$

and

$$\begin{array}{lcll}
y_{0,i} & = & 0 & \text{for} \quad i = 3N+1, \ldots, 6N, \\
y_{0,6N+j} & = & \frac{1}{2}\langle p_j(0), \widehat{f}_j \rangle & \text{for} \quad j = 1, \ldots, N, \\
y_{0,i} & = & 0 & \text{for} \quad i = 7N+1, \ldots, 8N,
\end{array}$$

where

$$p_j = \begin{pmatrix} y_{3(j-1)+1} \\ y_{3(j-1)+2} \\ y_{3(j-1)+3} \end{pmatrix}, \quad \widehat{f}_j = \begin{pmatrix} f_{3N+3(j-1)+1}((p(0), 0, \ldots, 0)^{\mathrm{T}}) \\ f_{3N+3(j-1)+2}((p(0), 0, \ldots, 0)^{\mathrm{T}}) \\ f_{3N+3(j-1)+3}((p(0), 0, \ldots, 0)^{\mathrm{T}}) \end{pmatrix}, \tag{14.2}$$

and $p = (y_1, y_2, \ldots, y_{3N})^{\mathrm{T}}$. The initial derivative vector reads $y'_0 = f(y_0)$. These definitions of y_0 and y'_0 yield consistent initial values. The first $6N$ components are of index 1, the last $2N$ of index 2.

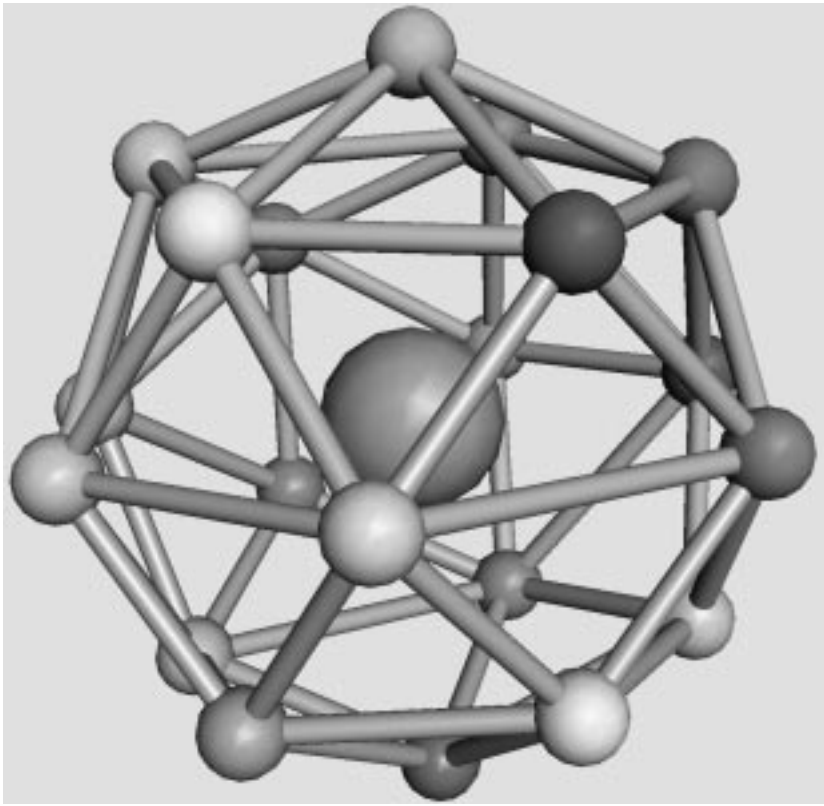

FIGURE 14.1: *Final configuration for $N = 20$. The large ball is centered at the origin and only added to facilitate the 3-D perception. (Taken from [PSS97] by courtesy of R. van Liere.)*

14.3 Origin of the problem

This problem is of interest for the computation of the elliptic Fekete points. Let us define the unit sphere in $\mathbb{R}^3$ by $\mathcal{S}^2$ and for any configuration $x := (x_1, x_2, \ldots, x_N)^{\mathrm{T}}$ of points $x_i \in \mathcal{S}^2$, the function

$$V(x) := \prod_{i<j} \|x_i - x_j\|_2. \tag{14.3}$$

We denote the value of x for which V reaches its global maximum by $\widehat{x} = (\widehat{x}_1, \ldots, \widehat{x}_N)$. The points $\widehat{x}_1, \widehat{x}_2, \ldots, \widehat{x}_N$ are called the elliptic Fekete points of order N. For example, for $N = 4$, the points of the optimal solution form a tetrahedron. But, in case of 8 points, intuition fails; the elliptic Fekete points do not form a cube in this case. A cube where, for example, the upper plane is rotated over 45° with respect to the bottom plane, gives already a larger value of V. It turns out (see e.g. [Par95]) that $\widehat{x}$ is difficult to compute as solution of an global optimization problem. For reasons that will become clear later, we differentiate $\log(V)$ with respect to x_k and apply the method of Lagrange multipliers, to see that $\widehat{x}$ fulfills

$$\nabla_k \log(V(x)) \mid_{x=\widehat{x}} = \sum_{j \neq k} \frac{\widehat{x}_k - \widehat{x}_j}{\|\widehat{x}_k - \widehat{x}_j\|_2^2} = \zeta_k \widehat{x}_k, \tag{14.4}$$

where the ζ_k are Lagrange multipliers.

We now discuss the Fekete points from another point of view. Consider on $\mathcal{S}^2$ a number of N particles, on which two forces are invoked: a repulsive force, by which the particles will start to move away from each other, and an adhesion force, by which the particles will reach a stationary state after a certain period of time.

We denote the position in Cartesian coordinates of particle i at time t by $p_i(t)$ and the configuration of N points at time t by $p(t) = (p_1(t), \ldots, p_N(t))^{\mathrm{T}}$. The stationary configuration is assumed to be obtained at $t = t_{\mathrm{stat}}$ and will be denoted by $\widehat{p} := (\widehat{p}_1, \widehat{p}_2, \ldots, \widehat{p}_N)$, where $\widehat{p}_i := p_i(t_{\mathrm{stat}})$. The repulsive force on particle i caused by particle j is defined by

$$F_{ij} = \frac{p_i - p_j}{\|p_i - p_j\|_2^{\gamma}}.$$

Note that the choice $\gamma = 3$ can be interpreted as an electrical force working on particles with unit charge. The adhesion force working on particle i is denoted by A_i and given by

$$A_i = -\alpha q_i.$$

Here, q is the velocity vector and α is valued 0.5.

We can compute the configuration of the particles as function of time, given that the particles cannot leave the unit sphere, as solution of the DAE system

$$\begin{aligned} p' &= q, && (14.5)\\ q' &= g(p,q) + G^{\mathrm{T}}(p)\lambda, && (14.6)\\ 0 &= \phi(p), && (14.7) \end{aligned}$$

where $G = \partial\phi/\partial p$ and $\lambda \in \mathbb{R}^N$. The function $\phi : \mathbb{R}^{3N} \to \mathbb{R}^N$ represents the constraint, which states that the particles remain on the unit sphere:

$$\phi_i(p) = p_{i,1}^2 + p_{i,2}^2 + p_{i,3}^2 - 1.$$

The function $g : \mathbb{R}^{6N} \to \mathbb{R}^{3N}$ is given by $g = (g_i)$, $i = 1, \ldots, N$, where

$$g_i(p,q) = \sum_{j \neq i} F_{ij}(p) + A_i(q).$$

The term $G^{\mathrm{T}}(p)\lambda$ in (14.6) represents the normal force which keeps the particle on $\mathcal{S}^2$.

Since we know that the speed of the final configuration at $t = t_{\mathrm{stat}}$ is 0, we can substitute $q = 0$ and $p = \widehat{p}$ in formula (14.6), thus arriving at

$$0 = \sum_{j \neq i} F_{ij}(\widehat{p}) + G^{\mathrm{T}}(\widehat{p})\lambda \ ,$$

which is equal to

$$\sum_{i \neq j} \frac{\widehat{p}_i - \widehat{p}_j}{\|\widehat{p}_i - \widehat{p}_j\ |^{\gamma}} = -2\lambda_i \widehat{p}_i \, . \qquad (14.8)$$

Comparing (14.4) and (14.8) tells us that computing $\widehat{p}$ for $\gamma = 2$ gives the local optima of the function V in (14.3). In [PSS97], it is showed that computing $\widehat{p}$ by solving the system (14.5)–(14.7) and then substituting $x = \widehat{p}$ in (14.3), results in values of V that are very competitive with those obtained by global optimization packages. For more details on elliptic Fekete points, we refer to [Par95] and [SS93].

The DAE system mentioned before is of index 3. To arrive at a more stable formulation of the problem, we stabilize the constraint (see [BCP89, p. 153]) by replacing (14.5) by

$$p' = q + G^{\mathrm{T}}(p)\mu, \qquad (14.9)$$

where $\mu \in \mathbb{R}^N$, and appending the differentiated constraint

$$0 = G(p)q. \qquad (14.10)$$

TABLE 14.1: *Reference solution at the end of the integration interval.*

$y(1)$	-0.4070263380333202	$y(7)$	0.7100577833343567
$y(2)$	0.3463758772791802	$y(8)$	0.1212948055586120
$y(3)$	0.8451942450030429	$y(9)$	0.6936177005172217
$y(4)$	0.0775293475252155	$y(10)$	0.2348267744557627
$y(5)$	-0.2628662719972299	$y(11)$	0.7449277976923311
$y(6)$	0.9617122871829146	$y(12)$	0.6244509285956391

The system (14.9), (14.6), (14.7), (14.10) is now of index 2; the variables p and q are of index 1, the variables λ and μ of index 2. We cast the system in the form (14.1) by setting $y = (p, q, \lambda, \mu)^{\mathrm{T}}$ and $f(y) = f(p, q, \lambda, \mu) = (q + G^{\mathrm{T}}\mu, g + G^{\mathrm{T}}\lambda, \phi, Gq)^{\mathrm{T}}$, where p_i is in Cartesian coordinates.

The choice for the initial configuration as defined in §14.2 is a rough attempt to spread out the points over the sphere. To arrive at a consistent set of initial values we choose $q(0) = 0$, yielding $\mu(0) = 0$ and $\phi_i'(0) = \langle 2p_i(0), q_i(0)\rangle = 0$. Consequently,

$$\begin{aligned}\phi_i''(0) &= \langle 2p_i(0), q_i'(0)\rangle \\ &= \langle 2p_i(0), g_i(p(0), q(0)) + 2\lambda_i(0)p_i(0)\rangle.\end{aligned}$$

Requiring $\phi_i''(0) = 0$ gives

$$\lambda_i(0) = -\frac{\langle p_i(0), g_i(p(0), q(0))\rangle}{2\langle p_i(0), p_i(0)\rangle} = -\frac{1}{2}\langle p_i(0), g_i(p(0), q(0))\rangle.$$

The initial derivative vector y_0' can be chosen equal to $f(y_0)$. For $N \le 20$, $t_{\mathrm{stat}} \le 1000$, therefore we chose $t_{\mathrm{end}} = 1000$.

In Figure 14.1 the final configuration for 20 points is plotted.

14.4 Numerical solution of the problem

All the tests concern the case with $N = 20$. Tables 14.1–14.2 and Figures 14.2–14.4 present the reference solution at the end of the integration interval (first 12 components), the run characteristics, the behavior of the first 6 solution components over the interval $[0, 20]$ and the work-precision diagrams, respectively. In computing the scd values, only the first sixty components were considered, since they refer to the position of the particles. The reference solution was computed using RADAU5, rtol $= 10^{-12}$, atol $= 10^{-12}$, and h0 $= 10^{-12}$. For the work-precision diagrams, we used: rtol $= 10^{-(2+m/16)}$, $m = 0, 1, \ldots, 32$; atol = rtol; h0 = rtol for RADAU, RADAU5 and MEBDFDAE. The speed-up factor for PSIDE is 3.28.

REFERENCES

[BCP89] K.E. Brenan, S.L. Campbell, and L.R. Petzold. *Numerical Solution of Initial–Value Problems in Differential–Algebraic Equations*. North–Holland, New York–Amsterdam–London, 1989.

[Par95] P.M. Pardalos. An open global optimization problem on the unit sphere. *Journal of Global Optimization*, 6:213, 1995.

[PSS97] J.D. Pintér, W.J.H. Stortelder, and J.J.B. de Swart. Computation of elliptic Fekete point sets. Report MAS-R9705, CWI, Amsterdam, 1997. To appear in CWI Quarterly.

[SS93] M. Shub and S. Smale. Complexity of Bezout's theorem III. Condition number and packing. *Journal of Complexity*, 9:4–14, 1993.

TABLE 14.2: *Run characteristics.*

solver	rtol	atol	h0	scd	steps	accept	# f	# Jac	# LU	CPU
MEBDFDAE	10^{-2}	10^{-2}	10^{-2}	-0.52	69	66	126	15	15	5.30
	10^{-3}	10^{-3}	10^{-3}	2.05	112	111	183	17	17	6.48
	10^{-4}	10^{-4}	10^{-4}	2.64	209	209	334	21	21	9.87
PSIDE-1	10^{-2}	10^{-2}		2.20	73	53	693	16	288	62.75
	10^{-3}	10^{-3}		3.19	88	59	779	11	344	68.47
	10^{-4}	10^{-4}		4.12	114	75	967	9	448	82.83
RADAU	10^{-2}	10^{-2}	10^{-2}	1.97	33	30	274	27	32	23.53
	10^{-3}	10^{-3}	10^{-3}	2.65	43	41	315	38	43	27.57
	10^{-4}	10^{-4}	10^{-4}	4.29	61	58	442	54	61	35.15
RADAU5	10^{-2}	10^{-2}	10^{-2}	1.97	33	30	274	27	32	23.56
	10^{-3}	10^{-3}	10^{-3}	2.65	43	41	315	38	43	27.58
	10^{-4}	10^{-4}	10^{-4}	4.29	61	58	442	54	61	35.18

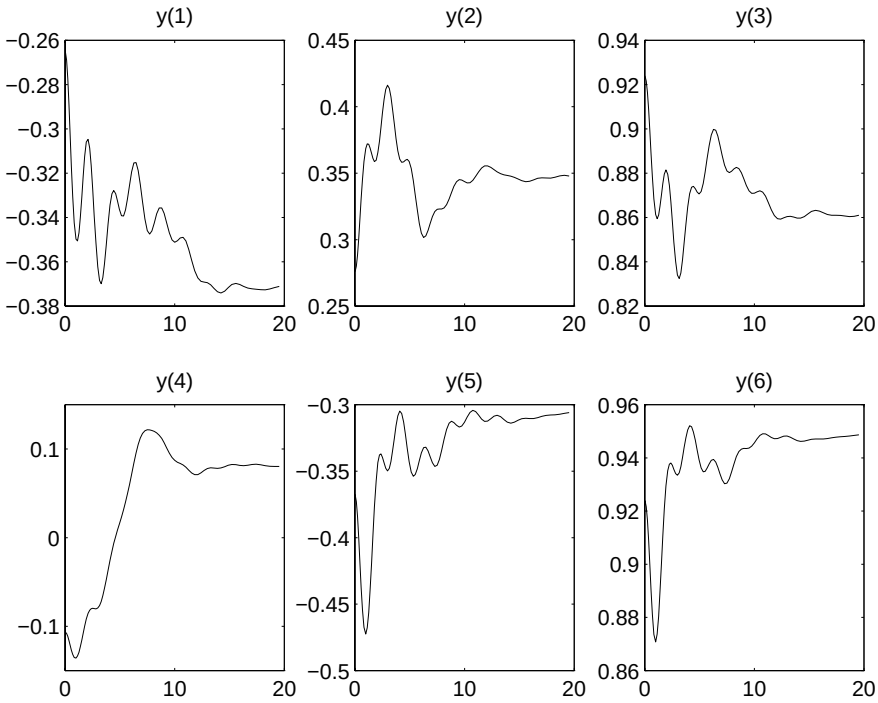

FIGURE 14.2: *Behavior of the solution over the integration interval.*

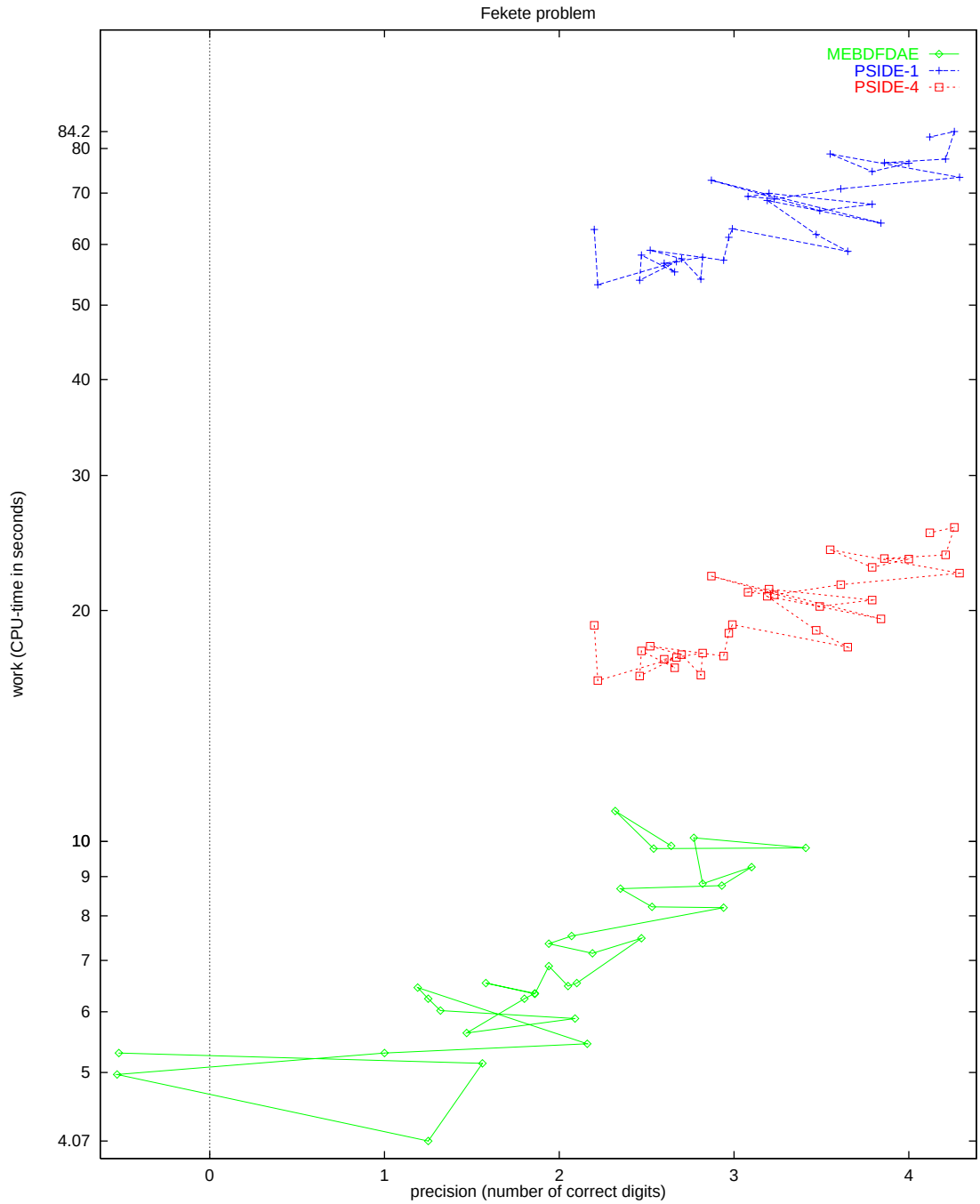

FIGURE 14.3: *Work-precision diagram.*

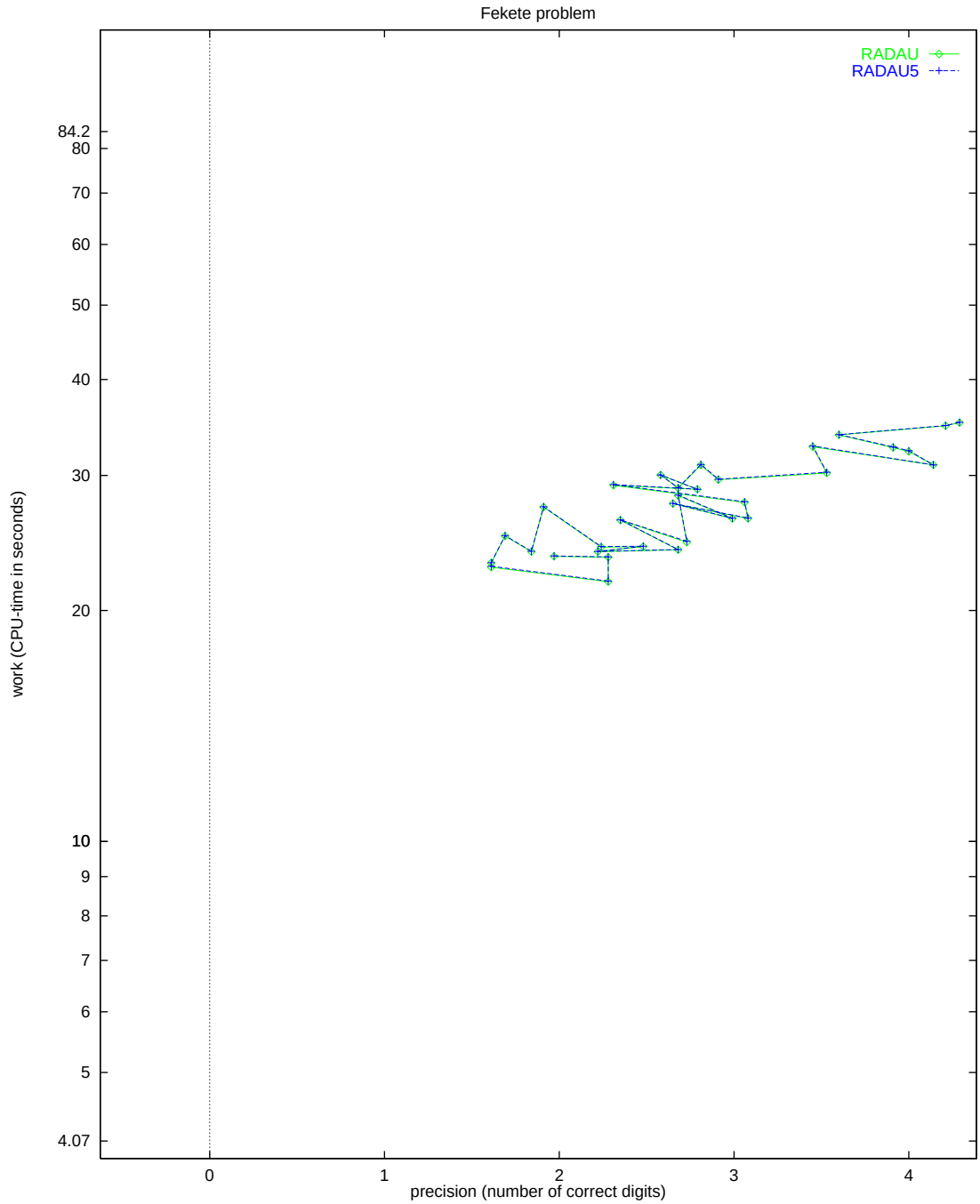

FIGURE 14.4: *Work-precision diagram.*

15. Pleiades problem

15.1 General information

The problem consists of a nonstiff system of 14 special second order differential equations rewritten to first order form, thus providing a nonstiff system of ordinary differential equations of dimension 28. The formulation and data have been taken from [HNW93]. E. Messina contributed this problem to the test set. Comments to `messina@matna2.dma.unina.it`.

15.2 Mathematical description of the problem

The problem is of the form

$$z'' \quad = \quad f(z), \quad z(0) = z_0, \quad z'(0) = z'_0, \tag{15.1}$$

with

$$z \in \mathbb{R}^{14}, \quad 0 \le t \le 3.$$

Defining $z := (x^{\mathrm{T}}, y^{\mathrm{T}})^{\mathrm{T}}$, $x, y \in \mathbb{R}^7$, the function $f : \mathbb{R}^{14} \to \mathbb{R}^{14}$ is given by $f(z) = f(x, y) = (f^{(1)}(x, y), f^{(2)}(x, y))^{\mathrm{T}}$, where $f^{(1,2)} : \mathbb{R}^{14} \to \mathbb{R}^7$ read

$$f_i^{(1)} = \sum_{j \neq i} m_j (x_j - x_i)/r_{ij}^{\frac{3}{2}}, \qquad f_i^{(2)} = \sum_{j \neq i} m_j (y_j - y_i)/r_{ij}^{\frac{3}{2}}, \qquad i = 1, \ldots, 7. \tag{15.2}$$

Here, $m_i = i$ and

$$r_{ij} = (x_i - x_j)^2 + (y_i - y_j)^2.$$

We write this problem to first order form by defining $w = z'$, yielding a system of 28 non-linear differential equations of the form

$$\begin{pmatrix} z \\ w \end{pmatrix}' = \begin{pmatrix} w \\ f(z) \end{pmatrix} \tag{15.3}$$

with

$$(z^{\mathrm{T}}, w^{\mathrm{T}})^{\mathrm{T}} \in \mathbb{R}^{28}, \quad 0 \le t \le 3.$$

The initial values are

$$\begin{pmatrix} z_0 \\ w_0 \end{pmatrix} = \begin{pmatrix} x_0 \\ y_0 \\ x'_0 \\ y'_0 \end{pmatrix}, \quad \text{where} \quad \begin{cases} x_0 &= (3, 3, -1, -3, 2, -2, 2)^{\mathrm{T}}, \\ y_0 &= (3, -3, 2, 0, 0, -4, 4)^{\mathrm{T}}, \\ x'_0 &= (0, 0, 0, 0, 0, 1.75, -1.5)^{\mathrm{T}}, \\ y'_0 &= (0, 0, 0, -1.25, 1, 0, 0)^{\mathrm{T}}. \end{cases}$$

15.3 Origin of the problem

The Pleiades problem is a celestial mechanics problem of seven stars in the plane of coordinates x_i, y_i and masses $m_i = i$ $(i = 1, \ldots, 7)$. We obtain the formulation of the problem by means of some mechanical considerations. Let us consider the body i. According to the second law of Newton this star is subjected to the action

$$F_i = m_i p_i'', \tag{15.4}$$

where $p_i := (x_i, y_i)^{\mathrm{T}}$. On the other hand, the law of gravity states that the force working on body i implied by body j, denoted by F_{ij}, is

$$F_{ij} = g \frac{m_i \cdot m_j}{\|p_i - p_j\|_2^2} d_{ij}. \tag{15.5}$$

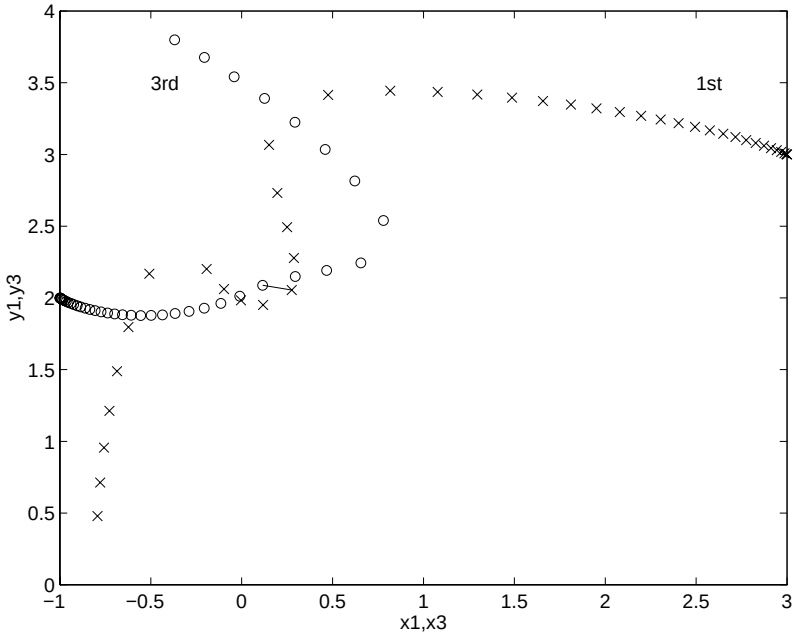

FIGURE 15.1: *Trajectories of the first and third body on* $[0, 2]$.

TABLE 15.1: *Quasi-collisions in Pleiades problem. The squared distance between body* i *and body* j *at* $t = \tau$ *is listed (values taken from [HNW93]).*

i	1	1	3	1	2	5
j	7	3	5	7	6	7
τ	1.23	1.46	1.63	1.68	1.94	2.14
$\|p_i - p_j\|_2^2$	0.0129	0.0193	0.0031	0.0011	0.1005	0.0700

Here, F_i, $F_{ij} \in \mathbb{R}^2$, g is the gravitational constant, which is assumed to be one here, and $d_{ij} = \frac{p_j - p_i}{\|p_j - p_i\|_2}$ represents the direction of the distance between the two stars. According to the principle of superposition of actions, F_i will be the sum of the interactions between body i and all the others,

$$F_i = \sum_{i \neq j} F_{ij}. \tag{15.6}$$

It is easily checked that (15.4)–(15.6) and (15.2) are the same.

During the movement of the 7 bodies several quasi-collisions occur which are displayed in Table 15.1. In Figure 15.1 the behaviors of the bodies 1 and 3 in the interval $[0, 2]$ are shown; the circles and the crosses represent data obtained every 0.05 sec, the link '—' indicates the distance occurring between the two stars at $t = 1.45$.

15.4 Numerical solution of the problem

One should be aware of the fact that the Pleiades problem is a nonstiff ODE. Therefore we also include the results obtained by the nonstiff solver DOPRI5[HW96], which is based on an explicit Runge–Kutta method.

Tables 15.2–15.3 and Figures 15.2–15.4 present the reference solution at the end of the integration interval, the run characteristics, the behavior of the solution components x_1 and y_1 over the integration

TABLE 15.2: *Reference solution at the end of the integration interval.*

x_1	0.3706139143970502	y_1	$-0.3943437585517392 \cdot 10$
x_2	$0.3237284092057233 \cdot 10$	y_2	$-0.3271380973972550 \cdot 10$
x_3	$-0.3222559032418324 \cdot 10$	y_3	$0.5225081843456543 \cdot 10$
x_4	0.6597091455775310	y_4	$-0.2590612434977470 \cdot 10$
x_5	0.3425581707156584	y_5	$0.1198213693392275 \cdot 10$
x_6	$0.1562172101400631 \cdot 10$	y_6	-0.2429682344935824
x_7	-0.7003092922212495	y_7	$0.1091449240428980 \cdot 10$
x'_1	$0.3417003806314313 \cdot 10$	y'_1	$-0.3741244961234010 \cdot 10$
x'_2	$0.1354584501625501 \cdot 10$	y'_2	0.3773459685750630
x'_3	$-0.2590065597810775 \cdot 10$	y'_3	0.9386858869551073
x'_4	$0.2025053734714242 \cdot 10$	y'_4	0.3667922227200571
x'_5	$-0.1155815100160448 \cdot 10$	y'_5	-0.3474046353808490
x'_6	-0.8072988170223021	y'_6	$0.2344915448180937 \cdot 10$
x'_7	0.5952396354208710	y'_7	$-0.1947020434263292 \cdot 10$

TABLE 15.3: *Run characteristics.*

solver	rtol	atol	h0	scd	steps	accept	# f	# Jac	# LU	CPU
DASSL	10^{-4}	10^{-4}		0.23	428	390	589	49		0.65
	10^{-7}	10^{-7}		3.30	1219	1204	1694	62		1.79
	10^{-10}	10^{-10}		5.78	3640	3635	4702	66		4.96
DOPRI5	10^{-4}	10^{-4}		0.50	100	74	602			0.21
	10^{-7}	10^{-7}		3.49	295	244	1772			0.61
	10^{-10}	10^{-10}		7.83	940	940	5642			1.94
MEBDFDAE	10^{-4}	10^{-4}	10^{-6}	0.76	402	379	593	56	56	0.81
	10^{-7}	10^{-7}	10^{-9}	3.61	834	815	1194	87	87	1.69
	10^{-10}	10^{-10}	10^{-12}	6.95	1867	1867	2573	191	191	3.75
PSIDE-1	10^{-4}	10^{-4}		1.82	102	76	1710	27	364	1.51
	10^{-7}	10^{-7}		4.70	248	223	3187	1	592	2.69
	10^{-10}	10^{-10}		7.55	807	807	9095	1	604	6.92
RADAU	10^{-4}	10^{-4}	10^{-6}	2.11	151	138	1053	132	151	1.14
	10^{-7}	10^{-7}	10^{-9}	6.17	112	95	2153	83	112	2.15
	10^{-10}	10^{-10}	10^{-12}	9.20	130	119	3001	91	130	2.94
RADAU5	10^{-4}	10^{-4}	10^{-6}	2.11	151	138	1053	132	151	1.14
	10^{-7}	10^{-7}	10^{-9}	4.51	394	394	2734	302	343	2.80
	10^{-10}	10^{-10}	10^{-12}	7.06	1237	1237	8626	174	732	7.66
VODE	10^{-4}	10^{-4}		-0.17	352	325	468	6	57	0.40
	10^{-7}	10^{-7}		2.57	1081	1043	1232	18	94	1.05
	10^{-10}	10^{-10}		5.20	3120	3079	3351	51	203	2.86

interval and the work-precision diagrams, respectively. The computation of the scd values is based on the first 14 components, since they refer to the physically important quantities. The reference solution was computed on the Cray C90, using PSIDE with Cray double precision and atol = rtol = 10^{-16}. For the work-precision diagrams, we used: rtol = $10^{-(4+m/4)}$, $m = 0, 1, \ldots, 24$; atol = rtol; h0 = $10^{-2} \cdot$rtol for RADAU, RADAU5 and MEBDFDAE. The speed-up factor for PSIDE is 2.50.

With respect to the RADAU and RADAU5 results in Table 15.3 and Figures 15.3–15.4, we remark

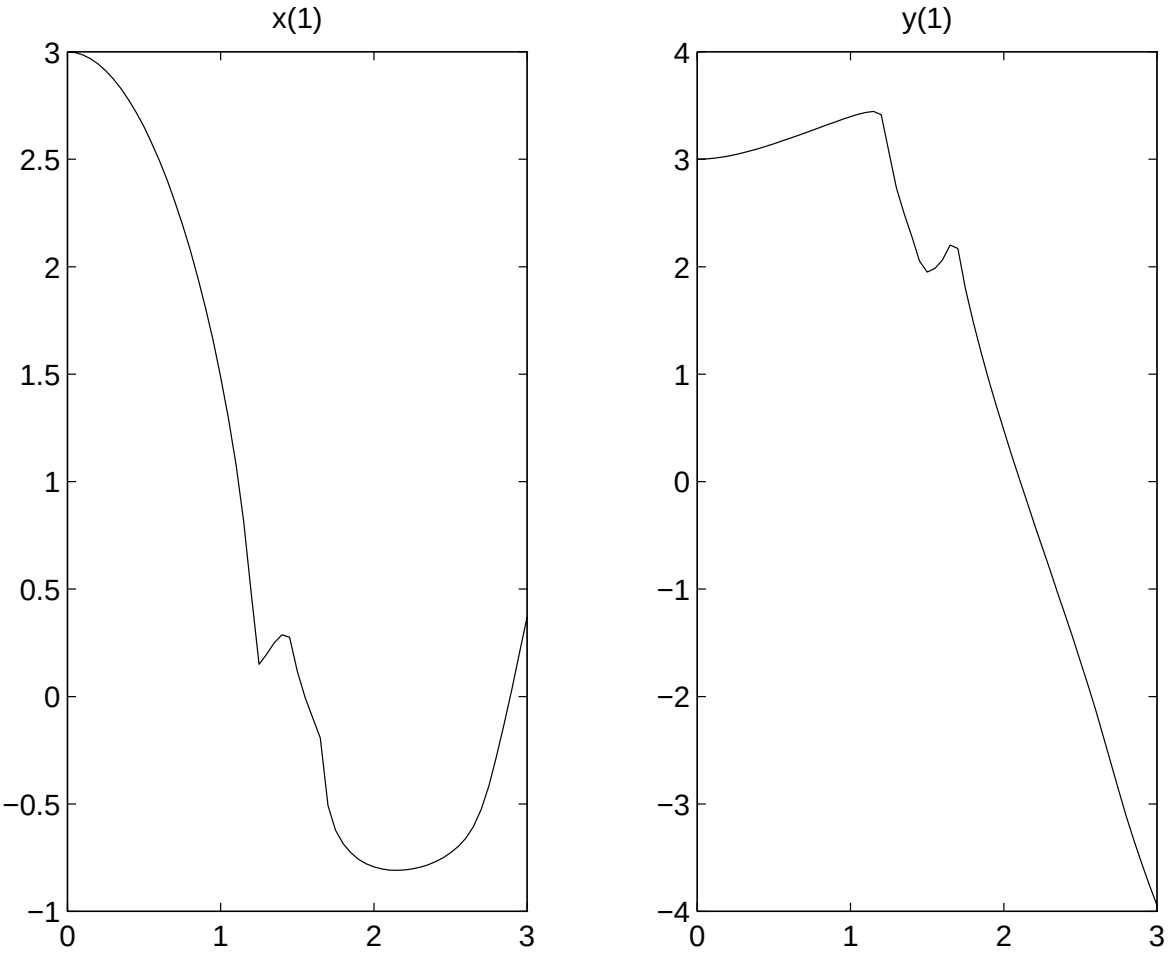

FIGURE 15.2: *Behavior of the two solution components corresponding to the first body over the integration interval.*

TABLE 15.4: *Run characteristics obtained by RADAU5 with exploited special structure.*

solver	rtol	atol	h0	scd	steps	accept	# f	# Jac	# LU	CPU
RADAU5	10^{-4}	10^{-4}	10^{-6}	2.11	151	138	1053	132	151	0.82
	10^{-7}	10^{-7}	10^{-9}	4.51	394	394	2734	302	343	2.06
	10^{-10}	10^{-10}	10^{-12}	7.06	1237	1237	8626	174	732	5.77

that for generality of the test set drivers, we did not use the facility to exploit the special structure of problems of the form (15.3). By setting the input parameter `IWORK(9)=14`, and adjusting the Jacobian routine appropriately, RADAU and RADAU5 produces considerably better results. These results are listed for RADAU5 in Table 15.4.

REFERENCES

[HNW93] E. Hairer, S.P. Nørsett, and G. Wanner. *Solving Ordinary Differential Equations I: Nonstiff Problems*. Springer-Verlag, second revised edition, 1993.

[HW96] E. Hairer and G. Wanner. *DOPRI5*, April 25, 1996. Bug fix release September 18, 1998.

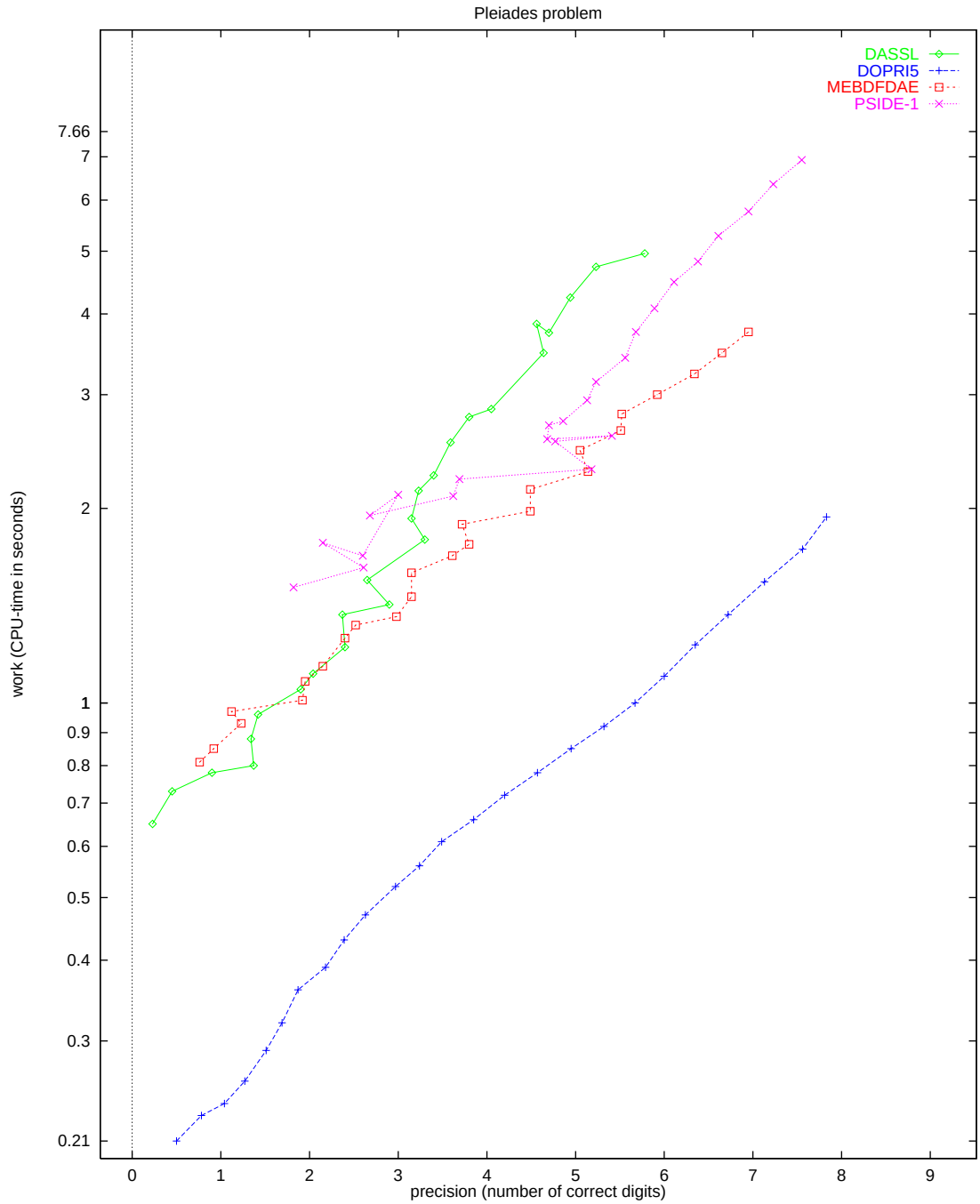

FIGURE 15.3: *Work-precision diagram.*

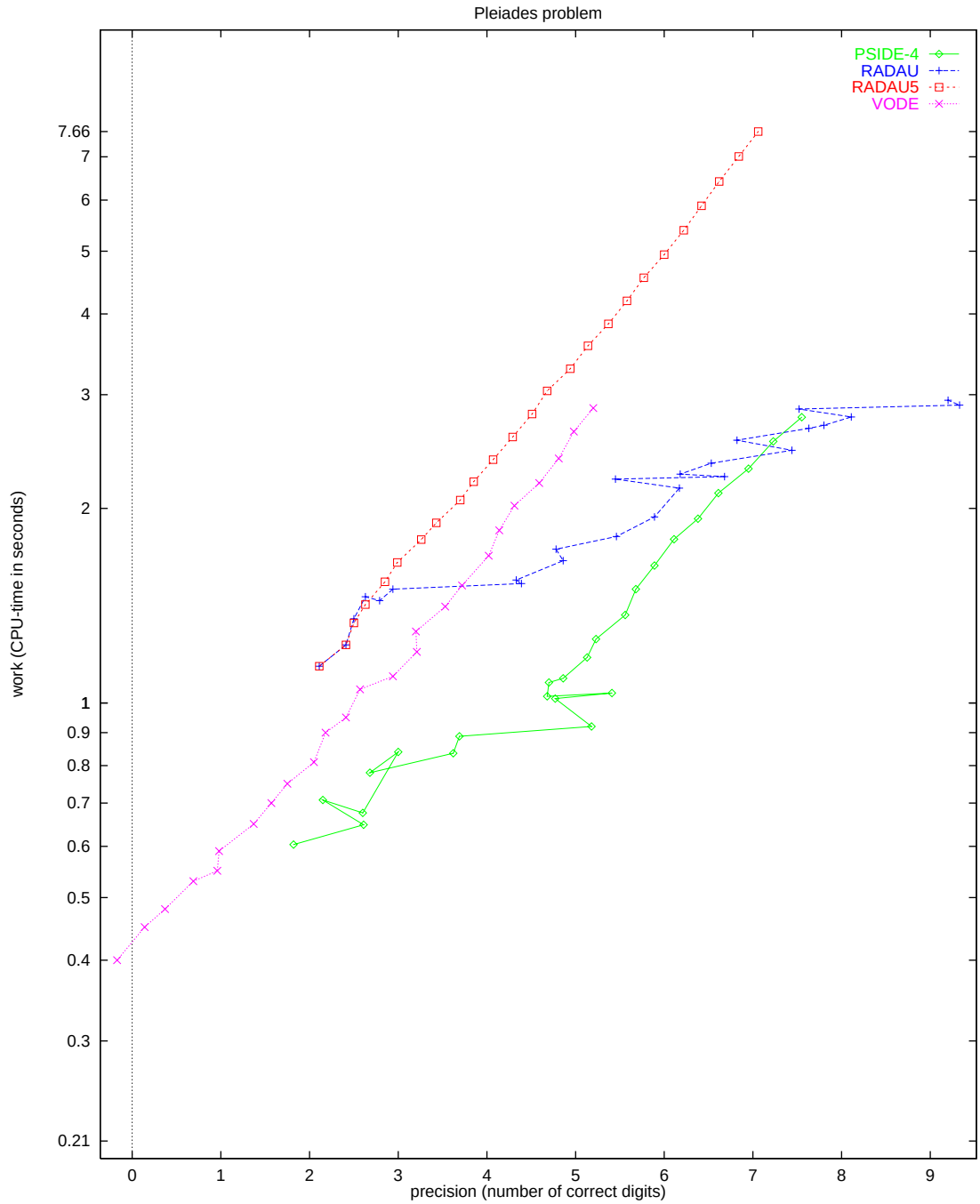

FIGURE 15.4: *Work-precision diagram.*

Available at ftp://ftp.unige.ch/pub/doc/math/nonstiff/dopri5.f.

16. Slider Crank

16.1 General Information

This problem was contributed by Bernd Simeon, March 1998. The slider crank shows some typical properties of simulation problems in *flexible multibody systems*, i.e., constrained mechanical systems which include both rigid and elastic bodies. It is also an example of a *stiff mechanical system* since it features large stiffness terms in the right hand side. Accordingly, there are some fast variables with high frequency oscillations.

This problem is originally described by a second order system of differential-algebraic equations (DAEs), but transformed to first order and semi-explicit system of dimension 24. The index of the problem is originally 3, but an index 1 and index 2 formulation are supplied as well. By default, the subroutines provide the index 2 formulation.

Comments to `bernd.simeon@mathematik.tu-darmstadt.de`.

16.2 Mathematical description of the problem

The original problem has the form

$$\begin{aligned} \boldsymbol{M}(p,q)\begin{pmatrix} \ddot{p} \\ \ddot{q} \end{pmatrix} &= \boldsymbol{f}(p,\dot{p},q,\dot{q}) - \boldsymbol{G}(p,q)^{\mathrm{T}}\lambda, \\ 0 &= \boldsymbol{g}(p,q) + \boldsymbol{r}(t), \end{aligned} \tag{16.1}$$

where $0 \le t \le 0.1$, $p \in \mathbb{R}^3$, $q \in \mathbb{R}^4$, $\lambda \in \mathbb{R}^3$, $\boldsymbol{M} : \mathbb{R}^7 \to \mathbb{R}^7 \times \mathbb{R}^7$, $\boldsymbol{f} : \mathbb{R}^{14} \to \mathbb{R}^7$, $\boldsymbol{g} : \mathbb{R}^7 \to \mathbb{R}^3$, $\boldsymbol{r} : \mathbb{R} \to \mathbb{R}^3$, and $\boldsymbol{G} = \partial \boldsymbol{g}/\partial(p,q)$. The matrix $\boldsymbol{M}(p,q)$ is symmetric positive semi-definite and rank $\boldsymbol{M}(p,q)$ is 3, which implies that the DAE (16.1) is of index 3. For the index 2 formulation, the position constraints are replaced by the velocity constraints

$$0 = \frac{\mathrm{d}}{\mathrm{d}t}\Big(\boldsymbol{g}(p,q) + \boldsymbol{r}(t)\Big) = \boldsymbol{G}(p,q)\begin{pmatrix} \dot{p} \\ \dot{q} \end{pmatrix} + \dot{\boldsymbol{r}}(t). \tag{16.2}$$

Additionally, the system is transformed to first order and semi explicit form

$$\begin{aligned} \begin{pmatrix} \dot{p} \\ \dot{q} \end{pmatrix} &= \begin{pmatrix} v_p \\ v_q \end{pmatrix}, \\ \begin{pmatrix} \dot{v}_p \\ \dot{v}_q \end{pmatrix} &= \begin{pmatrix} a_p \\ a_q \end{pmatrix}, \\ 0 &= \boldsymbol{M}(p,q)\begin{pmatrix} a_p \\ a_q \end{pmatrix} - \boldsymbol{f}(p,v_p,q,v_q) + \boldsymbol{G}(p,q)^{\mathrm{T}}\lambda\,, \\ 0 &= \boldsymbol{G}(p,q)\begin{pmatrix} v_p \\ v_q \end{pmatrix} + \dot{\boldsymbol{r}}(t)\,, \end{aligned} \tag{16.3}$$

which increases the dimension of the problem to 24. If we define $y := (p,q,v_p,v_q,a_p,a_q,\lambda)^{\mathrm{T}}$, then the consistent values are given by $y(0) := y_0$ and $y'(0) := y_0'$. The components of y_0 are zero, except for

$y_{0,3}$	$0.450016933 \cdot 10$	$y_{0,16}$	$-1.344541576008661 \cdot 10^{-3}$
$y_{0,6}$	$0.103339863 \cdot 10^{-4}$	$y_{0,17}$	$-5.062194923138079 \cdot 10^{3}$
$y_{0,7}$	$0.169327969 \cdot 10^{-4}$	$y_{0,18}$	$-6.833142732779555 \cdot 10^{-5}$
$y_{0,8}$	$0.150000000 \cdot 10^{3}$	$y_{0,19}$	$1.449382650173157 \cdot 10^{-8}$
$y_{0,9}$	$-0.749957670 \cdot 10^{2}$	$y_{0,20}$	$-4.268463211410861 \cdot 10$
$y_{0,10}$	$-0.268938672 \cdot 10^{-5}$	$y_{0,21}$	$2.098334687947376 \cdot 10^{-1}$
$y_{0,11}$	$0.444896105 \cdot 10$	$y_{0,22}$	$-6.397251492537153 \cdot 10^{-8}$
$y_{0,12}$	$0.463434311 \cdot 10^{-2}$	$y_{0,23}$	$3.824589508329281 \cdot 10^{2}$
$y_{0,13}$	$-0.178591076 \cdot 10^{-5}$	$y_{0,24}$	$-4.376060460948886 \cdot 10^{-9}$
$y_{0,14}$	$-0.268938672 \cdot 10^{-5}$		

The first 14 components of y_0' read $y'_{0,i} = y_{0,i+7}$, $i = 1, \ldots, 14$; the last 10 are zero.

For the index 2 formulation, the index of the variables p, q, v_p and v_q equals 1 and that of a_p, a_q and λ equals 2. The equations are given in detail in the next subsections, in which already some references to the origin of the problem, treated in §16.3, are given.

16.2.1 Equations of motion The position or gross motion coordinates p are

$$p := \begin{pmatrix} \phi_1 \\ \phi_2 \\ x_3 \end{pmatrix} \qquad \begin{matrix} \text{crank angle} \\ \text{connecting rod angle} \\ \text{sliding block displacement} \end{matrix}$$

The deformation coordinates q (of the elastic connecting rod, see below) are

$$q := \begin{pmatrix} q_1 \\ q_2 \\ q_3 \\ q_4 \end{pmatrix} \qquad \begin{matrix} \text{first lateral mode } \sin(\pi x/l_2) \\ \text{second lateral mode } \sin(2\pi x/l_2) \\ \text{longitudinal displacement midpoint} \\ \text{longitudinal displacement endpoint} \end{matrix}$$

The mass matrix $\boldsymbol{M}$ reads

$$\boldsymbol{M}(p,q) = \begin{pmatrix} M_r(p) + M_e(p,q) & C(p,q)^{\mathrm{T}} \\ C(p,q) & M_\Delta \end{pmatrix}$$

with rigid motion mass matrix

$$M_r(p) = \begin{pmatrix} J_1 + m_2 l_1^2 & 1/2\, l_1 l_2 m_2 \cos(\phi_1 - \phi_2) & 0 \\ 1/2\, l_1 l_2 m_2 \cos(\phi_1 - \phi_2) & J_2 & 0 \\ 0 & 0 & m_3 \end{pmatrix},$$

coupling blocks

$$M_e(p,q) = \begin{pmatrix} 0 & \rho l_1 (\cos(\phi_1 - \phi_2) c_1^{\mathrm{T}} + \sin(\phi_1 - \phi_2) c_2^{\mathrm{T}}) q & 0 \\ \rho l_1 (\cos(\phi_1 - \phi_2) c_1^{\mathrm{T}} + \sin(\phi_1 - \phi_2) c_2^{\mathrm{T}}) q & q^{\mathrm{T}} M_\Delta q + 2\rho c_{12}^{\mathrm{T}} q & 0 \\ 0 & 0 & 0 \end{pmatrix}$$

and

$$C(p,q)^{\mathrm{T}} = \begin{pmatrix} \rho l_1 (-\sin(\phi_1 - \phi_2) c_1 + \cos(\phi_1 - \phi_2) c_2) \\ \rho c_{21} + \rho q^{\mathrm{T}} B \\ 0 \end{pmatrix},$$

and elastic body space discretization mass matrix

$$M_\Delta = \rho\, d\, h\, l_2 \begin{pmatrix} 1/2 & 0 & 0 & 0 \\ 0 & 1/2 & 0 & 0 \\ 0 & 0 & 8 & 1 \\ 0 & 0 & 1 & 2 \end{pmatrix}.$$

The forces are given by

$$\boldsymbol{f}(p, \dot{p}, q, \dot{q}) = \begin{pmatrix} f_r(p, \dot{p}) + f_e(p, \dot{p}, q, \dot{q}) \\ f_\Delta(p, \dot{p}, q, \dot{q}) - \operatorname{grad} W_\Delta(q) - D_\Delta \dot{q} \end{pmatrix},$$

where the rigid motion terms are collected in

$$f_r(p,\dot p) = \begin{pmatrix} -1/2\, l_1(\gamma(m_1+2m_2)\cos\phi_1 + l_2 m_2 \dot\phi_2^2 \sin(\phi_1-\phi_2)) \\ -1/2\, l_2 \gamma m_2 \cos\phi_2 + 1/2\, l_1 l_2 m_2 \dot\phi_1^2 \sin(\phi_1-\phi_2) \\ 0 \end{pmatrix}.$$

For the force term $f_e(p,\dot p,q,\dot q)$ we have

$$\begin{pmatrix} \rho l_1 \dot\phi_2^2(-\sin(\phi_1-\phi_2)c_1^{\mathrm T} + \cos(\phi_1-\phi_2)c_2^{\mathrm T})q - 2\rho l_1 \dot\phi_2(\cos(\phi_1-\phi_2)c_1^{\mathrm T} + \sin(\phi_1-\phi_2)c_2^{\mathrm T})\dot q \\ \rho l_1 \dot\phi_1^2(\sin(\phi_1-\phi_2)c_1^{\mathrm T} - \cos(\phi_1-\phi_2)c_2^{\mathrm T})q - 2\rho\dot\phi_2 c_{12}^{\mathrm T}\dot q - 2\dot\phi_2 \dot q^{\mathrm T} M_\Delta q \\ -\rho \dot q^{\mathrm T} B \dot q - \rho\gamma(\cos\phi_2 c_1^{\mathrm T} q - \sin\phi_2 c_2^{\mathrm T} q) \\ 0 \end{pmatrix},$$

and for $f_\Delta(p,\dot p,q,\dot q)$ the expression

$$\dot\phi_2^2 M_\Delta q + \rho\Big(\dot\phi_2^2 c_{12}^{\mathrm T} + l_1\dot\phi_1^2(\cos(\phi_1-\phi_2)c_1^{\mathrm T} + \sin(\phi_1-\phi_2)c_2^{\mathrm T}) + 2\dot\phi_2 B\dot q\Big) - \rho\gamma\Big(\sin\phi_2 c_1^{\mathrm T} + \cos\phi_2 c_2^{\mathrm T}\Big).$$

The gradient of the elastic potential $W_\Delta(q)$ in case of linear elasticity (which is the default) is $\operatorname{grad} W_\Delta(q) = K_\Delta q$ with stiffness matrix

$$K_\Delta = E\, d\, h\, /l_2 \begin{pmatrix} \pi^4/24(h/l_2)^2 & 0 & 0 & 0 \\ 0 & \pi^4 2/3(h/l)^2 & 0 & 0 \\ 0 & 0 & 16/3 & -8/3 \\ 0 & 0 & -8/3 & 7/3 \end{pmatrix}.$$

Alternatively, in case of the nonlinear beam model (`IPAR(1) = 1`, see below), it holds $\operatorname{grad} W_\Delta(q) = K_\Delta q + k_\Delta(q)$,

$$k_\Delta(q) = 1/2\,\pi^2\, E\, d\, h/l_2^2 \begin{pmatrix} q_1 q_4 - \beta q_2(-4q_3+2q_4) \\ 4q_2 q_4 - \beta q_1(-4q_3+2q_4) \\ 4\beta q_1 q_2 \\ 1/2q_1^2 + 2q_2^2 - 2\beta q_1 q_2 \end{pmatrix}, \qquad \beta = 80/(9\pi^2).$$

The damping matrix D_Δ is by default zero. The coupling matrices and vectors arising from the space discretization read

$$B = d\, h\, l_2 \begin{pmatrix} 0 & 0 & -16/\pi^3 & 8/\pi^3 - 1/\pi \\ 0 & 0 & 0 & 1/(2\pi) \\ 16/\pi^3 & 0 & 0 & 0 \\ 1/\pi - 8/\pi^3 & -1/(2\pi) & 0 & 0 \end{pmatrix}$$

and

$$\begin{aligned} c_1 &= d\, h\, l_2(\,0,\,0,\,2/3,\,1/6\,)^{\mathrm T}, \\ c_2 &= d\, h\, l_2(\,2/\pi,\,0,\,0,\,0\,)^{\mathrm T}, \\ c_{12} &= d\, h\, l_2^2(\,0,\,0,\,1/3,\,1/6\,)^{\mathrm T}, \\ c_{21} &= d\, h\, l_2^2(\,1/\pi,\,-1/(2\pi),\,0,\,0\,)^{\mathrm T}. \end{aligned}$$

Finally, the position constraints $0 = \boldsymbol{g}(p,q) + \boldsymbol{r}(t)$ are given by

$$\begin{aligned} 0 &= l_1\sin\phi_1 + l_2\sin\phi_2 + q_4\sin\phi_2, \\ 0 &= x_3 - l_1\cos\phi_1 - l_2\cos\phi_2 - q_4\cos\phi_2, \\ 0 &= \phi_1 - \Omega t\,. \end{aligned}$$

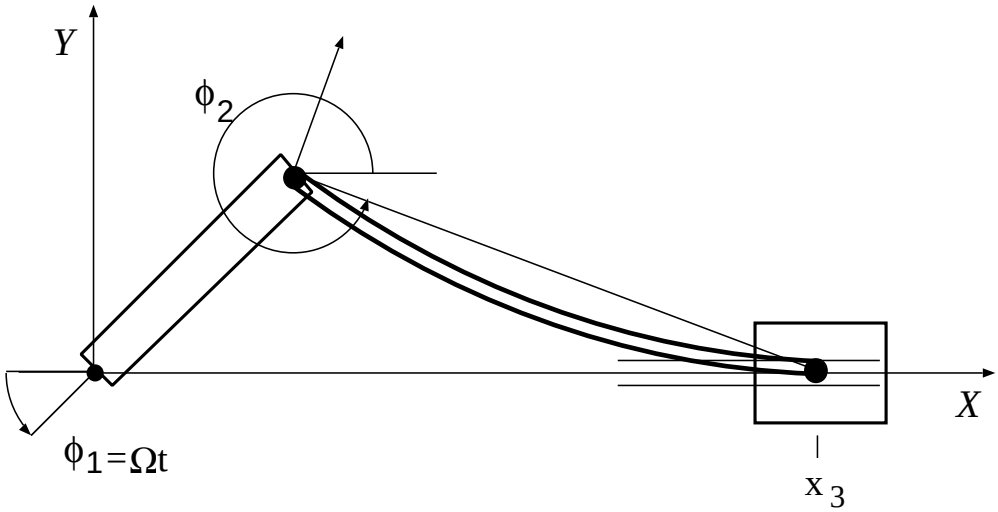

FIGURE 16.1: The multibody system with crank, connecting rod, sliding block.

16.2.2 Parameters For the simulation, the following data are used:
The bodies have lengths $l_1 = 0.15$, $l_2 = 0.30[m]$.
The masses of the bodies are $m_1 = 0.36$, $m_2 = 0.151104$, $m_3 = 0.075552[kg]$.
The moments of inertia are $J_1 = 0.002727$, $J_2 = 0.0045339259[kg\,m^2]$.
The flexible connecting rod has height and width $h = d = 0.008[m]$.
The mass density $\rho = 7870[kg/m^3]$, and Young's modulus $E = 2. \cdot 10^{11}[N/m^2]$.
The gravity constant was set to zero since gravitation plays no role here, $\gamma = 0$.
The angular velocity of the prescribed crank motion is $\Omega = 150[rad/s]$.

16.3 Origin of the problem
The planar slider crank mechanism, see Figure 16.1, consists of a rigid crank (body 1), an elastic connecting rod (body 2), a rigid sliding block (body 3) and two revolving and one translational joint. Koppens [Kop89] and Jahnke [JPD93] investigated this example using an ODE model in minimum coordinates. In [Sim96], an alternative DAE approach is introduced.

The mathematical model outlined above is derived in two steps. First, the elastic connecting rod is discretized in space. The geometry of the rod allows to apply an Euler-Bernoulli beam

$$\begin{aligned} u_1(x,y) &= w_1(x) - y w_2'(x), \\ u_2(x,y) &= w_2(x), \end{aligned}$$

to describe the longitudinal and lateral displacements u_1 and u_2 of material point (x, y) in the body-fixed coordinate system. For the longitudinal displacement w_1 of the neutral fiber, a simple quadratic model

$$w_1(x) \doteq \xi^2(-4q_3 + 2q_4) + \xi(4q_3 - q_4), \qquad \xi = x/l_2,$$

is sufficient to show the basic effects. The lateral displacement w_2 is approximated by the first two sinus shape functions

$$w_2(x) \doteq \sin(\pi\xi)q_1 + \sin(2\pi\xi)q_2\,.$$

These functions satisfy the boundary conditions $w_1(0) = 0$, $w_2(0) = 0$, $w_2(l_2) = 0$. Accordingly, the body-fixed coordinate system's origin is placed in $(x, y) = (0, 0)$, and its x-axis passes through the point $(l_2 + w_1(x), 0)$.

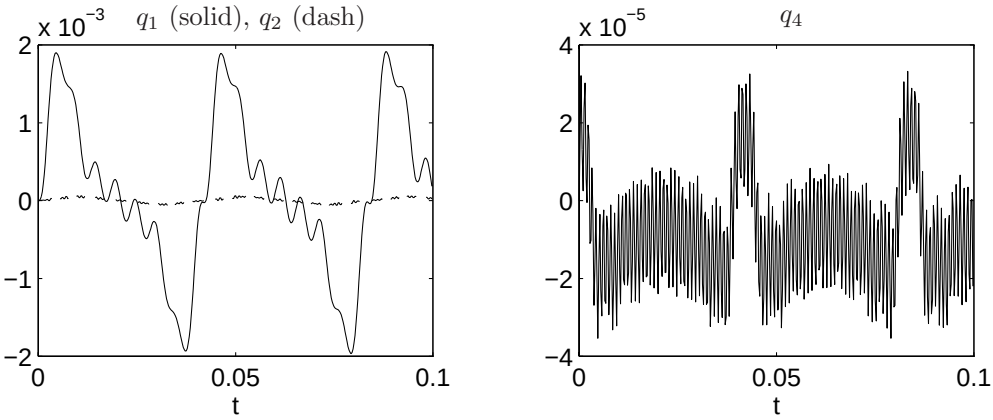

FIGURE 16.2: Solution of slider crank for 'rigid' initial values, i.e., deformation $q(0) = v_q(0) = 0$.

As already mentioned in §16.2, we provide two versions of the problem. The first one (default) assumes linear elasticity while the second takes the coupling of longitudinal and lateral displacements in terms of $k_\Delta(q)$ into account. Set `IPAR(1) = 1` to switch to this nonlinear beam model. See below for a comparison of the results.

In the second step, the equations of motion of the overall multibody system are assembled. Due to the choice of ϕ_2 as gross motion coordinate, there is no constraint equation necessary to express the revolving joint between crank and connecting rod. The revolving joint between sliding block and connecting rod and the translational joint lead to two constraints that depend on the deformation variable q_4. The third constraint equation defines the crank motion using $\boldsymbol{r}(t) = (0,\, 0,\, -\Omega t)^{\mathrm{T}}$. Here, other functions for the crank motion could also be prescribed.

The model described so far features no dissipation. Consequently, the solutions show a purely oscillatory behavior. We supply also a nonzero damping matrix D_Δ which can be activated by setting `IPAR(2) = 1`. Then, 0.5 percent dissipation is included in the right hand side of the elastic connecting rod.

In §16.4, we investigate the dynamic behavior of the slider crank model corresponding to the nonlinear model without damping with the initial values listed in §16.2, which were calculated such that the motion is almost smooth, using an asymptotic expansion technique [Sim97]. In Figure 16.4 we see the behavior of the numerical solution for this setting of the model. A close look at these plots reveals that both lateral displacements q_1, q_2 as well as longitudinal displacements q_3, q_4 still show some small oscillations. The corresponding frequencies as solutions of the eigenvalue problem $\omega^2 M_\Delta q = K_\Delta q$ are

$$\omega_1 = 1277, \quad \omega_2 = 5107, \quad \omega_3 = 6841, \quad \omega_4 = 24613 \ \ [rad/s]\,.$$

In particular, q_3 and q_4 are characterized by the relatively large frequency ω_4. Any explicit discretization in time will need stepsizes smaller than the shortest period of oscillation, even for tracking a smooth solution. On the other hand, the challenge for implicit methods is to be able to take larger steps. In this simulation the gross motion coordinates p differ only slightly from the motion of a mechanism with rigid connecting rod.

The subroutines that describe the model offer several possibilities to test other variants of the model than those tested in §16.4. We now discuss some of them.

Oscillatory solution We provide also a second set of initial values (`subroutine init2`) which lead to a strongly oscillatory solution. Here, the initial deformation as well as the corresponding velocity were set to zero, $q(0) = v_q(0) = 0$, which is equivalent to consistent initial values on a rigid motion trajectory. Figure 16.2 plots the behavior of q_1, q_2 and q_4 for this setting. Both lateral and longitudinal modes oscillate now with different frequencies.

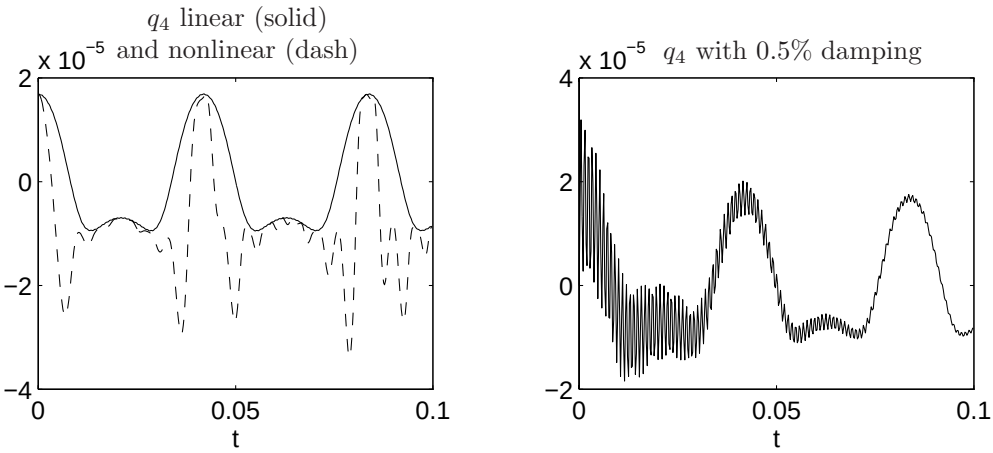

FIGURE 16.3: Left: Comparison of linear and nonlinear beam model. Right: Oscillatory solution with physical damping.

TABLE 16.1: *Failed runs.*

solver	m	reason
MEBDFDAE	$21, 22, 23, 24$	stepsize too small
PSIDE-1	$17, 18, \ldots, 24$	iteration matrix singular
RADAU	24	core dump / overflow in decomposition
RADAU5	24	core dump / overflow in decomposition

Nonlinear beam model and damping The left and right plot in Figure 16.3 show the effects of setting `IPAR(1) = 1` and `IPAR(2) = 1`, respectively. On the left, the difference between linear and nonlinear beam model is illustrated, with initial values close to the smooth motion. In particular, the components q_3 and q_4 change if the nonlinear model is employed. At points of maximum bending, the longitudinal displacement has now much smaller minima. If we increase the crank's angular velocity, the resulting forces acting on the connecting rod are much larger and we can then even observe how the sharp needles turn into a singularity, the buckling phenomenon.

On the right of Figure 16.3, the damping was activated by `IPAR(2) = 1`, with initial values on a rigid motion trajectory (`init2`). Obviously, the oscillation shown in Figure 16.2 on the right is now slowly damped out.

16.4 Numerical solution of the problem

The results presented here refer to index 2 formulation of the linear model without damping, using the initial values corresponding to a smooth solution.

Tables 16.2–16.3 and Figures 16.4–16.6 present the reference solution at the end of the integration interval, the run characteristics, the behavior of some of the solution components over the integration interval and the work-precision diagrams, respectively. The reference solution was computed using MDOP5 with atol $= 10^{-10}$ and rtol $= 10^{-8}$ for p and v. For the work-precision diagrams, we used: rtol $= 10^{-(4+m/4)}$, $m = 0, \ldots, 24$; atol = rtol; h0 $= 10^{-2} \cdot$ rtol for RADAU5, RADAU and MEBDFDAE. The failed runs are in Table 16.1; listed are the name of the solver that failed, for which values of m this happened, and the reason for failing. The speed-up factor for PSIDE is 2.69.

Remarks

- The slider crank is an example for a stiff mechanical system given in DAE form. See Lubich

TABLE 16.2: *Reference solution at the end of the integration interval.*

y_1	$1.500000000000000 \cdot 10^{1}$	y_{13}	$4.978243404809343 \cdot 10^{-4}$
y_2	$-3.311734987910881 \cdot 10^{-1}$	y_{14}	$1.104933470696396 \cdot 10^{-3}$
y_3	$1.697373326718410 \cdot 10^{-1}$	y_{15}	0
y_4	$1.893192460247178 \cdot 10^{-4}$	y_{16}	$6.488722210234531 \cdot 10^{3}$
y_5	$2.375751865617931 \cdot 10^{-5}$	y_{17}	$2.167924253080623 \cdot 10^{3}$
y_6	$-5.323907988763734 \cdot 10^{-6}$	y_{18}	$3.391435115267547 \cdot 10^{1}$
y_7	$-8.363283141616840 \cdot 10^{-6}$	y_{19}	$1.699107480197843 \cdot 10^{-1}$
y_8	$1.500000000000000 \cdot 10^{2}$	y_{20}	$-1.415799354959001 \cdot 10$
y_9	$6.025346682645789 \cdot 10^{1}$	y_{21}	$9.903251655235532 \cdot 10^{-1}$
y_{10}	$-8.753116989887888 \cdot 10$	y_{22}	$-6.232893262533717 \cdot 10^{1}$
y_{11}	$-3.005536801092212 \cdot 10^{-2}$	y_{23}	$-1.637910131687472 \cdot 10^{2}$
y_{12}	$-5.500488291932075 \cdot 10^{-3}$	y_{24}	$2.529853213732781 \cdot 10^{1}$

TABLE 16.3: *Run characteristics.*

solver	rtol	atol	h0	scd	steps	accept	# f	# Jac	# LU	CPU
MEBDFDAE	10^{-4}	10^{-4}	10^{-6}	-0.05	346	341	1691	45	45	0.82
	10^{-6}	10^{-6}	10^{-8}	-0.36	3780	3772	11960	284	284	7.68
	10^{-8}	10^{-8}	10^{-10}	2.16	6801	6778	19829	448	448	13.61
PSIDE-1	10^{-4}	10^{-4}		-0.06	45	41	858	29	180	0.84
	10^{-6}	10^{-6}		-0.07	259	235	5024	146	888	4.71
	10^{-8}	10^{-8}		1.50	1642	1437	32008	47	2652	24.37
RADAU	10^{-4}	10^{-4}	10^{-6}	-0.21	108	93	745	90	108	0.94
	10^{-6}	10^{-6}	10^{-8}	-0.04	172	171	2660	161	171	2.53
	10^{-8}	10^{-8}	10^{-10}	1.46	417	415	10492	396	412	8.80
RADAU5	10^{-4}	10^{-4}	10^{-6}	-0.21	108	93	745	90	108	0.94
	10^{-6}	10^{-6}	10^{-8}	0.00	294	289	2077	275	290	2.69
	10^{-8}	10^{-8}	10^{-10}	0.06	1957	1799	13526	1422	1880	16.05

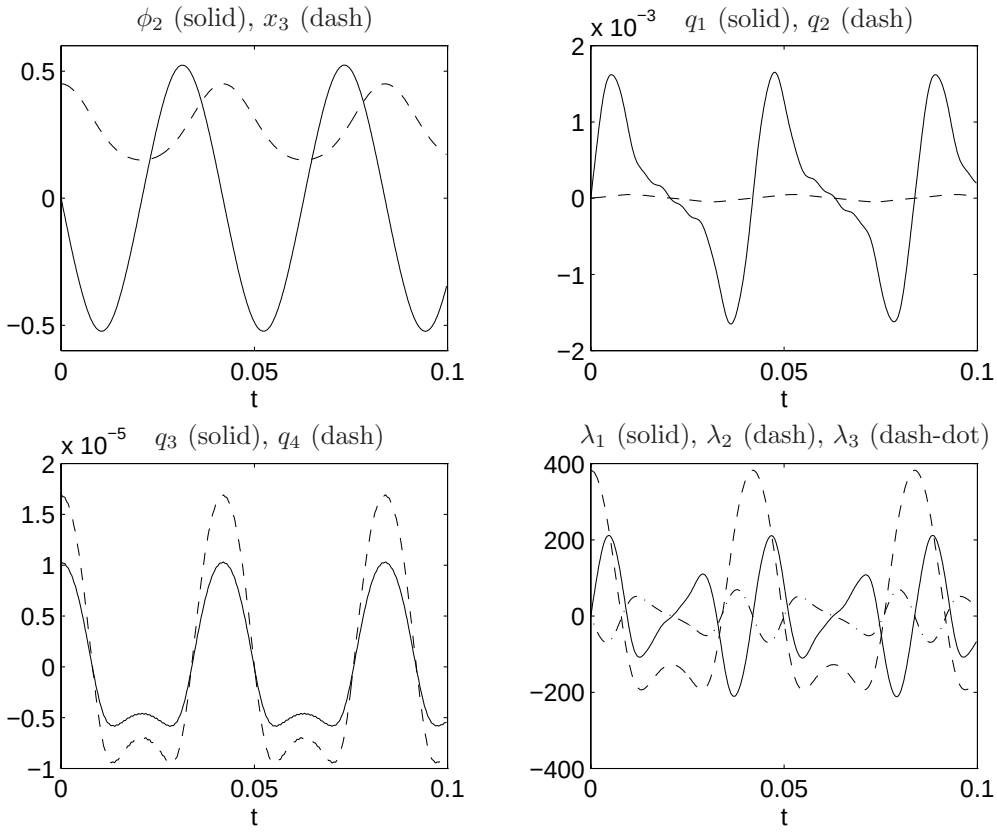

FIGURE 16.4: *Behavior of the ith solution component;* $i \in \{2, 3, \ldots, 7, 22, 23, 24\}$.

[Lub93] for an investigation of such systems and the implications for numerical methods in the ODE case.

- The nonlinear beam model leads to a higher computational effort but does not provoke convergence failures of Newton's method in RADAU5, as might be expected in case of nonlinear stiffness terms.

- As an alternative to stiff solvers, it is still possible to apply methods based on explicit discretizations, e.g., half-explicit or projection methods for constrained mechanical systems. The code MDOP5 [Sim95], a projection method based on DOPRI5, uses 2260 integration steps to solve this problem in the default setting, with atol = 10^{-6} and rtol = 10^{-5}, and initial values close to the smooth motion. Thus, the stiffness is no that severe in case of this carefully chosen one-dimensional elastic body model.

- There is also an extended version of the slider crank with a two-dimensional FE grid for the connecting rod. There, explicit methods do not work any longer. An animation of the system motion can be found at `http://www.mathematik.tu-darmstadt.de/~simeon/` .

REFERENCES

[JPD93] M. Jahnke, K. Popp, and B. Dirr. Approximate analysis of flexible parts in multibody systems using the finite element method. In Schiehlen W., editor, *Advanced Multibody System Dynamics*, pages 237–256, Stuttgart, 1993. Kluwer Academic Publishers.

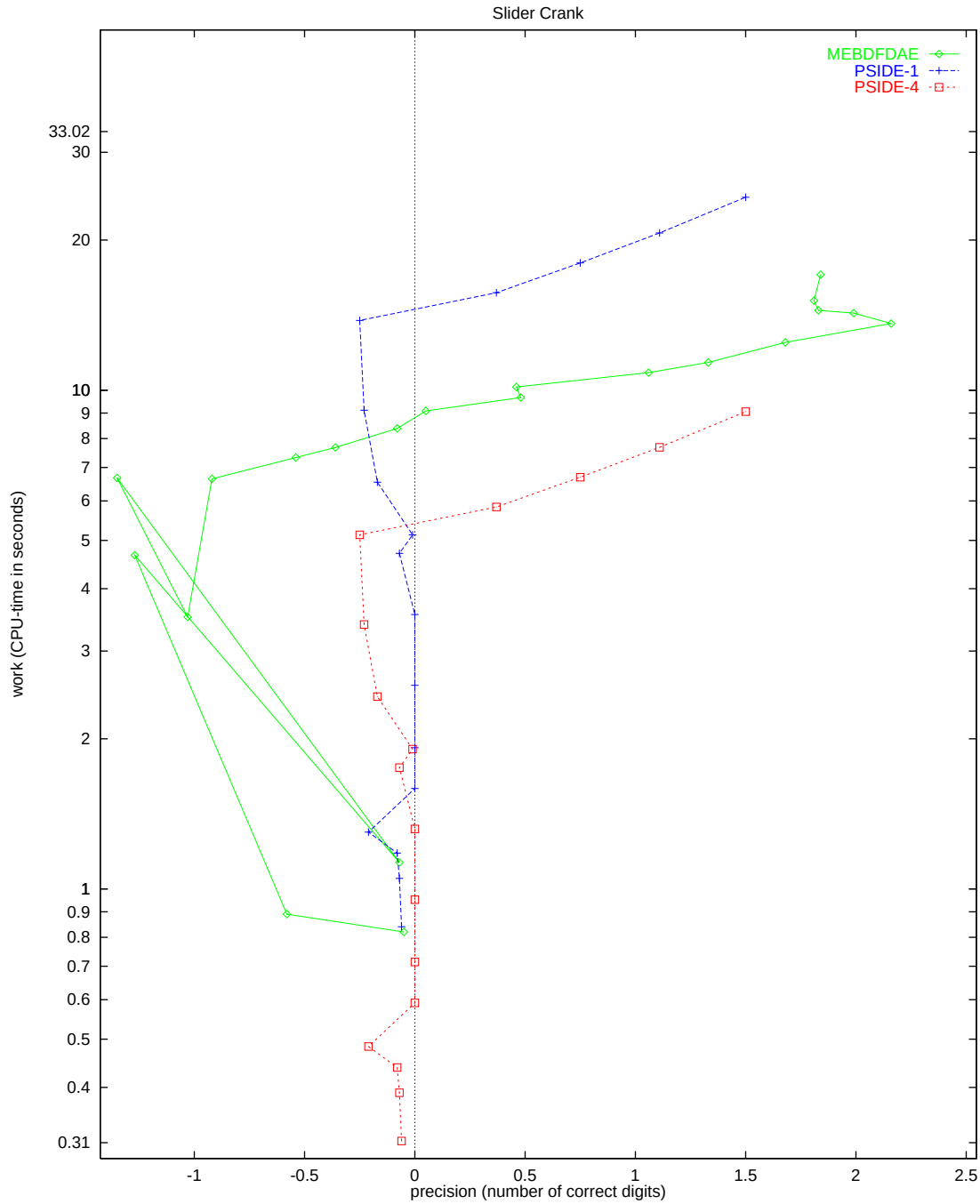

FIGURE 16.5: *Work-precision diagram.*

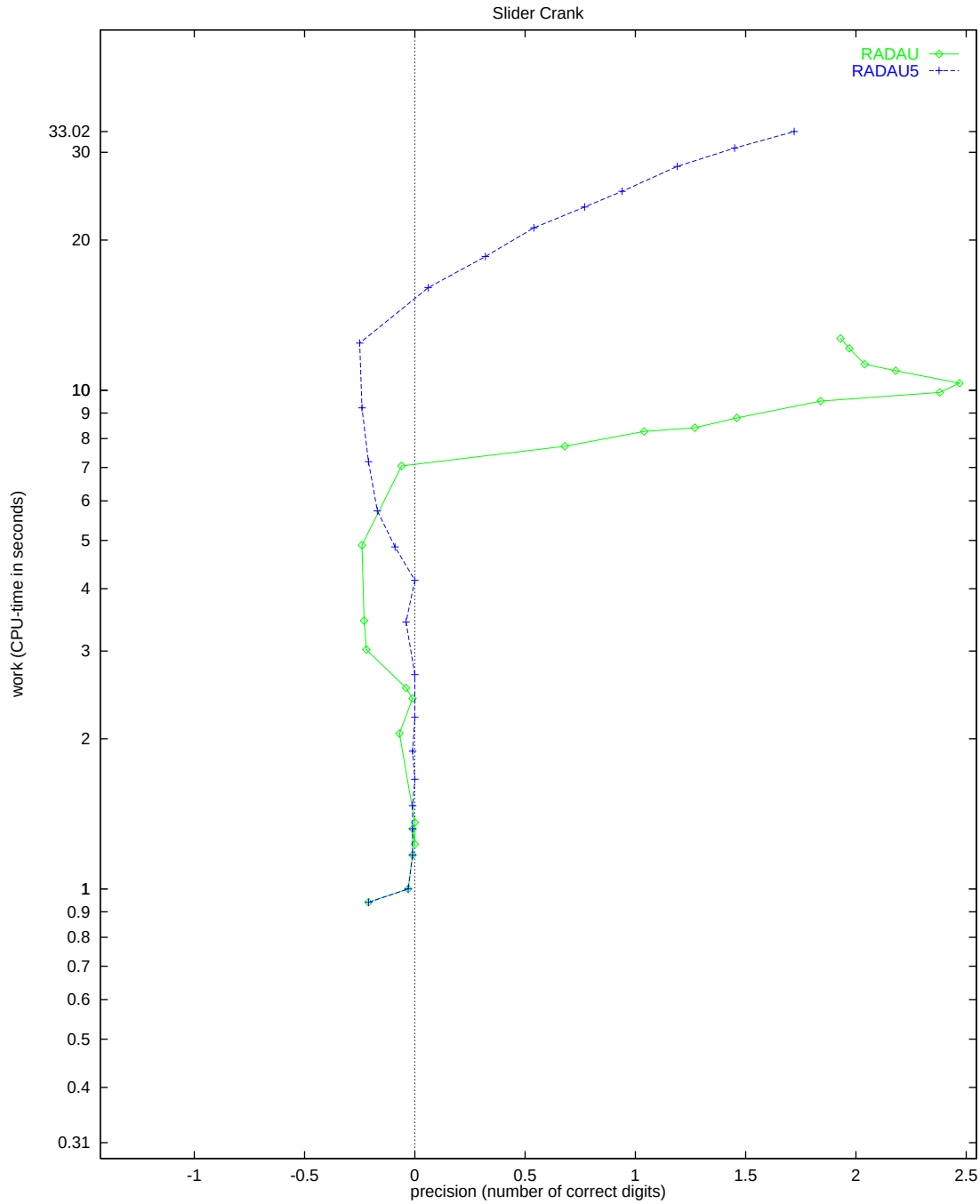

FIGURE 16.6: *Work-precision diagram.*

[Kop89] W. Koppens. *The dynamics of systems of deformable bodies.* PhD thesis, Technische Universiteit Eindhoven, 1989.

[Lub93] C. Lubich. Integration of stiff mechanical systems by Runge-Kutta methods. *ZAMP*, 44:1022–1053, 1993.

[Sim95] B. Simeon. MBSPACK - Numerical integration software for constrained mechanical motion. *Surv. on Math. in Ind.*, 5:169–202, 1995.

[Sim96] B. Simeon. Modelling a flexible slider crank mechanism by a mixed system of DAEs and PDEs. *Math. Modelling of Systems*, 2:1–18, 1996.

[Sim97] B. Simeon. DAEs and PDEs in elastic multibody systems, 1997. *To appear in Numerical Algorithms.*

17. Water tube system

17.1 General information

This IVP is an index 2 system of 49 non-linear Differential-Algebraic Equations and describes the water flow through a tube system, taking into account turbulence and the roughness of the tube walls. The parallel-IVP-algorithm group of CWI contributed this problem to the test set in cooperation with B. Koren (CWI) and Paragon Decision Technology B.V.

17.2 Mathematical description of the problem

The problem is of the form

$$M\frac{\mathrm{d}y}{\mathrm{d}t} = f(y), \qquad y(0) = y_0, \quad y'(0) = y'_0, \tag{17.1}$$

where $0 \le t \le 17 \cdot 3600$ and $y \in \mathbb{R}^{49}$. Furthermore,

$$M = \begin{bmatrix} M^\phi & O & O \\ O & O & O \\ O & O & M^p \end{bmatrix}, \tag{17.2}$$

where $M^\phi \in \mathbb{R}^{18\times 18}$ and $M^p \in \mathbb{R}^{13\times 13}$ are given by

$$M^\phi_{i,j} = \begin{cases} v_i & \text{for } i = j, \\ 0 & \text{otherwise.} \end{cases} \qquad M^p_{i,j} = \begin{cases} C_5 & \text{for } i = j = 1, \\ C_8 & \text{for } i = j = 2, \\ 0 & \text{otherwise,} \end{cases}$$

The first 38 components of y are of index 1, the last 11 are of index 2. For the definition of f and the values of C_5, C_8 and v we refer to §17.3.

The initial vectors y_0 and y'_0 are given by

$$y_0 = \begin{cases} 0 & \text{for} \quad i = 1, 2, \ldots, 18 \\ 0.047519404529185289807 & \text{for} \quad i = 19, 20, \ldots, 36 \\ 109800 & \text{for} \quad i = 37, 38, \ldots, 49 \end{cases} \quad \text{and} \quad y'_0 = (0, \ldots, 0)^{\mathrm{T}}. \tag{17.3}$$

The function f contains several square roots. It is clear that the function can not be evaluated if one of the arguments of one of these square roots becomes negative. To prevent this situation, we set `IERR=-1` in the Fortran subroutine that defines f if this happens. See page *III-vi* of the the description of the software part of the test set for more details on `IERR`.

17.3 Origin of the problem

This test example describes how water flows through a water tube system. The system is represented by a set of nodes, which are connected by tubes. The structure of the water tube system is depicted in Figure 17.1. There are two types of nodes: normal nodes and buffer nodes, to which a buffer is attached. We denote the set of all nodes by $\mathcal{N}$, and the set of buffer nodes by $\mathcal{B}$. For the system under consideration, $\mathcal{B} = \{5, 8\}$. The rectangles in Figure 17.1 represent the buffers. The pipes are in the horizontal plane; the buffers are connected to the nodes perpendicular to this plane. The pipes from the buffer nodes to the rectangles are virtual; in reality the buffers are directly attached to the buffer nodes. In the model every node can have inflow and outflow, which are denoted by $e_i^{\mathrm{in}}(t)$ and $e_i^{\mathrm{out}}(t)$. In our example, inflow occurs only at node 1 and node 13, whereas only node 10 has outflow. The unit of time in the model is second. Defining the time in hours by $\hat{t} = t/3600$, these flows are defined by

$$\begin{aligned} e_1^{\mathrm{in}}(t) &= (1 - \cos(\mathrm{e}^{-\hat{t}} - 1))/200, \\ e_{13}^{\mathrm{in}}(t) &= (1 - \cos(\mathrm{e}^{-\hat{t}} - 1))/80, \\ e_{10}^{\mathrm{out}}(t) &= \hat{t}^2(3\hat{t}^2 - 92\hat{t} + 720)/10^6. \end{aligned}$$

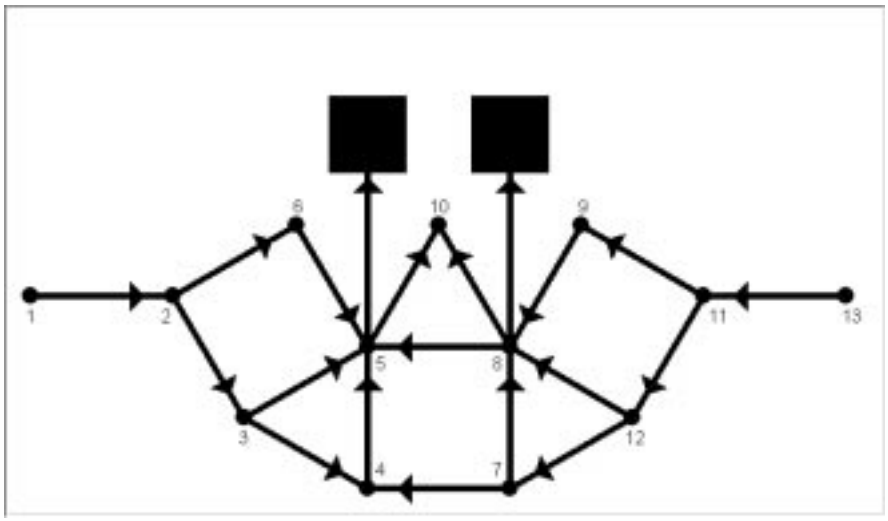

FIGURE 17.1: *Structure of water tube system.*

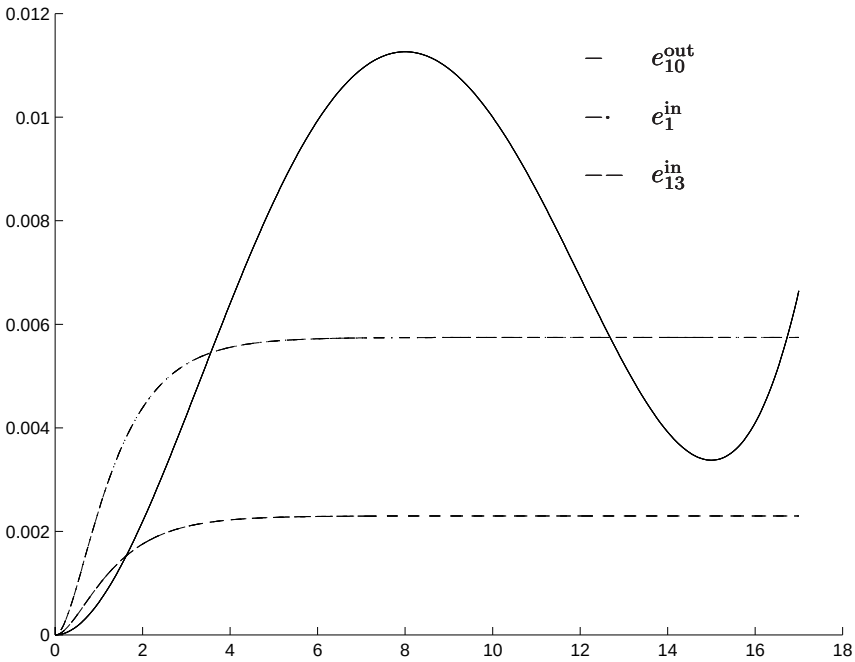

FIGURE 17.2: *Inflows and outflow in m^3/s as function of time in hours.*

Figure 17.2 shows plots of these flows as function of $\hat{t}$. Note that the outflow has a peak at 8 AM and is increasing again after 3 PM.

Although it seems that node 6 and node 9 could be omitted, we include them in the model, to leave open the possibility that these nodes have inflow or outflow. The arrows in Figure 17.1 denote the direction in which we compute the flows. For example, if there is a flow from node 4 to node 3, then this flow will be negative.

To model the flow of the water, we introduce some symbols, which are listed in Table 17.1. The roughness $k_{i,j}$ is measured as the average height of the obstacles on the tube wall. The structure $S_{i,j}$

TABLE 17.1: *List of symbols for modeling flow in tubes.*

Symbol	Unit	Meaning
$\phi_{i,j}(t)$	m^3/s	flow through tube from i to j at time t
$u_{i,j}(t)$	m/s	mean velocity of flow through tube from i to j at time t
$F_{i,j}(t)$	N	total force on water in tube from i to j at time t
$F^{\mathrm{a}}_{i,j}(t)$	N	adhesion force on water in tube from i to j at time t
$\lambda_{i,j}(t)$	-	coefficient of resistance of tube from i to j at time t
$R_{i,j}(t)$	-	Reynolds number of flow through tube from i to j at time t
$p_i(t)$	N/m^2	pressure in i at time t
$S_{i,j}$	-	incidence matrix for structure of the tube system
$m_{i,j}$	kg	mass of water in tube from i to j
$d_{i,j}$	m	diameter of tube from i to j
$l_{i,j}$	m	length of tube from i to j
$A_{i,j}$	m^2	area of tube from i to j
$k_{i,j}$	m	roughness of wall of tube from i to j
$e^{\mathrm{in}}_i(t)$	m^3/s	inflow at i at time t
$e^{\mathrm{out}}_i(t)$	m^3/s	outflow at i at time t
B_i $(i \in \mathcal{B})$	m^2	area of buffer i
R^{crit}	-	critical Reynolds number
g	m/s^2	gravity constant
ρ	kg/m^3	density of water
μ	$kg/(m \cdot s)$	viscosity of water
ν	m^2/s	kinematic viscosity of water
v	kg/m^4	auxiliary vector, see (17.15)

is defined as

$$S_{i,j} = \begin{cases} 1 & \text{if there is a tube from } i \text{ to } j, \\ 0 & \text{otherwise.} \end{cases}$$

From Figure 17.1 we see that

$$S = \begin{bmatrix} 0 & 1 & 0 & 0 & 0 & 0 & 0 & 0 & 0 & 0 & 0 & 0 & 0 \\ 0 & 0 & 1 & 0 & 0 & 1 & 0 & 0 & 0 & 0 & 0 & 0 & 0 \\ 0 & 0 & 0 & 1 & 1 & 0 & 0 & 0 & 0 & 0 & 0 & 0 & 0 \\ 0 & 0 & 0 & 0 & 1 & 0 & 0 & 0 & 0 & 0 & 0 & 0 & 0 \\ 0 & 0 & 0 & 0 & 0 & 0 & 0 & 0 & 0 & 1 & 0 & 0 & 0 \\ 0 & 0 & 0 & 0 & 1 & 0 & 0 & 0 & 0 & 0 & 0 & 0 & 0 \\ 0 & 0 & 0 & 1 & 0 & 0 & 0 & 1 & 0 & 0 & 0 & 0 & 0 \\ 0 & 0 & 0 & 0 & 1 & 0 & 0 & 0 & 0 & 1 & 0 & 0 & 0 \\ 0 & 0 & 0 & 0 & 0 & 0 & 0 & 1 & 0 & 0 & 0 & 0 & 0 \\ 0 & 0 & 0 & 0 & 0 & 0 & 0 & 0 & 0 & 0 & 0 & 0 & 0 \\ 0 & 0 & 0 & 0 & 0 & 0 & 0 & 0 & 1 & 0 & 0 & 1 & 0 \\ 0 & 0 & 0 & 0 & 0 & 0 & 1 & 1 & 0 & 0 & 1 & 0 & 0 \\ 0 & 0 & 0 & 0 & 0 & 0 & 0 & 0 & 0 & 0 & 1 & 0 & 0 \end{bmatrix}.$$

Some of the quantities in Table 17.1 can be computed directly from others:

$$\begin{aligned} \mu &= \nu \cdot \rho, \\ \phi_{i,j}(t) &= u_{i,j}(t) \cdot A_{i,j}, \\ A_{i,j} &= \pi \cdot d_{i,j}^2/4, \\ m_{i,j} &= A_{i,j} \cdot l_{i,j} \cdot \rho, \\ R_{i,j}(t) &= u_{i,j}(t) \cdot d_{i,j}/\nu. \end{aligned}$$

The definition of $R_{i,j}(t)$ was taken from [Sch78, p. 816].

We now explain how to model the flow through a tube, using Newton's second Law, which states that

$$m_{i,j}\frac{\mathrm{d}u_{i,j}(t)}{\mathrm{d}t} = F_{i,j}(t). \tag{17.4}$$

Assuming that gravity has no influence on the water flow in all tubes (remember that the pipes are

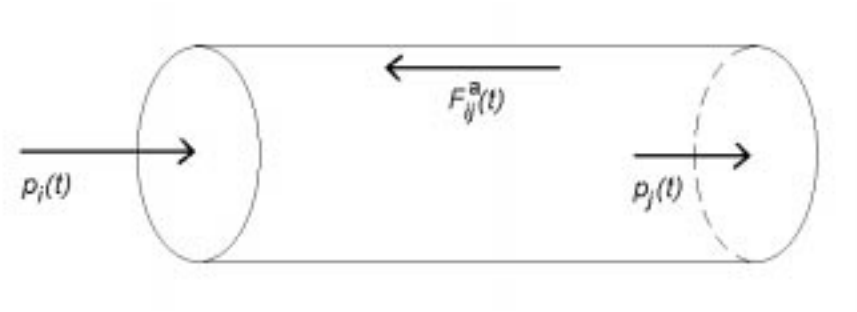

FIGURE 17.3: *Forces on water in tube.*

in the horizontal plane), we see from Figure 17.3 that the total force on the water in a tube equals

$$F_{i,j}(t) = A_{i,j}(p_i(t) - p_j(t)) - F_{i,j}^{\mathrm{a}}(t). \tag{17.5}$$

The magnitude of the adhesion force depends on the type of flow. For laminar flows ($|R_{i,j}(t)| \leq R^{\mathrm{crit}}$), we use the formula [Sch78, p. 12]

$$F_{i,j}^{\mathrm{a}}(t)/A_{i,j} = 32\mu \cdot l_{i,j} \cdot u_{i,j}(t)/d_{i,j}^2. \tag{17.6}$$

For turbulent flows ($|R_{i,j}(t)| > R^{\mathrm{crit}}$), we have [Sch78, p. 597]

$$F_{i,j}^{\mathrm{a}}(t)/A_{i,j} = \lambda_{i,j}(t) \cdot \rho \cdot l_{i,j} \cdot u_{i,j}(t)^2/d_{i,j}, \tag{17.7}$$

where the resistance $\lambda_{i,j}(t)$ is computed from Colebrook and White's formula [Sch78, p. 621]:

$$0 = \frac{1}{\sqrt{\lambda_{i,j}(t)}} - 1.74 + 2\log\left(\frac{2k_{i,j}}{d_{i,j}} + \frac{18.7}{|R_{i,j}(t)|\sqrt{\lambda_{i,j}(t)}}\right). \tag{17.8}$$

Although for laminar flows the adhesion force does not depend on the resistance coefficient (cf. (17.6)), we have to choose a value for $\lambda_{i,j}$ in case of laminar flows. We compute this value by replacing $R_{i,j}$ in (17.8) by R^{crit}, i.e., we choose the value such that if a flow changes from laminar into turbulent, the resistance coefficient changes gradually.

For the normal nodes, Kirchoff's law holds, which states that

$$\forall\, n \in \mathcal{N} - \mathcal{B}: \qquad 0 = \sum_{i|S_{i,n}=1} \phi_{i,n}(t) + e_n^{\text{in}}(t) - \sum_{j|S_{n,j}=1} \phi_{n,j}(t) - e_n^{\text{out}}(t) \tag{17.9}$$

For the buffer nodes, we add a term $\psi_n(t)$ that represents the flow to the buffer:

$$\forall\, n \in \mathcal{B}: \qquad \psi_n(t) = \sum_{i|S_{i,n}=1} \phi_{i,n}(t) + e_n^{\text{in}}(t) - \sum_{j|S_{n,j}=1} \phi_{n,j}(t) - e_n^{\text{out}}(t) \tag{17.10}$$

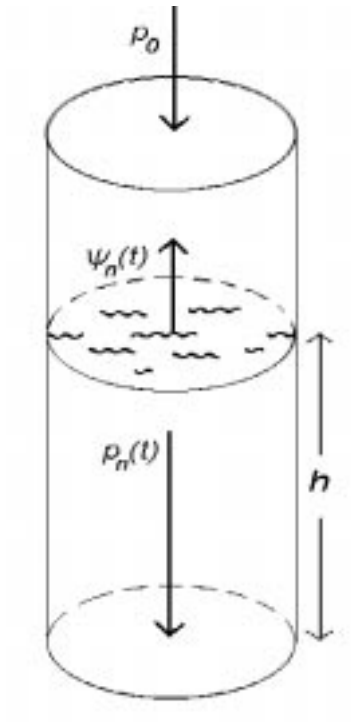

FIGURE 17.4: *Representation of water buffer.*

We now explain how to compute $\psi_n(t)$. A buffer can be interpreted as the water column in Figure 17.4, with ground area B_n and height h. Due to the flow $\psi_n(t)$ the height of the buffer changes at a rate $\psi_n(t)/B_n$. The difference between the pressure at the top and bottom of the column satisfies

$$p_n - p_0 = g \cdot \rho \cdot h.$$

Consequently, the pressure difference changes at a rate given by

$$\frac{\mathrm{d}(p_n - p_0)}{\mathrm{d}t} = g \cdot \rho \cdot \frac{\mathrm{d}h}{\mathrm{d}t} = g \cdot \rho \cdot \frac{\psi_n(t)}{B_n}. \tag{17.11}$$

Notice that the pressure p_0 is constant and therefore drops out in this formula. Substituting (17.11) in (17.10) gives

$$\forall\, n \in \mathcal{B}: \qquad C_n \frac{\mathrm{d}p_n(t)}{\mathrm{d}t} = \sum_{i|S_{i,n}=1} \phi_{i,n}(t) + e_n^{\text{in}}(t) - \sum_{j|S_{n,j}=1} \phi_{n,j}(t) - e_n^{\text{out}}(t), \tag{17.12}$$

where the quantity $C_n := B_n/(\rho \cdot g)$ can be interpreted as the capacity of the buffer at node n.

We arrive at the formulation in §17.2 by setting

$$\begin{aligned} y = (\quad & \phi_{1,2}(t), \phi_{2,3}(t), \phi_{2,6}(t), \phi_{3,4}(t), \phi_{3,5}(t), \phi_{4,5}(t), \phi_{5,10}(t), \phi_{6,5}(t), \phi_{7,4}(t), \\ & \phi_{7,8}(t), \phi_{8,5}(t), \phi_{8,10}(t), \phi_{9,8}(t), \phi_{11,9}(t), \phi_{11,12}(t), \phi_{12,7}(t), \phi_{12,8}(t), \phi_{13,11}(t), \\ & \lambda_{1,2}(t), \lambda_{2,3}(t), \lambda_{2,6}(t), \lambda_{3,4}(t), \lambda_{3,5}(t), \lambda_{4,5}(t), \lambda_{5,10}(t), \lambda_{6,5}(t), \lambda_{7,4}(t), \\ & \lambda_{7,8}(t), \lambda_{8,5}(t), \lambda_{8,10}(t), \lambda_{9,8}(t), \lambda_{11,9}(t), \lambda_{11,12}(t), \lambda_{12,7}(t), \lambda_{12,8}(t), \lambda_{13,11}(t), \\ & p_5(t), p_8(t), p_1(t), p_2(t), \ldots, p_4(t), p_6(t), p_7(t), p_9(t), p_{10}(t), \ldots, p_{13}(t) \qquad)^{\mathrm{T}}. \end{aligned} \tag{17.13}$$

All pressures are of index 2, except for those at the buffer nodes. The reordering of the pressures in (17.13) is such that the elements in y appear in order of increasing index, as required by RADAU, RADAU5 and MEBDFDAE.

The first 18 equations in (17.1) are obtained by first substituting (17.5) in (17.4). Next, we divide both sides by $A_{i,j}$, thus yielding

$$\frac{\rho \cdot l_{i,j}}{A_{i,j}} \frac{\mathrm{d}\phi_{i,j}(t)}{\mathrm{d}t} = p_i(t) - p_j(t) - F^{\mathrm{a}}_{i,j}(t)/A_{i,j}. \tag{17.14}$$

Finally, (17.6) and (17.7) are substituted in (17.14). Consequently, if we define $V_{i,j} = \rho \cdot l_{i,j}/A_{i,j}$, then the vector v in (17.2) is given by

$$\begin{aligned} v = (\quad & V_{1,2}, V_{2,3}, V_{2,6}, V_{3,4}, V_{3,5}, V_{4,5}, V_{5,10}, V_{6,5}, V_{7,4}, \\ & V_{7,8}, V_{8,5}, V_{8,10}, V_{9,8}, V_{11,9}, V_{11,12}, V_{12,7}, V_{12,8}, V_{13,11} \quad)^{\mathrm{T}}. \end{aligned} \tag{17.15}$$

The next 18 equations in (17.1) equal (17.8), whereas the last 13 equations are given by (17.9) and (17.12).

In this model, all tubes and buffers are equal with characteristics as specified in Table 17.2. Moreover, we assume that the temperature is constant. The values for the physical constants are listed

TABLE 17.2: *Characteristics of tubes.*

Quantity	Value
$l_{i,j}$	1000
$k_{i,j}$	0.000002
$d_{i,j}$	1
B_i	200

in Table 17.3. The values for ρ and ν correspond to a temperature of 10°C. The value for R^{crit} was

TABLE 17.3: *Values of physical constants.*

Constant	Value
ν	$1.31 \cdot 10^{-6}$
g	9.8
ρ	$1.0 \cdot 10^{3}$
R^{crit}	$2.3 \cdot 10^{3}$

taken from [Sch78, p. 39].

We now discuss how we derived the initial conditions in (17.3). First we note that (17.9) is an index 2 constraint. Therefore, the initial values also have to satisfy the once differentiated constraint (the so-called *hidden* constraint)

$$\forall\, n \in \mathcal{N} - \mathcal{B}: \qquad 0 = \sum_{i|S_{i,n}=1} \phi'_{i,n}(t) + e_n^{\text{in}'}(t) - \sum_{j|S_{n,j}=1} \phi'_{n,j}(t) - e_n^{\text{out}'}(t). \tag{17.16}$$

We are free to choose initial flows $\phi_{i,j}(0)$ as long as they satisfy (17.9); we chose these all equal to zero. This means that the resistance coefficients equal the value for the case of laminar flows, i.e., $0.047519\ldots$ The pressures at the buffer nodes, which can be selected freely, are chosen to be $10^5 + g\cdot\rho$, which corresponds to initial heights of one meter in the water columns, assuming that p_0 in Figure 17.4 equals one bar. From (17.12) it follows that $p'_n(0) = 0$, $n \in \mathcal{B}$ (note that the in- and outflows are initially zero). The initial pressures $p_n(0)$, $n \in \mathcal{N} - \mathcal{B}$, and the initial derivative flows $\phi'_{i,j}(0)$ follow from (17.14) and (17.16). Since the derivatives of the in- and outflows are initially zero, the initial values in (17.3) satisfy these equations. The other initial values, $\lambda'_{i,j}(0)$ and $p'_n(0)$, $n \in \mathcal{N} - \mathcal{B}$, appear neither in the system, nor in the hidden constraints, and can be chosen freely. We set these equal to 0.

Several observations can be made from the behavior of the flows, resistance coefficients and pressures, which are plotted in Figure 17.6–17.8:

- The rise and fall of the outflow in node 10 cause the flows to node 10 to change from laminar to turbulent and back, as can be seen from the resistance coefficients $\lambda_{5,10}$ and $\lambda_{8,10}$, which correspond to y_{25} and y_{30}.
- At 8 AM, the pressures in the buffer nodes drop below their original level, which means that some of the water that was present in the buffers initially, is used to meet the peak demand.
- The time period in which the flows to node 10 have become laminar again (this period is indicated by the vertical dashed lines in the plots of y_{25} and y_{30}, causes an irregular behavior (indicated again by dashed lines) of the solution components y_3, y_6, y_9, y_{10} and y_{11} which correspond to the flow from node 3 to node 4 and the flows in the cycle 4–7–8–5, respectively.
- Some of the flows contain high-frequent oscillations of small amplitude. To see this more clearly, we plotted $\phi_{3,4}$ for $6878 < t \le 17 \cdot 3600$ in Figure 17.5.

17.4 Numerical solution of the problem

Tables 17.4–17.5 and Figures 17.6–17.8 present the reference solution at the end of the integration interval, the run characteristics, the behavior of the solution over the integration interval and the work-precision diagrams, respectively.

Since the 13 last solution components (the pressures) are so much larger in magnitude than the other components, we used the following vector-valued input tolerances:

$$\begin{aligned} &\text{atol}(i) = \text{atol} && \text{for } i = 1,\ldots,36,\\ &\text{atol}(i) = 10^6 \cdot \text{atol} && \text{for } i = 37,\ldots,49,\\ &\text{rtol}(i) = \text{rtol} && \text{for } i = 1,\ldots,49. \end{aligned}$$

The reference solution was computed by PSIDE with `rtol = atol =` 10^{-14}. For the work-precision diagrams, we used: $\text{rtol} = 10^{-(4+m/4)}$, $m = 0, 1, \ldots, 24$; atol = rtol; h0 = rtol for RADAU, RADAU5 and MEBDFDAE.

The failed runs are in Table 17.6; listed are the name of the solver that failed, for which values of m this happened, and the reason for failing. The speed-up factor for PSIDE is 2.73.

References

[Sch78] H. Schlichting. *Boundary-Layer Theory.* Series in mechanical engineering. Mc Graw-Hill, seventh edition, 1978.

TABLE 17.4: *Reference solution at the end of the integration interval.*

y_1	$0.2298488296477430 \cdot 10^{-002}$	y_{26}	$0.4751940452918529 \cdot 10^{-001}$
y_2	$0.1188984650746585 \cdot 10^{-002}$	y_{27}	$0.4751940452918529 \cdot 10^{-001}$
y_3	$0.1109503645730845 \cdot 10^{-002}$	y_{28}	$0.4751940452918529 \cdot 10^{-001}$
y_4	$0.1589620100314825 \cdot 10^{-003}$	y_{29}	$0.4751940452918529 \cdot 10^{-001}$
y_5	$0.1030022640715102 \cdot 10^{-002}$	y_{30}	$0.4249217433601160 \cdot 10^{-001}$
y_6	$0.8710606306836165 \cdot 10^{-003}$	y_{31}	$0.4732336439609648 \cdot 10^{-001}$
y_7	$0.3243571480903489 \cdot 10^{-002}$	y_{32}	$0.4732336439609648 \cdot 10^{-001}$
y_8	$0.1109503645730845 \cdot 10^{-002}$	y_{33}	$0.4270002118868241 \cdot 10^{-001}$
y_9	$0.7120986206521341 \cdot 10^{-003}$	y_{34}	$0.4751940452918529 \cdot 10^{-001}$
y_{10}	$0.6414613963833099 \cdot 10^{-003}$	y_{35}	$0.4751940452918529 \cdot 10^{-001}$
y_{11}	$0.9416978549524347 \cdot 10^{-003}$	y_{36}	$0.3651427026675656 \cdot 10^{-001}$
y_{12}	$0.3403428519096511 \cdot 10^{-002}$	y_{37}	$0.1111268591478108 \cdot 10^{+006}$
y_{13}	$0.2397639310739395 \cdot 10^{-002}$	y_{38}	$0.1111270045592387 \cdot 10^{+006}$
y_{14}	$0.2397639310739395 \cdot 10^{-002}$	y_{39}	$0.1111271078730254 \cdot 10^{+006}$
y_{15}	$0.3348581430454180 \cdot 10^{-002}$	y_{40}	$0.1111269851929858 \cdot 10^{+006}$
y_{16}	$0.1353560017035444 \cdot 10^{-002}$	y_{41}	$0.1111269255355337 \cdot 10^{+006}$
y_{17}	$0.1995021413418736 \cdot 10^{-002}$	y_{42}	$0.1111269322658045 \cdot 10^{+006}$
y_{18}	$0.5746220741193575 \cdot 10^{-002}$	y_{43}	$0.1111269221703983 \cdot 10^{+006}$
y_{19}	$0.4751940452918529 \cdot 10^{-001}$	y_{44}	$0.1111270121140691 \cdot 10^{+006}$
y_{20}	$0.4751940452918529 \cdot 10^{-001}$	y_{45}	$0.1111274419515807 \cdot 10^{+006}$
y_{21}	$0.4751940452918529 \cdot 10^{-001}$	y_{46}	$0.1111255158881087 \cdot 10^{+006}$
y_{22}	$0.4751940452918529 \cdot 10^{-001}$	y_{47}	$0.1111278793439227 \cdot 10^{+006}$
y_{23}	$0.4751940452918529 \cdot 10^{-001}$	y_{48}	$0.1111270995171642 \cdot 10^{+006}$
y_{24}	$0.4751940452918529 \cdot 10^{-001}$	y_{49}	$0.1111298338971779 \cdot 10^{+006}$
y_{25}	$0.4311196778792902 \cdot 10^{-001}$		

TABLE 17.5: *Run characteristics.*

solver	rtol	atol	h0	scd	steps	accept	# f	# Jac	# LU	CPU
MEBDFDAE	10^{-4}	10^{-4}	10^{-4}	1.35	85	81	961	16	16	2.03
	10^{-7}	10^{-7}	10^{-7}	3.17	1224	1181	9279	150	150	20.93
	10^{-10}	10^{-10}	10^{-10}	5.90	3779	3432	37017	629	629	79.24
PSIDE-1	10^{-4}	10^{-4}		1.31	68	54	842	14	260	4.63
	10^{-7}	10^{-7}		2.20	120	100	2208	44	408	12.24
	10^{-10}	10^{-10}		5.72	868	730	14506	44	1512	57.36
RADAU	10^{-10}	10^{-10}	10^{-10}	3.34	380	284	5467	203	363	35.83
RADAU5	10^{-4}	10^{-4}	10^{-4}	1.49	41	35	251	18	37	2.39
	10^{-7}	10^{-7}	10^{-7}	2.33	165	119	1109	65	138	9.21
	10^{-10}	10^{-10}	10^{-10}	3.91	722	640	5365	403	559	51.05

TABLE 17.6: *Failed runs.*

solver	m	reason
MEBDFDAE	8	core dump / overflow
MEBDFDAE	$15, 19, 23$	tolerance too strict
RADAU	$0, 4, 5, 6, 9, 10, 12, 14, 16, 17, 19$	solver cannot handle `IERR=-1`.
RADAU5	6	stepsize too small

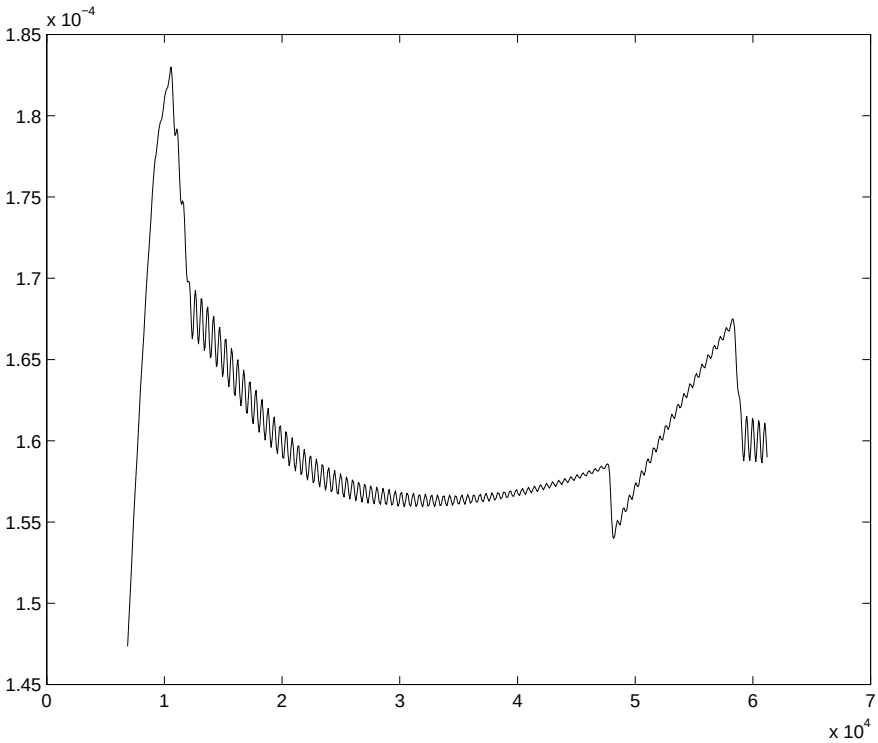

FIGURE 17.5: *Behavior of* $\phi_{3,4}$ *for* $6878 < t \leq 17 \cdot 3600$.

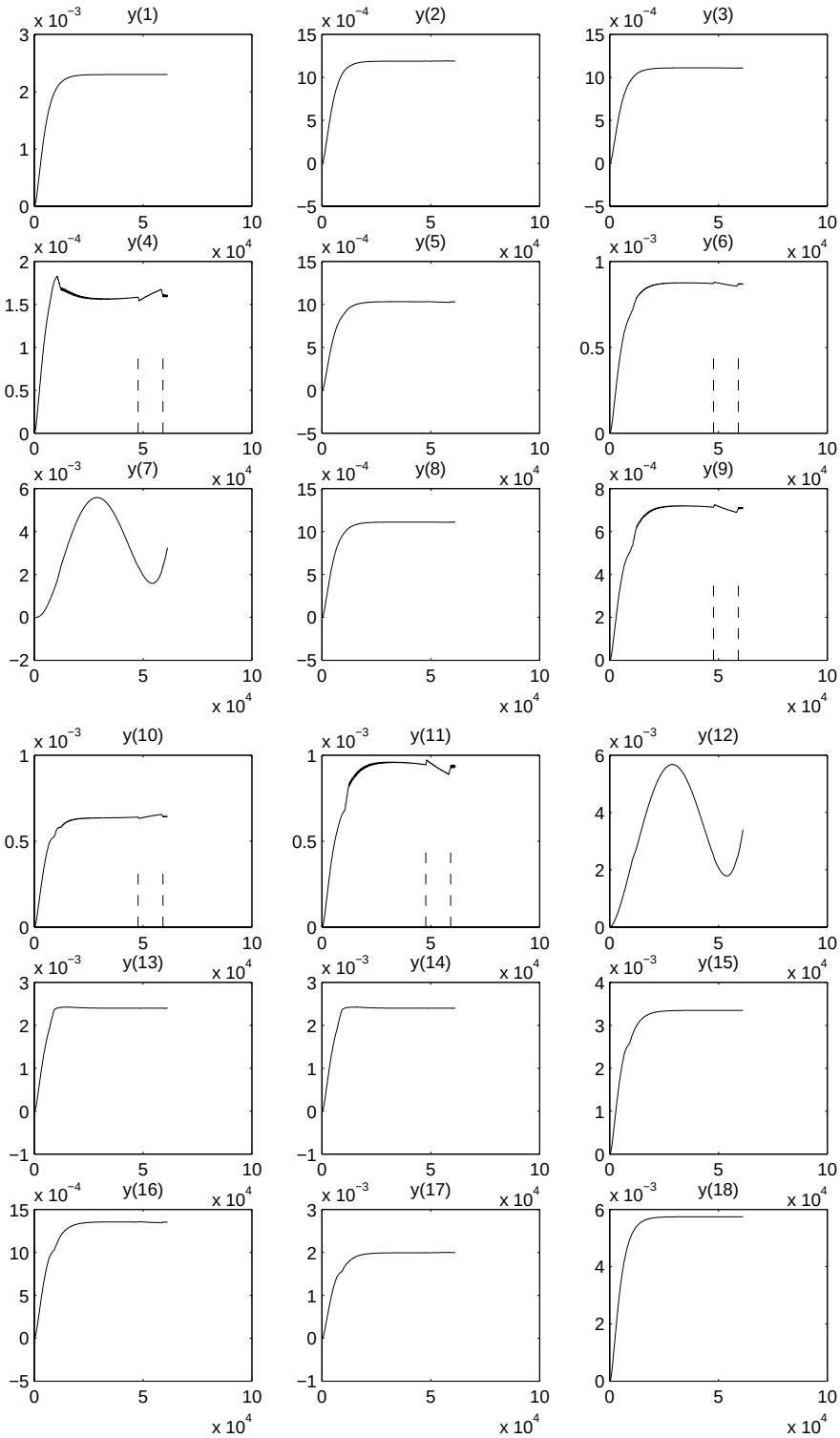

FIGURE 17.6: *Behavior of flows over the integration interval.*

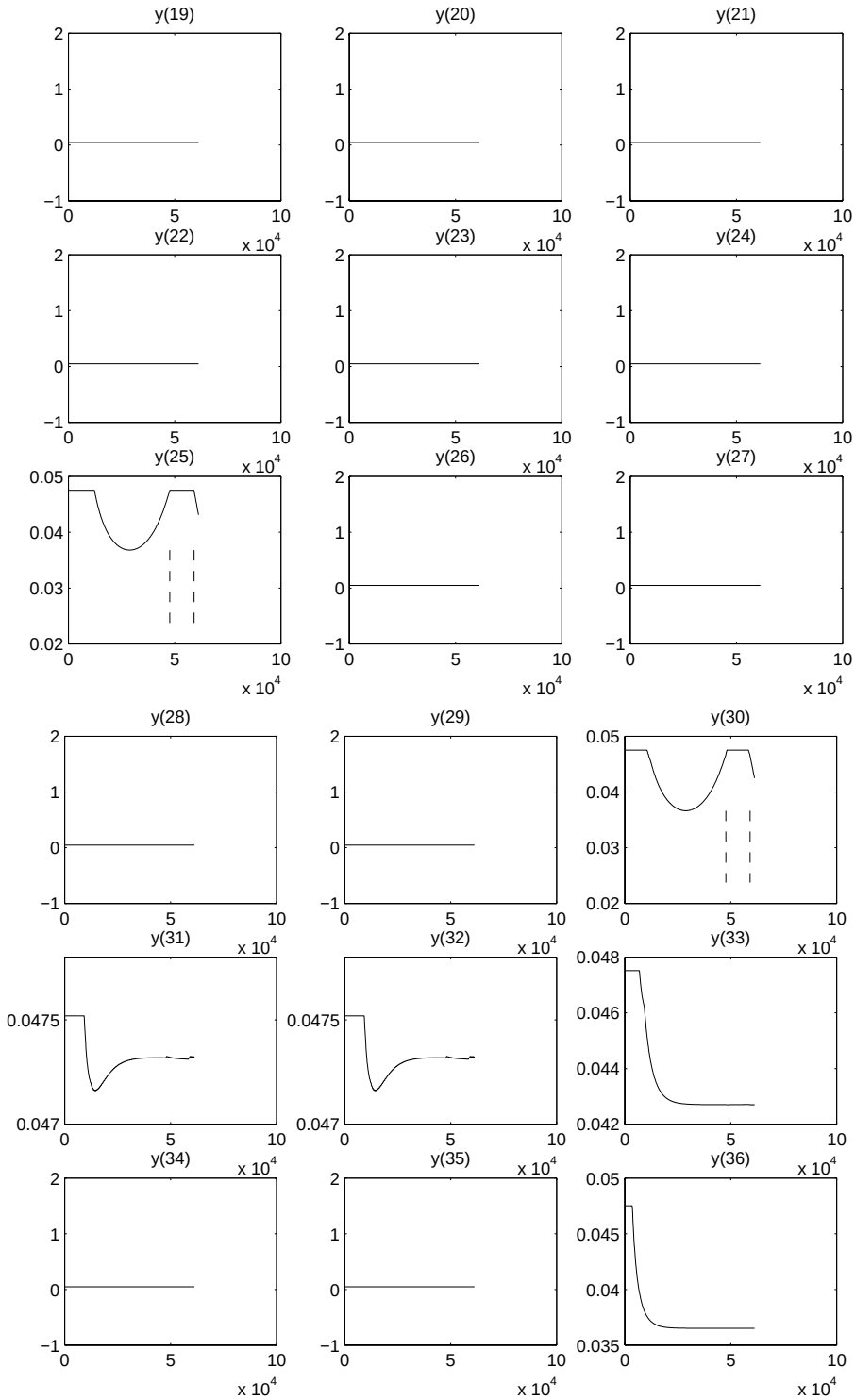

FIGURE 17.7: *Behavior of resistance coefficients over the integration interval.*

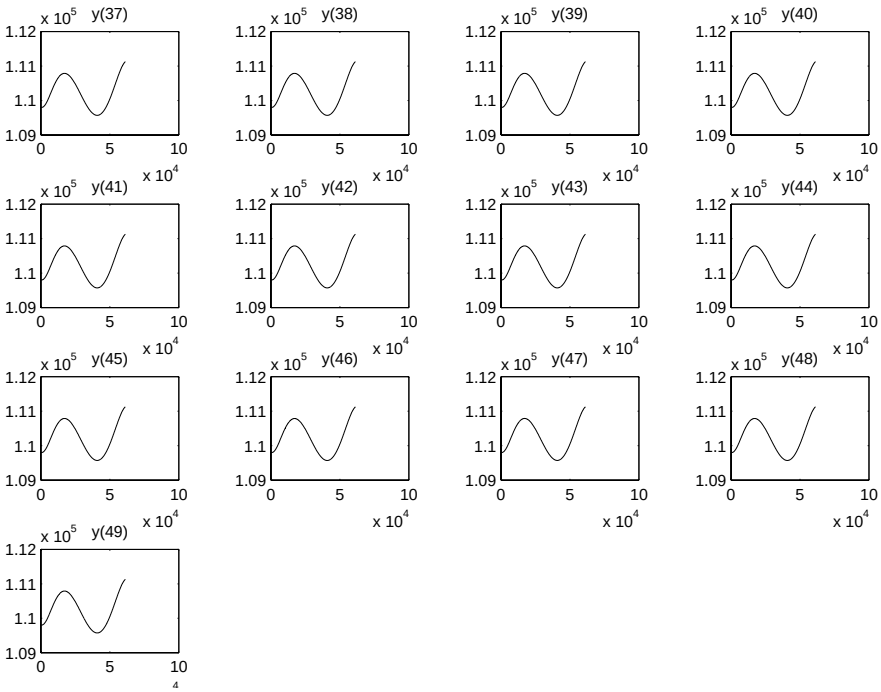

FIGURE 17.8: *Behavior of pressures over the integration interval.*

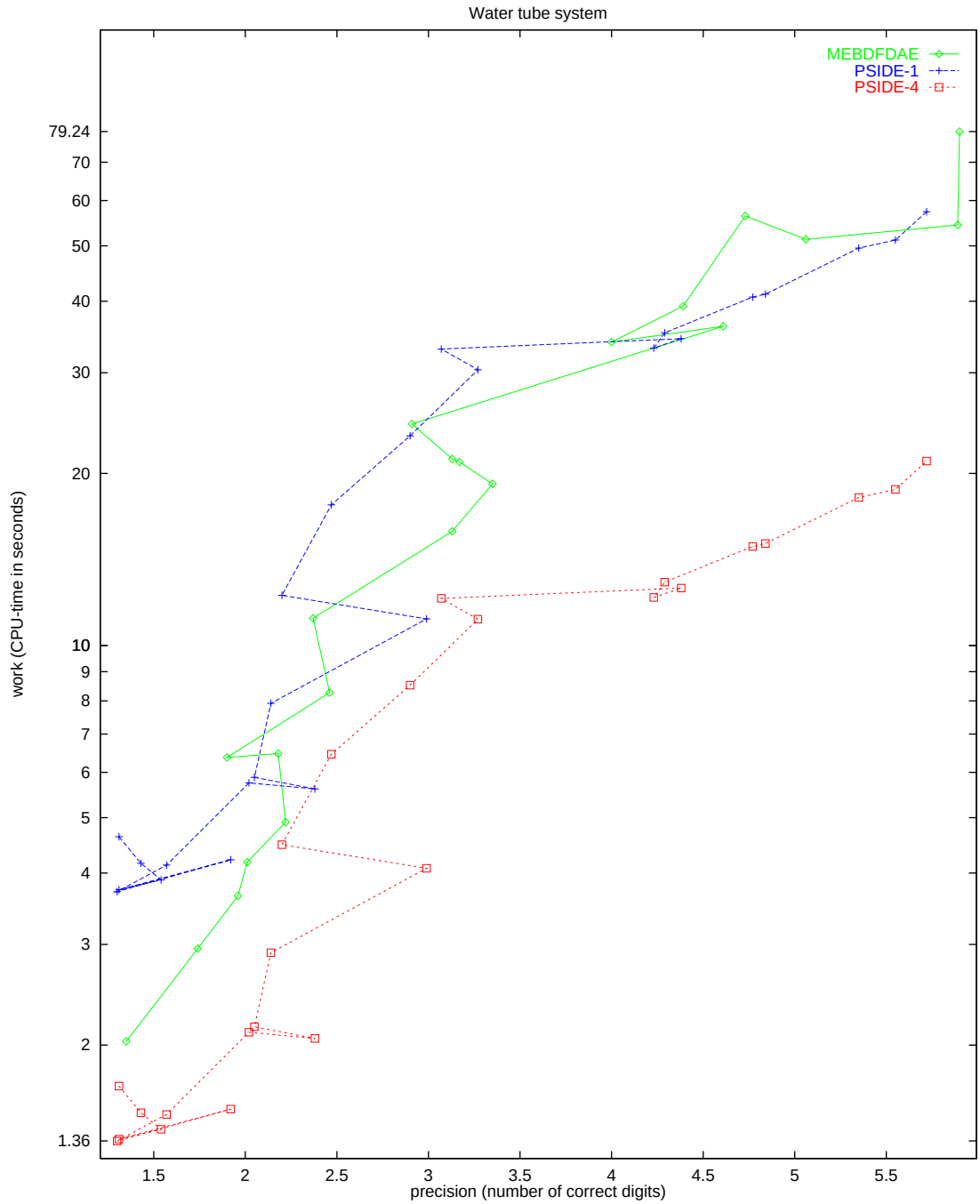

FIGURE 17.9: *Work-precision diagram.*

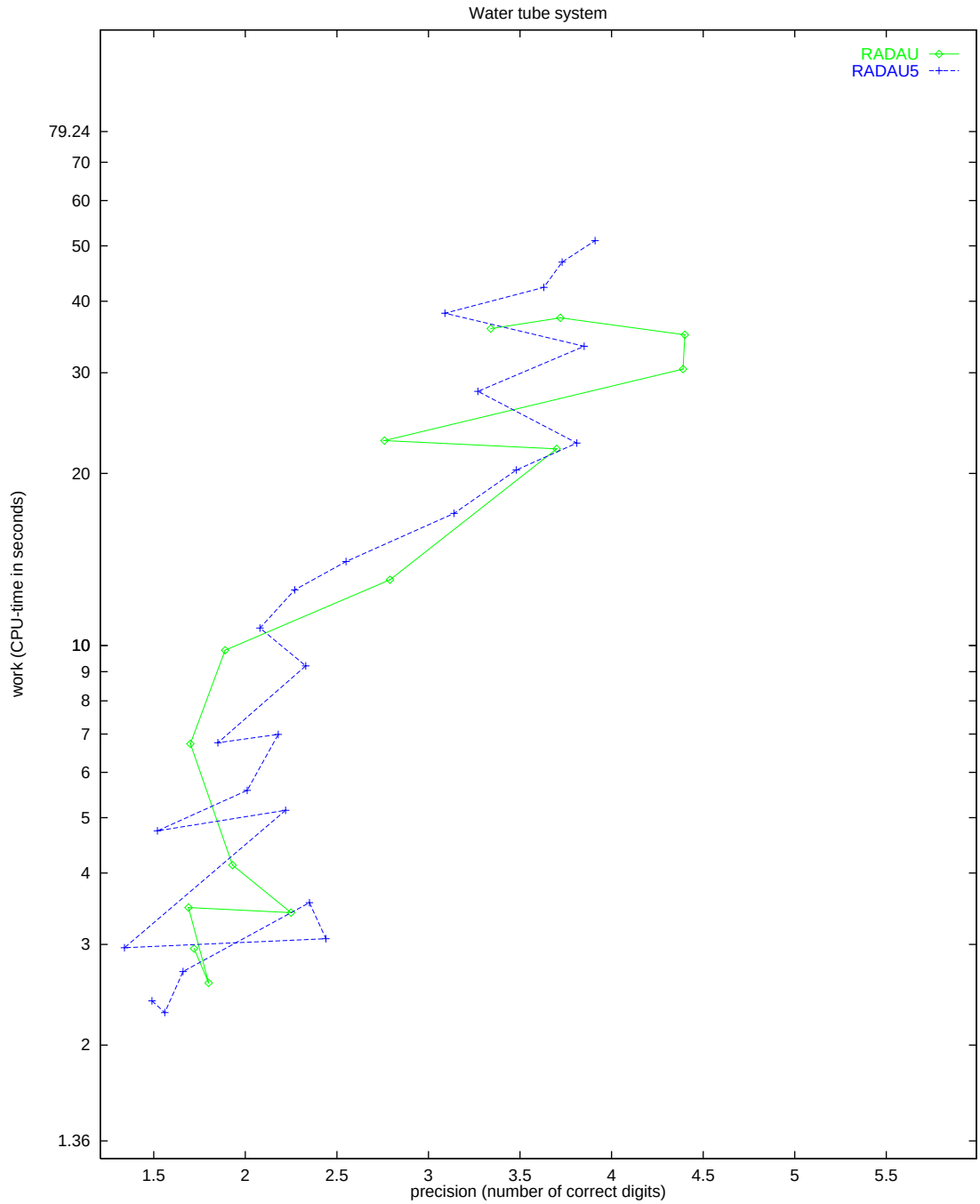

FIGURE 17.10: *Work-precision diagram.*